

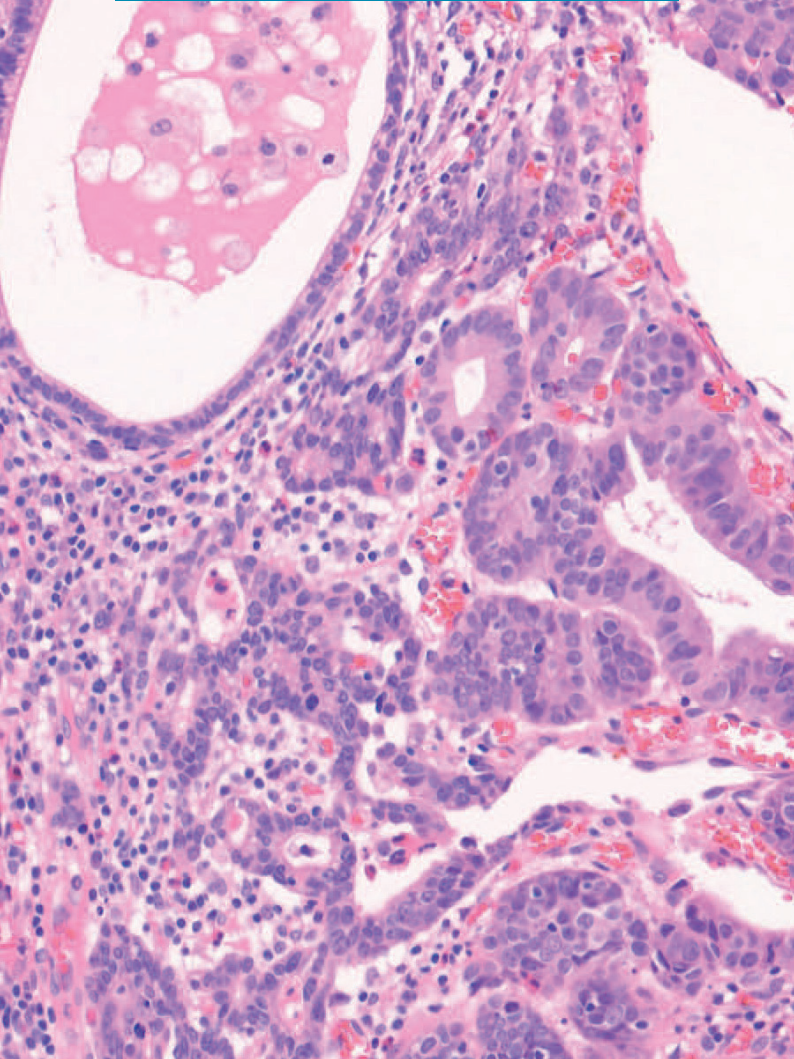
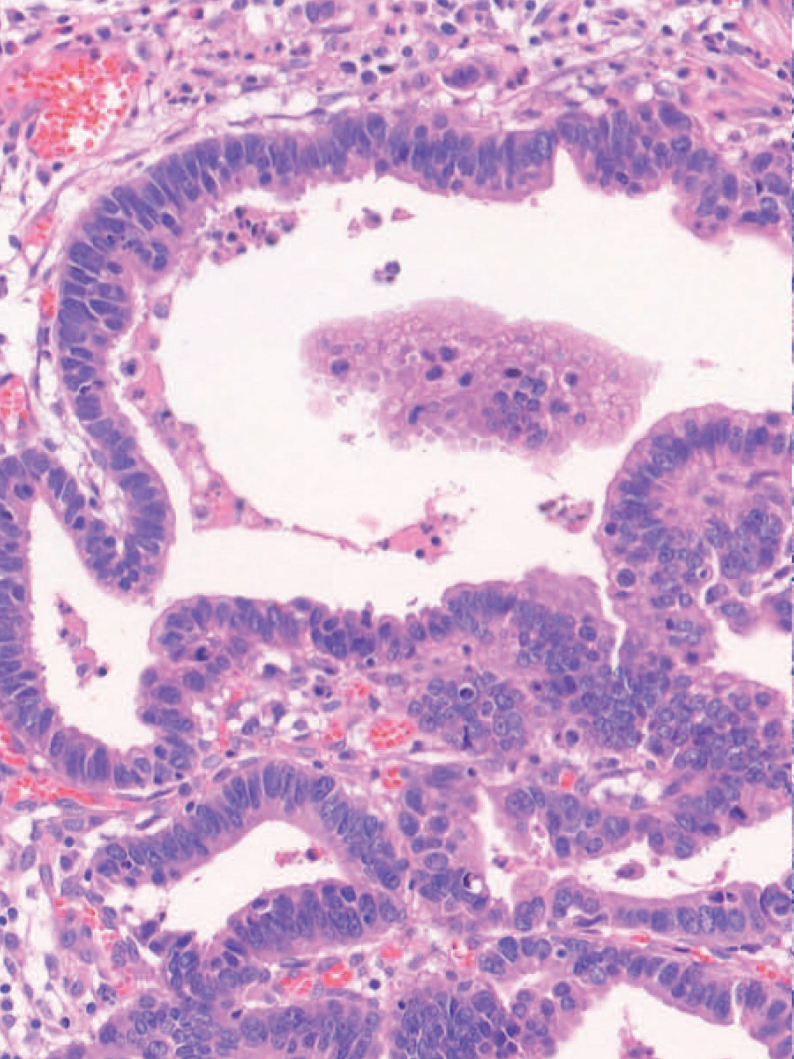
JPTM

Journal of Pathology
and Translational Medicine

January 2023
Vol. 57 / No.1
jpatholtm.org
pISSN: 2383-7837
eISSN: 2383-7845



*A Standardized
Pathology Report
for Gastric Cancer*



Aims & Scope

The *Journal of Pathology and Translational Medicine* is an open venue for the rapid publication of major achievements in various fields of pathology, cytopathology, and biomedical and translational research. The Journal aims to share new insights into the molecular and cellular mechanisms of human diseases and to report major advances in both experimental and clinical medicine, with a particular emphasis on translational research. The investigations of human cells and tissues using high-dimensional biology techniques such as genomics and proteomics will be given a high priority. Articles on stem cell biology are also welcome. The categories of manuscript include original articles, review and perspective articles, case studies, brief case reports, and letters to the editor.

Subscription Information

To subscribe to this journal, please contact the Korean Society of Pathologists/the Korean Society for Cytopathology. Full text PDF files are also available at the official website (<https://jpatholm.org>). *Journal of Pathology and Translational Medicine* is indexed by Emerging Sources Citation Index (ESCI), PubMed, PubMed Central, Scopus, KoreaMed, KoMCI, WPRIM, Directory of Open Access Journals (DOAJ), and CrossRef. Circulation number per issue is 50.

Editors-in-Chief

Jung, Chan Kwon, MD (*The Catholic University of Korea, Korea*) <https://orcid.org/0000-0001-6843-3708>

Park, So Yeon, MD (*Seoul National University, Korea*) <https://orcid.org/0000-0002-0299-7268>

Associate Editors

Bychkov, Andrey, MD (*Kameda Medical Center, Japan; Nagasaki University Hospital, Japan*) <https://orcid.org/0000-0002-4203-5696>

Kim, Haeryoung, MD (*Seoul National University, Korea*) <https://orcid.org/0000-0002-4205-9081>

Lee, Hee Eun, MD (*Mayo Clinic, USA*) <https://orcid.org/0000-0001-6335-7312>

Shin, Eunah, MD (*Yongin Severance Hospital, Yonsei University, Korea*) <https://orcid.org/0000-0001-5961-3563>

Editorial Board

Avila-Casado, Maria del Carmen, MD (*University of Toronto, Toronto General Hospital UHN, Canada*)

Bae, Jeong Mo, MD (*Seoul National University, Korea*)

Bae, Young Kyung, MD (*Yeungnam University, Korea*)

Bongiovanni, Massimo, MD (*Lausanne University Hospital, Switzerland*)

Bova, G. Steven, MD (*University of Tampere, Finland*)

Choi, Joon Hyuk (*Yeungnam University, Korea*)

Chong, Yo Sep, MD (*The Catholic University of Korea, Korea*)

Chung, Jin-Haeng, MD (*Seoul National University, Korea*)

Fadda, Guido, MD (*Catholic University of Rome-Foundation Agostino Gemelli University Hospital, Italy*)

Fukushima, Noriyoshi, MD (*Jichi Medical University, Japan*)

Go, Heounjeong (*University of Ulsan, Korea*)

Hong, Soon Won, MD (*Yonsei University, Korea*)

Jain, Deepali, MD (*All India Institute of Medical Sciences, India*)

Kakudo, Kennichi, MD (*Izumi City General Hospital, Japan*)

Kim, Jang-Hee, MD (*Ajou University, Korea*)

Kim, Jung Ho, MD (*Seoul National University, Korea*)

Kim, Se Hoon, MD (*Yonsei University, Korea*)

Komuta, Mina, MD (*Keio University, Tokyo, Japan*)

Kwon, Ji Eun (*Ajou University, Korea*)

Lai, Chiung-Ru, MD (*Taipei Veterans General Hospital, Taiwan*)

Lee, C. Soon, MD (*University of Western Sydney, Australia*)

Lee, Hwajeong, MD (*Albany Medical College, USA*)

Lee, Sung Hak, MD (*The Catholic University, Korea*)

Liu, Zhiyan, MD (*Shanghai Jiao Tong University, China*)

Lkhagvadorj, Sayamaa, MD (*Mongolian National University of Medical Sciences, Mongolia*)

Moran, Cesar, MD (*MD Anderson Cancer Center, U.S.A.*)

Paik, Jin Ho, MD (*Seoul National University, Korea*)

Park, Jeong Hwan (*Seoul National University, Korea*)

Ro, Jae Y., MD (*Cornell University, The Methodist Hospital, U.S.A.*)

Sakhuja, Puja, MD (*Govind Ballabh Pant Hospital, India*)

Shahid, Pervez, MD (*Aga Khan University, Pakistan*)

Song, Joon Seon, MD (*University of Ulsan, Korea*)

Tan, Puay Hoon, MD (*National University of Singapore, Singapore*)

Than, Nandor Gabor, MD (*Semmelweis University, Hungary*)

Tse, Gary M., MD (*The Chinese University of Hong Kong, Hong Kong*)

Yatabe, Yasushi, MD (*Aichi Cancer Center, Japan*)

Zhu, Yun, MD (*Jiangsu Institution of Nuclear Medicine, China*)

Ethic Editor

Choi, In-Hong, MD (*Yonsei University, Korea*)

Huh, Sun, MD (*Hallym University, Korea*)

Statistics Editors

Kim, Dong Wook (*National Health Insurance Service Ilsan Hospital, Korea*)

Lee, Hye Sun (*Yonsei University, Korea*)

Manuscript Editor

Chang, Soo-Hee (*InfoLumi Co., Korea*)

Layout Editor

Kim, Haeja (*iMiS Company Co., Ltd., Korea*)

Website and JATS XML File Producers

Cho, Yoonsang (*M2Community Co., Korea*)

Im, Jeonghee (*M2Community Co., Korea*)

Administrative Assistants

Kim, Da Jeong (*The Korean Society of Pathologists*)

Jeon, Anmi (*The Korean Society for Cytopathology*)

Contact the Korean Society of Pathologists/the Korean Society for Cytopathology

Publishers: Choe, Gheeyoung, MD, Lee, Seung-Sook, MD

Editors-in-Chief: Jung, Chan Kwon, MD, Park, So Yeon, MD

Published by the Korean Society of Pathologists/the Korean Society for Cytopathology

Editorial Office

Room 1209 Gwanghwamun Officia, 92 Saemunan-ro, Jongno-gu, Seoul 03186, Korea

Tel: +82-2-795-3094 Fax: +82-2-790-6635 E-mail: office@jpatholm.org

#1508 Renaissancetower, 14 Mallijae-ro, Mapo-gu, Seoul 04195, Korea

Tel: +82-2-593-6943 Fax: +82-2-593-6944 E-mail: office@jpatholm.org

Printed by iMiS Company Co., Ltd. (JMC)

Jungang Bldg. 18-8 Wonhyo-ro 89-gil, Yongsan-gu, Seoul 04314, Korea

Tel: +82-2-717-5511 Fax: +82-2-717-5515 E-mail: ml@smileml.com

Manuscript Editing by InfoLumi Co.

210-202, 421 Pangyo-ro, Bundang-gu, Seongnam 13522, Korea

Tel: +82-70-8839-8800 E-mail: infolumi.chang@gmail.com

Front cover image: Representative images of gastric low-grade/high-grade adenoma and adeonocarcinoma (p55).

© Copyright 2023 by the Korean Society of Pathologists/the Korean Society for Cytopathology

© Journal of Pathology and Translational Medicine is an Open Access journal under the terms of the Creative Commons Attribution Non-Commercial License (<https://creativecommons.org/licenses/by-nc/4.0>).

© This paper meets the requirements of KS X ISO 9706, ISO 9706-1994 and ANSI/NISO Z.39.48-1992 (Permanence of Paper).

CONTENTS

REVIEWS

- 1 **A standardized pathology report for gastric cancer: 2nd edition**
Young Soo Park, Myeong-Cherl Kook, Baek-hui Kim, Hye Seung Lee, Dong-Wook Kang, Mi-Jin Gu, Ok Ran Shin, Younghee Choi, Wonae Lee, Hyunki Kim, In Hye Song, Kyoung-Mee Kim, Hee Sung Kim, Guhyun Kang, Do Youn Park, So-Young Jin, Joon Mee Kim, Yoon Jung Choi, Hee Kyung Chang, Soomin Ahn, Mee Soo Chang, Song-Hee Han, Yoonjin Kwak, An Na Seo, Sung Hak Lee, Mee-Yon Cho, The Gastrointestinal Pathology Study Group of the Korean Society of Pathologists
- 28 **Infections and immunity: associations with obesity and related metabolic disorders**
Amitabha Ray, Melissa J. L. Bonorden, Rajashree Pandit, Katai J. Nkhata, Anupam Bishayee
- 43 **Single-cell and spatial sequencing application in pathology**
Yoon-Seob Kim, Jinyong Choi, Sug Hyung Lee
- 52 **Perspectives on single-nucleus RNA sequencing in different cell types and tissues**
Nayoung Kim, Huiram Kang, Areum Jo, Seung-Ah Yoo, Hae-Ock Lee
- 60 **Inflammatory bowel disease-associated intestinal fibrosis**
Ji Min Park, Jeongseok Kim, Yoo Jin Lee, Sung Uk Bae, Hye Won Lee

ORIGINAL ARTICLE

- 67 **The proteomic landscape shows oncologic relevance in cystitis glandularis**
Jun Yong Kim, Dohyun Han, Hyeyoon Kim, Minsun Jung, Han Suk Ryu

CASE REPORT

- 75 **Metallic implant-associated lymphoma: ALK-negative anaplastic large cell lymphoma associated with total knee replacement arthroplasty**
Jai-Hyang Go

NEWSLETTER

- 79 **What's new in neuromuscular pathology 2022: myopathy updates and gene therapies**
Chunyu Cai

A standardized pathology report for gastric cancer: 2nd edition

Young Soo Park^{1*}, Myeong-Cherl Kook^{2*}, Baek-hui Kim^{3*}, Hye Seung Lee^{4*}, Dong-Wook Kang⁵, Mi-Jin Gu⁶, Ok Ran Shin⁷, Younghee Choi⁸, Wonae Lee⁹, Hyunki Kim¹⁰, In Hye Song¹, Kyoung-Mee Kim¹¹, Hee Sung Kim¹², Guhyun Kang¹³, Do Youn Park¹⁴, So-Young Jin¹⁵, Joon Mee Kim¹⁶, Yoon Jung Choi¹⁷, Hee Kyung Chang¹⁸, Soomin Ahn¹¹, Mee Soo Chang¹⁹, Song-Hee Han²⁰, Yoonjin Kwak⁴, An Na Seo²¹, Sung Hak Lee²², Mee-Yon Cho²³,

The Gastrointestinal Pathology Study Group of the Korean Society of Pathologists

¹Department of Pathology, Asan Medical Center, University of Ulsan College of Medicine, Seoul; ²Center for Gastric Cancer, National Cancer Center, Goyang;

³Department of Pathology, Korea University Guro Hospital, Seoul;

⁴Department of Pathology, Seoul National University Hospital, Seoul National University College of Medicine, Seoul;

⁵Department of Pathology, Chungnam National University Sejong Hospital, Chungnam National University School of Medicine, Sejong;

⁶Department of Pathology, Yeungnam University College of Medicine, Daegu;

⁷Department of Hospital Pathology, Uijeongbu St. Mary's Hospital, College of Medicine, The Catholic University of Korea, Uijeongbu;

⁸Department of Pathology, Hallym University Dongtan Sacred Heart Hospital, Hwaseong; ⁹Department of Pathology, Dankook University College of Medicine, Cheonan;

¹⁰Department of Pathology, Yonsei University College of Medicine, Seoul;

¹¹Department of Pathology and Translational Genomics, Samsung Medical Center, Sungkyunkwan University School of Medicine, Seoul;

¹²Department of Pathology, Chung-Ang University Hospital, Chung-Ang University College of Medicine, Seoul;

¹³LabGenomics Clinical Laboratories, Seongnam; ¹⁴St. Maria Pathology Laboratory, Busan; ¹⁵Department of Pathology, Soonchunhyang University Seoul Hospital, Seoul;

¹⁶Department of Pathology, Inha University School of Medicine, Incheon;

¹⁷Department of Pathology, Yongin Severance Hospital, Yonsei University College of Medicine, Yongin;

¹⁸Department of Pathology, Kosin University Gospel Hospital, Kosin University College of Medicine, Busan;

¹⁹Department of Pathology, Seoul National University Boramae Hospital, Seoul National University College of Medicine, Seoul;

²⁰Department of Pathology, Dong-A University College of Medicine, Busan;

²¹Department of Pathology, School of Medicine, Kyungpook National University, Kyungpook National University Chilgok Hospital, Daegu;

²²Department of Hospital Pathology, Seoul St. Mary's Hospital, College of Medicine, The Catholic University of Korea, Seoul;

²³Department of Pathology, Wonju Severance Christian Hospital, Yonsei University Wonju College of Medicine, Wonju, Korea

The first edition of 'A Standardized Pathology Report for Gastric Cancer' was initiated by the Gastrointestinal Pathology Study Group of the Korean Society of Pathologists and published 17 years ago. Since then, significant advances have been made in the pathologic diagnosis, molecular genetics, and management of gastric cancer (GC). To reflect those changes, a committee for publishing a second edition of the report was formed within the Gastrointestinal Pathology Study Group of the Korean Society of Pathologists. This second edition consists of two parts: standard data elements and conditional data elements. The *standard data elements* contain the basic pathologic findings and items necessary to predict the prognosis of GC patients, and they are adequate for routine surgical pathology service. Other diagnostic and prognostic factors relevant to adjuvant therapy, including molecular biomarkers, are classified as *conditional data elements* to allow each pathologist to selectively choose items appropriate to the environment in their institution. We trust that the standardized pathology report will be helpful for GC diagnosis and facilitate large-scale multidisciplinary collaborative studies.

Key Words: Stomach neoplasms; Gastrectomy; Endoscopic resection; Molecular pathology; Pathology report; Standardization

Received: December 1, 2022 **Revised:** December 22, 2022 **Accepted:** December 23, 2022

Corresponding Author: Sung Hak Lee, MD, PhD, Department of Hospital Pathology, Seoul St. Mary's Hospital, College of Medicine, The Catholic University of Korea, 222 Banpo-daero, Seocho-gu, Seoul 06591, Korea

Tel: +82-2-2258-1617, Fax: +82-2-2258-1627, E-mail: hakjang@catholic.ac.kr

Corresponding Author: Mee-Yon Cho, MD, PhD, Department of Pathology, Wonju Severance Christian Hospital, Yonsei University Wonju College of Medicine, 20 Ilson-ro, Wonju 26426, Korea

Tel: +82-33-741-1553, Fax: +82-33-731-6590, E-mail: meeyon@yonsei.ac.kr

*Young Soo Park, Myeong-Cherl Kook, Baek-hui Kim, and Hye Seung Lee contributed equally to this work.

This article has been published jointly, with consent, in both *Journal of Pathology and Translational Medicine* and *Journal of Gastric Cancer*.

Gastric cancer (GC) is the fifth most commonly diagnosed cancer and has the fourth-highest mortality rate worldwide [1]. Although the incidence and mortality rates of GC have decreased markedly during the past 50 years, Korean cancer registry data show that GC was still the most diagnosed cancer in 2018 [2]. The Gastrointestinal Pathology Study Group (GIPSG) of the Korean Society of Pathologists developed the first edition of 'A Standardized Pathology Report for Gastric Cancer' in 2005 to give pathologists a standard reporting format for GC diagnosis in daily practice [3].

Considerable changes in the pathology of GC have happened since then, such as the development of the histopathological classification for carcinoma and several pathologic features for prognostication [4,5]. In addition, molecular pathology tests for GC have become essential as treatment strategies for GC have developed rapidly, including advances in targeted therapy and immunotherapy [6,7]. Therefore, it is necessary to provide a second edition of the standardization report that reflects those changes.

In March 2022, a committee for revision of the report was formed within the GIPSG of the Korean Society of Pathologists. The committee consisted of subcommittees to discuss four topics: (1) radical resection specimens, (2) endoscopic resection specimens, (3) histologic classification, and (4) molecular markers for GC. This second edition of 'A Standardized Pathology Report for Gastric Cancer' was developed after several meetings of the subcommittees and entire committee.

The purpose of this report form is to standardize pathologic diagnosis of GC and enhance treatment capacity by facilitating communication between clinicians and pathologists. The basic pathologic findings for prognostication of GC are described in the "Standard data elements" section of the form, and other factors related to diagnosis and adjuvant therapy, including molecular biomarkers, are documented in the "Conditional data elements" section. A Korean version as well as an English version is also provided to enable Korean pathologists to use this report (Supplementary Material S1).

APPLICATION OF STANDARD PATHOLOGY REPORT

This standard pathology report is for use with primary gastric carcinomas. Neuroendocrine tumors, lymphomas, gastrointestinal stromal tumors, and other sarcomas are excluded. Carcinomas involving the esophagogastric junction (EGJ) with a center ≤ 2 cm into the proximal stomach are considered to be distal esophageal carcinoma and excluded, as defined in the American Joint

Committee on Cancer (AJCC), 8th edition [8]. This pathology report is also used for residual (post-chemotherapy or post-endoscopic resection) carcinomas. The report forms for pathologic diagnosis from radical resection and endoscopic resection specimens are shown in Tables 1 and 2, respectively.

Radical resection specimens

Gastrectomy (specimen) type

The type of surgical procedure should be mentioned in the surgical record.

Gross type

The gross type of each lesion should be recorded individually. The classification of early gastric cancer (EGC) uses the Japanese guideline (subclassification of type 0) [9], and classification of advanced gastric cancer (AGC) uses the Borrmann classification. The unclassifiable type is Borrmann type 5, according to the Japanese guideline [9]. The gross type is determined by macroscopic examination. If there is discrepancy between the macroscopic and microscopic findings, i.e., EGC on macroscopic examination but tumor invades the proper muscle microscopically (AGC), the macroscopic type should remain as the gross finding and not be corrected according to the microscopic finding. In such cases, the following descriptions are recommended: AGC, mimicking EGC type X or EGC, mimicking Borrmann type X. If the lesion is AGC grossly, at least four representative sections should be submitted for microscopic examination, including the deepest invasion, and ink should be applied at the serosal surface nearest the tumor. If the lesion is EGC grossly, grid mapping should be performed at 4 to 5 mm width.

Previous treatment

Any treatment before surgical resection should be recorded when applicable. If there are residual tumor foci, it should be mentioned that these are residual tumors. In post-chemotherapy gastrectomy situations, representative sections are sufficient if the lesion is large and obvious. However, the entire tumor bed must be microscopically examined when the representative sections contain no residual cancer cells or the residual lesion is small or inconspicuous grossly. For post-endoscopic resection specimens, the entire tumor bed should be submitted for microscopic evaluation.

Tumor focality

Tumor focality should record whether it is a single lesion or

Table 1. Report form for pathologic diagnosis using radical resection specimens

Standard and Conditional data elements
Gastrectomy (specimen) type^a <ul style="list-style-type: none"> <input type="checkbox"/> Total gastrectomy <input type="checkbox"/> Distal (subtotal) gastrectomy <input type="checkbox"/> Proximal gastrectomy <input type="checkbox"/> Wedge resection <input type="checkbox"/> Others (_____)
Gross type^a <ul style="list-style-type: none"> <input type="checkbox"/> EGC type <ul style="list-style-type: none"> <input type="checkbox"/> EGC type I/IIa/IIb/IIc/III <input type="checkbox"/> Mixed EGC type (_____) <input type="checkbox"/> AGC type <ul style="list-style-type: none"> <input type="checkbox"/> Borrmann type 1/2/3/4/unclassifiable <input type="checkbox"/> Others (_____)
Residual with previous treatment^a (when applicable) <ul style="list-style-type: none"> <input type="checkbox"/> Residual <input type="checkbox"/> Previous treatment <ul style="list-style-type: none"> <input type="checkbox"/> Chemotherapy <input type="checkbox"/> Chemoradiotherapy <input type="checkbox"/> Endoscopic mucosal resection <input type="checkbox"/> Endoscopic submucosal dissection <input type="checkbox"/> Unknown <input type="checkbox"/> Others (_____)
Tumor focality^a <ul style="list-style-type: none"> <input type="checkbox"/> Single <input type="checkbox"/> Multiple
Tumor location^a <ul style="list-style-type: none"> <input type="checkbox"/> Involvement <ul style="list-style-type: none"> <input type="checkbox"/> Esophagus/Upper/Middle/Lower third of the stomach/Duodenum <input type="checkbox"/> Center <ul style="list-style-type: none"> <input type="checkbox"/> Cardia/Fundus/Body/Antrum/Pylorus <input type="checkbox"/> Lesser curvature/Greater curvature/Anterior wall/Posterior wall <input type="checkbox"/> Others (_____)
Tumor size^a <p><i>One largest dimension</i></p> <ul style="list-style-type: none"> <input type="checkbox"/> ____ cm <p>Tumor size^b</p> <p><i>Secondary or tertiary tumor dimensions</i></p> <ul style="list-style-type: none"> <input type="checkbox"/> ____ × ____ cm <input type="checkbox"/> ____ × ____ × ____ cm
Histologic type^a <p><i>According to the principles described in "Histologic classification" section</i></p> <ul style="list-style-type: none"> <input type="checkbox"/> WHO <input type="checkbox"/> Lauren
Tumor regression grade^a (when applicable) <ul style="list-style-type: none"> <input type="checkbox"/> Grade 0: Complete response (no viable cancer cells) <input type="checkbox"/> Grade 1: Near complete response (single cells or rare small groups of cancer cells) <input type="checkbox"/> Grade 2: Partial response (residual cancer with evident tumor regression, but more than single cells or rare small groups of cancer cells) <input type="checkbox"/> Grade 3: Poor or no response (extensive residual cancer with no evident tumor regression)
Lymph node tumor regression^b (when applicable) <ul style="list-style-type: none"> <input type="checkbox"/> Not identified <input type="checkbox"/> Present
Depth of invasion (pT)^a <ul style="list-style-type: none"> <input type="checkbox"/> Invades lamina propria (pT1a) <input type="checkbox"/> Invades muscularis mucosae (pT1a) <input type="checkbox"/> Invades submucosa (sm1/sm2/sm3) (pT1b) <input type="checkbox"/> Invades proper muscle (pT2) <input type="checkbox"/> Invades subserosa (pT3) <input type="checkbox"/> Invades serosa (visceral peritoneum) (pT4a) <input type="checkbox"/> Directly invades adjacent structure (pT4b) specify (_____)
Resection margin^a <ul style="list-style-type: none"> <input type="checkbox"/> Proximal margin <ul style="list-style-type: none"> <input type="checkbox"/> Free from carcinoma (safety margin, ____ cm) <input type="checkbox"/> Involved by carcinoma

(Continued to the next page)

Table 1. Continued

Standard and Conditional data elements
<input type="checkbox"/> Distal margin <input type="checkbox"/> Free from carcinoma (safety margin, ___ cm) <input type="checkbox"/> Involved by carcinoma
Circumferential resection margin^b <i>Applied in EGJ or cardia cancer</i> <input type="checkbox"/> Free from carcinoma (safety margin, ___ cm) <input type="checkbox"/> Involved by carcinoma
Regional lymph node metastasis^a <i>At least 16 regional lymph nodes should be assessed</i> <input type="checkbox"/> no metastasis in ___ regional lymph nodes <input type="checkbox"/> metastasis in ___ out of ___ regional lymph nodes
Extranodal tumor extension^b <input type="checkbox"/> Not identified <input type="checkbox"/> Present
Isolated tumor cell clusters^b <i>Applied in incidentally identified tumor cell cluster less than 0.2 mm in greatest dimension with no other regional lymph node metastasis (pN0)</i> <input type="checkbox"/> Present [pN0 (+)]
Lymphovascular invasion^a <input type="checkbox"/> Not identified <input type="checkbox"/> Present
Venous invasion^b <i>Applied when identified in large vessels with an identifiable smooth muscle layer or elastic lamina</i> <input type="checkbox"/> Not identified <input type="checkbox"/> Present
Perineural invasion^a <input type="checkbox"/> Not identified <input type="checkbox"/> Present
Pre-existing adenoma^a (when present) <i>Used if the carcinoma is within the adenoma</i> <input type="checkbox"/> Tubular/Tubulovillous/Villous adenoma <input type="checkbox"/> Low grade dysplasia/High grade dysplasia
Associated findings^a (when present) <input type="checkbox"/> Tumor perforation <input type="checkbox"/> Serosal (peritoneal, mesenteric) seeding <input type="checkbox"/> Distant metastasis Other organ, specify: _____ Distant lymph node
Separate lesions^a (when present) <input type="checkbox"/> Peptic ulcer <input type="checkbox"/> Adenoma <input type="checkbox"/> GIST <input type="checkbox"/> Others (_____)

EGC, early gastric cancer; AGC, advanced gastric cancer; WHO, World Health Organization; EGJ, esophagogastric junction.

^aStandard data elements; ^bConditional data elements.

multiple lesions. Multiple lesions should be evaluated individually both macroscopically and microscopically in descending order from the tumor with the deepest level of invasion. However, regional lymph node metastasis, associated findings, and separate lesions are listed only for the deepest lesion.

Tumor location

The description of the tumor location is recorded in two parts: involvement and center. The *involvement* of the tumor uses up to three portions from the esophagus to duodenum beginning with the most involved area. The delineation of the upper, middle, and lower thirds of the stomach follows the Japanese guideline [9].

The *center* of the tumor is described using a combination of locations according to the International Classification of Diseases for Oncology classification [10] (cardia, fundus, body, antrum, pylorus, lesser curvature, greater curvature) plus the anterior wall and posterior wall [11]. If none of those options appropriately describes the location of the tumor, other can be used.

Tumor size

The tumor size is recorded using the largest dimension of the tumor [11]. Secondary or tertiary dimensions can be measured as conditional data elements. However, the tumor size is not used in the current staging of GC [8], and it is sometimes very difficult to

Table 2. Report form for pathologic diagnosis using endoscopic resection specimens

Standard and Conditional data elements
Specimen size^a <input type="checkbox"/> ___ x ___ cm
Gross type of tumor^a <i>Same as method of surgical specimen</i>
Tumor size^a <i>One largest dimension</i> <input type="checkbox"/> ___ cm
Histologic type^a <i>According to the principles described in "Histologic classification" section</i> <input type="checkbox"/> WHO <input type="checkbox"/> Lauren
Histologic components^b <i>All morphologic components of tumor cell may be described</i>
Depth of invasion (pT)^a <input type="checkbox"/> Invades lamina propria (pT1a) <input type="checkbox"/> Invades muscularis mucosae (pT1a) <input type="checkbox"/> Invades submucosa (submucosal depth: ___ mm or μ m) <input type="checkbox"/> Invades proper muscle (pT2)
Depth of invasion (pT)^b <i>In case of submucosa invasion, the invasion width can be additionally described</i> <input type="checkbox"/> invades submucosa (submucosal depth: ___ mm or μ m) (submucosal width: ___ mm)
Resection margin^a <input type="checkbox"/> Lateral margin <input type="checkbox"/> Free from carcinoma (safety margin, ___ cm) <input type="checkbox"/> Involved by carcinoma <input type="checkbox"/> Deep margin <input type="checkbox"/> Free from carcinoma (safety margin, ___ cm) <input type="checkbox"/> Involved by carcinoma
Resection margin^b <input type="checkbox"/> Proximal margin <input type="checkbox"/> Free from carcinoma (safety margin, ___ cm) <input type="checkbox"/> Involved by carcinoma <input type="checkbox"/> Distal margin <input type="checkbox"/> Free from carcinoma (safety margin, ___ cm) <input type="checkbox"/> Involved by carcinoma <input type="checkbox"/> Anterior margin <input type="checkbox"/> Free from carcinoma (safety margin, ___ cm) <input type="checkbox"/> Involved by carcinoma <input type="checkbox"/> Posterior margin <input type="checkbox"/> Free from carcinoma (safety margin, ___ cm) <input type="checkbox"/> Involved by carcinoma <input type="checkbox"/> Deep margin <input type="checkbox"/> Free from carcinoma (safety margin, ___ cm) <input type="checkbox"/> Involved by carcinoma
Ulceration^a <input type="checkbox"/> Absent <input type="checkbox"/> Present
Ulceration^b <input type="checkbox"/> Absent <input type="checkbox"/> Non-significant (≤ 4 mm) <input type="checkbox"/> Significant (> 4 mm)
Cases with adenoma components^a <input type="checkbox"/> Absent <input type="checkbox"/> Present specify: _____
En bloc resection^a <input type="checkbox"/> Yes <input type="checkbox"/> No (piecemeal/tearing)
Lymphatic invasion^a <input type="checkbox"/> Not identified <input type="checkbox"/> Present
Venous invasion^a <input type="checkbox"/> Not identified <input type="checkbox"/> Present

WHO, World Health Organization.

^aStandard data elements; ^bConditional data elements.

measure accurately, such as in Borrmann type 4 cancer. For scattered residual tumor foci following previous treatment, it is recommended to measure the maximum diameter that includes all foci [12].

Tumor regression grade

Although preoperative chemotherapy has not been established as a standard treatment for patients in Korea [5], studies have shown survival benefits in local AGC in European [13], Asian [14], and Korean patients [15]. Therefore, the need to adequately evaluate the tumor response to chemotherapy is increasing [16]. Various tumor regression grading (TRG) methods are available for gastrointestinal cancers [17,18]. The Becker system [19] is one that has been proposed for GC. The previous edition of "A Standardized Pathology Report for Gastric Cancer" [3] used the Japanese guideline [9]. The Becker and Japanese systems both estimate the proportion of residual tumor and use it as a cutoff value between TRGs. However, because some tumors have more abundant fibrosis than tumor cells (before chemotherapy), estimation of the residual tumor proportion could show low concordance between observers [20,21]. Therefore, we suggest a new TRG system: the modified Ryan system currently recommended in the College of American Pathologists (CAP) guideline [11] and the second edition of the standardized pathology report for colorectal cancer in Korea [22]. It is a descriptive four-tier system that evaluates residual cancer rather than fibrosis as none, single cells or rare small groups, more than single cells but evident tumor response, and extensive residual cancer cells. Acellular mucin pools and necrotic or degenerative cells are not considered to be residual cancer [8]. Only the primary tumor is evaluated in this TRG, but tumor regression of the regional lymph nodes [16,23] can be reported as a conditional data element when there is evidence of partial (viable cancer cells with regressive changes) or complete tumor regression (only fibrosis, mucin pool, or foam cells without viable cells) in the regional lymph nodes. Evidence suggests that the presence of tumor regression in the lymph nodes is associated with better clinical outcomes [24,25].

Depth of invasion

The depth of the tumor invasion follows the AJCC 8th edition [8] and Japanese guidelines [9]. Notably, the Japanese guideline does not accept carcinoma *in situ* (pTis). In the AJCC 8th edition, pTis is defined as an intraepithelial tumor without invasion of the lamina propria, which is equivalent to high-grade dysplasia. pT1b is subdivided into sm1, sm2, and sm3. If cancer cells are present below an imaginary line dividing the submucosa and

proper muscle, the case is considered pT2 even if the cancer cells are not actually within the muscle fibers. If there is no proper muscle layer due to ulceration, and the cancer cells are below the imaginary line drawn at the lower border of the proper muscle, the case is considered pT3. Invasion of the omentum and perigastric fat is considered pT3. Ink should be applied at the serosal surface nearest the tumor during gross examination to properly evaluate serosal (visceral peritoneum) invasion. The case is considered pT4a if the cancer cells are adherent to or exposed beyond mesothelial cells. Because the mesocolon and gastric serosa (including the greater and lesser omentum) have different embryological origins, invasion of the mesocolon should be classified as pT4b. However, some areas are tightly fused, such as the posterior wall of the antrum, the gastric serosa, and the anterior side of the transverse mesocolon. Therefore, the Japanese guideline indicates that invasion of the transverse mesocolon is not pT4b unless it extends to the colic vessels or penetrates the posterior surface of the mesocolon [9]. Some cases can be either pT4a or pT4b, depending on the site of the tumor. Invasion of the pancreas capsule is considered pT4b. Direct duodenal or esophageal invasion is not considered pT4b. Any involvement of other organs, such as the liver, pancreas, colon, spleen, diaphragm, or kidney, should be recorded. Cancer cells within lymphatic or vascular spaces are not considered in the determination of invasion depth [8]. The presence of lymphatic or vascular invasion should be recorded separately in parentheses (e.g., tumor invades proper muscle [involvement of subserosa by lymphatic emboli]).

Resection margin

The distance from the proximal or distal resection margin is the length from the edge of the carcinoma to the nearest resection margin. It is important to locate the true resection margin in the gross specimen, especially when the stomach is opened along the lesser curvature or obliquely along the anterior or posterior wall. In some cases, cancer cells approach the resection margin much more closely than can be observed grossly (cancer spreading underneath the mucosa). Therefore, the resection margin is finalized in a microscopic evaluation. The circumferential and radial resection margin statuses can be reported as conditional data elements. Determination of the circumferential margin is often required if the tumor is located near the EGJ.

Regional lymph node metastasis

The presence of lymph node metastasis is one of the most important prognostic factors, even post-chemotherapy [26,27]. Both the total number of evaluated lymph nodes and the number of

metastatic lymph nodes are reported. Although pathological evaluation of more than 30 regional lymph nodes is desirable according to the AJCC 8th edition [8], a minimum of 16 regional lymph nodes is acceptable per the CAP guideline [11] because the definition of pN3b is 16 or more metastases. Therefore, if fewer than 16 lymph nodes were initially retrieved for evaluation, additional effort to recover more lymph nodes should be made and reported. This does not apply in cases of previous partial gastrectomy, preoperative chemotherapy, or radiation therapy. Microscopic evaluation should be performed on the largest plane of each lymph node. In general, if the size of the metastasis observed in the lymph node is ≤ 0.2 mm, the metastasis is called isolated tumor cells (ITCs); if the size is more than 0.2 mm but not greater than 2 mm, it is a micrometastasis. Because micrometastases are not reported separately in GC, they are considered to be positive lymph nodes [8]. According to the AJCC 8th edition, ITCs should not be reflected in the pN stage and should be reported as pN0 (i+) in the absence of another lymph node metastasis. However, it is hard to ignore ITCs, which are readily seen on hematoxylin and eosin (H&E) slides. Therefore, in most practices, all metastatic tumor cell clusters in the lymph nodes are reflected in the pN stage regardless of size, and only ITCs incidentally detected by cytokeratin immunohistochemistry (IHC) are excluded from the pN stage. The stations of the lymph nodes are not reported unless they are separately submitted with corresponding labels. Tumor deposit (TD) is defined as discrete tumor nodules separate from the tumor bed (within the lymphatic drainage of the primary tumor) without identifiable lymph node tissue or vascular or neural structure (Fig. 1) [8]. Unlike colorectal carcinoma, TDs are considered to be metastatic lymph nodes in

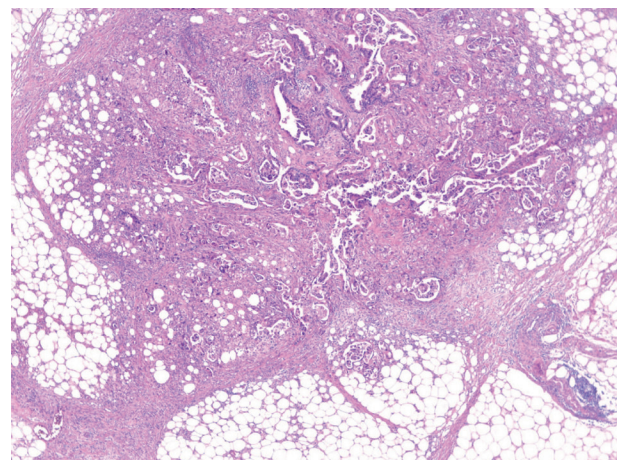


Fig. 1. An example of a tumor deposit. It usually has irregular outlines without identifiable lymph node tissue or identifiable vascular or neural structures.

GC and are thus reflected in the pN stage. TD and serosal (peritoneal) seeding nodules should be distinguished because peritoneal seeding is graded as pM1. Metastasis to a distant lymph node is pM1 and should not be considered in the pN stage. The definition of distant lymph nodes is different in the AJCC 8th edition than in the Japanese guideline, and we recommend following the AJCC 8th edition, in which superior mesenteric lymph node metastasis is pM1 [8].

Extranodal tumor extension

If the cancer cells show infiltration of the extranodal adipose tissue beyond the capsule of the lymph node, extranodal tumor extension (ENE) can be reported. ENE is associated with poor prognosis in GC [28-30].

Lymphovascular invasion

Lymphovascular invasion includes both lymphatic and vascular invasion. Discrimination of lymphatics from blood vessels on H&E slides is often difficult, especially when they are small (Fig. 2A, B). Although IHC for D2-40 or CD31 can be used, the prognostic differences between lymphatic and blood vessel invasion have not been sufficiently evaluated in GC [12]; therefore, we recommend using 'lymphovascular invasion.' However, when tumor invasion or emboli are observed in large vessels with an identifiable smooth muscle layer or elastic lamina, it is called venous invasion and can be reported as a conditional data element (Fig. 2C). Venous invasion has been reported as a risk factor for recurrence in both early [31,32] and advanced GCs [33].

Perineural invasion

Perineural invasion is reported when cancer cells are observed within or around the nerve [34].

Pre-existing adenoma

Pre-existing adenoma is reported when carcinoma is observed within an adenoma. If the adenoma is discrete from the carcinoma,

it is reported as a separate lesion.

Associated findings

Tumor perforation, serosal (peritoneal, mesenteric) seeding, and distant metastasis (including specific site) are reported when present.

Separate lesions

Peptic ulcers, adenomas, gastrointestinal stromal tumors, and other separate lesions are reported when present.

Endoscopic resection specimens

Description of the specimen

The size of the specimen is expressed as the length of the longest axis and the length perpendicular to the longest axis. The size of the tumor is indicated only by the length of the largest axis. The gross type of the tumor is described in the same way as for a surgical specimen.

Sectioning of the specimen

Apply ink to the entire deep margin and lateral margins of the specimen so that it can be viewed under a microscope. Prepare paraffin blocks by sequential parallel sectioning of the entire specimen at 2 mm intervals. Among the lateral margins of the four directions, the closest margin and the tumor should be included together in the sectioning direction.

For gastrointestinal specimens, the distal part is generally placed at the 9 o'clock position in a gross photograph. If the distances from each of the lateral margins are similar, serial sectioning of the specimen is commonly performed in the same direction. When visual observation indicates that the closest lateral margin is not included in this general sectioning direction, however, the direction of the sample or mapping frame should be turned so that the closest lateral margin and the tumor appear together on the section (Fig. 3).

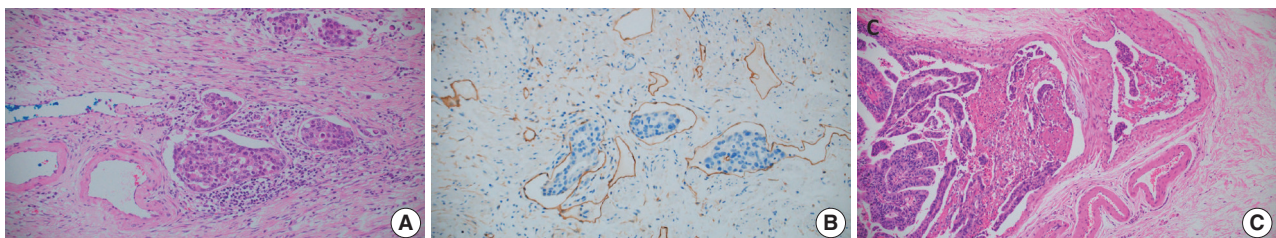


Fig. 2. Histologic features of lymphovascular invasion in sections of gastric cancer. An example of lymphovascular invasion on hematoxylin and eosin examination (A) and stained for D2-40 (B). Tumors involving vessels with an identifiable smooth muscle layer are considered to have venous invasion (C).

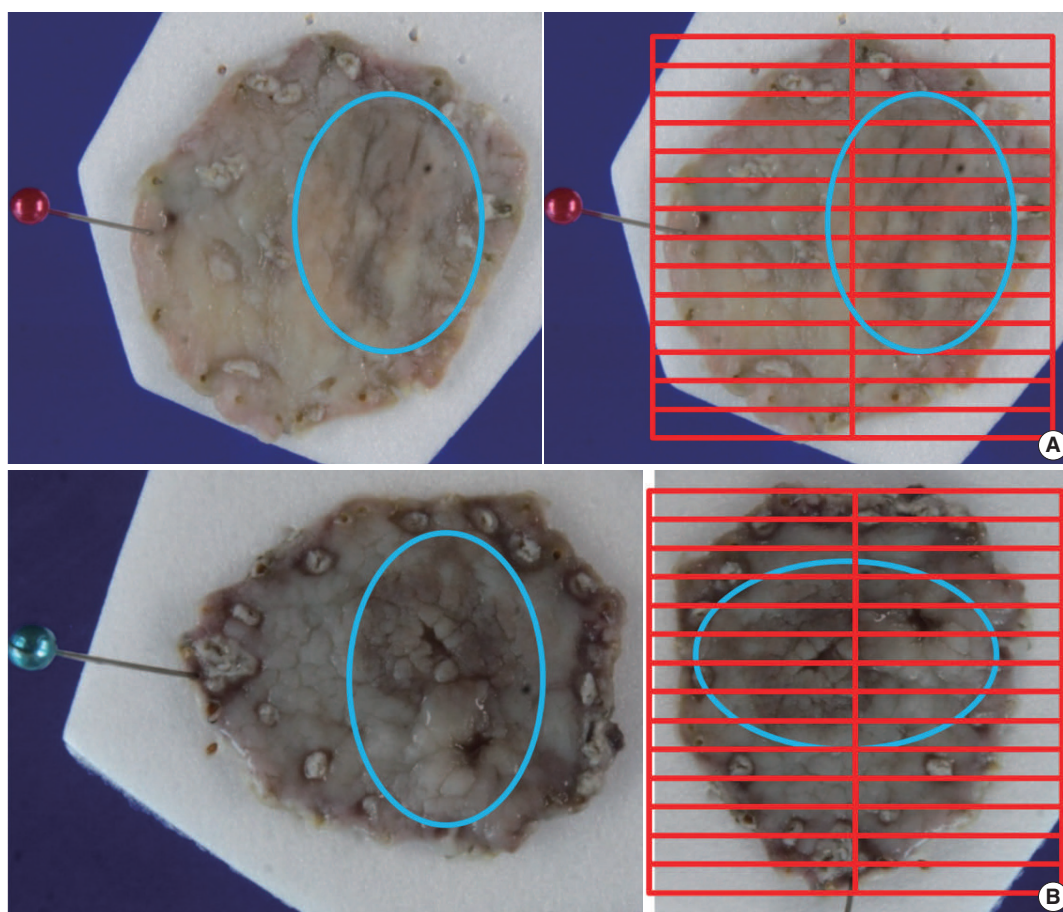


Fig. 3. Sectioning of an endoscopically resected specimen. When the direction of the photograph matches the direction of the closest lateral margin (A). If the direction of the photograph does not match, turn the specimen toward the closest lateral margin for mapping (B).

Histologic type and components

The histologic type of the tumor is described in the same way as for a surgical specimen. For the criteria and description of each type, refer to the information in the “Histologic classification” section below. The histologic type of the tumor should be described; the histologic diversity of tumor cells may be described separately as histologic components. If various morphologic components are observed within the tumor, all are described according to the histologic type. In such a case, the description should signify the quantitative majority of the tumor components. The description method can be selected according to institutional preferences. For example, record in order: well differentiated (WD)–moderately differentiated (MD) > poorly differentiated (PD) > signet ring cell (SRC) carcinoma; interval variable: WD-MD > 50%, PD < 50%, SRC < 10%; and continuous variable: WD-MD 65%, PD 30%, SRC 5%. Many studies have reported that tumors with a mixture of differentiated-type and undifferentiated-type components have a higher risk of lymph node metastasis than tu-

ors with only one component [35–40]. Within the undifferentiated type, SRC has a lower lymph node metastasis frequency, which is reported to be at a level similar to that of the differentiated type [41–43]. In addition, some reports indicate that the lymph node metastasis frequency is lower in pure SRC cases than in SRC cases mixed with other component types [44–47]. However, only the histologic type is applied for determining whether an endoscopic resection is curative, and because differences in histologic components are not applied, they are reflected as conditional elements rather than a standard element. A pathological study of the criteria for determining whether an endoscopic resection is curative is currently underway by the GIPSG of the Korean Society of Pathology as a research project of the National Evidence-based Healthcare Collaborating Agency. If important results are obtained from that study, they should be reflected in the elements of this guideline.

Tumor size

Only the length of the largest axis of a histologically confirmed tumor is recorded.

Depth of invasion

The method for describing the depth of invasion is basically the same as for a surgical specimen. The difference is that the invasion depth in the submucosal layer is measured and described in cases of submucosal invasion, and it is measured in mm or μm . The measurement is the length from the lowest surface of the muscularis mucosae to the most deeply invaded point. In some cases, the muscularis mucosae are modified by tumor invasion (hypertrophied, displaced, completely disappeared). In these cases, depth is measured using an imaginary line extending from adjacent muscularis mucosae in the normal area not deformed by the tumor (Fig. 4A). Always ensure that the lowest surface of the original, unmodified muscularis mucosae is used as the reference point. If the progressing course of the adjacent muscularis mucosae forms a curve, the virtual line is set as a matching curve (Fig. 4B).

No definitive description or research results indicate how to measure the depth of invasion when muscularis mucosae are modified. In the Japanese guideline, an explanation first appeared in the 14th edition from 2010: “if the muscularis mucosae are obscure due to ulcerative changes, the length should be measured on the virtual line based on the adjacent normal layer” [9]. In the

15th edition from 2017, it changed to recommend measuring from the surface of the tumor [48]. When muscularis mucosae are modified, some Korean pathologists measure from the lowest muscle fiber of the modified layer, and some measure from the imaginary line of the adjacent normal area. Two Korean studies reported that it is appropriate to measure from the imaginary line of the adjacent normal area in all modified situations [49,50]; accordingly, we use that recommendation as the standard measurement method in this guideline.

In cases of submucosal invasion, studies have shown that not only the invasion depth, but also the invasion width are significant risk factors for lymph node metastasis [50,51]. However, because few multicenter studies have been done and it has not yet been applied to the curative resection criteria, the invasion width is a conditional data element. This point is being addressed in the ongoing GIPSG pathological study on the criteria for determining whether an endoscopic resection is curative. The method for measuring the invasion width is as follows (Fig. 5): if submucosal invasion is observed on only one section, write the actual size measured on the slide of that section. If submucosal invasion is observed across two or more slices, write the larger of the following two values: (1) the actual size measured on the slide with the largest invasion width, or (2) the number of slices spanned by the invasion \times 2 mm (thickness of slice).

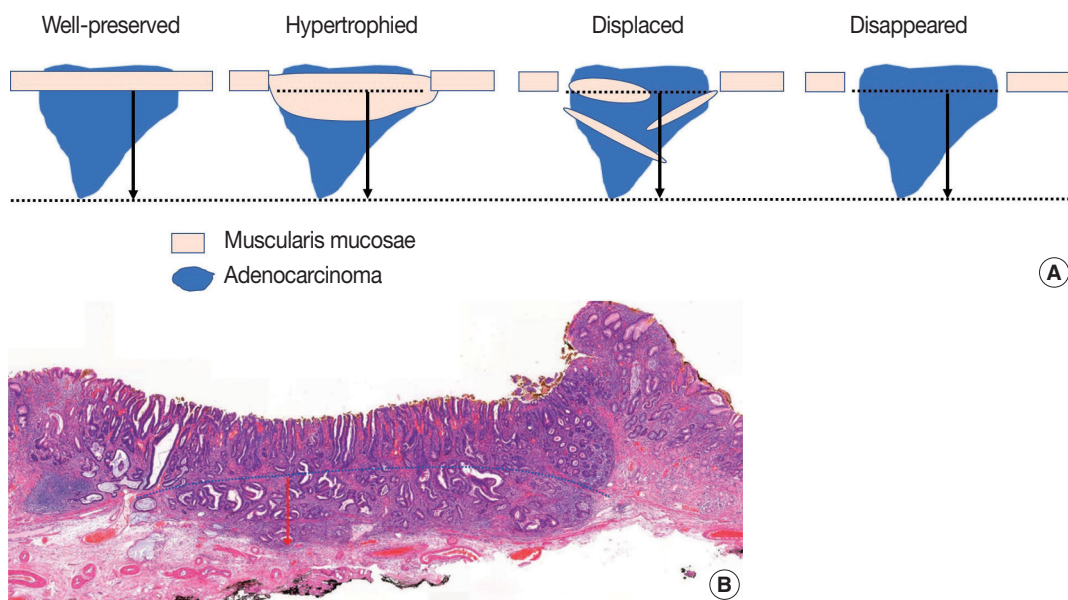


Fig. 4. Method to measure submucosal invasion depth. Always use the lowest surface of the original, unmodified muscularis mucosae as the reference point (A). When the progressing course of the adjacent muscularis mucosae forms a curve, the virtual line is set as a matching curve (B).

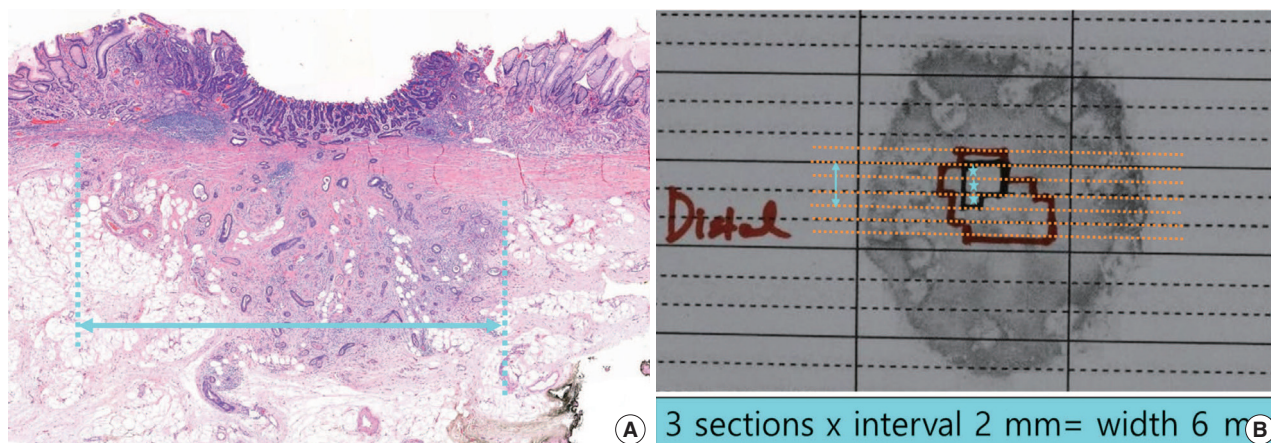


Fig. 5. Method to measure submucosal invasion width. The actual size measured within the slide (A). Number of slices that the invasion spans $\times 2$ mm (thickness of slice) (B).

Resection margin

The resection margin is described for the nearest lateral margin and deep margin. If the lateral margin is close (≤ 0.2 cm) or is involved in the tumor, the corresponding directions should be written together. If multiple margins are involved, all should be written. This is the information needed by the gastroenterologist to decide whether to perform additional procedures (endoscopic resection, argon plasma coagulation, follow-up biopsy). As a conditional element, the distance in all four directions of the lateral margin can be described.

The degree of invasion of the lateral resection margin and the probability of residual cancer are related. A high risk of residual cancer was reported when two or more of the four lateral margins were involved (multiple involvement) or when the length of involvement was large (more than 4 mm or 6 mm). However, it has not been determined whether additional treatment can be decided according to the degree of margin involvement because the risk is low but present in the group with a small degree of margin involvement.

Ulcer

Ulceration is defined as a full-thickness disruption of muscularis mucosae, both active and scarring, and determined by histological findings, not endoscopic findings [5,9,52]. The presence or absence of an ulcer is an important criterion for judging whether an endoscopic resection is curative in mucosal cancer [5], so it must be described in the pathology report for mucosal cancer. Because ulcers are included in the indications for an endoscopic resection, the presence of ulcers is determined by endoscopic findings. Ultimately, however, it must be confirmed by pathological examination findings of the resected specimen. En-

doscopic diagnosis is difficult in the absence of a mucosal break [53], and ulcer-negative endoscopy findings with ulcer-positive pathology findings were reported in 4.6%–5.5% of cases [54,55].

Another problem that occurs in practice is a lack of clarity in the criteria for differentiating original small ulcers from biopsy-induced changes after endoscopic biopsy in a case that did not originally have ulcers. Due to the low accuracy of ulcer determination in endoscopic findings, a finding of no ulcer during endoscopy cannot guarantee a biopsy-induced change. Diagnostic criteria for this have been suggested by Shimoda et al. [56], and the Japanese gastric cancer treatment guidelines describe this as follows: “A biopsy-derived scar is usually observed histologically as fibrosis restricted to small areas just beneath the muscularis mucosae. If it cannot be discriminated from the ulcer scar, it should be classified as UL1.” [57]. According to JCOG1009/1010, a clinical study on undifferentiated-type EGC: “UL was judged as present if the muscularis propria was completely disrupted and if fibrosis in the submucosal layer was observed to be wider than the range of disrupted muscularis propria.” [58]. In our study group, ulcer size was measured in the ongoing GIPSG study on the criteria for curative resection, and the possibility of offering differentiation criteria for this problem was investigated. We found that the risk of lymph node metastasis with an ulcer of 4 mm or less was the same as in cases with no ulcer. Using that criterion, very small ulcers can be excluded from the risk factors for lymph node metastasis, which removes the need to differentiate them from biopsy-induced changes. The grading of ulcer size is reflected as a conditional element. The method for measuring the size of an ulcer (Fig. 6) is similar to that used to measure the submucosal invasion width. If an ulcer (full-thickness disruption of the muscularis mucosae) is observed on only one section, write the

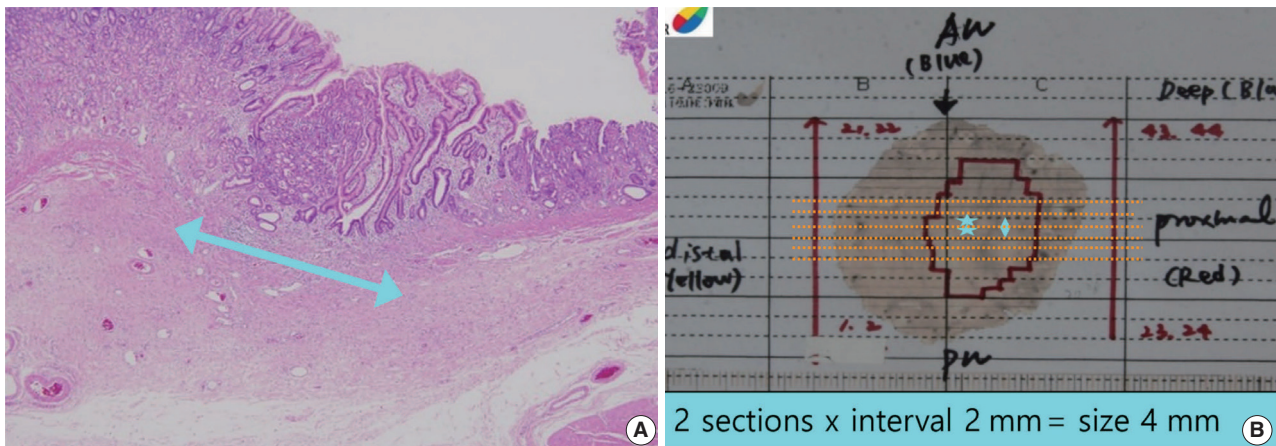


Fig. 6. Method to measure ulcer size. The actual size measured within the slide (arrow: ulcer size within the slide) (A). Number of slices that the ulcer spans $\times 2$ mm (thickness of slice) (star: ulcer-positive slices, arrow: slices that the ulcer spans) (B).

actual size measured on the slide. If it is observed across two or more slices, write the larger of the following two values: (1) the actual size measured on the slide with the largest disruption size or (2) the number of slices spanned by the disruption $\times 2$ mm (thickness of slice). The ulcer size is measured only within the tumor. If the ulcer spans the tumor and surrounding mucosa, measure the ulcer size only within the tumor area.

Cases with adenoma components

The adenoma component should be described only when the histological findings of adenoma are clear, and the intratumoral region is distinct from the adenocarcinoma component.

In diagnosis, only the adenocarcinoma contents should be described, and adenomas should be described separately as an additional item. For the size of the tumor, the size of the adenocarcinoma is described first, followed by the size of the total tumor. The distance from the resection margin describes the closest distance to any tumor component. If the resection margin is involved in a tumor or is less than 0.2 cm, the component should be described.

Unlike colorectal cancer, GC occurs in the adenoma-adenocarcinoma pathway in only a small number of cases, and adenocarcinomas of very small size are common. In addition, in many cases of WD adenocarcinoma, structural abnormalities are not severe, so areas that are difficult to differentiate from adenoma can be mixed in the tumor. Therefore, a background adenoma is identified only when the histological findings are clear and the area within the tumor is distinct from the adenocarcinoma component. If it is difficult to distinguish the mixed components, the entire lesion is treated as an adenocarcinoma. For example, if one component corresponds to adenocarcinoma and another compo-

nent is severely dysplastic but difficult to determine as adenocarcinoma, the whole is treated as an adenocarcinoma component. For an adenoma, only the presence of the adenoma component is briefly described in a separate section.

En bloc resection

Piecemeal resection or full-thickness tearing should be confirmed and documented in the histological examination. Even if the specimen is resected into several pieces, it is not piecemeal if the tumor is intact within one piece.

Lymphatic/venous invasion

Unlike surgical specimens, lymphatic and venous invasions are recorded separately in endoscopic resection specimens because of the differing risks of lymph node metastasis. Both lymphatic invasion and venous invasion are criteria for determining a non-curative resection. However, the risk of lymph node metastasis posed by lymphatic invasion is times higher than that from venous invasion, and a higher score is assigned in the risk prediction model [59]. This information is helpful when clinicians decide whether or not to perform gastrectomy; thus, it is recommended to report them separately. The standard method for differentiating lymphatic and venous invasion is H&E staining with the following criteria: it is determined as a lymphatic vessel when there is a thin wall or lymphatic fluid and as a venous vessel when there is a thick muscle wall or many red blood cells in the lumen. When it is difficult to distinguish between lymphatic vessels and small venules, classify them as lymphatic vessels.

IHC staining may be performed to better observe lymphatic or venous vessels. However, because H&E and other immunostained slides are obtained from different levels, they should be

interpreted separately. A specimen is deemed to be positive even if invasion is observed on only one slide.

Histologic classification

Histologic classification of GC is based on the 5th edition of the World Health Organization (WHO) blue book [4]. Representative histopathologic types described in the WHO classification are summarized in Table 3 and Fig. 7. The diagnosis of GC is usually determined according to the component that occupies the largest portion of the tumor, but the diagnosis of special histologic subtypes is based on the diagnostic criteria of each subtype. The most common subtype is tubular adenocarcinoma, characterized by prominent dilated or slit-like tubules. Carcinomas composed of solid tumor clusters with rare tubule formation are also classified as tubular adenocarcinoma. Tumor cells can be columnar, cuboidal, or flat, and luminal mucin/cell debris is common.

Papillary adenocarcinoma shows a papillary tumor structure with a central fibrovascular core and columnar or cuboidal tumor cells. For a diagnosis of papillary adenocarcinoma, more than 50% of the tumor area must contain the papillary tumor component [60-62]. High rates of liver metastasis, lymphovascular invasion, lymph node metastasis, and poor prognosis are reported in papillary adenocarcinoma [61-64].

Mucinous adenocarcinoma is defined when more than 50% of the tumor area shows extracellular mucin. Tumor cells in mucinous adenocarcinoma can show a glandular growth pattern, solid pattern, or scattered single cell pattern, including SRC carcinoma-

ma [4]. Mucinous adenocarcinoma is classified as the intestinal, diffuse, or indeterminate type according to the main component of tumor cell differentiation [4]. Mucinous adenocarcinoma tends to be diagnosed at an advanced stage [65,66].

Poorly cohesive carcinoma (PCC) is the second most common subtype of GC and is composed of isolated or small groups of tumor cells without gland formation [4]. Until the 3rd edition of

Table 3. Histopathologic classification of gastric carcinoma

Histopathologic classification	
WHO classification	
<input type="checkbox"/>	Tubular adenocarcinoma
<input type="checkbox"/>	Tubular adenocarcinoma, well differentiated
<input type="checkbox"/>	Tubular adenocarcinoma, moderately differentiated
<input type="checkbox"/>	Tubular adenocarcinoma, poorly differentiated
<input type="checkbox"/>	Papillary adenocarcinoma
<input type="checkbox"/>	Mucinous adenocarcinoma
<input type="checkbox"/>	Poorly cohesive carcinoma
<input type="checkbox"/>	Poorly cohesive carcinoma, signet-ring cell type
<input type="checkbox"/>	Poorly cohesive carcinoma, not otherwise specified
<input type="checkbox"/>	Mixed adenocarcinoma
<input type="checkbox"/>	Adenocarcinoma with lymphoid stroma
<input type="checkbox"/>	Hepatoid adenocarcinoma
<input type="checkbox"/>	Micropapillary adenocarcinoma
<input type="checkbox"/>	Adenocarcinoma of fundic-gland type
<input type="checkbox"/>	Undifferentiated carcinoma
<input type="checkbox"/>	Squamous cell carcinoma
<input type="checkbox"/>	Adenosquamous carcinoma
<input type="checkbox"/>	Gastroblastoma
<input type="checkbox"/>	Others (specify: _____)
Lauren classification	
<input type="checkbox"/>	Intestinal
<input type="checkbox"/>	Diffuse
<input type="checkbox"/>	Indeterminate
<input type="checkbox"/>	Mixed

WHO, World Health Organization.

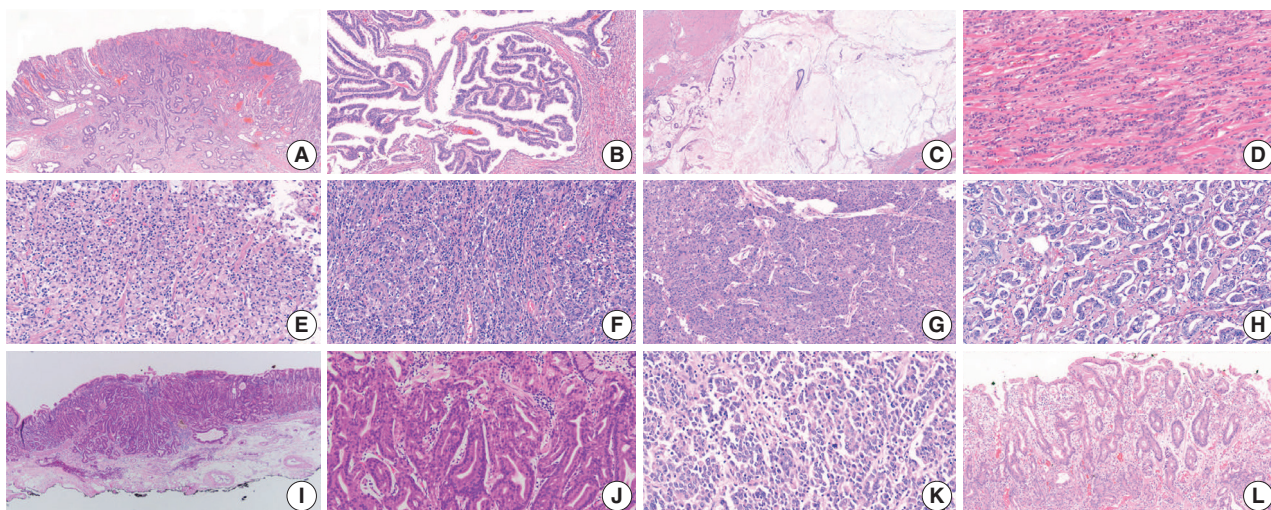


Fig. 7. Representative pictures of each histologic subtype of gastric carcinoma. Tubular adenocarcinoma (A), papillary adenocarcinoma (B), mucinous adenocarcinoma (C), poorly cohesive carcinoma, not otherwise specified (D), poorly cohesive carcinoma, signet-ring cell type (E), adenocarcinoma with lymphoid stroma (F), hepatoid adenocarcinoma (G), micropapillary adenocarcinoma (H), adenocarcinoma of the fundic-gland type (I, J), undifferentiated carcinoma (K), and crawling-type adenocarcinoma (L).

the WHO classification, SRC carcinoma was an independent subtype, but since the 4th edition of WHO classification, SRC has been included in the PCC category. Recently, several studies have suggested that non-SRC PCC (PCC-NOS) has a relatively poor prognosis compared with SRC and that SRC and PCC-NOS have different molecular profiles [67-70]. The WHO classification defines SRC as “composed predominantly or exclusively of signet-ring cell components” [4]. A European group suggested a PCC classification definition according to the percentage of the SRC component (SRC, > 90%; PCC-NOS, < 10%; PCC with SRC component, 10%–90%), but no definite criteria for diagnosing PCC-NOS and SRC have been established, so more studies are required [71].

Mixed adenocarcinomas, according to the WHO definition, are carcinomas with both glandular (tubular adenocarcinoma/papillary adenocarcinoma) and poorly cohesive (PCC/SRC) components [4]. Some reports recently suggested that mixed adenocarcinomas have poorer prognosis, such as frequent local recurrence and lymph node metastasis, than a pure subtype of carcinoma, especially in EGC [72,73]. However, no clear criteria have established a minimum ratio of glandular/poorly cohesive components for a diagnosis of mixed adenocarcinoma. Contrary to the WHO definition, many studies define mixed adenocarcinoma as PD adenocarcinoma or a PCC/SRC component mixed with gland-forming components; those studies also report that the prognosis of mixed adenocarcinoma in EGC is worse than that of pure subtypes [39,74,75]. Although mixed adenocarcinoma does not have a clear definition, it seems that EGC has a poor prognosis when a glandular component coexists with other components in the same tumor; therefore, when both a glandular component and other components are observed in an EGC, it is recommended that they be mentioned separately.

Adenocarcinoma with lymphoid stroma (medullary carcinoma with lymphoid stroma) was previously called ‘lymphoepithelioma-like carcinoma’ or ‘medullary carcinoma.’ Tumor cells of this subtype show irregular sheets, poorly defined clusters or tubules, trabeculae, or syncytial cells with dense lymphocytic infiltration and intraepithelial lymphocytes [4,76]. Such a tumor usually shows a well-defined margin without infiltrative growth and minimal desmoplasia. This type of tumor is frequently associated with Epstein-Barr virus (EBV) infection and sometimes shows microsatellite instability/mismatch repair deficiency [4,76]. Patients with this subtype show a lower number of lymph node metastases and better prognosis after surgery than those with other subtypes [77,78].

Hepatoid adenocarcinoma is composed of hepatocyte-like tu-

mor cells, which are large polygonal cells with eosinophilic-abundant cytoplasm arranged in a trabecular pattern [4,79]. This alpha-fetoprotein-positive tumor is often diagnosed preoperatively with multiple liver and lymph node metastases [4,79].

Micropapillary adenocarcinoma is characterized by an inside-out pattern of tumor clusters, which are small tumor clusters without a fibrovascular core, in clear spaces [4,80]. Micropapillary adenocarcinoma can be diagnosed when more than 10% of the tumor comprises micropapillary components [4,81]. This subtype is associated with poor prognosis and lymph node metastasis [4,80,81].

Adenocarcinoma of the fundic-gland type is composed of tumor cells showing chief cell differentiation, parietal cell differentiation, or both. Because this tumor does not show obvious nuclear dysplasia or structural abnormalities, it would be reasonable to regard it as adenocarcinoma only when it invades the submucosal layer. Lymph node metastasis is very rare in this subtype [4,82,83].

Undifferentiated carcinoma is composed of anaplastic cells without specific differentiation [4]. Grossly, a large ulcerating or fungating mass with necrosis is common. Tumor giant cells and rhabdoid tumor cells are common in this subtype, and spindle sarcomatoid cells can be seen [84,85]. Most patients show dismal prognosis with distant metastasis.

Squamous cell carcinoma is a very rare gastric tumor and shows morphology similar to that found in other organs. Adenosquamous carcinoma has both glandular and squamous tumor components, with $\geq 25\%$ squamous component [4]. Gastroblastoma is a biphasic tumor composed of spindle and epithelial cells.

Crawling-type adenocarcinomas are characterized by complex branching or anastomotic structures and low-grade nuclei and have not yet been classified as a distinct subtype in the WHO classification [4]. Because of their low-grade nuclear atypia, reactive looking structural change, and mucosal location, crawling-type adenocarcinomas were once called a very WD form of gastric adenocarcinoma. Recent studies have shown that large crawling-type adenocarcinomas are often accompanied by PD components, and one report indicates that lymph node metastasis occurs frequently when the cancer invades beyond the submucosal layer [86,87]. Although it has not yet been classified as a formal subtype, some research results on crawling-type adenocarcinoma have recently been published, and attention needs to be paid in terms of prognosis.

Tubular adenocarcinoma and papillary adenocarcinoma can be graded. When two or more differentiations are mixed in an adenocarcinoma, the differentiation grade reflects the largest tumor

area. A distinct glandular structure composed of columnar cells is classified as WD, and a small glandular structure composed of cuboidal or flat cells is classified as MD. In a tumor with an indistinct glandular structure, carcinoma forming frequent luminal structures is classified as MD, and that with a rare luminal structure is classified as PD (Fig. 8) [3]. Although the WHO recommends a two-tier grading system of low- (WD and MD) and high-grade (PD), most pathologists and clinicians use a three-tier grading system. We have agreed to use a three-tier grading system that can be easily switched to a two-tier grading system.

Histologic types in biopsy specimens

In endoscopic gastric biopsy samples, it is often difficult to diagnose a specific subtype of gastric carcinoma. However, histologic subtypes and differentiation are important in the selection of a treatment modality. We recommend reporting a histologic component or subtype if there is a PD component or subtypes associated with poor prognosis (such as PCC, PD tubular adenocarcinoma, or micropapillary feature), irrespective of the proportion. Some peculiar subtypes of adenocarcinomas, such as adenocarcinoma of the fundic-gland type and EBV-associated gastric carcinoma, have a lower rate of lymph node metastasis than other subtypes with similar invasion depth, especially in EGC [82,88,89]. Reporting these subtypes and testing for EBV in situ in biopsy specimens could thus be helpful for patient management [89].

Lauren classification

The Lauren classification has been one of the most commonly used classification systems for GC worldwide since its publication in 1965 (Table 3) [90]. According to the WHO 5th edition, WD and MD papillary adenocarcinoma and tubular adenocarcinoma are classified as the intestinal type, and PCC and SRC are classified as the diffuse type (Fig. 9). In the Lauren classification, the mixed type (not the same as mixed adenocarcinoma in the histological classification) is used when intestinal and diffuse

tumor components coexist in similar proportions. Although a table in the WHO blue book indicates that solid type, PD adenocarcinoma is classified as indeterminate type, this does not mean that all PD adenocarcinoma should be classified as such, and there is some disagreement among pathologists about the definition of the indeterminate type. Further discussion is needed to decide whether other special histological types of adenocarcinoma are excluded from the Lauren classification or whether they can be classified as intestinal, diffuse, or indeterminate according to their morphology.

To determine the feasibility of an endoscopic resection of tumors, most clinical guidelines and studies apply the differentiated type (papillary adenocarcinoma, tubular adenocarcinoma, WD and MD)/undifferentiated type (tubular adenocarcinoma, PD and poorly cohesive carcinoma, including SRC carcinoma) criteria of the Japanese guidelines [57]. In these criteria, PD adenocarcinoma is classified as the undifferentiated type. To prevent confusion with undifferentiated carcinoma, we do not recommend using the 'differentiated type/undifferentiated type' criteria in pathology reports. Instead, using the histologic classification and/or Lauren classification can provide sufficient information to clinicians and researchers.

Adenoma

Neoplastic epithelial proliferation without stromal invasion is called either adenoma or dysplasia. This intraepithelial neoplasia is usually called an adenoma by Western pathologists when the tumor shows a protruding, polypoid appearance with a distinct border and dysplasia when the tumor appears as a flat, depressed lesion or elevated indistinct lesion [4]. The Japanese classification tends to refer to elevated, flat, and depressed intraepithelial lesions as adenomas. Both adenoma and dysplasia can be used as terms for intraepithelial neoplasia in Korea.

Gastric adenomas can be subclassified into the intestinal type, foveolar type, pyloric gland type, and oxyntic gland type. Intestinal-type adenomas are the most common adenomas and usually

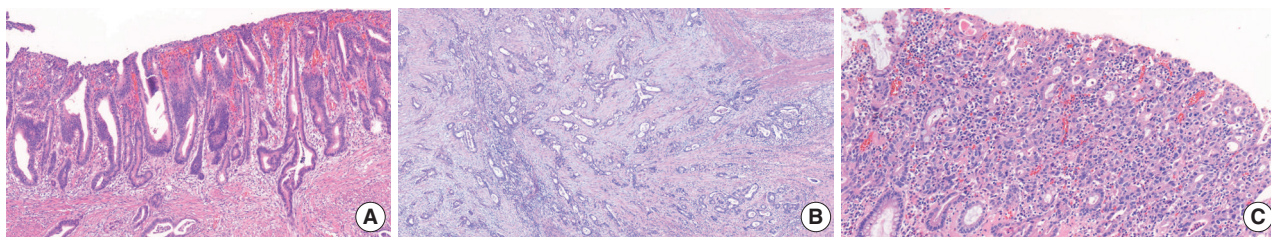


Fig. 8. Grading of gastric tubular adenocarcinoma. Well-differentiated adenocarcinoma showing glandular structures composed of columnar tumor cells (A). Moderately differentiated adenocarcinoma exhibits more complex tubular structures with cuboidal and/or flat epithelial cells (B). Tubular structure is unclear in most tumor glands in poorly differentiated adenocarcinoma (C).

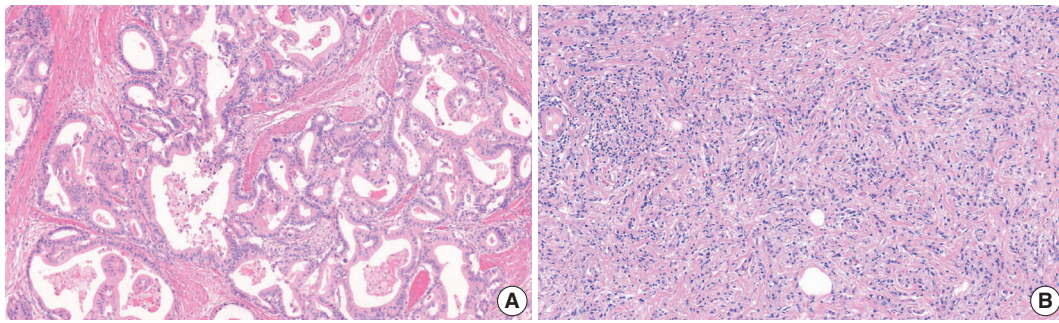


Fig. 9. Intestinal (A) and diffuse (B) Lauren type gastric adenocarcinomas characterized by well-formed tumor glands and interspersed tumor cells, respectively.

show tubule formation and columnar cells with elongated nuclei, with or without goblet cells and Paneth cells [4]. Foveolar-type adenomas are the second most common type of gastric adenoma, and an apical mucin cap is characteristic [91]. Pyloric gland type adenomas consist of columnar cells with ground-glass-like cytoplasm, basally located nuclei, and closely packed tubular glands with occasional dilatation [92]. Oxyntic gland type adenomas, also called oxyntic gland neoplasms because they can be diagnosed as adenocarcinoma only when submucosal invasion is confirmed, can progress into adenocarcinoma of the fundic gland type. This adenoma is composed of tumor cells with an oxyntic gland (chief cells, parietal cells, and mucous neck cells) and exhibits structural irregularity and minimal to mild nuclear atypia [82,88].

A two-tier system (low-grade/high-grade) is recommended for grading adenomas. Low-grade adenomas are characterized by a simple tubular or papillary architecture, hyperchromatic elongated or ovoid nuclei without severe atypia, preserved cellular polarity with basally located nuclei, and relatively regular intervening stroma without structural disruption. Goblet cells, apoptotic features, and mild to moderate mitotic features can be observed in low-grade adenomas (Fig. 10A). High-grade adenomas show more complex structures such as fusion, crowding, and budding of glands and the formation of glands with varying diameters. Cellular atypia is more pronounced in high-grade adenomas, such as loss of polarity, a high nuclear/cytoplasm ratio, pleomorphic nuclei, frequent mitosis, and atypical mitosis [93,94]. Intraglandular necrotic debris is also a diagnostic clue for high-grade dysplasia and, more commonly, adenocarcinoma (Fig. 10B) [95]. A diagnosis of adenocarcinoma should be considered when more than one of the following is present: evidence of stromal invasion (including single cell invasion into stroma and desmoplastic reaction), marked structural atypia, and marked glandular crowding (Fig. 10C) [94].

Helicobacter pylori

H. pylori infection is the most common cause of gastric adenocarcinoma, and eradication of *H. pylori* is associated with metachronous GC [96,97]. To detect *H. pylori* infection in a pathology specimen, additional staining (such as the Wright-Giemsa stain or Warthin-starry stain) is recommended. The proportion of drug-resistant *H. pylori* is increasing, and in patients with clarithromycin-resistant *H. pylori* infection, the failure rate of standard eradication treatment is also increasing. In patients with *H. pylori* infection, testing for clarithromycin-resistance is helpful for *H. pylori* eradication.

Molecular markers

All molecular tests are optional, conditional data elements. All report forms for the pathologic diagnosis of molecular markers are shown in Table 4.

Human epidermal growth factor receptor 2 testing

Determination of human epidermal growth factor receptor 2 (HER2) status is critical to identify patients with advanced-stage cancer for appropriate precision therapy. HER2-positive GC patients are currently treated with trastuzumab in combination with chemotherapy as first-line therapy, and fam-trastuzumab deruxtecan-nxki, a.k.a. trastuzumab deruxtecan, was recently approved by the Food and Drug Administration as a third- or later-line treatment [5,7,98,99]. HER2 status is principally determined by IHC or in situ hybridization (ISH) assays. HER2-positivity is defined as IHC 3+ or IHC 2+/ISH-positive [100,101]. HER2 testing requires formalin-fixed paraffin-embedded biopsy tissues with an adequate number of tumor fragments (ideally at least four) or representative surgical specimens with more differentiated components [102,103].

In currently recommended testing algorithms, HER2 status should be initially established using IHC [7,100] to estimate the

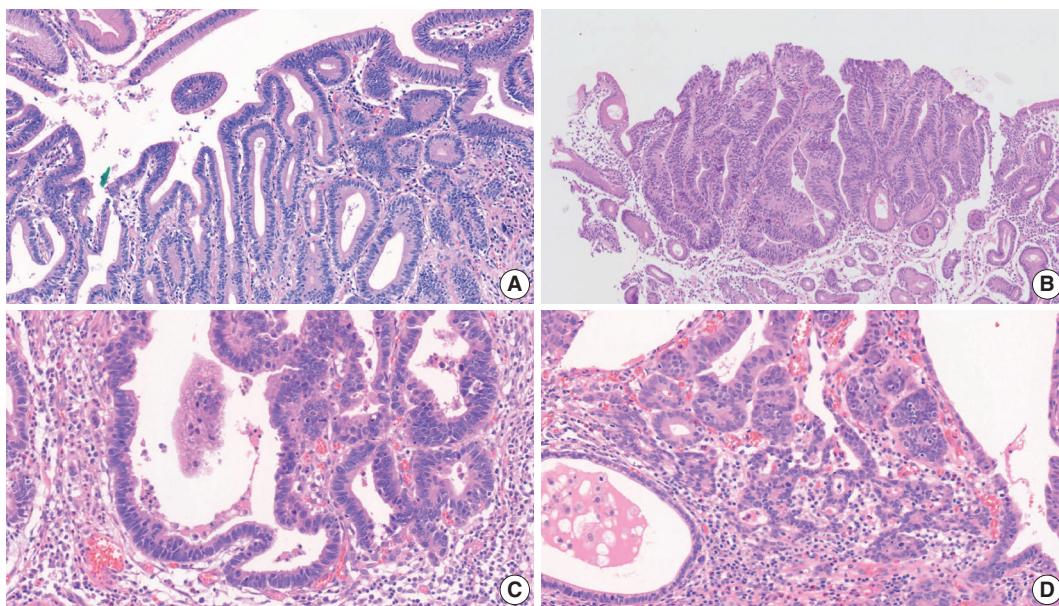


Fig. 10. Tubular adenoma with low-grade dysplasia shows simple tubular architecture composed of elongated tumor cells with preserved polarity (A). More crowding and variation in the size of the tumor glands are noted in high-grade adenoma (B). The diagnosis of adenocarcinoma can be made when tumor cells show single-cell infiltration into the lamina propria (C) and/or marked structural fusion and atypia (D).

immunoreactive intensity and percentage of basolateral membranous expression on cancer cells [7,104]. The score ranges from 0 to 3 based on $\geq 10\%$ cutoff level of HER2 expression in surgical specimens and ≥ 5 clustered cells in biopsy specimens as follows: 0 (negative), no reactivity or membranous reactivity in $< 10\%$ of cancer cells from surgical specimens or any cancer cells in biopsy specimens; 1+ (negative), faint or barely perceptible membrane reactivity; 2+ (equivocal), weak to moderate complete or basolateral membrane reactivity; and 3+ (positive), strong complete or basolateral membrane reactivity (Fig. 11).

Cases with a score of 2+ or indeterminate by IHC should be confirmed with ISH techniques to determine the final HER2 status [7,100]. Positive *HER2* amplification is defined as a *HER2*:CEP17 (centromeric region of chromosome 17) ratio ≥ 2.0 . To evaluate the ISH results, first check the HER2 IHC slide to select the most strongly stained region that might predict a higher level of *HER2* amplification. Next, at least 20 evaluable, non-overlapping invasive tumor cells should be counted. If CEP17 signals are ≥ 3 and the ratio of *HER2*:CEP17 is < 2.0 , an average *HER2* copy number > 6 signals/cell is considered positive for *HER2* amplification by ISH and < 4 signals/cell is considered negative. If an average *HER2* copy number is between four and six signals/cell, another 20 cells should be counted in a different area. Sometimes, the determination of HER2 status is uncertain due to sample problems or technical issues [103,105]. In that case, the test should be reported as “cannot be determined.”

Some studies have revealed a significant correlation between HER2 expression and histologic subtype in GC. The Trastuzumab for Gastric Cancer (ToGA) trial and other published studies showed that the HER2 positivity rate was higher in differentiated subtypes (Lauren intestinal type and WD and MD type) than in the Lauren diffuse type or PD type [106-108]. Furthermore, intratumor heterogeneity of HER2 expression was reported in approximately 50% of GC cases [106,109]. Inter-lesional heterogeneity of HER2 expression for either positive or negative shifting has been reported between primary carcinomas and synchronous or metachronous locoregional/distant metastases at a rate of 2%–14% [110-115].

Therefore, HER2 status should be re-evaluated for all newly diagnosed secondary, recurrent, and metastatic lesions, regardless of the HER2 status of the primary cancer because it affects the therapeutic strategy and prognosis of patients [116,117].

Microsatellite instability and mismatch repair deficiency

Microsatellites, also called short tandem repeats, consist of repeats of a sequence that ranges from 1–6 nucleotides in length [103,118,119]. DNA mismatch repair (MMR) is a highly conserved mechanism to recognize and replace or repair mismatched nucleotides during DNA replication [119]. MMR deficiency (dMMR) is commonly caused by a germline mutation or sporadic epigenetic silencing and leads to insertions or deletions of nucleotides in microsatellite regions during DNA replication [119,120].

Table 4. Report form for pathologic diagnosis using molecular markers

Molecular markers
<i>All molecular markers are "conditional data element"</i>
HER2 immunohistochemistry
<input type="checkbox"/> Negative (0/1+)
<input type="checkbox"/> Equivocal (2+)
<input type="checkbox"/> Positive (3+)
<input type="checkbox"/> Undetermined (explain):
HER2 (ERBB2) in situ hybridization
Number of invasive cancer cells counted: _____ cells
<input type="checkbox"/> Using dual-probe assay
<input type="checkbox"/> HER2 (ERBB2)/CEP17 ratio: _____
<input type="checkbox"/> Average number of HER2 (ERBB2) signals per cancer cell: _____
<input type="checkbox"/> Average number of CEP17 signals per cancer cell: _____
<input type="checkbox"/> Using single-probe assay
<input type="checkbox"/> Average number of HER2 (ERBB2) signals per cancer cell: _____
Summary: Negative/Positive for HER2 (ERBB2) gene amplification
<input type="checkbox"/> Undetermined (explain):
Microsatellite instability (MSI)
Summary:
<input type="checkbox"/> Microsatellite stable (MSS)
<input type="checkbox"/> Microsatellite instability-low (MSI-L)
<input type="checkbox"/> Microsatellite instability-high (MSI-H)
<input type="checkbox"/> Undetermined (explain) ^a
DNA mismatch repair immunohistochemistry
MLH1:
<input type="checkbox"/> Positive (retained expression)
<input type="checkbox"/> Negative (loss of expression)
<input type="checkbox"/> Undetermined (explain):
MSH2:
<input type="checkbox"/> Positive (retained expression)
<input type="checkbox"/> Negative (loss of expression)
<input type="checkbox"/> Undetermined (explain):
PMS2:
<input type="checkbox"/> Positive (retained expression)
<input type="checkbox"/> Negative (loss of expression)
<input type="checkbox"/> Undetermined (explain):
MSH6:
<input type="checkbox"/> Positive (retained expression)
<input type="checkbox"/> Negative (loss of expression)
<input type="checkbox"/> Undetermined (explain):
Summary:
<input type="checkbox"/> DNA mismatch repair deficiency (was/was not) observed
<input type="checkbox"/> Because it is difficult to determine DNA mismatch repair deficiency, PCR-based testing and/or NGS for MSI is recommended.
In situ hybridization for Epstein-Barr virus–encoded small RNAs
<input type="checkbox"/> Positive [diffuse/heterogenous (focal and/or mixed intensity)] ^{b,c}
<input type="checkbox"/> Negative
Summary: Epstein-Barr virus–associated gastric carcinoma
PD-L1 immunohistochemistry
PD-L1 [Antibody (22C3 PharmDx/22C3 conc. Ventana/28-8 PharmDx/others: _____)]:
<input type="checkbox"/> CPS = _____

HER2, human epidermal growth factor receptor 2; CEP17, centromeric region of chromosome 17; MLH1, mutL homolog 1; MSH2, mutS homolog 2; PMS2, PMS1 homolog 2; MSH6, mutS homolog 6; PCR, polymerase chain reaction; NGS, next-generation sequencing; PD-L1, programmed death ligand 1; CPS, combined positive score.

^aBecause it is difficult to determine MSI status, mismatch repair immunohistochemistry and/or NGS is recommended; ^bChecking the signal pattern is optional; ^cThe term "Epstein-Barr virus–associated gastric carcinoma" applies to positive cases.

The four genes that play an important role in this process are mutL homolog 1 (*MLH1*), mutS homolog 2 (*MSH2*), mutS homolog 6 (*MSH6*), and PMS1 homolog 2 (*PMS2*) [103,119-121]. When MMR does not function normally, it is called microsatellite instability (MSI) [119,122].

MSI is the hallmark of Lynch syndrome and is found in many sporadic cancers [103,123]. MSI-high (MSI-H) is observed in 6.9%–22.7% of sporadic GC cases [124-127]. As a distinct molecular subtype, MSI-GC is characterized by the gastric CpG island methylator phenotype with *MLH1* silencing [124]. The clinical characteristics of MSI-GC are antrum (distal) locations, intestinal type of Lauren histology, early disease stage, and favorable prognosis [5,103,125,126]. Clinically, MSI is an actionable predictive biomarker for resistance to 5-fluorouracil-based adjuvant chemotherapy and indicates good suitability for immunotherapy [128-132]. For this reason, clinician requests for MSI and/or MMR test are increasing. In the National Comprehensive Cancer Network Guidelines for Gastric Cancer V.2.2022, universal MSI and MMR testing is recommended for all newly diagnosed GC patients, in accordance with the CAP DNA Mismatch Repair Biomarker Reporting Guidelines [100].

The three main methods used to detect MSI/dMMR are as follows: (1) polymerase chain reaction (PCR) amplification of microsatellite sequences; (2) IHC staining to determine the expression of the four MMR proteins MLH1, MSH2, MSH6, and PMS2; and (3) next-generation sequencing (NGS) [103,119,120,133]. Additionally, a new kit enables diagnosis of MSI according to the number of deleted base mutations by using a melting curve analysis with a peptide nucleic acid (PNA) probe [134].

PCR can compare the allelic position of the microsatellite locus in the tumor with that in normal tissue [103,120,133]. The National Cancer Institute recommends the so-called Bethesda Panel as reference [133,135]. This panel is composed of two mononucleotide repeats (BAT-25 and BAT-26) and three dinucleotide repeats (D2S123, D5S346, and D17S250) [22,103,133,135]. These regions are amplified in parallel using fluorescent PCR, and their sizes are assessed by capillary electrophoresis [133,136]. However, because the dinucleotide markers are less sensitive and specific than the mononucleotide markers [137], an alternative panel with five poly-A mononucleotide repeats (NR-21, NR-24, NR-27 [or Mono-27], BAT-25, and BAT-26) has also been suggested [22,103,119].

MSI-H is defined as instability of two or more of five microsatellite loci; MSI-low (MSI-L) is defined as instability of one site, and microsatellite stable (MSS) is defined as no instability at any site. Currently, clinical studies tend to categorize MSI-L and MSS

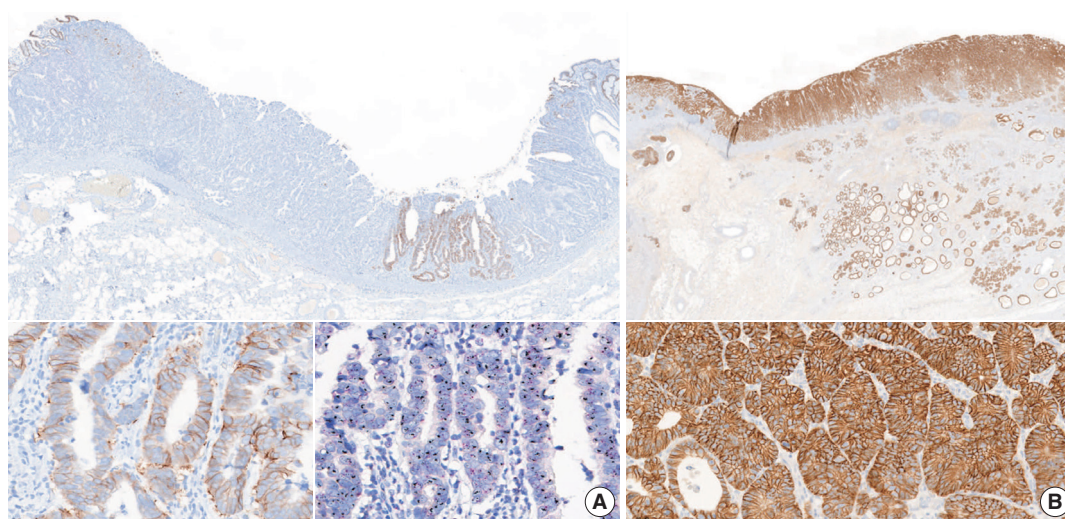


Fig. 11. Representative images of human epidermal growth factor receptor 2 (HER2)-positive gastric cancer. HER2 immunohistochemistry (IHC) of this case showed heterogeneous intratumoral expression, composed of some areas featuring a score of 2+ with *HER2* gene amplification and others scoring 0 (A). HER2 IHC of this case showed homogeneous HER2 positivity (score of 3+) (B).

as one type. This PCR method enables a functional measure of dMMR by directly measuring DNA changes. However, the method does not identify the MMR gene to be investigated. When the PCR test fails or the interpretation of the results is difficult, the test should be reported as “undetermined,” and IHC testing or NGS is recommended.

IHC for MMR proteins in GC samples is a simple and useful practice to determine dMMR. This method shows performance characteristics similar to MSI detection by PCR and a high concordance rate (> 90%) [138]. The use of all four proteins, MLH1, MSH2, MSH6, and PMS2, is recommended for the IHC test. However, in more than 90% of cases, MSI-GC is associated with MLH1 and/or PMS2 losses by hypermethylation of the *MLH1* gene. Because this IHC method is based on the ubiquitous expression of the MMR proteins in cell nuclei, nuclear staining should be checked when determining MMR positivity [22,119]. The presence of internal positive controls such as normal mucosa, lymphocytes, or stromal cells is essential for the interpretation of results [119]. dMMR is determined when the nuclear expression of at least one MMR protein is absent (Fig. 12) [22]. Heterogeneity of IHC or abnormal staining (cytoplasmic or membranous staining) is sometimes observed [138-143]. When it is difficult to interpret the IHC results, the test should be reported as “undetermined,” and PCR-based testing or NGS is recommended to confirm the MMR status. Using both IHC and PCR analyses for the detection of MSI-H/dMMR can reduce indeterminacy in the results.

EBV testing

EBV-associated gastric carcinoma belongs to one of four types of molecular classification suggested by the Cancer Genome Atlas (TCGA) [124]. Virus-host interactions play a pivotal role in EBV-induced carcinogenesis [144]. In EBV-associated gastric carcinoma, BamHI-A rightward frame 1 (*BARF1*) and latent membrane 2A (*LMP2A*) are putative viral oncogenes [145-147]. Once EBV enters the epithelium, EBV DNA methylation occurs globally. Hypermethylation of the CpG island promoter occurs throughout human cellular progress, which inactivates tumor suppressor genes [148]. Unique methylation leading to *CDKN2A* (p16) downregulation seems to be essential [124]. Eventually, EBV-infected gastric epithelial cells begin clonal growth, and gene mutations in EBV-infected cells lead to carcinogenesis [144]. EBV-associated gastric carcinoma is molecularly characterized by frequent mutations in phosphatidylinositol-4,5-bisphosphate 3-kinase catalytic subunit α (*PIK3CA*) [124] and AT-rich interaction domain 1A (*ARID1A*) [125], rare *TP53* mutations [124], and the overexpression of interferon- γ [149] and programmed death ligand 1 (PD-L1) [124,150].

EBV-associated gastric carcinoma has distinct histologic, genetic, and immune microenvironmental features. Notably, EBV-associated gastric carcinomas exhibit a dramatic response to pembrolizumab immunotherapy (100% overall response rate) [130]. EBV positivity can be a good indication for immunotherapy in GC. Moreover, in submucosal invasive GC, EBV positivity has been associated with a low risk of lymph node metastasis [151,152].

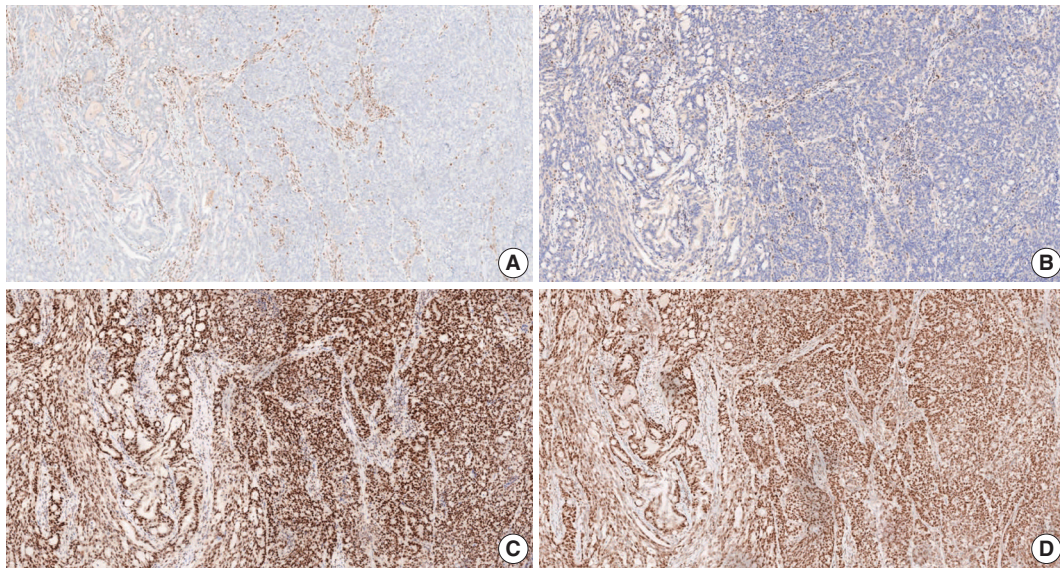


Fig. 12. A representative figure of gastric cancer with DNA mismatch repair deficiency. Immunohistochemistry for MLH1 (A) and PMS2 (B) showed loss of nuclear expression in tumor cells and positive nuclear expression in adjacent inflammatory cells. In contrast, immunohistochemistry for MSH2 (C) and MSH6 (D) showed retained nuclear expression in tumor cells. MLH, mutL homolog 1; PMS2, PMS1 homolog 2; MSH2, mutS homolog 2; MSH6, mutS homolog 6.

ISH for EBV-encoded small RNAs (EBERs) is the most suitable and widely used method to detect EBV in formalin-fixed paraffin-embedded tissues and cytology specimens [153,154]. It is a highly sensitive detection method because of the large number of EBERs (10^6 – 10^7 copies/cell) [19], but it cannot be used for quantitative analysis of viral particles. Several commercial probes for EBERs are available, in which EBERs labeled with biotin, digoxigenin, or fluorescein can be visualized by microscopic examination. In most EBV-associated GCs, EBER signals are observed with strong intensity in almost all cancer cell nuclei. In certain cases, EBER signals are heterogeneous, i.e., positive only in a focal portion of the cancer or mixed—weak to strong—intensity (Fig. 13). Recently, focal positivity of EBER signals was reported in 18% of EBV-associated GC cases in Germany [155]. In daily practice in Korea, however, intratumoral heterogeneity of EBER signals is not as high as in those German cases. Whether focal negative/weak intensity represents an absence of EBV infection or a subcritical or insufficient copy number of EBERs remains unclear [156]. EBER signals are rarely detected in intratumoral or peritumoral lymphocytes, which originate from peripheral B lymphocytes infected with EBV in a latent state.

PD-L1 immunohistochemistry

The programmed death-1 receptor (PD-1)–PD-L1 interaction is one of the major mechanisms of immune modulation that allow T-cell inactivation and tumor immune evasion [157].

Blocking the PD-1/PD-L1 pathway is a standard therapeutic strategy for various solid tumors, including GCs [158].

Pembrolizumab was granted accelerated FDA-approval as a third-line treatment of GC based on the findings of the phase 2 KEYNOTE-059 trial, which demonstrated its treatment benefit in advanced GC patients with PD-L1 combined positive score (CPS) positivity (CPS ≥ 1). Accompanying approval was granted for the PD-L1 IHC 22C3 pharmDx assay on the Autostainer Link 48 platform as a companion diagnostic assay [159]. However, the subsequent phase 3 KEYNOTE-061 trial failed to demonstrate a significant survival improvement in PD-L1-positive GC patients [160].

Another phase 3 trial, CheckMate-649, demonstrated the efficacy of nivolumab in combination with fluoropyrimidine and platinum-based chemotherapy as a first-line treatment for HER2-negative advanced or metastatic GC, gastroesophageal junction cancer, and esophageal adenocarcinoma patients with PD-L1 CPS ≥ 5 [161]. In that trial, PD-L1 expression was determined using the PD-L1 IHC 28-8 pharmDx assay on the Autostainer Link 48 platform. Recently, that assay earned the CE-IVD mark in Europe as a companion diagnostic for identifying candidates for nivolumab treatment.

Both assays share the CPS scoring system to determine PD-L1 expression, which is the number of PD-L1–stained cells (tumor cells, lymphocytes, and macrophages) divided by the total number of viable tumor cells, multiplied by 100. For adequate evalu-

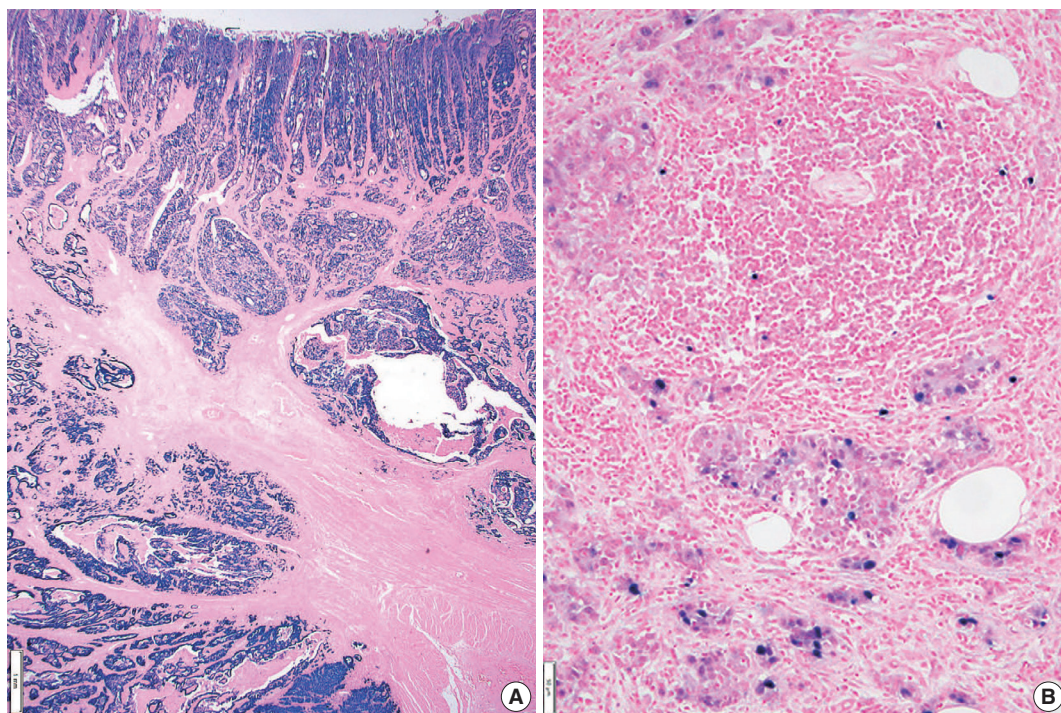


Fig. 13. A representative figure of Epstein-Barr virus (EBV) in situ hybridization. Diffuse positive EBV-encoded small RNA (EBER) signals (A). Heterogenous pattern of EBER signals in cancer cells. EBER signals appear within a few intratumoral lymphocytes (B).

ation, a specimen containing a minimum of 100 viable tumor cells is required [162]. A PD-L1–stained tumor cell should present partial or complete membrane staining of viable cells with more than faint staining intensity ($\geq 1+$). PD-L1–stained immune cells include only mononuclear inflammatory cells (lymphocytes or macrophages) within tumor nests and adjacent stroma and show membrane and/or cytoplasmic staining. Other stromal cells such as fibroblasts, neutrophils, and plasma cells should be excluded from the CPS numerator. If the result of the calculation exceeds 100, it is presented as a maximum score of 100. If the PD-L1 staining shows heterogeneous results, the final CPS should be estimated by calculating each area's CPS result (Fig. 14).

Because two different PD-L1 assays have been approved based on different CPS cutoff values, the interpretation of PD-L1 positivity should be based on the CPS cutoff value appropriate to the assay used for evaluation. The PD-L1 IHC 22C3 pharmDx assay uses CPS ≥ 1 for CPS positivity, and the 28-8 pharmDx assay uses CPS ≥ 5 . The report should specify the assay type and appropriate cutoff value used for the PD-L1 positivity interpretation.

Previous studies have reported changes in PD-L1 expression during chemotherapy [163,164] and discrepancies between primary and metastatic lesions [164,165]. Therefore, re-evaluation of PD-L1 IHC in secondary, recurrent, and metastatic lesions is recommended for GC patients.

Next generation sequencing

Recently identified molecular profiles are not only important for improving our understanding of driver alterations involved in gastric carcinogenesis, but also for identifying clinically relevant biomarkers and new potential therapeutic targets [124,125]. Therefore, the clinical need for NGS in AGCs is increasing.

According to the recent National Comprehensive Cancer Network (NCCN) guideline, the biomarkers implicated in clinical management of AGC include HER2, MSI, PD-L1, tumor mutation burden (TMB) status, and neurotrophic tyrosine receptor kinase (*NTRK*) gene fusion [100]. Among these, TMB can only be assessed using NGS, and *NTRK* fusion is best evaluated using NGS (preferential RNA sequencing) [166]. Alternatively, it can be screened with TRK IHC, and then sequencing can be performed in positive cases [166]. Some other targets also showed promising clinical results in advanced GC, such as fibroblast growth factor receptor 2 (*FGFR2*) amplification [167], epidermal growth factor receptor (*EGFR*) amplification [168], *MET* amplification [169], and alterations of homologous recombination deficiency–related genes [170]. In addition, there are very rare (prevalence $<1\%$) targetable tissue–agnostic variants [171] such as *BRAF* V600E [172], anaplastic lymphoma kinase (*ALK*) fusion [173], and reactive oxygen species 1 (*ROS1*) fusion [174].

TMB is defined as the total number of somatic coding muta-

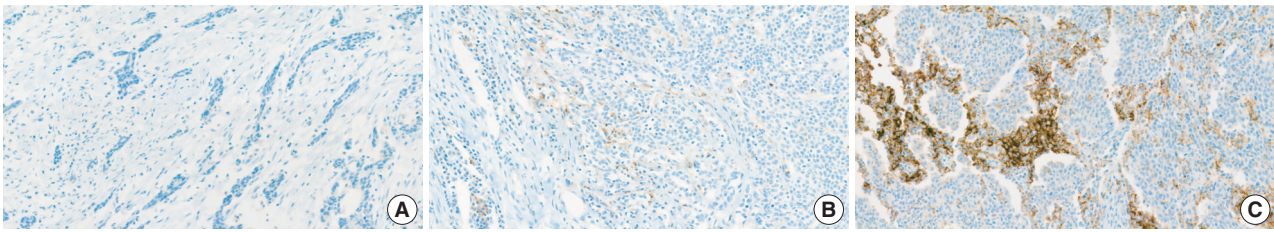


Fig. 14. A representative example of programmed death ligand 1 staining. Combined positive score (CPS) < 1 (A), CPS > 1 and < 5 (B), CPS > 5 (C).

tions in a tumor and represents an emerging biomarker for immunotherapy response in cancer patients [175]. The exploratory analysis for KEYNOTE-062 suggested an association between TMB and the clinical efficacy of first-line pembrolizumab-based therapy in patients with advanced GC [176]. Although whole exome sequencing is considered the gold standard for TMB, recent targeted gene panels have also provided accurate quantification [175]. The lack of harmonization in panel-based TMB quantification and lack of robust predictive cutoffs are currently some of the main limitations of TMB as a biomarker in clinical practice [175].

The gold standard for MSI detection is PCR or IHC. Recently, several MSI detection methods based on NGS have shown high concordance (> 95%) with the conventional PCR-based assay [171,177,178]. The recent NCCN guidelines indicate that sequencing via a validated NGS assay may be used to determine MSI status and other biomarkers when limited tissue is available for testing [100].

Tissue preparation is one of the most important factors for getting accurate and reliable results from NGS. In general, the total DNA and RNA requirements range from 10 to 300 ng for targeted gene panels [179]. Tissue specimen requirements are formalin-fixed, paraffin-embedded tissue or cytology specimens [179]. The minimum sample requirement for reliable sequencing results is a specimen with a tumor fraction and surface area > 10%–20% and 5 mm², respectively [179].

Mucin phenotype

GC is classified as the gastric type, intestinal type, mixed type, or unclassified type based on the expression of MUC5AC, MUC6, MUC2, and CD10 [3]. The gastric type is positive for MUC5AC and/or MUC6, and the intestinal type is positive for MUC2 and/or CD10. The mixed type is positive for both gastric and intestinal mucins, and the unclassified type is negative for both.

Easy methods for molecular classification

Molecular profiles of GCs have been published in recent stud-

ies by TCGA and the Asian Cancer Research Group (ACRG). TCGA classified GCs into EBV, MSI, genomically stable, and chromosomally unstable [124]. In contrast, ACRG published a molecular classification of MSI, microsatellite stable/epithelial mesenchymal transition (MSS/EMT), MSS/TP53+, and MSS/TP53– [125]. The MSS/EMT subtype is closely associated with the SRC and PCC histology and Lauren's diffuse type, and patient survival is poor. The EBV and MSI subtypes are related to the histologic type of adenocarcinoma with lymphoid stroma and have relatively better prognosis. High TMB and increased expression of PD-L1 are commonly reported in the EBV and MSI subtypes.

Several studies have reported that these molecular classifications could be reproduced in GCs using simple techniques, including EBV ISH, MSI testing, MMR IHC, E-cadherin IHC, and p53 IHC [127,180,181]. Using those tests, GC is classified as EBV, MSI, EMT, altered p53, and not altered p53. Those molecular subtypes showed distinct clinicopathologic characteristics.

Supplementary Information

The Data Supplement is available with this article at <https://doi.org/10.4132/jptm.2022.12.23>.

Ethics Statement

Not applicable.

Availability of Data and Material

Data sharing not applicable to this article as no datasets were generated or analyzed during the study.

Code Availability

Not applicable.

ORCID

Young Soo Park	https://orcid.org/0000-0001-5389-4245
Myeong-Cherl Kook	https://orcid.org/0000-0002-3435-3301
Baek-hui Kim	https://orcid.org/0000-0001-6793-1991
Hye Seung Lee	https://orcid.org/0000-0002-1667-7986
Dong-Wook Kang	https://orcid.org/0000-0002-4300-3469
Mi-Jin Gu	https://orcid.org/0000-0002-8350-3038
Ok Ran Shin	https://orcid.org/0000-0003-4506-5150
Younghee Choi	https://orcid.org/0000-0002-3882-4000

Wonaee Lee <https://orcid.org/0000-0001-9266-6640>
 Hyunki Kim <https://orcid.org/0000-0003-2292-5584>
 In Hye Song <https://orcid.org/0000-0001-6325-3548>
 Kyoung-Mee Kim <https://orcid.org/0000-0002-1162-9205>
 Hee Sung Kim <https://orcid.org/0000-0002-8154-2391>
 Guhyun Kang <https://orcid.org/0000-0001-7730-1686>
 Do Youn Park <https://orcid.org/0000-0001-7641-1509>
 So-Young Jin <https://orcid.org/0000-0002-9900-8322>
 Joon Mee Kim <https://orcid.org/0000-0003-1355-4187>
 Yoon Jung Choi <https://orcid.org/0000-0002-5701-8864>
 Hee Kyung Chang <https://orcid.org/0000-0002-4843-5316>
 Soomin Ahn <https://orcid.org/0000-0002-1979-4010>
 Mee Soo Chang <https://orcid.org/0000-0002-0948-799X>
 Song-Hee Han <https://orcid.org/0000-0002-4564-7014>
 Yoonjin Kwak <https://orcid.org/0000-0001-5314-2465>
 An Na Seo <https://orcid.org/0000-0001-6412-3067>
 Sung Hak Lee <https://orcid.org/0000-0003-1020-5838>
 Mee-Yon Cho <https://orcid.org/0000-0002-7955-4211>

Author Contributions

Conceptualization: YSP, MCK, BHK, HSL, KMK, JMK, SHL, MYC. Project administration: KMK, JMK, SHL, MYC. Supervision: DWK, YC, HK, KMK, DYP, SYJ, JMK, YJC, HKC, MSC, MYC. Writing—original draft preparation: YSP, MCK, BHK, HSL, SHL. Writing—review & editing: YSP, MCK, BHK, HSL, DWK, MJG, ORS, YC, WL, HK, HIS, KMK, HSK, GK, DYP, SYJ, JMK, YJC, HKC, SA, MSC, SHH, YK, ANS, SHL, MYC. Approval of final manuscript: all authors.

Conflicts of Interest

S.H.L., a contributing editor of the *Journal of Pathology and Translational Medicine*, was not involved in the editorial evaluation or decision to publish this article. All remaining authors have declared no conflicts of interest.

Funding Statement

This research was supported by a grant of Patient-Centered Clinical Research Coordinating Center (PACEN) funded by the Ministry of Health & Welfare, Republic of Korea (grant number: HC20C0123).

References

1. Sung H, Ferlay J, Siegel RL, et al. Global cancer statistics 2020: GLOBOCAN estimates of incidence and mortality worldwide for 36 cancers in 185 countries. *CA Cancer J Clin* 2021; 71: 209-49.
2. Hong S, Won YJ, Lee JJ, et al. Cancer statistics in Korea: incidence, mortality, survival, and prevalence in 2018. *Cancer Res Treat* 2021; 53: 301-15.
3. Kim WH, Park CK, Kim YB, et al. A standardized pathology report for gastric cancer. *Korean J Pathol* 2005; 39: 106-13.
4. World Health Organization. WHO classification of tumours: digestive system tumours. Geneva: World Health Organization, 2019.
5. Guideline Committee of the Korean Gastric Cancer Association (KGCA), Development Working Group and Review Panel. Korean practice guideline for gastric cancer 2018: an evidence-based, multi-disciplinary approach. *J Gastric Cancer* 2019; 19: 1-48.
6. Muro K, Chung HC, Shankaran V, et al. Pembrolizumab for patients with PD-L1-positive advanced gastric cancer (KEYNOTE-012): a multicentre, open-label, phase 1b trial. *Lancet Oncol* 2016; 17: 717-26.
7. Bang YJ, Van Cutsem E, Feyereislova A, et al. Trastuzumab in combination with chemotherapy versus chemotherapy alone for treat-

- ment of HER2-positive advanced gastric or gastro-oesophageal junction cancer (ToGA): a phase 3, open-label, randomised controlled trial. *Lancet* 2010; 376: 687-97.
8. Amin MB, Edge SB, Greene FL, et al. *AJCC cancer staging manual*. 8th ed. Cham: Springer, 2017.
9. Japanese Gastric Cancer Association. Japanese classification of gastric carcinoma: 3rd English edition. *Gastric Cancer* 2011; 14: 101-12.
10. Fritz A, Percy C, Jack A, et al. *International Classification of Diseases for Oncology (ICD-O)*. 3rd ed. Lyon: International Agency for Research on Cancer, 2013.
11. Shi C, Berlin J, Branton PA, et al. Protocol for the examination of specimens from patients with carcinoma of the stomach [Internet]. Northfield: College of American Pathologists, 2020 [cited 2022 Dec 1]. Available from: <https://documents.cap.org/protocols/cp-gi-upper-esophagus-20-4100.pdf>.
12. Shi C, Badgwell BD, Grabsch HI, et al. Data set for reporting carcinoma of the stomach in gastrectomy. *Arch Pathol Lab Med* 2022; 146: 1072-83.
13. Cunningham D, Allum WH, Stenning SP, et al. Perioperative chemotherapy versus surgery alone for resectable gastroesophageal cancer. *N Engl J Med* 2006; 355: 11-20.
14. Zhang X, Liang H, Li Z, et al. Perioperative or postoperative adjuvant oxaliplatin with S-1 versus adjuvant oxaliplatin with capecitabine in patients with locally advanced gastric or gastro-oesophageal junction adenocarcinoma undergoing D2 gastrectomy (RESOLVE): an open-label, superiority and non-inferiority, phase 3 randomised controlled trial. *Lancet Oncol* 2021; 22: 1081-92.
15. Kang YK, Yook JH, Park YK, et al. PRODIGY: a phase III study of neoadjuvant docetaxel, oxaliplatin, and S-1 plus surgery and adjuvant S-1 versus surgery and adjuvant S-1 for resectable advanced gastric cancer. *J Clin Oncol* 2021; 39: 2903-13.
16. Langer R, Becker K. Tumor regression grading of gastrointestinal cancers after neoadjuvant therapy. *Virchows Arch* 2018; 472: 175-86.
17. Mandard AM, Dalibard F, Mandard JC, et al. Pathologic assessment of tumor regression after preoperative chemoradiotherapy of esophageal carcinoma: clinicopathologic correlations. *Cancer* 1994; 73: 2680-6.
18. Dworak O, Keilholz L, Hoffmann A. Pathological features of rectal cancer after preoperative radiochemotherapy. *Int J Colorectal Dis* 1997; 12: 19-23.
19. Becker K, Mueller JD, Schulmacher C, et al. Histomorphology and grading of regression in gastric carcinoma treated with neoadjuvant chemotherapy. *Cancer* 2003; 98: 1521-30.
20. Mirza A, Naveed A, Hayes S, et al. Assessment of histopathological response in gastric and gastro-oesophageal junction adenocarcinoma following neoadjuvant chemotherapy: which scoring system to use? *ISRN Pathol* 2012; 2012: 519351.
21. Karamitopoulou E, Thies S, Zlobec I, et al. Assessment of tumor regression of esophageal adenocarcinomas after neoadjuvant chemotherapy: comparison of 2 commonly used scoring approaches. *Am J Surg Pathol* 2014; 38: 1551-6.
22. Kim BH, Kim JM, Kang GH, et al. Standardized pathology report for colorectal cancer, 2nd edition. *J Pathol Transl Med* 2020; 54: 1-19.
23. Tsekrekos A, Vieth M, Ndegwa N, et al. Interobserver agreement of a gastric adenocarcinoma tumor regression grading system that

- incorporates assessment of lymph nodes. *Hum Pathol* 2021; 116: 94-101.
24. Davies AR, Myoteri D, Zylstra J, et al. Lymph node regression and survival following neoadjuvant chemotherapy in oesophageal adenocarcinoma. *Br J Surg* 2018; 105: 1639-49.
 25. Reim D, Novotny A, Friess H, et al. Significance of tumour regression in lymph node metastases of gastric and gastro-oesophageal junction adenocarcinomas. *J Pathol Clin Res* 2020; 6: 263-72.
 26. Smyth EC, Fassan M, Cunningham D, et al. Effect of pathologic tumor response and nodal status on survival in the Medical Research Council adjuvant gastric infusional chemotherapy Trial. *J Clin Oncol* 2016; 34: 2721-7.
 27. Koh YW, Park YS, Ryu MH, et al. Postoperative nodal status and diffuse-type histology are independent prognostic factors in resectable advanced gastric carcinomas after preoperative chemotherapy. *Am J Surg Pathol* 2013; 37: 1022-9.
 28. Veronese N, Fassan M, Wood LD, et al. Extranodal extension of nodal metastases is a poor prognostic indicator in gastric cancer: a systematic review and meta-analysis. *J Gastrointest Surg* 2016; 20: 1692-8.
 29. Lee IS, Park YS, Ryu MH, et al. Impact of extranodal extension on prognosis in lymph node-positive gastric cancer. *Br J Surg* 2014; 101: 1576-84.
 30. Lee IS, Kang HJ, Park YS, et al. Prognostic impact of extranodal extension in stage 1B gastric carcinomas. *Surg Oncol* 2018; 27: 299-305.
 31. Araki I, Hosoda K, Yamashita K, et al. Prognostic impact of venous invasion in stage 1B node-negative gastric cancer. *Gastric Cancer* 2015; 18: 297-305.
 32. Takeuchi A, Ojima T, Katsuda M, et al. Venous invasion is a risk factor for recurrence of pT1 gastric cancer with lymph node metastasis. *J Gastrointest Surg* 2022; 26: 757-63.
 33. Nishibeppu K, Komatsu S, Ichikawa D, et al. Venous invasion as a risk factor for recurrence after gastrectomy followed by chemotherapy for stage III gastric cancer. *BMC Cancer* 2018; 18: 108.
 34. Liebig C, Ayala G, Wilks JA, Berger DH, Albo D. Perineural invasion in cancer: a review of the literature. *Cancer* 2009; 115: 3379-91.
 35. Hanaoka N, Tanabe S, Mikami T, Okayasu I, Saigenji K. Mixed-histologic-type submucosal invasive gastric cancer as a risk factor for lymph node metastasis: feasibility of endoscopic submucosal dissection. *Endoscopy* 2009; 41: 427-32.
 36. Takizawa K, Ono H, Kakushima N, et al. Risk of lymph node metastases from intramucosal gastric cancer in relation to histological types: how to manage the mixed histological type for endoscopic submucosal dissection. *Gastric Cancer* 2013; 16: 531-6.
 37. Lee JH, Choi IJ, Han HS, et al. Risk of lymph node metastasis in differentiated type mucosal early gastric cancer mixed with minor undifferentiated type histology. *Ann Surg Oncol* 2015; 22: 1813-9.
 38. Sekiguchi M, Oda I, Taniguchi H, et al. Risk stratification and predictive risk-scoring model for lymph node metastasis in early gastric cancer. *J Gastroenterol* 2016; 51: 961-70.
 39. Seo HS, Lee GE, Kang MG, Han KH, Jung ES, Song KY. Mixed histology is a risk factor for lymph node metastasis in early gastric cancer. *J Surg Res* 2019; 236: 271-7.
 40. Horiuchi Y, Ida S, Yamamoto N, et al. Feasibility of further expansion of the indications for endoscopic submucosal dissection in undifferentiated-type early gastric cancer. *Gastric Cancer* 2020; 23: 285-92.
 41. Ha TK, An JY, Youn HK, Noh JH, Sohn TS, Kim S. Indication for endoscopic mucosal resection in early signet ring cell gastric cancer. *Ann Surg Oncol* 2008; 15: 508-13.
 42. Kim BS, Oh ST, Yook JH, Kim BS. Signet ring cell type and other histologic types: differing clinical course and prognosis in T1 gastric cancer. *Surgery* 2014; 155: 1030-5.
 43. Guo CG, Zhao DB, Liu Q, et al. Risk factors for lymph node metastasis in early gastric cancer with signet ring cell carcinoma. *J Gastrointest Surg* 2015; 19: 1958-65.
 44. Huh CW, Jung DH, Kim JH, et al. Signet ring cell mixed histology may show more aggressive behavior than other histologies in early gastric cancer. *J Surg Oncol* 2013; 107: 124-9.
 45. Lee IS, Lee S, Park YS, Gong CS, Yook JH, Kim BS. Applicability of endoscopic submucosal dissection for undifferentiated early gastric cancer: Mixed histology of poorly differentiated adenocarcinoma and signet ring cell carcinoma is a worse predictive factor of nodal metastasis. *Surg Oncol* 2017; 26: 8-12.
 46. Kim YH, Park JH, Park CK, et al. Histologic purity of signet ring cell carcinoma is a favorable risk factor for lymph node metastasis in poorly cohesive, submucosa-invasive early gastric carcinoma. *Gastric Cancer* 2017; 20: 583-90.
 47. Chu Y, Mao T, Li X, et al. Predictors of lymph node metastasis and differences between pure and mixed histologic types of early gastric signet-ring cell carcinomas. *Am J Surg Pathol* 2020; 44: 934-42.
 48. Japanese Gastric Cancer Society. Regulations for the treatment of gastric cancer. 15th ed. Tokyo: Kanehara Publishing, 2017.
 49. Kim JY, Kim WG, Jeon TY, et al. Lymph node metastasis in early gastric cancer: evaluation of a novel method for measuring submucosal invasion and development of a nodal predicting index. *Hum Pathol* 2013; 44: 2829-36.
 50. Ma DW, Lee SJ, Kook MC, et al. The suggestion of revised criteria for endoscopic resection of differentiated-type submucosal gastric cancer. *Ann Surg Oncol* 2020; 27: 795-801.
 51. Choi JY, Park YS, Jung HY, et al. Identifying predictors of lymph node metastasis after endoscopic resection in patients with minute submucosal cancer of the stomach. *Surg Endosc* 2015; 29: 1476-83.
 52. Gotoda T, Yanagisawa A, Sasako M, et al. Incidence of lymph node metastasis from early gastric cancer: estimation with a large number of cases at two large centers. *Gastric Cancer* 2000; 3: 219-25.
 53. Park SM, Kim BW, Kim JS, Kim YW, Kim GJ, Ryu SJ. Can endoscopic ulcerations in early gastric cancer be clearly defined before endoscopic resection? A survey among endoscopists. *Clin Endosc* 2017; 50: 473-8.
 54. Kim JM, Sohn JH, Cho MY, et al. Pre- and post-ESD discrepancies in clinicopathologic criteria in early gastric cancer: the NECA-Korea ESD for Early Gastric Cancer Prospective Study (N-Keep). *Gastric Cancer* 2016; 19: 1104-13.
 55. Yabuuchi Y, Takizawa K, Kakushima N, et al. Discrepancy between endoscopic and pathological ulcerative findings in clinical intramucosal early gastric cancer. *Gastric Cancer* 2021; 24: 691-700.
 56. Shimoda T, Kushima R, Ono H. Histological features of peptic ulceration and biopsy scar of gastric ESD specimen. *Stomach Intestine* 2013; 48: 16-24.

57. Japanese Gastric Cancer Association. Japanese gastric cancer treatment guidelines 2018 (5th edition). *Gastric Cancer* 2021; 24: 1-21.
58. Takizawa K, Ono H, Hasuike N, et al. A nonrandomized, single-arm confirmatory trial of expanded endoscopic submucosal dissection indication for undifferentiated early gastric cancer: Japan Clinical Oncology Group study (JCOG1009/1010). *Gastric Cancer* 2021; 24: 479-91.
59. Hatta W, Gotoda T, Oyama T, et al. A scoring system to stratify curability after endoscopic submucosal dissection for early gastric cancer: "eCura system". *Am J Gastroenterol* 2017; 112: 874-81.
60. Uesugi N, Sugai T, Sugimoto R, et al. Clinicopathological and molecular stability and methylation analyses of gastric papillary adenocarcinoma. *Pathology* 2017; 49: 596-603.
61. Lee HJ, Kim GH, Park DY, et al. Endoscopic submucosal dissection for papillary adenocarcinoma of the stomach: is it really safe? *Gastric Cancer* 2017; 20: 978-86.
62. Min BH, Byeon SJ, Lee JH, et al. Lymphovascular invasion and lymph node metastasis rates in papillary adenocarcinoma of the stomach: implications for endoscopic resection. *Gastric Cancer* 2018; 21: 680-8.
63. Yasuda K, Adachi Y, Shiraishi N, Maeo S, Kitano S. Papillary adenocarcinoma of the stomach. *Gastric Cancer* 2000; 3: 33-8.
64. Yu H, Fang C, Chen L, et al. Worse prognosis in papillary, compared to tubular, early gastric carcinoma. *J Cancer* 2017; 8: 117-23.
65. Kawamura H, Kondo Y, Osawa S, et al. A clinicopathologic study of mucinous adenocarcinoma of the stomach. *Gastric Cancer* 2001; 4: 83-6.
66. Lee HH, Song KY, Park CH, Jeon HM. Undifferentiated-type gastric adenocarcinoma: prognostic impact of three histological types. *World J Surg Oncol* 2012; 10: 254.
67. Nakamura K, Eto K, Iwagami S, et al. Clinicopathological characteristics and prognosis of poorly cohesive cell subtype of gastric cancer. *Int J Clin Oncol* 2022; 27: 512-9.
68. Roviello F, Marano L, Ambrosio MR, et al. Signet ring cell percentage in poorly cohesive gastric cancer patients: a potential novel predictor of survival. *Eur J Surg Oncol* 2022; 48: 561-9.
69. Garcia-Pelaez J, Barbosa-Matos R, Gullo I, Carneiro F, Oliveira C. Histological and mutational profile of diffuse gastric cancer: current knowledge and future challenges. *Mol Oncol* 2021; 15: 2841-67.
70. Kwon CH, Kim YK, Lee S, et al. Gastric poorly cohesive carcinoma: a correlative study of mutational signatures and prognostic significance based on histopathological subtypes. *Histopathology* 2018; 72: 556-68.
71. Mariette C, Carneiro F, Grabsch HI, et al. Consensus on the pathological definition and classification of poorly cohesive gastric carcinoma. *Gastric Cancer* 2019; 22: 1-9.
72. Han JP, Hong SJ, Kim HK. Long-term outcomes of early gastric cancer diagnosed as mixed adenocarcinoma after endoscopic submucosal dissection. *J Gastroenterol Hepatol* 2015; 30: 316-20.
73. Park HK, Lee KY, Yoo MW, Hwang TS, Han HS. Mixed carcinoma as an independent prognostic factor in submucosal invasive gastric carcinoma. *J Korean Med Sci* 2016; 31: 866-72.
74. Horiuchi Y, Fujisaki J, Yamamoto N, et al. Undifferentiated-type predominant mixed-type early gastric cancer is a significant risk factor for requiring additional surgeries after endoscopic submucosal dissection. *Sci Rep* 2020; 10: 6748.
75. Ozeki Y, Hirasawa K, Sawada A, et al. Mixed histology poses a greater risk for noncurative endoscopic resection in early gastric cancers regardless of the predominant histologic types. *Eur J Gastroenterol Hepatol* 2021; 32: 186-93.
76. Shin DH, Kim GH, Lee BE, et al. Clinicopathologic features of early gastric carcinoma with lymphoid stroma and feasibility of endoscopic submucosal dissection. *Surg Endosc* 2017; 31: 4156-64.
77. Iwasaki K, Suda T, Takano Y, et al. Postoperative outcomes of gastric carcinoma with lymphoid stroma. *World J Surg Oncol* 2020; 18: 102.
78. Huh CW, Jung DH, Kim H, et al. Clinicopathologic features of gastric carcinoma with lymphoid stroma in early gastric cancer. *J Surg Oncol* 2016; 114: 769-72.
79. Inagawa S, Shimazaki J, Hori M, et al. Hepatoid adenocarcinoma of the stomach. *Gastric Cancer* 2001; 4: 43-52.
80. Roh JH, Srivastava A, Lauwers GY, et al. Micropapillary carcinoma of stomach: a clinicopathologic and immunohistochemical study of 11 cases. *Am J Surg Pathol* 2010; 34: 1139-46.
81. Fujita T, Gotohda N, Kato Y, et al. Clinicopathological features of stomach cancer with invasive micropapillary component. *Gastric Cancer* 2012; 15: 179-87.
82. Benedict MA, Lauwers GY, Jain D. Gastric adenocarcinoma of the fundic gland type: update and literature review. *Am J Clin Pathol* 2018; 149: 461-73.
83. Miyazawa M, Matsuda M, Yano M, et al. Gastric adenocarcinoma of the fundic gland (chief cell-predominant type): a review of endoscopic and clinicopathological features. *World J Gastroenterol* 2016; 22: 10523-31.
84. Agaimy A, Rau TT, Hartmann A, Stoehr R. SMARCB1 (INI1)-negative rhabdoid carcinomas of the gastrointestinal tract: clinicopathologic and molecular study of a highly aggressive variant with literature review. *Am J Surg Pathol* 2014; 38: 910-20.
85. Willems S, Carneiro F, Geboes K. Gastric carcinoma with osteoclast-like giant cells and lymphoepithelioma-like carcinoma of the stomach: two of a kind? *Histopathology* 2005; 47: 331-3.
86. Woo HY, Bae YS, Kim JH, et al. Distinct expression profile of key molecules in crawling-type early gastric carcinoma. *Gastric Cancer* 2017; 20: 612-9.
87. Okamoto N, Kawachi H, Yoshida T, et al. "Crawling-type" adenocarcinoma of the stomach: a distinct entity preceding poorly differentiated adenocarcinoma. *Gastric Cancer* 2013; 16: 220-32.
88. Ushiku T, Kunita A, Kuroda R, et al. Oxyntic gland neoplasm of the stomach: expanding the spectrum and proposal of terminology. *Mod Pathol* 2020; 33: 206-16.
89. Tsuji Y, Ushiku T, Shinozaki T, et al. Risk for lymph node metastasis in Epstein-Barr virus-associated gastric carcinoma with submucosal invasion. *Dig Endosc* 2021; 33: 592-7.
90. Lauren P. The two histological main types of gastric carcinoma: diffuse and so-called intestinal-type carcinoma: an attempt at a histo-clinical classification. *Acta Pathol Microbiol Scand* 1965; 64: 31-49.
91. Park DY, Srivastava A, Kim GH, et al. Adenomatous and foveolar gastric dysplasia: distinct patterns of mucin expression and background intestinal metaplasia. *Am J Surg Pathol* 2008; 32: 524-33.
92. Choi WT, Brown I, Ushiku T, et al. Gastric pyloric gland adenoma: a multicentre clinicopathological study of 67 cases. *Histopa-*

- thology 2018; 72: 1007-14.
93. Kim JM, Sohn JH, Cho MY, et al. Inter-observer reproducibility in the pathologic diagnosis of gastric intraepithelial neoplasia and early carcinoma in endoscopic submucosal dissection specimens: a multi-center study. *Cancer Res Treat* 2019; 51: 1568-77.
 94. Kim JM, Cho MY, Sohn JH, et al. Diagnosis of gastric epithelial neoplasia: dilemma for Korean pathologists. *World J Gastroenterol* 2011; 17: 2602-10.
 95. Watanabe Y, Shimizu M, Itoh T, Nagashima K. Intraglandular necrotic debris in gastric biopsy and surgical specimens. *Ann Diagn Pathol* 2001; 5: 141-7.
 96. Choi IJ, Kook MC, Kim YI, et al. *Helicobacter pylori* therapy for the prevention of metachronous gastric cancer. *N Engl J Med* 2018; 378: 1085-95.
 97. Ono H, Yao K, Fujishiro M, et al. Guidelines for endoscopic submucosal dissection and endoscopic mucosal resection for early gastric cancer (second edition). *Dig Endosc* 2021; 33: 4-20.
 98. Shitara K, Bang YJ, Iwasa S, et al. Trastuzumab deruxtecan in previously treated HER2-positive gastric cancer. *N Engl J Med* 2020; 382: 2419-30.
 99. FDA approves fam-trastuzumab deruxtecan-nxki for HER2-positive gastric adenocarcinomas [Internet]. Silver Spring: U.S. Food and Drug Administration, 2021 [cited 2022 Dec 1]. Available from: <https://www.fda.gov/drugs/resources-information-approved-drugs/fda-approves-fam-trastuzumab-deruxtecan-nxki-her2-positive-gastric-adenocarcinomas>.
 100. Ajani JA, D'Amico TA, Bentrem DJ, et al. Gastric cancer, version 2.2022, NCCN Clinical Practice Guidelines in Oncology. *J Natl Compr Canc Netw* 2022; 20: 167-92.
 101. Hofmann M, Stoss O, Shi D, et al. Assessment of a HER2 scoring system for gastric cancer: results from a validation study. *Histopathology* 2008; 52: 797-805.
 102. Ahn S, Ahn S, Van Vrancken M, et al. Ideal number of biopsy tumor fragments for predicting HER2 status in gastric carcinoma resection specimens. *Oncotarget* 2015; 6: 38372-80.
 103. Lee HS, Kim WH, Kwak Y, et al. Molecular testing for gastrointestinal cancer. *J Pathol Transl Med* 2017; 51: 103-21.
 104. Bartley AN, Washington MK, Colasacco C, et al. HER2 testing and clinical decision making in gastroesophageal adenocarcinoma: guideline from the College of American Pathologists, American Society for Clinical Pathology, and the American Society of Clinical Oncology. *J Clin Oncol* 2017; 35: 446-64.
 105. Wolff AC, Hammond ME, Hicks DG, et al. Recommendations for human epidermal growth factor receptor 2 testing in breast cancer: American Society of Clinical Oncology/College of American Pathologists clinical practice guideline update. *J Clin Oncol* 2013; 31: 3997-4013.
 106. Van Cutsem E, Bang YJ, Feng-Yi F, et al. HER2 screening data from ToGA: targeting HER2 in gastric and gastroesophageal junction cancer. *Gastric Cancer* 2015; 18: 476-84.
 107. Tsapralis D, Panayiotides I, Peros G, Liakakos T, Karamitopoulou E. Human epidermal growth factor receptor-2 gene amplification in gastric cancer using tissue microarray technology. *World J Gastroenterol* 2012; 18: 150-5.
 108. Liu W, Zhong S, Chen J, Yu Y. HER-2/neu overexpression is an independent prognostic factor for intestinal-type and early-stage gastric cancer patients. *Journal of clinical gastroenterology* 2012; 46: e31-7.
 109. Lee HE, Park KU, Yoo SB, et al. Clinical significance of intratumoral HER2 heterogeneity in gastric cancer. *European Journal of Cancer* 2013; 49: 1448-57.
 110. Kim MA, Lee HJ, Yang HK, Bang YJ, Kim WH. Heterogeneous amplification of ERBB2 in primary lesions is responsible for the discordant ERBB2 status of primary and metastatic lesions in gastric carcinoma. *Histopathology* 2011; 59: 822-31.
 111. Peng Z, Zou J, Zhang X, et al. HER2 discordance between paired primary gastric cancer and metastasis: a meta-analysis. *Chin J Cancer Res* 2015; 27: 163-71.
 112. Kim JH, Kim MA, Lee HS, Kim WH. Comparative analysis of protein expressions in primary and metastatic gastric carcinomas. *Hum Pathol* 2009; 40: 314-22.
 113. Fusco N, Rocco EG, Del Conte C, et al. HER2 in gastric cancer: a digital image analysis in pre-neoplastic, primary and metastatic lesions. *Mod Pathol* 2013; 26: 816-24.
 114. Geng Y, Chen X, Qiu J, et al. Human epidermal growth factor receptor-2 expression in primary and metastatic gastric cancer. *Int J Clin Oncol* 2014; 19: 303-11.
 115. Kochi M, Fujii M, Masuda S, et al. Differing deregulation of HER2 in primary gastric cancer and synchronous related metastatic lymph nodes. *Diagn Pathol* 2013; 8: 191.
 116. Ieni A, Barresi V, Rigoli L, Caruso RA, Tuccari G. HER2 status in premalignant, early, and advanced neoplastic lesions of the stomach. *Dis Markers* 2015; 2015: 234851.
 117. Zhao W, Sun L, Dong G, Wang X, Jia Y, Tong Z. Receptor conversion impacts outcomes of different molecular subtypes of primary breast cancer. *Ther Adv Med Oncol* 2021; 13: 17588359211012982.
 118. Garrido-Ramos MA. Satellite DNA: an evolving topic. *Genes (Basel)* 2017; 8: 230.
 119. Luchini C, Bibeau F, Ligtenberg MJL, et al. ESMO recommendations on microsatellite instability testing for immunotherapy in cancer, and its relationship with PD-1/PD-L1 expression and tumour mutational burden: a systematic review-based approach. *Ann Oncol* 2019; 30: 1232-43.
 120. Li K, Luo H, Huang L, Luo H, Zhu X. Microsatellite instability: a review of what the oncologist should know. *Cancer Cell Int* 2020; 20: 16.
 121. Jiricny J. Postreplicative mismatch repair. *Cold Spring Harb Perspect Biol* 2013; 5: a012633.
 122. Ma J, Setton J, Lee NY, Riaz N, Powell SN. The therapeutic significance of mutational signatures from DNA repair deficiency in cancer. *Nat Commun* 2018; 9: 3292.
 123. Peltomaki P. Role of DNA mismatch repair defects in the pathogenesis of human cancer. *J Clin Oncol* 2003; 21: 1174-9.
 124. Cancer Genome Atlas Research Network. Comprehensive molecular characterization of gastric adenocarcinoma. *Nature* 2014; 513: 202-9.
 125. Cristescu R, Lee J, Nebozhyn M, et al. Molecular analysis of gastric cancer identifies subtypes associated with distinct clinical outcomes. *Nat Med* 2015; 21: 449-56.
 126. Setia N, Agoston AT, Han HS, et al. A protein and mRNA expression-based classification of gastric cancer. *Mod Pathol* 2016; 29: 772-84.
 127. Ahn S, Lee SJ, Kim Y, et al. High-throughput protein and mRNA expression-based classification of gastric cancers can identify clinically distinct subtypes, concordant with recent molecular classifications. *Am J Surg Pathol* 2017; 41: 106-15.

128. Choi YY, Kim H, Shin SJ, et al. Microsatellite instability and programmed cell death-ligand 1 expression in stage II/III gastric cancer: post hoc analysis of the CLASSIC randomized controlled study. *Ann Surg* 2019; 270: 309-16.
129. Guastadisegni C, Colafranceschi M, Ottini L, Dogliotti E. Microsatellite instability as a marker of prognosis and response to therapy: a meta-analysis of colorectal cancer survival data. *Eur J Cancer* 2010; 46: 2788-98.
130. Kim ST, Cristescu R, Bass AJ, et al. Comprehensive molecular characterization of clinical responses to PD-1 inhibition in metastatic gastric cancer. *Nat Med* 2018; 24: 1449-58.
131. Le DT, Uram JN, Wang H, et al. PD-1 blockade in tumors with mismatch-repair deficiency. *N Engl J Med* 2015; 372: 2509-20.
132. Le DT, Durham JN, Smith KN, et al. Mismatch repair deficiency predicts response of solid tumors to PD-1 blockade. *Science* 2017; 357: 409-13.
133. Ratti M, Lampis A, Hahne JC, Passalacqua R, Valeri N. Microsatellite instability in gastric cancer: molecular bases, clinical perspectives, and new treatment approaches. *Cell Mol Life Sci* 2018; 75: 4151-62.
134. Jang M, Kwon Y, Kim H, et al. Microsatellite instability test using peptide nucleic acid probe-mediated melting point analysis: a comparison study. *Bmc Cancer* 2018; 18: 1218.
135. Murphy KM, Zhang S, Geiger T, et al. Comparison of the microsatellite instability analysis system and the Bethesda panel for the determination of microsatellite instability in colorectal cancers. *J Mol Diagn* 2006; 8: 305-11.
136. Berg KD, Glaser CL, Thompson RE, Hamilton SR, Griffin CA, Esheleman JR. Detection of microsatellite instability by fluorescence multiplex polymerase chain reaction. *J Mol Diagn* 2000; 2: 20-8.
137. Deschoolmeester V, Baay M, Wuys W, et al. Detection of microsatellite instability in colorectal cancer using an alternative multiplex assay of quasi-monomorphic mononucleotide markers. *J Mol Diagn* 2008; 10: 154-9.
138. Shia J, Ellis NA, Klimstra DS. The utility of immunohistochemical detection of DNA mismatch repair gene proteins. *Virchows Arch* 2004; 445: 431-41.
139. McCarthy AJ, Capo-Chichi JM, Spence T, et al. Heterogenous loss of mismatch repair (MMR) protein expression: a challenge for immunohistochemical interpretation and microsatellite instability (MSI) evaluation. *J Pathol Clin Res* 2019; 5: 115-29.
140. Renkonen E, Zhang Y, Lohi H, et al. Altered expression of MLH1, MSH2, and MSH6 in predisposition to hereditary nonpolyposis colorectal cancer. *J Clin Oncol* 2003; 21: 3629-37.
141. Graham RP, Kerr SE, Butz ML, et al. Heterogenous MSH6 loss is a result of microsatellite instability within MSH6 and occurs in sporadic and hereditary colorectal and endometrial carcinomas. *Am J Surg Pathol* 2015; 39: 1370-6.
142. Jansson A, Arbmán G, Zhang H, Sun XF. Combined deficiency of hMLH1, hMSH2, hMSH3 and hMSH6 is an independent prognostic factor in colorectal cancer. *Int J Oncol* 2003; 22: 41-9.
143. Ruzkiewicz A, Bennett G, Moore J, et al. Correlation of mismatch repair genes immunohistochemistry and microsatellite instability status in HNPCC-associated tumours. *Pathology* 2002; 34: 541-7.
144. Fukayama M, Abe H, Kunita A, et al. Thirty years of Epstein-Barr virus-associated gastric carcinoma. *Virchows Arch* 2020; 476: 353-65.
145. Chang MS, Kim DH, Roh JK, et al. Epstein-Barr virus-encoded BART1 promotes proliferation of gastric carcinoma cells through regulation of NF-kappaB. *J Virol* 2013; 87: 10515-23.
146. Hoebe EK, Le Large TY, Greijer AE, Middeldorp JM. BamHI-A rightward frame 1, an Epstein-Barr virus-encoded oncogene and immune modulator. *Rev Med Virol* 2013; 23: 367-83.
147. zur Hausen A, Brink AA, Craanen ME, Middeldorp JM, Meijer CJ, van den Brule AJ. Unique transcription pattern of Epstein-Barr virus (EBV) in EBV-carrying gastric adenocarcinomas: expression of the transforming BART1 gene. *Cancer Res* 2000; 60: 2745-8.
148. Kang GH, Lee S, Kim WH, et al. Epstein-barr virus-positive gastric carcinoma demonstrates frequent aberrant methylation of multiple genes and constitutes CpG island methylator phenotype-positive gastric carcinoma. *Am J Pathol* 2002; 160: 787-94.
149. Strong MJ, Xu G, Coco J, et al. Differences in gastric carcinoma microenvironment stratify according to EBV infection intensity: implications for possible immune adjuvant therapy. *PLoS Pathog* 2013; 9: e1003341.
150. Gu L, Chen M, Guo D, et al. PD-L1 and gastric cancer prognosis: a systematic review and meta-analysis. *PLoS One* 2017; 12: e0182692.
151. Park JH, Kim EK, Kim YH, et al. Epstein-Barr virus positivity, not mismatch repair-deficiency, is a favorable risk factor for lymph node metastasis in submucosa-invasive early gastric cancer. *Gastric Cancer* 2016; 19: 1041-51.
152. Cheng Y, Zhou X, Xu K, Huang J, Huang Q. Very low risk of lymph node metastasis in Epstein-Barr virus-associated early gastric carcinoma with lymphoid stroma. *BMC Gastroenterol* 2020; 20: 273.
153. Yoon CJ, Chang MS, Kim DH, et al. Epstein-Barr virus-encoded miR-BART5-5p upregulates PD-L1 through PIAS3/pSTAT3 modulation, worsening clinical outcomes of PD-L1-positive gastric carcinomas. *Gastric Cancer* 2020; 23: 780-95.
154. Lee HS, Chang MS, Yang HK, Lee BL, Kim WH. Epstein-barr virus-positive gastric carcinoma has a distinct protein expression profile in comparison with epstein-barr virus-negative carcinoma. *Clin Cancer Res* 2004; 10: 1698-705.
155. Longnecker RM, Kieff E, Cohen JI. Epstein-Barr virus. In: Knipe DM, Howley PM, eds. *Fields virology*. 6th ed. Philadelphia: Lippincott Williams & Wilkins, 2013; 1898-959.
156. Boger C, Kruger S, Behrens HM, et al. Epstein-Barr virus-associated gastric cancer reveals intratumoral heterogeneity of PIK3CA mutations. *Ann Oncol* 2017; 28: 1005-14.
157. Ribas A. Tumor immunotherapy directed at PD-1. *N Engl J Med* 2012; 366: 2517-9.
158. Kwak Y, Seo AN, Lee HE, Lee HS. Tumor immune response and immunotherapy in gastric cancer. *J Pathol Transl Med* 2020; 54: 20-33.
159. Fuchs CS, Doi T, Jang RW, et al. Safety and efficacy of pembrolizumab monotherapy in patients with previously treated advanced gastric and gastroesophageal junction cancer: phase 2 clinical KEYNOTE-059 trial. *JAMA Oncol* 2018; 4: e180013.
160. Shitara K, Ozguroglu M, Bang YJ, et al. Pembrolizumab versus paclitaxel for previously treated, advanced gastric or gastro-oesophageal junction cancer (KEYNOTE-061): a randomised, open-label, controlled, phase 3 trial. *Lancet* 2018; 392: 123-33.
161. Janjigian YY, Shitara K, Moehler M, et al. First-line nivolumab plus chemotherapy versus chemotherapy alone for advanced gastric, gastro-oesophageal junction, and oesophageal adenocarcinoma (CheckMate 649): a randomised, open-label, phase 3 trial. *Lan-*

- cet 2021; 398: 27-40.
162. DAKO Agilent Technologies. Interpretation manual: gastric or gastroesophageal junction adenocarcinoma. PD-L1 IHC 22C3 pharmDx interpretation manual: gastric or gastroesophageal junction adenocarcinoma. Santa Clara: DAKO Agilent Technologies, 2018.
 163. Yang JH, Kim H, Roh SY, et al. Discordancy and changes in the pattern of programmed death ligand 1 expression before and after platinum-based chemotherapy in metastatic gastric cancer. *Gastric Cancer* 2019; 22: 147-54.
 164. Zhou KI, Peterson B, Serritella A, et al. Spatial and temporal heterogeneity of PD-L1 expression and tumor mutational burden in gastroesophageal adenocarcinoma at baseline diagnosis and after chemotherapy. *Clin Cancer Res* 2020; 26: 6453-63.
 165. Son SM, Woo CG, Kim DH, et al. Distinct tumor immune microenvironments in primary and metastatic lesions in gastric cancer patients. *Sci Rep* 2020; 10: 14293.
 166. Marchio C, Scaltriti M, Ladanyi M, et al. ESMO recommendations on the standard methods to detect NTRK fusions in daily practice and clinical research. *Ann Oncol* 2019; 30: 1417-27.
 167. Catenacci DV, Rasco D, Lee J, et al. Phase I escalation and expansion study of bemarituzumab (FPA144) in patients with advanced solid tumors and FGFR2b-selected gastroesophageal adenocarcinoma. *J Clin Oncol* 2020; 38: 2418-26.
 168. Maron SB, Alpert L, Kwak HA, et al. Targeted therapies for targeted populations: anti-EGFR treatment for *EGFR*-amplified gastroesophageal adenocarcinoma. *Cancer Discov* 2018; 8: 696-713.
 169. Lee J, Kim ST, Kim K, et al. Tumor genomic profiling guides patients with metastatic gastric cancer to targeted treatment: the VIKTORY Umbrella Trial. *Cancer Discov* 2019; 9: 1388-405.
 170. Smyth EC, Cafferkey C, Loehr A, et al. Genomic loss of heterozygosity and survival in the REAL3 trial. *Oncotarget* 2018; 9: 36654-65.
 171. Nakamura Y, Kawazoe A, Lordick F, Janjigian YY, Shitara K. Biomarker-targeted therapies for advanced-stage gastric and gastroesophageal junction cancers: an emerging paradigm. *Nat Rev Clin Oncol* 2021; 18: 473-87.
 172. van Grieken NC, Aoyama T, Chambers PA, et al. *KRAS* and *BRAF* mutations are rare and related to DNA mismatch repair deficiency in gastric cancer from the East and the West: results from a large international multicentre study. *Br J Cancer* 2013; 108: 1495-501.
 173. Wen Z, Xiong D, Zhang S, et al. Case report: RAB10-ALK: a novel *ALK* fusion in a patient with gastric cancer. *Front Oncol* 2021; 11: 645370.
 174. Lee J, Lee SE, Kang SY, et al. Identification of *ROS1* rearrangement in gastric adenocarcinoma. *Cancer* 2013; 119: 1627-35.
 175. Fancello L, Gandini S, Pelicci PG, Mazzarella L. Tumor mutational burden quantification from targeted gene panels: major advancements and challenges. *J Immunother Cancer* 2019; 7: 183.
 176. Lee KW, Van Cutsem E, Bang YJ, et al. Association of tumor mutational burden with efficacy of pembrolizumab+/-chemotherapy as first-line therapy for gastric cancer in the phase III KEYNOTE-062 study. *Clin Cancer Res* 2022; 28: 3489-98.
 177. Kang SY, Kim DG, Ahn S, Ha SY, Jang KT, Kim KM. Comparative analysis of microsatellite instability by next-generation sequencing, MSI PCR and MMR immunohistochemistry in 1942 solid cancers. *Pathol Res Pract* 2022; 233: 153874.
 178. Ratovomanana T, Cohen R, Svrcek M, et al. Performance of next-generation sequencing for the detection of microsatellite instability in colorectal cancer with deficient DNA mismatch repair. *Gastroenterology* 2021; 161: 814-26.
 179. Ascierto PA, Bifulco C, Palmieri G, Peters S, Sidiropoulos N. Preanalytic variables and tissue stewardship for reliable next-generation sequencing (NGS) clinical analysis. *J Mol Diagn* 2019; 21: 756-67.
 180. Koh J, Lee KW, Nam SK, et al. Development and validation of an easy-to-implement, practical algorithm for the identification of molecular subtypes of gastric cancer: prognostic and therapeutic implications. *Oncologist* 2019; 24: e1321-30.
 181. Ramos M, Pereira MA, Amorim LC, et al. Gastric cancer molecular classification and adjuvant therapy: is there a different benefit according to the subtype? *J Surg Oncol* 2020; 121: 804-13.

Infections and immunity: associations with obesity and related metabolic disorders

Amitabha Ray¹, Melissa J. L. Bonorden², Rajashree Pandit³, Katai J. Nkhata⁴, Anupam Bishayee⁵

¹College of Medical Science, Alderson Broaddus University, Philippi, WV;

²Division of Research and Development, Hormel Foods Corporation, Austin, MN;

³Division of Medical & Behavioral Health, Pueblo Community College, Pueblo, CO;

⁴WuXi AppTec, St. Paul, MN;

⁵Lake Erie College of Osteopathic Medicine, Bradenton, FL, USA

About one-fourth of the global population is either overweight or obese, both of which increase the risk of insulin resistance, cardiovascular diseases, and infections. In obesity, both immune cells and adipocytes produce an excess of pro-inflammatory cytokines that may play a significant role in disease progression. In the recent coronavirus disease 2019 (COVID-19) pandemic, important pathological characteristics such as involvement of the renin-angiotensin-aldosterone system, endothelial injury, and pro-inflammatory cytokine release have been shown to be connected with obesity and associated sequelae such as insulin resistance/type 2 diabetes and hypertension. This pathological connection may explain the severity of COVID-19 in patients with metabolic disorders. Many studies have also reported an association between type 2 diabetes and persistent viral infections. Similarly, diabetes favors the growth of various microorganisms including protozoal pathogens as well as opportunistic bacteria and fungi. Furthermore, diabetes is a risk factor for a number of prion-like diseases. There is also an interesting relationship between helminths and type 2 diabetes; helminthiasis may reduce the pro-inflammatory state, but is also associated with type 2 diabetes or even neoplastic processes. Several studies have also documented altered circulating levels of neutrophils, lymphocytes, and monocytes in obesity, which likely modifies vaccine effectiveness. Timely monitoring of inflammatory markers (e.g., C-reactive protein) and energy homeostasis markers (e.g., leptin) could be helpful in preventing many obesity-related diseases.

Key Words: Metabolic disorders; Infections; COVID-19; Parasites; Immune cells

Received: September 10, 2022 **Revised:** November 13, 2022 **Accepted:** November 14, 2022

Corresponding Author: Amitabha Ray, MD, PhD, College of Medical Science, Alderson Broaddus University, 101 College Hill Drive, Philippi, WV 26416, USA
 Tel: +1-304-457-6587, Fax: +1-304-457-6308, E-mail: ray.amit213@gmail.com

Several investigators have reported that obesity or obesity-related complications appeared to be associated with increased risk of hospitalization of coronavirus disease 2019 (COVID-19) patients and death [1-3]. In general, overweight or obese persons are at higher risk for infections and respond poorly to therapies [4,5]. Being obese or overweight corresponds to a state of energy imbalance and is caused by inappropriate intake of energy-dense foods and physical inactivity. According to the World Health Organization (WHO), more than 1.9 billion adults were overweight (body mass index [BMI], 25.0 to <30) in 2016; of these over 650 million were obese (BMI, 30 or higher). In addition, over 340 million children and adolescents aged 5–19 were overweight or obese in 2016. Elevated BMI is an important risk factor for various non-communicable diseases such as type 2 dia-

betes and insulin resistance, hypertension, coronary artery disease, stroke, osteoarthritis, and certain cancers such as postmenopausal breast cancer, endometrial cancer, and renal cell carcinoma. With increasing BMI, the risk for these diseases also increases.

Obesity and its intimately associated disorder— type 2 diabetes or insulin resistance – are associated with gradual alterations in cellular physiology. Many investigators believe that the poor outcomes observed in individuals with obesity and type 2 diabetes/insulin resistance are due to immune system dysfunction that is triggered by chronic low-grade inflammation present in both health problems [6]. Interestingly, these patients also are at increased risk of infections and mortality from sepsis. Recent data suggest that infections may precipitate insulin resistance via multiple mechanisms such as the pro-inflammatory cytokine response,

the acute-phase response, and alteration of nutrient status [7]. In general, excessive adipose tissue in the body is known to hinder immune function, altering leucocyte counts as well as cell-mediated immune responses [8]. These immune cells are an intimate part of adipose tissue and an important source of pro-inflammatory cytokines/products, which ultimately contribute to the development of local adipose tissue inflammation and several metabolic complications [9].

In fact, adipose tissue acts as an endocrine organ; it secretes a number of hormone-like cytokines or adipokines, e.g., leptin, tumor necrosis factor α (TNF- α), monocyte chemoattractant protein-1 (MCP-1/CCL2), plasminogen activator inhibitor-1, resistin, adiponectin, and adiponectin among others. The majority of these adipokines participate in pro-inflammatory processes in obesity and perpetuate the state of insulin resistance [10]. Among these adipokines, several studies have suggested that leptin has an important role in major obesity-related health problems such as type 2 diabetes, hypertension, and different cancers [11]. Under normal conditions, leptin primarily maintains energy homeostasis through the central/hypothalamic anorexigenic pathway. However, in obesity, leptin possibly acts differently and supports a pro-inflammatory milieu. The long isoform of the leptin receptor (Ob-Rb) may play a key role in both physiologic and pathologic conditions. Interestingly, both long and short forms of the leptin receptor are expressed by different immune cells, e.g., B-cells, T-cells, neutrophils, eosinophils, monocytes, and macrophages [12–14]. Therefore, leptin can modulate both innate and adaptive immune response. An appropriate understanding of the complicated network of infectious pathologies and immune responses in obesity would help to formulate novel preventive strategies.

CORONAVIRUS DISEASE, OTHER VIRAL INFECTIONS, AND OBESITY-RELATED PROBLEMS

During the last two decades, there have been three coronavirus disease outbreaks. The first was the 2002–2004 outbreak of severe acute respiratory syndrome coronavirus (SARS-CoV or SARS-CoV-1) that emerged in China. A similar disease, caused by Middle East respiratory syndrome coronavirus (MERS-CoV), was initially detected in Saudi Arabia in 2012. The latest coronavirus pandemic (COVID-19) caused by SARS-CoV-2 began in December 2019 in China. The rapid spread of this infectious disease has been documented in different parts of the world, and about 6.7 million deaths have been recorded so far. SARS-CoV-2 is an enveloped positive-sense single-stranded linear RNA virus; the

envelope is coated with envelope (E) and membrane (M) proteins as well as a spike (S) glycoprotein that is responsible for binding to the host target cell receptor angiotensin-converting enzyme 2 (ACE-2). In addition, other cellular components such as extracellular matrix metalloproteinase inducer/CD147, transmembrane serine protease 2, and ADAM metalloproteinase domain 17 are implicated in viral endocytosis [15].

ACE catalyzes the conversion of angiotensin I to angiotensin II, which is an important step in the regulation of blood pressure via the renin-angiotensin-aldosterone system (RAAS). Moreover, ACE acts on several biomolecules including bradykinin, enkephalin, substance P, and amyloid β -peptide (A β), as well as in various physiological processes such as renal development, male fertility, hematopoiesis, and immune responses [16,17]. Conversely, ACE-2 is an important homolog of ACE and responsible for the conversion of angiotensin II to angiotensin 1-7, thereby counterbalancing ACE activity [18]. Both ACE and ACE-2 are cell membrane-anchored proteins, expressed in several organs, and functionally antagonistic to each other.

As mentioned earlier, to enter host cells, SARS-CoV-2 utilizes ACE-2 expressed in various organs, e.g., lung cells (pneumocytes and bronchial epithelium), gastrointestinal epithelium, and endothelial cells. Besides the lung parenchymal injury, there may be generalized endotheliitis (accumulation of lymphocytes, plasma cells and macrophages below the endothelium and in the perivascular spaces) [19]. In COVID-19, endothelial dysfunction is associated with the recruitment of immune cells and can result in many complications such as vasoconstriction, ischemia, inflammation, a pro-coagulant state, edema, and finally organ damage [20]. Moreover, abnormally increased levels of immune reaction and cytokines in different organs may cause a cytokine storm that can lead to additional organ dysfunction.

Obesity and insulin resistance are strongly connected to the activity of RAAS. Interestingly, expression of ACE-2, the functional receptor for viral entry, has been found to be higher in adipose tissue (and therefore higher in obesity) [21,22]. Furthermore, obesity and its complications such as hypertension, insulin resistance, and type 2 diabetes are associated with a higher risk of COVID-19 disease severity and mortality [22–24]. The impact of obesity and/or diabetes on SARS-CoV-1 infection has not been properly evaluated, although a few studies have investigated MERS-CoV-linked pathologies. One study of 32 MERS-CoV infected patients observed that mortality was significantly correlated with both obesity and diabetes [25]. A meta-analysis of 637 MERS-CoV cases revealed that diabetes and hypertension were present in roughly 50% of the patients [26]. Addition-

ally, in the 2009 H1N1 influenza pandemic, obesity was also identified as an important risk factor for a poor prognosis [27,28]. In general, a number of reports have documented an association between type 2 diabetes and chronic viral infections (Table 1) [29-48].

In addition to the disrupted immune response in obesity, other plausible mechanisms responsible for the poor prognosis of SARS-CoV-2 infection include obesity-associated pre-existing endothe-

lial dysfunction, a reduction in respiratory compliance, dysregulated lipid metabolism, and an overabundance of pro-inflammatory cytokines [20,22,49]. It is worth mentioning that obese individuals have defective/decreased responses to vaccination [49]. As a result, the combined effects of obesity and viral infection may worsen the existing status of cytokines, which normally coordinate the immune system and physiological homeostasis.

Table 1. Association between type 2 diabetes and common chronic viral infections

Study	Patients' details	Finding
Ndako et al. (2021); Nigeria [29]	180 Diabetic patients and 100 non-diabetics controls	Higher risk of HBV infection among type 2 diabetic patients than non-diabetics
Iovanescu et al. (2015); Romania [30]	246 Patients with chronic liver disease (136 chronic viral hepatitis, 110 viral liver cirrhosis)	A significant association between diabetes mellitus and HCV-induced chronic liver disease
Cheng et al. (2006); Hong Kong [31]	2,838 Type 2 diabetes patients	HBV-infected patients had earlier onset of diabetes, higher frequency of retinopathy, and increased risk of end-stage renal disease than non-HBV-infected patients
Virsedá Chamorro et al. (2006); Spain [32]	305 Patients who came for HCV assessment	A relationship between HCV infection and type 2 diabetes
Arao et al. (2003); Japan [33]	866 Patients with chronic viral disease (707 HCV-infected and 159 HBV-infected)	HCV infection was closely associated with diabetes, and cirrhosis was an independent risk factor for diabetes
Dworzanski et al. (2019); Poland [34]	173 Diabetic patients and 50 persons without diabetes	Prevalence of EBV, HPV, and EBV+HPV co-infection was significantly higher in diabetic patients than those without diabetes
Karjala et al. (2011); USA [35]	Data from the National Health and Examination and Nutritional Examination Survey (NHANES) 2007–2008	Obesity was significantly associated with HSV-1 infection
Fernandez-Real et al. (2007); Spain [36]	74 Healthy middle-aged men from the general population	Significant positive relation between HSV-1 titer and fat mass
Sun et al. (2003); China [37]	1,244 Inpatients (408 with dyslipidemia and 836 controls)	Prevalence of HSV-2 seropositivity was significantly higher in patients with dyslipidemia. BMI, diabetes, and hypertension were more common in patients with dyslipidemia than those without
Woelfle et al. (2022); Germany [38]	From the German population-based KORA cohort (pre-diabetes, n = 1,257)	HSV-2 and CMV were associated with pre-diabetes incidence
Yoo et al. (2019); Korea [39]	576 Adults with CMV diseases	Type 2 diabetes cases had a higher incidence of CMV diseases
Chen et al. (2012); Netherlands [40]	549 Participants	CMV seropositive subjects were more likely to have type 2 diabetes
Roberts and Cech (2005); USA [41]	113 Hemodialysis patients (83 type 2 diabetes and 30 controls)	A higher seroprevalence of anti-CMV IgG among diabetes patients
Chiu et al. (1997); Canada [42]	Endarterectomy specimens from 76 patients with carotid artery stenosis and 20 normal carotid artery and aortic tissue autopsy specimens	CMV was detected in carotid atherosclerotic plaques from 27 cases (35.5%)
Reinholdt et al. (2021); Denmark [43]	Male population (n = 2,528,756), nationwide registry-based cohort study	Increased incidence rate of HPV-related anogenital intraepithelial neoplasia and cancer among men with diabetes than non-diabetic men
Sobti et al. (2019); UK [44]	210 Patients with HNSCC	Prevalence of developing HPV-16-positive HNSCC was 3.79 times higher in diabetic patients than in those without diabetes. Moreover, diabetes was a risk factor for a poorer prognosis
Slama et al. (2021); USA [45]	1,584 Men with pre-diabetes (793 with HIV, 791 without HIV), over a median 12-year follow-up	40% higher risk for the development of diabetes among men with HIV
Kubiak et al. (2021); South Africa [46]	1,369 Persons with HIV	Among adults with HIV, diabetes and pre-diabetes were common
Hema et al. (2021); Burkina Faso [47]	4,259 Patients in a cross-sectional study	Prevalence of diabetes and hypertension was higher among persons with HIV on ART than the general population
Jeremiah et al. (2020); Tanzania [48]	1,947 Adults (336 with HIV on ART, 956 with HIV ART-naïve, 655 without HIV)	Prevalence of diabetes was high, particularly among HIV-infected ART-naïve persons

HBV, hepatitis B virus; HCV, hepatitis C virus; EBV, Epstein-Barr virus; HPV, human papillomavirus; HSV, herpes simplex virus; BMI, body mass index; CMV, cytomegalovirus; HNSCC, head and neck squamous cell carcinoma; HIV, human immunodeficiency virus; ART, antiretroviral therapy.

COVID-19–ASSOCIATED OPPORTUNISTIC FUNGAL DISEASES AND DIABETES

Generally, the majority of COVID-19 patients are asymptomatic or have minor symptoms. Less than 20% of cases require medical attention. According to the National Institutes of Health (NIH, USA), approximately 65% of individuals with serious illness from SARS-CoV-2 infection also had metabolic disorders such as obesity, type 2 diabetes, hypertension, and heart issues. Disease severity is associated with an uncontrolled immune response involving macrophages, neutrophils, different complement components, and a number of cytokines including TNF- α and interleukin-6 (IL-6). All these factors ultimately lead to a ‘cytokine storm’ and accompanying problems such as acute respiratory distress syndrome (ARDS), widespread vascular inflammation, and disseminated intravascular coagulation.

Therefore, to prevent the aforementioned abnormal immune reactions, intervention with corticosteroids (like dexamethasone) has been considered [50]. Of note, apart from immune suppression, corticosteroid therapy can aggravate insulin resistance/type 2 diabetes, which is a risk factor for COVID-19 disease severity. Moreover, immune suppression can also allow the growth of opportunistic bacterial and fungal pathogens. Among hospitalized COVID-19 patients, investigators have isolated various bacterial strains such as coagulase-negative staphylococci, *Klebsiella pneumoniae*, and *Pseudomonas aeruginosa*, as well as a number of fungal agents including *Candida albicans*, *Aspergillus fumigatus*, and *Cryptococcus neoformans* [51–53]. Although *Aspergillus* and *Candida* species are commonly found in severely ill COVID-19 patients, studies have also documented other fungal pathogens. For example, researchers detected *Histoplasma capsulatum* complement fixation titers in patients with serious SARS-CoV-2 infection [53,54]. Other factors also thought to play a key role in fungal co-infection include hypoxemia/lack of tissue oxygenation, mechanical ventilation, and type 2 diabetes and associated hyperglycemia [55].

Inappropriately managed diabetes increases the risk of infection of various body organs. Furthermore, diabetes can hinder both innate and adaptive immune mechanisms [56]. In the second wave of the COVID-19 pandemic in India (roughly from March to July 2021), there was a mysterious outbreak of mucormycosis or black fungus infection among patients with SARS-CoV-2 infection, and diabetic patients were more susceptible to mucormycosis [57]. In the normal immune system, all three complement activation pathways (classical, lectin, and alternative) play an important role protecting against fungal pathogens through

mechanisms such as opsonization, humoral immune response stimulation, and chemotaxis of immune cells [58,59]. In diabetes, glycation of complement components (functional low levels) may lead to an impaired immune response [55,60]. Consequently, the impaired immune response in severe COVID-19 illness allows fungal infection.

OTHER NON-VIRAL PATHOLOGIES: PRION AND PRION-LIKE DISEASES

Prions or protease-resistant misfolded proteins are unusual protein aggregates (also termed amyloids/amyloid fibrils) that have a high proportion of β -sheets. The first prion identified was the PrP protein [61]. The gene encoding the normal cellular prion protein (PrP^C, misfolded–PrP^S) is located on chromosome 20, and this glycoprotein is commonly present on the cell surface and can serve as a receptor for the A β peptide [62]. In addition, PrP^C is expressed in different organs, particularly in the nervous and immune systems, and is thought to have numerous physiological functions such as cell surface scaffolding. Nevertheless, the mechanism of misfolding and aggregation into an abnormal prion-like conformation that again influences the misfolding of other associated protein copies in a self-propagating manner is indeed a unique biological process, and we can see this phenomenon even in yeast and fungi.

Apart from typical prion diseases, which include Creutzfeldt-Jakob disease (CJD), kuru, Gerstmann-Sträussler-Scheinker disease, and fatal familial insomnia [63], there are other prion-like diseases such as Alzheimer’s disease, Parkinson’s disease, Huntington’s disease, type 2 diabetes, and amyloidosis. Certain proteins such as A β , tau, α -synuclein, and serum amyloid-A, which share some pathological characteristics with prions, have been implicated in these prion-like diseases [64,65]. For example, in Alzheimer’s and Parkinson’s diseases, aggregates of A β , tau, and α -synuclein can transmit the disease-pathology to experimental animals [65]. Of note, the fundamental features of Alzheimer’s disease lesions are the formation of A β in plaques and tau in tangles—both are β -sheet-rich misfolded variants of normal proteins.

Currently, about 50 different proteins are thought to form various human disease-related amyloid fibrils [66]. Furthermore, some of these abnormal proteins can cross species barriers and affect humans such as bovine spongiform encephalopathy or mad-cow disease, which is linked to variant CJD (vCJD) [67]. Interestingly, aggregation of amylin or islet amyloid polypeptide has been found in the pancreatic islets of Langerhans in individuals with type 2 diabetes [66]. In addition, patients with type 2 dia-

betes have an increased risk of developing Alzheimer's disease. Of note, a number of pathophysiological associations have been documented between Alzheimer's disease and metabolic disorders such as type 2 diabetes, obesity, and metabolic syndrome [68]. On the other hand, both Alzheimer's and prion diseases are neurodegenerative disorders, and there are several neuropathological commonalities and genetic connections between these diseases [69].

In humans, the most common prion disease is CJD with an incidence of about 1 case per 1 million population per year worldwide [70]. The majority (~85%) of cases of this rare disease occur sporadically, while ~10%–15% cases are due to familial or genetic mutations. The remaining cases (less than 1%) are linked to obvious environmental causes such as contaminated tissue transplant or surgical instruments (i.e., iatrogenic CJD) and contaminated meat consumption (i.e., vCJD). Another prion disease, kuru, once endemic in the Eastern Highlands of Papua New Guinea, disappeared rapidly after the cessation of ritual cannibalism. Clinically, kuru has a prodromal phase and three stages. Interestingly, in the second stage, obesity is a common feature, which could also exist in early disease in association with bulimia

[71]. However, unlike dissemination of microbial infections, prion disease is spread through ingestion or inoculation of contaminated materials (aside from sporadic and genetic inheritance). Therefore, different mechanisms by which conventional infectious diseases are spread, e.g., skin/mucosal contact, droplet/aerosol (airborne, coughs or sneezes), body fluids (like urine), fecal-oral route, vector-borne transmission, and fomites, have no role in the spread of prion diseases.

A number of investigators recorded an alteration of gut microbiota (dysbiosis) in prion disease and other neurodegenerative disorders such as Alzheimer's and Parkinson's disease [72–76]. Gut microbiota dysbiosis has also been reported in obesity and metabolic disorders including type 2 diabetes [77–80]. Nonetheless, there is a close similarity between protein misfolding disorders and pathogenesis of prions (infectious/transmissible proteins). For example, misfolded A β and tau (of Alzheimer's disease) spread in a way very similar to misfolded PrP [81–83]. As mentioned above, PrP^C functions as a cell surface receptor for A β . Fascinatingly, PrP^C acts in the propagation of prions as well as to transduce the neurotoxic signals from A β oligomers [82]. Experimentally, the transmission of kuru and CJD to various in

Table 2. Selected observations that displayed prion-like transmission characteristics of the most common neurodegenerative disease-related proteins

Study	Study design	Finding
Ayers et al. (2017) [87]	Injection of β -synuclein fibrils in M83 transgenic mice ^a through different peripheral routes, i.e., intramuscular (hind limb muscle), intravenous (tail veins), and intraperitoneal.	Injection of α -synuclein fibrils via these peripheral routes in M83 mice induced a robust α -synuclein pathology in the central nervous system.
Betemps et al. (2014) [88]	Transgenic M83 mice were inoculated intracerebrally in the striato-cortical area ^b with brain homogenates from sick M83 mice.	Disease acceleration following intracerebral inoculation suggests that disease propagation involves a prion-like mechanism.
Boluda et al. (2015) [89]	Intracerebral injection of Alzheimer's disease brain extracts enriched in pathological tau in young mutant P301S tau transgenic mice (PS19) ^c approximately 6–9 months before they show the onset of mutant tau transgene-induced tau pathology.	At 1-month post-injection, inoculated Alzheimer's disease-tau in young PS19 mice induced tau pathology predominantly in neuronal perikarya (neuron cell body). With longer post-injection survival periods of up to 6 months, tau pathology spread to different brain regions distant from the inoculated sites.
Guo et al. (2016) [90]	2–3-Month-old C57BL6 and C57BL6/C3H F1 mice were intracerebrally inoculated with different tau fibrils; 15–19-month-old C57BL6 mice were injected with Alzheimer's disease-tau.	Intracerebral inoculation of tau fibrils purified from Alzheimer's disease brains, but not synthetic tau fibrils, resulted in the formation of abundant tau inclusions in the brain of non-transgenic mice.
Lam et al. (2021) [91]	The posterior cingulate cortex ^d areas of 1.5-year-old male mouse lemurs (<i>Microcebus murinus</i>) were inoculated with either Alzheimer's disease or control brain extracts.	After 21 months, amyloid beta (A β) and tau pathologies developed in all Alzheimer-inoculated animals (n = 12) while no control brain extract-inoculated animals (n = 6) developed such lesions.
Morales et al. (2015) [92]	Brain extracts from 18–20 months old tg2576 mice ^e (having significant amyloid deposits) were serially diluted (10 ⁻⁷ dilution) and intracerebrally injected into 50–55-day-old tg2576 mice.	Administration of misfolded A β significantly accelerated amyloid deposition in young mice.

^aThe M83 transgenic mouse model overexpresses A53T mutated human α -synuclein protein, which is connected with buildup of pathognomonic Ser129-phosphorylated α -synuclein in the central nervous system. Abnormal accumulation of misfolded α -synuclein is linked to synucleinopathies including Parkinson's disease; ^bStriato-cortical area: The corpus striatum (subcortical basal ganglia) and the adjacent cerebral cortex in the forebrain region; ^cPS19 transgenic mouse expresses the P301S mutant form of human microtubule-associated protein tau. This hyper-phosphorylated and insoluble protein accumulates in the brain; ^dPosterior cingulate cortex: Situated at the posterior part of the cingulate gyrus in the medial part of the inferior parietal lobe, above the posterior end of the corpus callosum; ^eThe Tg2576 mouse model overexpresses a mutant form of amyloid precursor protein (APP₆₉₅SWE, found in early-onset familial Alzheimer's disease), which has the double mutation- APPK670M/671L. The most common neurodegenerative diseases: Alzheimer's disease and Parkinson's disease.

vivo models has been performed by different laboratories [84-86]. Similarly, the pathologies of A β , tau, and α -synuclein could be transmitted in a prion-like manner to in vivo models by injecting the misfolded proteins. In this connection, the results of selected studies have been mentioned briefly in Table 2 [87-92].

Both in vitro and in vivo studies have identified a number of compounds that have anti-prion activity. Congo red, polyanionic glycans, quinacrine, and compB either inhibit the formation of PrP^{Sc} or enhance the degradation of PrP^{Sc}. Interestingly, in experimental studies, anle138b (a recently developed drug) has been documented to inhibit the formation of pathological aggregates of α -synuclein (Parkinson's disease) and tau (Alzheimer's disease) proteins in addition to inhibiting aggregation of prion protein (PrP^{Sc}) [93,94]. A clear understanding of protein misfolding and its association with metabolic disorders at the molecular level may provide insights into their precise pathogenesis and result in the development of prevention strategies. Furthermore, early diagnosis (preferably in the preclinical stage) and prompt intervention are critical when there are few pathological protein aggregates in the brain. Accordingly, identification of appropriate early diagnostic markers is essential.

PARASITES IN OBESITY-RELATED PATHOLOGIES

Parasitic infestations can have a diverse range of consequences/ sequelae. Ryan et al. [95] posited that helminth-related anti-inflammatory mechanisms may be beneficial. Lifestyle-linked chronic diseases usually have a strong connection with inflammation. In this context, hookworm species, particularly *Necator americanus*, may have a protective effect in inflammatory bowel diseases such as Crohn's disease and ulcerative colitis as well as in celiac disease. In addition, these authors reported an inverse association between human helminth infection and insulin resistance/type 2 diabetes. In an experimental study on male C57BL/6 wild-type mice, infection with *Nippostrongylus brasiliensis* (rodent hookworm) significantly decreased various diabetes-associated parameters such as fasting blood glucose and weight gain [96]. Similarly, studies in human subjects have demonstrated that infection with *Strongyloides stercoralis* (threadworm) can reduce the risk of type 2 diabetes by modulating the expression of different pro-inflammatory cytokines [97-99]. A study from Thailand showed that *Opisthorchis viverrini* (liver fluke) infection had a protective effect against hyperglycemia and metabolic disease risk [100]. In contrast, many studies have reported that individuals with parasitic diseases are more susceptible to diabetes

or that diabetic persons are at higher risk of infection with various parasites, e.g., *Ascaris lumbricoides*, *Echinococcus granulosus*, *Enterobius vermicularis*, *Schistosoma mansoni*, *S. haematobium*, *Hymenolepis nana*, hookworm, and *Taenia* species, as well as protozoan parasites such as *Giardia lamblia*, *Entamoeba histolytica*, and *Cryptosporidium* species (Table 3) [101-116]. Some of these helminths are also considered to be responsible for cancer development. For example, *S. haematobium* can induce squamous cell carcinoma of the urinary bladder, and *O. viverrini* may cause cholangiocarcinoma/bile duct cancer [117]. Unprecedentedly, a report revealed the dissemination of cancer cells from *H. nana* to different organs of a human host [118].

Two major types of primary liver cancer, i.e., hepatocellular carcinoma (~75% of all liver cancers) and cholangiocarcinoma (10%–20% of cases), are uniquely linked to a diverse group of risk factors namely viral hepatitis (hepatitis B virus and hepatitis C virus), obesity, type 2 diabetes, alcohol consumption, smoking, and toxic substances including aflatoxins produced by *Aspergillus* species. Moreover, risk factors for cholangiocarcinoma are inflammatory bowel disease, parasitic infections, and hepatolithiasis. Along with *O. viverrini*, infection with *Clonorchis sinensis* (another liver fluke) can cause the development of cholangiocarcinoma, particularly in Southeast Asia [119]. In addition, *C. sinensis* and *A. lumbricoides* may promote hepatolithiasis [119,120]. Interestingly, the co-occurrence of *O. viverrini* infection and diabetes has been shown to be associated with hepatobiliary tract damage and malignant transformation [121,122].

For helminthic infestations that are predominantly connected with tissue migration, numerous studies have documented the presence of peripheral eosinophilia (or increased number of eosinophils in the peripheral blood) or Loeffler's syndrome (i.e., accumulation of eosinophils in the lung) [123,124]. Although eosinophils play a significant role in various physiologic processes including innate and adaptive immunity, data on the precise role of human eosinophils in defense against helminths are limited. Data on the specific anti-parasitic role of mast cells and basophils, which behave functionally similar to eosinophils in hypersensitivity/allergic inflammation, are also inadequate [125-127]. By contrast, there is a growing body of evidence that neutrophils play a protective role against several parasitic infections such as *E. histolytica*, *Leishmania*, and *Plasmodium* infections [128-130]. Neutrophils may clear the parasites by a number of mechanisms including phagocytosis, generation of reactive oxygen species (ROS), and formation of neutrophil extracellular traps.

Table 3. Selected studies that recorded a positive association between metabolic disorders and protozoan parasites

Study	Subject	Important finding
Udoh et al. (2020); Nigeria [105]	Cross-sectional study of 208 diabetic patients	Diabetic patients were reservoirs of asymptomatic <i>Plasmodium falciparum</i> .
Wyss et al. (2017); Sweden [106]	Retrospective observational study on 937 adults with malaria	Comorbidities, specifically obesity and diabetes, were risk factors for severe malaria in adults diagnosed with <i>Plasmodium falciparum</i> .
Danquah et al. (2010); Ghana [107]	Case-control study of 946 diabetic patients and 520 controls	Patients with type 2 diabetes had a 46% increased risk for infection with <i>Plasmodium falciparum</i> .
Vizzoni et al. (2018); Brazil [108]	Cross-sectional study of 619 patients with Chagas disease	Elderly patients had a high frequency of hypertension and other comorbidities such as diabetes and dyslipidemia.
dos Santos et al. (1999); Brazil [109]	Cross-sectional study of female patients with Chagas disease (n=362) and controls (n=285)	Diabetes/hyperglycemia was more prevalent in patients with the cardiac form of Chagas disease than in controls, or patients with gastrointestinal problems or the asymptomatic form of the disease.
Soltani et al. (2021); Iran [110]	Case-control study of 105 diabetic patients and 150 controls	Chronic <i>Toxoplasma gondii</i> infection was significantly associated with diabetes.
Li et al. (2018); China [111]	Case-control study of 1,200 diabetic patients (type 1, 2, and gestational) and 1,200 matched controls	Diabetic patients had a significantly higher <i>Toxoplasma gondii</i> seroprevalence than controls.
Reeves et al. (2013); Germany [112]	999 Randomly selected adults	Obese persons had significantly higher <i>Toxoplasma gondii</i> seropositivity than non-obese individuals.
Machado et al. (2018); Brazil [113]	Descriptive study of 156 diabetic individuals	Frequencies of <i>Giardia lamblia</i> were higher in individuals with type 2 diabetes than those without.
Sisu et al. (2021); Ghana [114]	Cross-sectional study of 152 diabetes patients	Diabetes patients appeared susceptible to infections with <i>Giardia lamblia</i> , <i>Entamoeba histolytica</i> , and <i>Cryptosporidium parvum</i> .
Akinbo et al. (2013); Nigeria [115]	150 Diabetic patients and 30 controls	Diabetes was significantly associated with intestinal parasitic infections (like <i>Entamoeba histolytica</i>).
Alemu et al. (2018); Ethiopia [116]	Cross-sectional study of 215 diabetic patients	Intestinal parasites were found more frequently in diabetic patients compared to data from other similar studies. <i>Cryptosporidium parvum</i> was the parasite found with the highest frequency.

IMMUNE CELLS IN OBESITY

White blood cells (WBCs or leukocytes) are fundamental components of the immune system. Several studies have reported a quantitative increase in WBCs among obese people [131-133]. A major component of the observed increase in WBC counts is neutrophils. In peripheral blood, more than half of the WBCs (up to about 70%) are neutrophils. It is notable that these cells are present in marginated (recoverable part) and circulating pools in almost equal proportions, while circulating cells have a remarkably short lifespan. Nonetheless, along with increased WBC counts, many investigators have noticed significantly higher levels of neutrophils in obese people [134-136]. Neutrophils from obese subjects have also been found to be functionally more active than neutrophils from lean controls. In obesity, the levels of neutrophil-released superoxides are significantly greater than in normal controls [137]. Apart from an elevated leukocyte count and release of ROS like superoxide (i.e., oxidative burst), the lymphocyte count is also elevated in obesity. In a community-based study of 116 obese women, investigators found that obesity was connected with an increase in certain lymphocyte subset counts, excepting natural killer (NK) and cytotoxic/suppressor T cells [138]. Multivariate analyses of 322 women who were

longitudinally followed from 1999 through 2003 revealed that increasing body weight was independently related to higher WBC, total lymphocyte, CD4, and CD8 counts [139]. Similarly, a study of 119 Saudi female university students showed that both BMI and waist-to-hip ratio (WHR) were significantly correlated with WBC, neutrophil, and CD4 lymphocyte counts [140]. Furthermore, in a cross-sectional, retrospective study of 223 participants (female- 104), BMI was found to have a significant positive relationship with WBC, neutrophil, and lymphocyte counts [141]. These findings indicate that being overweight or obese may impact both innate and adaptive immune responses to numerous pathophysiological phenomena including infections by various pathogens.

Obesity is associated with chronic low-grade inflammation. A relatively inexpensive method to assess the systemic pro-inflammatory state is to determine the blood neutrophil-to-lymphocyte ratio (NLR) [142]. It is believed that this parameter also indicates the stress situation of our body. A healthy range is between 1 and 2; values more than 3 or less than 0.7 in adults are pathognomonic [142]. In a study that compared NLR between obese individuals with insulin resistance (n = 46) and those without (n = 51), both the neutrophil count and NLR were found to be significantly higher in the insulin resistance group [143]. It is worth

mentioning that insulin resistance or type 2 diabetes, which is a common sequela of obesity, is also associated with elevated total and differential WBC counts [131,132,144]. In a study of 600 subjects (BMI: 27.9 ± 4.7) selected from 474,616 patients who visited Severance Hospital, Seoul, South Korea between January 2008 and March 2017, NLR was significantly associated with intra-abdominal visceral adipose tissue volume [145]. In addition, WBCs and levels of the serum inflammatory marker high-sensitivity C-reactive protein (hs-CRP) were strongly correlated with visceral adipose tissue. In a cross-sectional study in Taiwan, a total of 26,016 subjects with metabolic syndrome were recruited between 2004 and 2013 [146]. Of note, the American Heart Association criteria for metabolic syndrome are central obesity, hypertension, high blood glucose and triglycerides, and lower high-density lipoprotein cholesterol levels in the blood. In this study, obesity and related anthropometric parameters such as WHR were positively associated with NLR and C-reactive protein (CRP) in both sexes. Another study of 1,267 subjects (1,068 female and 199 male) collected from the out-patient clinic of Düzce University Hospital, Turkey during 2012–2013 reported that while WBC, neutrophil, and lymphocyte counts as well as level of hs-CRP exhibited a significant interrelationship with BMI, BMI was not correlated with NLR [147]. NLR may not be a better pro-inflammatory indicator than CRP or hs-CRP. Nonetheless, a different study from Turkey of 306 morbidly obese subjects (BMI ≥ 40) demonstrated significantly higher NLR levels in these subjects than normal controls [148]. Moreover, the authors concluded that elevated NLR was an independent and strong predictor of type 2 diabetes in morbidly obese individuals. A cross-sectional study from the 2011–2016 National Health and Nutrition Examination Survey (NHANES 2011–2016, a US population database) recorded a positive association between BMI and NLR in healthy adult female participants ($n = 3,201$) [149]. The above studies indicate that being overweight or obese is linked with certain circulating markers that can be used affordably to evaluate systemic inflammatory status.

Lymphocytes (T-cells, B-cells, NK cells) play a significant role in obesity-linked inflammation [150]. A study from Germany revealed an impaired NK cells phenotype and subset alterations in obesity [151]. Another study of 169 subjects demonstrated an increase in total lymphocytes along with granulocytes and a decrease in the NK cell population among persons with metabolic syndrome and increased visceral adipose tissue [152]. Furthermore, an increase in memory cells was also documented in those subjects with an increased BMI and visceral adipose tissue. Impaired B-cell and T-cell function has been observed in high-fat

(HF) diet-induced obese mice [153].

In HF diet-induced obese C57BL/6J female mice, investigators noted higher circulating monocytes in the HF group than the standard chow diet-fed mice [154]. Likewise, a number of studies involving human subjects have recorded an increased monocyte count in obese individuals [132,138,155,156]. However, other studies found no correlation between BMI and blood monocyte count [140,151]. Monocytes are the largest cells in our blood and normally up to 10% of WBCs are monocytes. Monocytes can be classified into three categories depending on their surface receptors: classical (CD14⁺), intermediate (CD14⁺ and low levels of CD16⁺), and non-classical (CD16⁺ along with lower levels of CD14⁺). In a study of 58 obese subjects and 25 metabolically healthy lean controls, numbers of both intermediate and non-classical monocytes were higher in obese subjects than lean controls [157]. Interestingly, these investigators also found that the levels of intermediate monocytes were positively and significantly related with the obese group's serum triglyceride levels and mean blood pressure. Monocytes can differentiate into macrophages after migration to different tissues of our body—therefore, macrophages are present in the extracellular space. A number of reports have confirmed the accumulation of macrophages in the excess adipose tissue of obese individuals [157–159]. These infiltrated macrophages in adipose tissue create an inflammatory environment due to their production of several pro-inflammatory molecules. Consequently, macrophage infiltration and adipose tissue inflammation are important pathological processes that contribute to systemic inflammation and various complications such as insulin resistance and metabolic syndrome.

INFLUENCE OF OBESITY ON VACCINE EFFECTIVENESS

The efficacy and effectiveness of any vaccine varies considerably and no vaccines can provide 100% protection. According to the WHO, vaccine effectiveness is associated with a number of factors including age, gender, ethnicity, and other accompanying health conditions. The efficacy of a vaccine is evaluated by estimating the development of disease among vaccinated people in comparison with a placebo/control group in controlled clinical trials (i.e., ideal conditions). Conversely, vaccine effectiveness refers to how a vaccine actually performs in different populations.

The basic biological mechanisms underlying vaccine non-responsiveness are not well known. However, there is evidence that both carbohydrate and fat metabolic pathways are involved in responsiveness to vaccines [160]. Furthermore, obesity has been

proposed to be associated with inadequate vaccine responsiveness [161]. Apart from well-established health-related problems such as insulin resistance and hypertension, the obesity-related chronic low-grade inflammatory state has adverse effects on the immune system [162]. Obviously, more research is needed to understand the effects of obesity on vaccine effectiveness.

POTENTIAL INDICATORS OF OBESITY AND INFLAMMATION

Obesity and CRP have been demonstrated to be positively correlated [163]. Furthermore, CRP is widely used as a marker of inflammation. Along with its role in inflammation, CRP also functions significantly in host defense against different pathogenic organisms [164]. CRP is present in at least two distinct forms: pentameric and monomeric (mCRP) isoforms, which have diverse activities and functional characteristics. Dissociation of the pentameric group into monomeric forms occurs at sites of inflammation and the monomeric form then may participate in local inflammation. CRP is primarily produced by the liver and its blood levels may increase from 0.8 mg/L (approximate normal value) to

more than 500 mg/L in inflammatory conditions [165]. However, CRP is involved in several pathophysiological processes such as activation of the complement system, phagocytosis, promotion of apoptosis, release of nitric oxide (NO), and biosynthesis of various cytokines particularly pro-inflammatory cytokines such as TNF- α , MCP-1, and IL-6 [166]. In addition, it is believed that mCRP can stimulate the process of chemotaxis and recruitment of circulating WBCs to sites of inflammation. Studies have documented associations (both positive and negative) between CRP and various hormone-like cytokines (adipokines) that are released from adipose tissue [167-169]; in particular, with the pro-inflammatory adipokine leptin (Fig. 1).

Adipose tissue behaves like an endocrine organ. As mentioned earlier, several hormone-like cytokines or adipokines are secreted from adipose tissue or fat cells. In general, the majority of these adipokines are pro-inflammatory, for example, leptin, visfatin, and resistin. However, a few anti-inflammatory adipokines such as omentin, apelin, and adiponectin are also secreted. Nevertheless, the majority of published studies have focused mainly on two adipokines— pro-inflammatory leptin and anti-inflammatory adiponectin. These two adipokines are involved in a number of

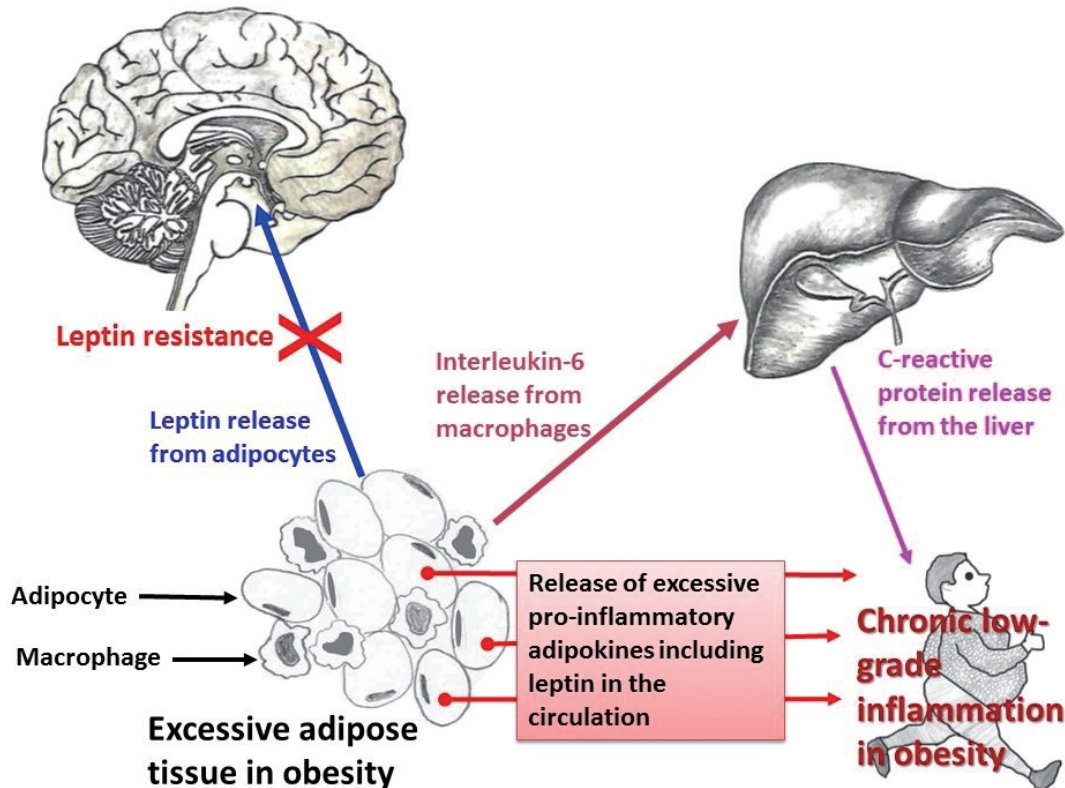


Fig. 1. Relationship among pro-inflammatory adipokines, interleukin-6 (IL-6), and C-reactive protein (CRP) in obesity. Infiltration of macrophages in excess adipose tissue is a common phenomenon. The pleiotropic pro-inflammatory cytokine IL-6, secreted by monocytes/macrophages, induces the biosynthesis of CRP from the liver.

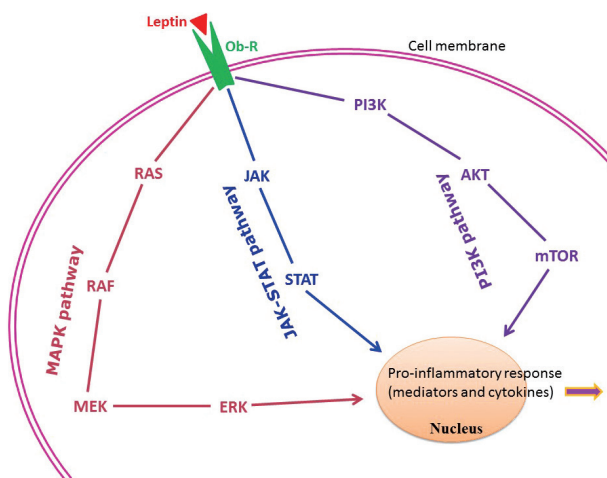


Fig. 2. Principal intracellular signaling pathways of leptin in connection with the chronic low-grade inflammatory state found in obesity. AKT, protein kinase B/serine-threonine kinase; ERK, extracellular signal-regulated kinase; JAK, Janus kinase; MAPK, mitogen-activated protein kinase; MEK, mitogen-activated protein kinase kinase; mTOR, mechanistic/mammalian target of rapamycin; Ob-R, leptin receptor; PI3K, phosphatidylinositol-3-kinase; STAT, signal transducer and activator of transcription.

biological mechanisms both under normal health conditions as well as under pathological circumstances. Interestingly, both adipokines are closely linked with our immune system. Leptin is a 16-kD protein produced primarily by adipocytes. Its main function is maintenance of energy homeostasis through regulation of the arcuate nucleus of the hypothalamus. Leptin is associated with both innate and adaptive immune responses [170]. This adipokine has a close connection with inflammatory molecules including IL-6, TNF- α , NO, eicosanoid, and cyclooxygenase (particularly cyclooxygenase 2) [171], as well as intracellular signaling pathways connected with inflammation such as mitogen-activated protein kinase, Janus kinase/signal transducer and activator of transcription, and phosphatidylinositol-3-kinase (Fig. 2). In addition, leptin promotes chemotaxis, phagocytosis, and release of ROS [170,172].

Higher circulating levels of both leptin and CRP have been demonstrated to be correlated with disease severity and poor prognosis in patients with COVID-19 [173-175]. In a recently published report from Italy, COVID-19 patients with pneumonia had increased circulating levels of leptin and IL-6 and lower adiponectin levels than age- and sex-matched healthy controls [176]. Similar findings were documented in another study from the Netherlands [177]. In contrast, a group of investigators hypothesized that increased blood levels of leptin could be due to patients' obesity and unrelated to disease pathology [178,179]. A number of mechanisms have been proposed to explain the poor prognostic

role of leptin in COVID-19. van der Voort et al. reasoned that SARS-CoV-2 infection, by inducing higher leptin production, might overactivate leptin receptors in pulmonary tissue, ultimately enhancing local inflammation in the lungs [177]. Higher leptin levels could also activate monocytes and thus upregulate the expression of pro-inflammatory cytokines in monocytes, resulting in dysregulation of immune responses, finally leading to ARDS and multiple organ failure [173,180]. As mentioned earlier, leptin receptors are present in all immune cells. Therefore, leptin may affect the functions of these cells. Understanding the precise role of leptin and its interactions with different adipokines (both pro-inflammatory and anti-inflammatory) and other classical hormones such as insulin, insulin-like growth factors, and estrogen, will help elucidate the relationships between obesity-related problems and immune mechanisms.

CONCLUSION

The recent COVID-19 pandemic has renewed interest in infectious diseases, and the disease pathology itself is a meeting place of both communicable and non-communicable diseases. For this reason, many authors have described the grave situation of 2020 and 2021 as 'double pandemics'— the pandemic of COVID-19 and the long-continued global problem of obesity [1,181,182]. Apart from bacterial and fungal infections that are a common occurrence in obesity-related health conditions like type 2 diabetes, a number of prion-like diseases have a close link with these metabolic disorders. Regular assessment of a few markers such as CRP and leptin and adjustment of lifestyle factors could help protect against pathogens as well as metabolic diseases.

Ethics Statement

Not applicable.

Availability of Data and Material

The datasets generated or analyzed during the current study are available in the [MEDLINE] repository.

Code Availability

Not applicable.

ORCID

Amitabha Ray	https://orcid.org/0000-0003-1240-6887
Melissa J. L. Bonorden	https://orcid.org/0000-0003-4786-3164
Rajashree Pandit	https://orcid.org/0000-0002-3219-1126
Katai J. Nkhata	https://orcid.org/0000-0002-5119-8278
Anupam Bishayee	https://orcid.org/0000-0001-9159-960X

Author Contributions

Conceptualization: AR. Data collection and assembly: RP. Formal analysis:

KJN. Project administration: MJLB, RP. Supervision: MJLB, RP. Writing—original draft: AR, MJLB. Figures: KJN. Writing—review & editing: RP, KJN, AB. Approval of final manuscript: all authors.

Conflicts of Interest

The authors declare that they have no potential conflicts of interest.

Funding Statement

No funding to declare.

References

- Gammone MA, D'Orazio N. COVID-19 and obesity: overlapping of two pandemics. *Obes Facts* 2021; 14: 579-85.
- Sattar N, Valabhji J. Obesity as a risk factor for severe COVID-19: summary of the best evidence and implications for health care. *Curr Obes Rep* 2021; 10: 282-9.
- Dayaramani C, De Leon J, Reiss AB. Cardiovascular disease complicating COVID-19 in the elderly. *Medicina (Kaunas)* 2021; 57: 833.
- Ghilotti F, Bellocco R, Ye W, Adami HO, Trolle Lagerros Y. Obesity and risk of infections: results from men and women in the Swedish National March Cohort. *Int J Epidemiol* 2019; 48: 1783-94.
- Dhurandhar NV, Bailey D, Thomas D. Interaction of obesity and infections. *Obes Rev* 2015; 16: 1017-29.
- Frydrych LM, Bian G, O'Lone DE, Ward PA, Delano MJ. Obesity and type 2 diabetes mellitus drive immune dysfunction, infection development, and sepsis mortality. *J Leukoc Biol* 2018; 104: 525-34.
- Chakraborty S, Bhattacharyya R, Banerjee D. Infections: a possible risk factor for type 2 diabetes. *Adv Clin Chem* 2017; 80: 227-51.
- de Heredia FP, Gomez-Martinez S, Marcos A. Obesity, inflammation and the immune system. *Proc Nutr Soc* 2012; 71: 332-8.
- Cinkajzlova A, Mraz M, Haluzik M. Adipose tissue immune cells in obesity, type 2 diabetes mellitus and cardiovascular diseases. *J Endocrinol* 2021; 252: R1-22.
- Iskander K, Farhour R, Ficek M, Ray A. Obesity-related complications: few biochemical phenomena with reference to tumorigenesis. *Malays J Pathol* 2013; 35: 1-15.
- Ray A. Cancer and comorbidity: the role of leptin in breast cancer and associated pathologies. *World J Clin Cases* 2018; 6: 483-92.
- Taylor EB. The complex role of adipokines in obesity, inflammation, and autoimmunity. *Clin Sci (Lond)* 2021; 135: 731-52.
- Fernandez-Riejos P, Najib S, Santos-Alvarez J, et al. Role of leptin in the activation of immune cells. *Mediators Inflamm* 2010; 2010: 568343.
- Conus S, Bruno A, Simon HU. Leptin is an eosinophil survival factor. *J Allergy Clin Immunol* 2005; 116: 1228-34.
- Ahmetaj-Shala B, Vaja R, Atanur SS, George PM, Kirkby NS, Mitchell JA. Cardiorenal tissues express SARS-CoV-2 entry genes and basigin (BSG/CD147) increases with age in endothelial cells. *JACC Basic Transl Sci* 2020; 5: 1111-23.
- Lubbe L, Cozier GE, Oosthuizen D, Acharya KR, Sturrock ED. ACE2 and ACE: structure-based insights into mechanism, regulation and receptor recognition by SARS-CoV. *Clin Sci (Lond)* 2020; 134: 2851-71.
- Wong MK. Angiotensin converting enzymes. In: Takei Y, Ando H, Tsutsui K, eds. *Handbook of hormones*. Oxford: Elsevier Academic Press, 2016; 263-e29D-4.
- Kuba K, Imai Y, Penninger JM. Multiple functions of angiotensin-converting enzyme 2 and its relevance in cardiovascular diseases. *Circ J* 2013; 77: 301-8.
- Varga Z. Endotheliitis in COVID-19. *Pathologe* 2020; 41(Suppl 2): 99-102.
- Varga Z, Flammer AJ, Steiger P, et al. Endothelial cell infection and endotheliitis in COVID-19. *Lancet* 2020; 395: 1417-8.
- Al-Benna S. Association of high level gene expression of ACE2 in adipose tissue with mortality of COVID-19 infection in obese patients. *Obes Med* 2020; 19: 100283.
- Al-Sabah S, Al-Haddad M, Al-Youha S, Jamal M, Almazeedi S. COVID-19: impact of obesity and diabetes on disease severity. *Clin Obes* 2020; 10: e12414.
- Cevik M, Kuppalli K, Kindrachuk J, Peiris M. Virology, transmission, and pathogenesis of SARS-CoV-2. *BMJ* 2020; 371: m3862.
- Albini A, Di Guardo G, Noonan DM, Lombardo M. The SARS-CoV-2 receptor, ACE-2, is expressed on many different cell types: implications for ACE-inhibitor- and angiotensin II receptor blocker-based cardiovascular therapies. *Intern Emerg Med* 2020; 15: 759-66.
- Halim AA, Alsayed B, Embarak S, Yaseen T, Dabbous S. Clinical characteristics and outcome of ICU admitted MERS corona virus infected patients. *Egypt J Chest Dis Tuberc* 2016; 65: 81-7.
- Badawi A, Ryoo SG. Prevalence of comorbidities in the Middle East respiratory syndrome coronavirus (MERS-CoV): a systematic review and meta-analysis. *Int J Infect Dis* 2016; 49: 129-33.
- Honce R, Schultz-Cherry S. Impact of obesity on influenza A virus pathogenesis, immune response, and evolution. *Front Immunol* 2019; 10: 1071.
- Bhattacharya I, Ghayor C, Perez Dominguez A, Weber FE. From influenza virus to novel corona virus (SARS-CoV-2): the contribution of obesity. *Front Endocrinol (Lausanne)* 2020; 11: 556962.
- Ndako JA, Nwankiti OO, Olorundare JO, et al. Studies on the serological markers for hepatitis B virus infection among type 2 diabetic patients. *J Clin Lab Anal* 2021; 35: e23464.
- Iovanescu VE, Streba CT, Ionescu M, et al. Diabetes mellitus and renal involvement in chronic viral liver disease. *J Med Life* 2015; 8: 483-7.
- Cheng AY, Kong AP, Wong VW, et al. Chronic hepatitis B viral infection independently predicts renal outcome in type 2 diabetic patients. *Diabetologia* 2006; 49: 1777-84.
- Virseda Chamorro I, Virseda Chamorro M, Prieto Carbajo RI, Jaqueti Aroca J. Hepatitis C as a risk factor of diabetes mellitus type 2. *Rev Clin Esp* 2006; 206: 167-71.
- Arao M, Murase K, Kusakabe A, et al. Prevalence of diabetes mellitus in Japanese patients infected chronically with hepatitis C virus. *J Gastroenterol* 2003; 38: 355-60.
- Dworzanski J, Drop B, Kliszczewska E, Strycharz-Dudziak M, Polz-Dacewicz M. Prevalence of Epstein-Barr virus, human papillomavirus, cytomegalovirus and herpes simplex virus type 1 in patients with diabetes mellitus type 2 in south-eastern Poland. *PLoS One* 2019; 14: e0222607.
- Karjala Z, Neal D, Rohrer J. Association between HSV1 seropositivity and obesity: data from the National Health and Nutritional Examination Survey, 2007-2008. *PLoS One* 2011; 6: e19092.
- Fernandez-Real JM, Ferri MJ, Vendrell J, Ricart W. Burden of infection and fat mass in healthy middle-aged men. *Obesity (Silver Spring)* 2007; 15: 245-52.
- Sun YH, Pei WD, Wu YJ, Wang GG. Association of herpes simplex virus type 2 infection with dyslipidemia in Chinese. *Zhong-*

- hua Yi Xue Za Zhi 2003; 83: 1774-7.
38. Woelfle T, Linkohr B, Waterboer T, et al. Health impact of seven herpesviruses on (pre)diabetes incidence and HbA(1c): results from the KORA cohort. *Diabetologia* 2022; 65: 1328-38.
 39. Yoo SG, Han KD, Lee KH, La Y, Kwon DE, Han SH. Impact of cytomegalovirus disease on new-onset type 2 diabetes mellitus: population-based matched case-control cohort study. *Diabetes Metab J* 2019; 43: 815-29.
 40. Chen S, de Craen AJ, Raz Y, et al. Cytomegalovirus seropositivity is associated with glucose regulation in the oldest old: results from the Leiden 85-plus study. *Immun Ageing* 2012; 9: 18.
 41. Roberts BW, Cech I. Association of type 2 diabetes mellitus and seroprevalence for cytomegalovirus. *South Med J* 2005; 98: 686-92.
 42. Chiu B, Viira E, Tucker W, Fong IW. Chlamydia pneumoniae, cytomegalovirus, and herpes simplex virus in atherosclerosis of the carotid artery. *Circulation* 1997; 96: 2144-8.
 43. Reinholdt K, Thomsen LT, Munk C, et al. Incidence of HPV-related anogenital intraepithelial neoplasia and cancer in men with diabetes compared with the general population. *Epidemiology* 2021; 32: 705-11.
 44. Sobti A, Sharif-Askari FS, Khan S, et al. Logistic regression prediction model identify type 2 diabetes mellitus as a prognostic factor for human papillomavirus-16 associated head and neck squamous cell carcinoma. *PLoS One* 2019; 14: e0217000.
 45. Slama L, Barrett BW, Abraham AG, et al. Risk for incident diabetes is greater in prediabetic men with HIV than without HIV. *AIDS* 2021; 35: 1605-14.
 46. Kubiak RW, Kratz M, Motala AA, et al. Clinic-based diabetes screening at the time of HIV testing and associations with poor clinical outcomes in South Africa: a cohort study. *BMC Infect Dis* 2021; 21: 789.
 47. Hema A, Poda A, Tougouma JB, et al. Diabetes mellitus and high blood pressure over risk in HIV-infected people followed at Sourou Sanou University Hospital Day Hospital, Bobo-Dioulasso 2018. *Rev Epidemiol Sante Publique* 2021; 69: 72-7.
 48. Jeremiah K, Filteau S, Faurholt-Jepsen D, et al. Diabetes prevalence by HbA1c and oral glucose tolerance test among HIV-infected and uninfected Tanzanian adults. *PLoS One* 2020; 15: e0230723.
 49. Albashir AA. The potential impacts of obesity on COVID-19. *Clin Med (Lond)* 2020; 20: e109-13.
 50. Singh AK, Majumdar S, Singh R, Misra A. Role of corticosteroid in the management of COVID-19: a systemic review and a Clinician's perspective. *Diabetes Metab Syndr* 2020; 14: 971-8.
 51. Hughes S, Troise O, Donaldson H, Mughal N, Moore LS. Bacterial and fungal coinfection among hospitalized patients with COVID-19: a retrospective cohort study in a UK secondary-care setting. *Clin Microbiol Infect* 2020; 26: 1395-9.
 52. Rawson TM, Wilson RC, Holmes A. Understanding the role of bacterial and fungal infection in COVID-19. *Clin Microbiol Infect* 2021; 27: 9-11.
 53. Cafardi J, Haas D, Lamarre T, Feinberg J. Opportunistic fungal infection associated with COVID-19. *Open Forum Infect Dis* 2021; 8: ofab016.
 54. Taylor M, Ghodasara A, Ismail A, Gauhar U, El-Kersh K. Disseminated histoplasmosis in an immunocompetent patient after COVID-19 pneumonia. *Cureus* 2021; 13: e17269.
 55. Amin A, Vartanian A, Poladian N, et al. Root causes of fungal coinfections in COVID-19 infected patients. *Infect Dis Rep* 2021; 13: 1018-35.
 56. Erener S. Diabetes, infection risk and COVID-19. *Mol Metab* 2020; 39: 101044.
 57. Choudhary NK, Jain AK, Soni R, Gahlot N. Mucormycosis: a deadly black fungus infection among COVID-19 patients in India. *Clin Epidemiol Glob Health* 2021; 12: 100900.
 58. Kuchi Bhotla H, Balasubramanian B, Meyyazhagan A, et al. Opportunistic mycoses in COVID-19 patients/survivors: epidemic inside a pandemic. *J Infect Public Health* 2021; 14: 1720-6.
 59. Speth C, Rambach G, Wurzner R, Lass-Flörl C. Complement and fungal pathogens: an update. *Mycoses* 2008; 51: 477-96.
 60. Soni S, Namdeo Pudake R, Jain U, Chauhan N. A systematic review on SARS-CoV-2-associated fungal coinfections. *J Med Virol* 2022; 94: 99-109.
 61. Prusiner SB. Novel proteinaceous infectious particles cause scrapie. *Science* 1982; 216: 136-44.
 62. Linden R. The biological function of the prion protein: a cell surface scaffold of signaling modules. *Front Mol Neurosci* 2017; 10: 77.
 63. Sikorska B, Liberski PP. Human prion diseases: from Kuru to variant Creutzfeldt-Jakob disease. *Subcell Biochem* 2012; 65: 457-96.
 64. Aguilar-Calvo P, Garcia C, Espinosa JC, Andreoletti O, Torres JM. Prion and prion-like diseases in animals. *Virus Res* 2015; 207: 82-93.
 65. Duyckaerts C, Clavaguera F, Potier MC. The prion-like propagation hypothesis in Alzheimer's and Parkinson's disease. *Curr Opin Neurol* 2019; 32: 266-71.
 66. Iadanza MG, Jackson MP, Hewitt EW, Ranson NA, Radford SE. A new era for understanding amyloid structures and disease. *Nat Rev Mol Cell Biol* 2018; 19: 755-73.
 67. Lee J, Kim SY, Hwang KJ, Ju YR, Woo HJ. Prion diseases as transmissible zoonotic diseases. *Osong Public Health Res Perspect* 2013; 4: 57-66.
 68. Tumminia A, Vinciguerra F, Parisi M, Frittitta L. Type 2 diabetes mellitus and Alzheimer's disease: role of insulin signalling and therapeutic implications. *Int J Mol Sci* 2018; 19: 3306.
 69. Kellett KA, Hooper NM. Prion protein and Alzheimer disease. *Prion* 2009; 3: 190-4.
 70. Sitamagari KK, Masood W. Creutzfeldt Jakob disease [Internet]. Treasure Island: StatPearls Publishing, 2022 [cited 2022 Mar 9]. Available from: <https://www.ncbi.nlm.nih.gov/books/NBK507860/>.
 71. Collinge J, Whitfield J, McKintosh E, et al. A clinical study of kuru patients with long incubation periods at the end of the epidemic in Papua New Guinea. *Philos Trans R Soc Lond B Biol Sci* 2008; 363: 3725-39.
 72. Guo Y, Xu Y, Lin X, et al. Creutzfeldt-Jakob disease: alterations of gut microbiota. *Front Neurol* 2022; 13: 832599.
 73. Yang D, Zhao D, Shah SZA, et al. Implications of gut microbiota dysbiosis and metabolic changes in prion disease. *Neurobiol Dis* 2020; 135: 104704.
 74. Fang P, Kazmi SA, Jameson KG, Hsiao EY. The microbiome as a modifier of neurodegenerative disease risk. *Cell Host Microbe* 2020; 28: 201-22.
 75. Liu S, Gao J, Zhu M, Liu K, Zhang HL. Gut microbiota and dysbiosis in Alzheimer's disease: implications for pathogenesis and treatment. *Mol Neurobiol* 2020; 57: 5026-43.
 76. Nishiwaki H, Ito M, Ishida T, et al. Meta-analysis of gut dysbiosis in Parkinson's disease. *Mov Disord* 2020; 35: 1626-35.
 77. Gasmi Benahmed A, Gasmi A, Dosa A, et al. Association between the gut and oral microbiome with obesity. *Anaerobe* 2021; 70:

- 102248.
78. Thomas MS, Blesso CN, Calle MC, Chun OK, Puglisi M, Fernandez ML. Dietary influences on gut microbiota with a focus on metabolic syndrome. *Metab Syndr Relat Disord* 2022; 20: 429-39.
 79. Gradisteanu Pircalabioru G, Liaw J, Gundogdu O, et al. Effects of the lipid profile, type 2 diabetes and medication on the metabolic syndrome-associated gut microbiome. *Int J Mol Sci* 2022; 23: 7509.
 80. Bielka W, Przekaz A, Pawlik A. The role of the gut microbiota in the pathogenesis of diabetes. *Int J Mol Sci* 2022; 23: 480.
 81. Gomez-Gutierrez R, Morales R. The prion-like phenomenon in Alzheimer's disease: evidence of pathology transmission in humans. *PLoS Pathog* 2020; 16: e1009004.
 82. Zhou J, Liu B. Alzheimer's disease and prion protein. *Intractable Rare Dis Res* 2013; 2: 35-44.
 83. Soto C. Transmissible proteins: expanding the prion heresy. *Cell* 2012; 149: 968-77.
 84. Liberski PP, Gajos A, Sikorska B, Lindenbaum S. Kuru, the first human prion disease. *Viruses* 2019; 11: 232.
 85. Brandner S, Jaunmuktane Z. Prion disease: experimental models and reality. *Acta Neuropathol* 2017; 133: 197-222.
 86. Manuelidis L, Chakrabarty T, Miyazawa K, Nduom NA, Emmerling K. The kuru infectious agent is a unique geographic isolate distinct from Creutzfeldt-Jakob disease and scrapie agents. *Proc Natl Acad Sci U S A* 2009; 106: 13529-34.
 87. Ayers JL, Brooks MM, Rutherford NJ, et al. Robust central nervous system pathology in transgenic mice following peripheral injection of alpha-synuclein fibrils. *J Virol* 2017; 91: e02095-16.
 88. Betemps D, Verchere J, Brot S, et al. Alpha-synuclein spreading in M83 mice brain revealed by detection of pathological alpha-synuclein by enhanced ELISA. *Acta Neuropathol Commun* 2014; 2: 29.
 89. Boluda S, Iba M, Zhang B, Raible KM, Lee VM, Trojanowski JQ. Differential induction and spread of tau pathology in young PS19 tau transgenic mice following intracerebral injections of pathological tau from Alzheimer's disease or corticobasal degeneration brains. *Acta Neuropathol* 2015; 129: 221-37.
 90. Guo JL, Narasimhan S, Changolkar L, et al. Unique pathological tau conformers from Alzheimer's brains transmit tau pathology in nontransgenic mice. *J Exp Med* 2016; 213: 2635-54.
 91. Lam S, Petit F, Herard AS, et al. Transmission of amyloid-beta and tau pathologies is associated with cognitive impairments in a primate. *Acta Neuropathol Commun* 2021; 9: 165.
 92. Morales R, Bravo-Alegria J, Duran-Aniotz C, Soto C. Titration of biologically active amyloid-beta seeds in a transgenic mouse model of Alzheimer's disease. *Sci Rep* 2015; 5: 9349.
 93. Wagner J, Ryazanov S, Leonov A, et al. Anle138b: a novel oligomer modulator for disease-modifying therapy of neurodegenerative diseases such as prion and Parkinson's disease. *Acta Neuropathol* 2013; 125: 795-813.
 94. Wagner J, Krauss S, Shi S, et al. Reducing tau aggregates with anle138b delays disease progression in a mouse model of tauopathies. *Acta Neuropathol* 2015; 130: 619-31.
 95. Ryan SM, Eichenberger RM, Ruscher R, Giacomin PR, Loukas A. Harnessing helminth-driven immunoregulation in the search for novel therapeutic modalities. *PLoS Pathog* 2020; 16: e1008508.
 96. Khudhair Z, Alhallaif R, Eichenberger RM, et al. Gastrointestinal helminth infection improves insulin sensitivity, decreases systemic inflammation, and alters the composition of gut microbiota in distinct mouse models of type 2 diabetes. *Front Endocrinol (Lausanne)* 2020; 11: 606530.
 97. Hays R, Esterman A, Giacomin P, Loukas A, McDermott R. Does *Strongyloides stercoralis* infection protect against type 2 diabetes in humans? Evidence from Australian Aboriginal adults. *Diabetes Res Clin Pract* 2015; 107: 355-61.
 98. Rajamanickam A, Munisankar S, Bhootra Y, et al. Metabolic consequences of concomitant *Strongyloides stercoralis* infection in patients with type 2 diabetes mellitus. *Clin Infect Dis* 2019; 69: 697-704.
 99. Rajamanickam A, Munisankar S, Dolla C, et al. Helminth infection modulates systemic pro-inflammatory cytokines and chemokines implicated in type 2 diabetes mellitus pathogenesis. *PLoS Negl Trop Dis* 2020; 14: e0008101.
 100. Muthukumar R, Suttiaprapa S, Mairiang E, et al. Effects of *Opisthorchis viverrini* infection on glucose and lipid profiles in human hosts: a cross-sectional and prospective follow-up study from Thailand. *Parasitol Int* 2020; 75: 102000.
 101. Htun NS, Odermatt P, Paboriboune P, et al. Association between helminth infections and diabetes mellitus in adults from the Lao People's Democratic Republic: a cross-sectional study. *Infect Dis Poverty* 2018; 7: 105.
 102. Moudgil V, Rana R, Tripathi PK, Farooq U, Sehgal R, Khan MA. Coprevalence of parasitic infections and diabetes in Sub-Himalayan region of Northern India. *Int J Health Sci (Qassim)* 2019; 13: 19-24.
 103. Ambachew S, Assefa M, Tegegne Y, Zeleke AJ. The prevalence of intestinal parasites and their associated factors among diabetes mellitus patients at the University of Gondar Referral Hospital, northwest Ethiopia. *J Parasitol Res* 2020; 2020: 8855965.
 104. Almugadam BS, Ibrahim MK, Liu Y, et al. Association of urogenital and intestinal parasitic infections with type 2 diabetes individuals: a comparative study. *BMC Infect Dis* 2021; 21: 20.
 105. Udoh BE, Iwalokun BA, Etukumana E, Amoo J. Asymptomatic falciparum malaria and its effects on type 2 diabetes mellitus patients in Lagos, Nigeria. *Saudi J Med Med Sci* 2020; 8: 32-40.
 106. Wyss K, Wangdahl A, Vesterlund M, et al. Obesity and diabetes as risk factors for severe *Plasmodium falciparum* malaria: results from a Swedish nationwide study. *Clin Infect Dis* 2017; 65: 949-58.
 107. Danquah I, Bedu-Addo G, Mockenhaupt FP. Type 2 diabetes mellitus and increased risk for malaria infection. *Emerg Infect Dis* 2010; 16: 1601-4.
 108. Vizzoni AG, Varela MC, Sangenis LH, Hasslocher-Moreno AM, do Brasil P, Saraiva RM. Ageing with Chagas disease: an overview of an urban Brazilian cohort in Rio de Janeiro. *Parasit Vectors* 2018; 11: 354.
 109. dos Santos VM, da Cunha SF, Teixeira Vde P, et al. Frequency of diabetes mellitus and hyperglycemia in chagasic and non-chagasic women. *Rev Soc Bras Med Trop* 1999; 32: 489-96.
 110. Soltani S, Tavakoli S, Sabaghan M, Kahvaz MS, Pashmforosh M, Foroutan M. The probable association between chronic *Toxoplasma gondii* infection and type 1 and type 2 diabetes mellitus: a case-control study. *Interdiscip Perspect Infect Dis* 2021; 2021: 2508780.
 111. Li YX, Xin H, Zhang XY, et al. *Toxoplasma gondii* infection in diabetes mellitus patients in China: seroprevalence, risk factors, and case-control studies. *Biomed Res Int* 2018; 2018: 4723739.
 112. Reeves GM, Mazaheri S, Snitker S, et al. A Positive association between *T. gondii* seropositivity and obesity. *Front Public Health* 2013; 1: 73.

113. Machado ER, Matos NO, Rezende SM, et al. Host-parasite interactions in individuals with type 1 and 2 diabetes result in higher frequency of *Ascaris lumbricoides* and *Giardia lamblia* in type 2 diabetic individuals. *J Diabetes Res* 2018; 2018: 4238435.
114. Sisu A, Abugri J, Ephraim RK, et al. Intestinal parasite infections in diabetes mellitus patients: a cross-sectional study of the Bolgatanga municipality, Ghana. *Sci Afr* 2021; 11: e00680.
115. Akinbo FO, Olujobi SO, Omoregie R, Egbe C. Intestinal parasitic infections among diabetes mellitus patients. *Biomark Genom Med* 2013; 5: 44-7.
116. Alemu G, Jemal A, Zerdo Z. Intestinal parasitosis and associated factors among diabetic patients attending Arba Minch Hospital, Southern Ethiopia. *BMC Res Notes* 2018; 11: 689.
117. van Tong H, Brindley PJ, Meyer CG, Velavan TP. Parasite infection, carcinogenesis and human malignancy. *EBioMedicine* 2017; 15: 12-23.
118. Muehlenbachs A, Bhatnagar J, Agudelo CA, et al. Malignant transformation of *Hymenolepis nana* in a human host. *N Engl J Med* 2015; 373: 1845-52.
119. Tyson GL, El-Serag HB. Risk factors for cholangiocarcinoma. *Hepatology* 2011; 54: 173-84.
120. Huang MH, Chen CH, Yen CM, et al. Relation of hepatolithiasis to helminthic infestation. *J Gastroenterol Hepatol* 2005; 20: 141-6.
121. Chaidee A, Onsurathum S, Intuyod K, et al. Co-occurrence of opisthorchiasis and diabetes exacerbates morbidity of the hepatobiliary tract disease. *PLoS Negl Trop Dis* 2018; 12: e0006611.
122. Thinkhamrop K, Khuntikeo N, Laohasiriwong W, Chupanit P, Kelly M, Suwannatrai AT. Association of comorbidity between *Opisthorchis viverrini* infection and diabetes mellitus in the development of cholangiocarcinoma among a high-risk population, northeastern Thailand. *PLoS Negl Trop Dis* 2021; 15: e0009741.
123. Klion AD, Ackerman SJ, Bochner BS. Contributions of eosinophils to human health and disease. *Annu Rev Pathol* 2020; 15: 179-209.
124. Shibuya T. Eosinophilic response in parasitic diseases. *Nihon Rinsho* 1993; 51: 825-31.
125. Linnemann LC, Reitz M, Feyerabend TB, Breloer M, Hartmann W. Limited role of mast cells during infection with the parasitic nematode *Litomosoides sigmodontis*. *PLoS Negl Trop Dis* 2020; 14: e0008534.
126. Lu F, Huang S. The roles of mast cells in parasitic protozoan infections. *Front Immunol* 2017; 8: 363.
127. Mitre E, Nutman TB. Lack of basophilia in human parasitic infections. *Am J Trop Med Hyg* 2003; 69: 87-91.
128. Rosales C. Neutrophils vs. amoebas: immunity against the protozoan parasite *Entamoeba histolytica*. *J Leukoc Biol* 2021; 110: 1241-52.
129. Passelli K, Billion O, Tacchini-Cottier F. The impact of neutrophil recruitment to the skin on the pathology induced by *Leishmania* infection. *Front Immunol* 2021; 12: 649348.
130. Aitken EH, Alemu A, Rogerson SJ. Neutrophils and malaria. *Front Immunol* 2018; 9: 3005.
131. Marzullo P, Minocci A, Giarda P, et al. Lymphocytes and immunoglobulin patterns across the threshold of severe obesity. *Endocrine* 2014; 45: 392-400.
132. Yoshimura A, Ohnishi S, Orito C, et al. Association of peripheral total and differential leukocyte counts with obesity-related complications in young adults. *Obes Facts* 2015; 8: 1-16.
133. Erdal E, Inanir M. Platelet-to-lymphocyte ratio (PLR) and platelet-crit (PCT) in young patients with morbid obesity. *Rev Assoc Med Bras* (1992) 2019; 65: 1182-7.
134. Dixon JB, O'Brien PE. Obesity and the white blood cell count: changes with sustained weight loss. *Obes Surg* 2006; 16: 251-7.
135. Xu X, Su S, Wang X, et al. Obesity is associated with more activated neutrophils in African American male youth. *Int J Obes (Lond)* 2015; 39: 26-32.
136. Raghavan V, Gunasekar D, Rao KR. Relevance of haematologic parameters in obese women with or without metabolic syndrome. *J Clin Diagn Res* 2016; 10: EC11-6.
137. Brotfain E, Hadad N, Shapira Y, et al. Neutrophil functions in morbidly obese subjects. *Clin Exp Immunol* 2015; 181: 156-63.
138. Nieman DC, Henson DA, Nehlsen-Cannarella SL, et al. Influence of obesity on immune function. *J Am Diet Assoc* 1999; 99: 294-9.
139. Womack J, Tien PC, Feldman J, et al. Obesity and immune cell counts in women. *Metabolism* 2007; 56: 998-1004.
140. Al-Sufyani AA, Mahassni SH. Obesity and immune cells in Saudi females. *Innate Immun* 2011; 17: 439-50.
141. Furuncuoglu Y, Tulgar S, Dogan AN, Cakar S, Tulgar YK, Cakiroglu B. How obesity affects the neutrophil/lymphocyte and platelet/lymphocyte ratio, systemic immune-inflammatory index and platelet indices: a retrospective study. *Eur Rev Med Pharmacol Sci* 2016; 20: 1300-6.
142. Zahorec R. Neutrophil-to-lymphocyte ratio, past, present and future perspectives. *Bratisl Lek Listy* 2021; 122: 474-88.
143. Karakaya S, Altay M, Kaplan Efe F, et al. The neutrophil-lymphocyte ratio and its relationship with insulin resistance in obesity. *Turk J Med Sci* 2019; 49: 245-8.
144. Kim DJ, Noh JH, Lee BW, et al. The associations of total and differential white blood cell counts with obesity, hypertension, dyslipidemia and glucose intolerance in a Korean population. *J Korean Med Sci* 2008; 23: 193-8.
145. Yu JY, Choi WJ, Lee HS, Lee JW. Relationship between inflammatory markers and visceral obesity in obese and overweight Korean adults: an observational study. *Medicine (Baltimore)* 2019; 98: e14740.
146. Syauby A, Hsu CY, Rau HH, Chao JC. Association of dietary patterns, anthropometric measurements, and metabolic parameters with C-reactive protein and neutrophil-to-lymphocyte ratio in middle-aged and older adults with metabolic syndrome in Taiwan: a cross-sectional study. *Nutr J* 2018; 17: 106.
147. Bahadir A, Baltaci D, Turker Y, et al. Is the neutrophil-to-lymphocyte ratio indicative of inflammatory state in patients with obesity and metabolic syndrome? *Anatol J Cardiol* 2015; 15: 816-22.
148. Yilmaz H, Ucan B, Sayki M, et al. Usefulness of the neutrophil-to-lymphocyte ratio to prediction of type 2 diabetes mellitus in morbid obesity. *Diabetes Metab Syndr* 2015; 9: 299-304.
149. Thavaraputta S, Dennis JA, Ball S, Laoveeravat P, Nugent K. Relation of hematologic inflammatory markers and obesity in otherwise healthy participants in the National Health and Nutrition Examination Survey, 2011-2016. *Proc (Bayl Univ Med Cent)* 2020; 34: 17-21.
150. Ip BC, Hogan AE, Nikolajczyk BS. Lymphocyte roles in metabolic dysfunction: of men and mice. *Trends Endocrinol Metab* 2015; 26: 91-100.
151. Bahr I, Jahn J, Zipprich A, Pahlow I, Spielmann J, Kielstein H. Impaired natural killer cell subset phenotypes in human obesity. *Immunol Res* 2018; 66: 234-44.

152. Rodriguez CP, Gonzalez MC, Aguilar-Salinas CA, Najera-Medina O. Peripheral lymphocytes, obesity, and metabolic syndrome in young adults: an immunometabolism study. *Metab Syndr Relat Disord* 2018; 16: 342-9.
153. Sato Mito N, Suzui M, Yoshino H, Kaburagi T, Sato K. Long term effects of high fat and sucrose diets on obesity and lymphocyte proliferation in mice. *J Nutr Health Aging* 2009; 13: 602-6.
154. Breznik JA, Foley KP, Maddiboina D, Schertzer JD, Sloboda DM, Bowdish DM. Effects of obesity-associated chronic inflammation on peripheral blood immunophenotype are not mediated by TNF in female C57BL/6J mice. *Immunohorizons* 2021; 5: 370-83.
155. Tenorio TR, Farah BQ, Ritti-Dias RM, et al. Relation between leukocyte count, adiposity, and cardiorespiratory fitness in pubertal adolescents. *Einstein (Sao Paulo)* 2014; 12: 420-4.
156. Friedrich K, Sommer M, Strobel S, et al. Perturbation of the monocyte compartment in human obesity. *Front Immunol* 2019; 10: 1874.
157. Christou KA, Christou GA, Karamoutsios A, et al. Metabolically healthy obesity is characterized by a proinflammatory phenotype of circulating monocyte subsets. *Metab Syndr Relat Disord* 2019; 17: 259-65.
158. Subramanian V, Ferrante AW Jr. Obesity, inflammation, and macrophages. *Nestle Nutr Workshop Ser Pediatr Program* 2009; 63: 151-9.
159. Bastarrachea RA, Lopez-Alvarenga JC, Bolado-Garcia VE, Tellez-Mendoza J, Laviada-Molina H, Comuzzie AG. Macrophages, inflammation, adipose tissue, obesity and insulin resistance. *Gac Med Mex* 2007; 143: 505-12.
160. Shehata HM, Murphy AJ, Lee MK, et al. Sugar or fat?: metabolic requirements for immunity to viral infections. *Front Immunol* 2017; 8: 1311.
161. Wiedermann U, Garner-Spitzer E, Wagner A. Primary vaccine failure to routine vaccines: why and what to do? *Hum Vaccin Immunother* 2016; 12: 239-43.
162. Young KM, Gray CM, Bekker LG. Is obesity a risk factor for vaccine non-responsiveness? *PLoS One* 2013; 8: e82779.
163. Choi J, Joseph L, Pilote L. Obesity and C-reactive protein in various populations: a systematic review and meta-analysis. *Obes Rev* 2013; 14: 232-44.
164. Wu Y, Potempa LA, El Kebir D, Filep JG. C-reactive protein and inflammation: conformational changes affect function. *Biol Chem* 2015; 396: 1181-97.
165. Pepys MB, Hirschfield GM. C-reactive protein: a critical update. *J Clin Invest* 2003; 111: 1805-12.
166. Sproston NR, Ashworth JJ. Role of C-reactive protein at sites of inflammation and infection. *Front Immunol* 2018; 9: 754.
167. Viikari LA, Huupponen RK, Viikari JS, et al. Relationship between leptin and C-reactive protein in young Finnish adults. *J Clin Endocrinol Metab* 2007; 92: 4753-8.
168. Hribal ML, Fiorentino TV, Sesti G. Role of C reactive protein (CRP) in leptin resistance. *Curr Pharm Des* 2014; 20: 609-15.
169. Liu Y, Liu C, Jiang C, et al. C-reactive protein inhibits high-molecular-weight adiponectin expression in 3T3-L1 adipocytes via PI3K/Akt pathway. *Biochem Biophys Res Commun* 2016; 472: 19-25.
170. Naylor C, Petri WA Jr. Leptin regulation of immune responses. *Trends Mol Med* 2016; 22: 88-98.
171. La Cava A. Leptin in inflammation and autoimmunity. *Cytokine* 2017; 98: 51-8.
172. Dayakar A, Chandrasekaran S, Veronica J, Maurya R. Leptin induces the phagocytosis and protective immune response in Leishmania donovani infected THP-1 cell line and human PBMCs. *Exp Parasitol* 2016; 160: 54-9.
173. Baltodano-Calle MJ, Polo-Vasquez JS, Romani-Pozo A, Gutarra-Saldana D, Guija-Poma E. Leptin as a potential prognostic marker of the severity of COVID-19 infection in obese patients. *Nutr Metab Cardiovasc Dis* 2022; 32: 743-4.
174. Smilowitz NR, Kunichoff D, Garshick M, et al. C-reactive protein and clinical outcomes in patients with COVID-19. *Eur Heart J* 2021; 42: 2270-9.
175. Giner-Galvan V, Pomares-Gomez FJ, Quesada JA, et al. C-Reactive protein and serum albumin ratio: a feasible prognostic marker in hospitalized patients with COVID-19. *Biomedicines* 2022; 10: 1393.
176. Tonon F, Di Bella S, Giudici F, et al. Discriminatory value of adiponectin to leptin ratio for COVID-19 pneumonia. *Int J Endocrinol* 2022; 2022: 9908450.
177. van der Voort PHJ, Moser J, Zandstra DF, et al. Leptin levels in SARS-CoV-2 infection related respiratory failure: a cross-sectional study and a pathophysiological framework on the role of fat tissue. *Heliyon* 2020; 6: e04696.
178. Larsson A, Lipcsey M, Hultstrom M, Frithiof R, Eriksson M. Plasma leptin is increased in intensive care patients with COVID-19: an investigation performed in the PronMed-Cohort. *Biomedicines* 2021; 10: 4.
179. Blot M, David M, Nguyen M, et al. Are adipokines the missing link between obesity, immune response, and outcomes in severe COVID-19? *Int J Obes (Lond)* 2021; 45: 2126-31.
180. Wang J, Xu Y, Zhang X, et al. Leptin correlates with monocytes activation and severe condition in COVID-19 patients. *J Leukoc Biol* 2021; 110: 9-20.
181. Honce R, Schultz-Cherry S. A tale of two pandemics: obesity and COVID-19. *J Travel Med* 2020; 27: taaa097.
182. Brandao SCS, Godoi E, de Oliveira Cordeiro LH, et al. COVID-19 and obesity: the meeting of two pandemics. *Arch Endocrinol Metab* 2021; 65: 3-13.

Single-cell and spatial sequencing application in pathology

Yoon-Seob Kim^{1,2}, Jinyong Choi^{1,3}, Sug Hyung Lee^{3,4,5}

¹Department of Microbiology, ²Precision Medicine Research Center/Integrated Research Center for Genome Polymorphism, ³Biomedicine & Health Sciences, ⁴Department of Pathology, and ⁵Cancer Evolution Research Center, College of Medicine, The Catholic University of Korea, Seoul, Korea

Traditionally, diagnostic pathology uses histology representing structural alterations in a disease's cells and tissues. In many cases, however, it is supplemented by other morphology-based methods such as immunohistochemistry and fluorescent in situ hybridization. Single-cell RNA sequencing (scRNA-seq) is one of the strategies that may help tackle the heterogeneous cells in a disease, but it does not usually provide histologic information. Spatial sequencing is designed to assign cell types, subtypes, or states according to the mRNA expression on a histological section by RNA sequencing. It can provide mRNA expressions not only of diseased cells, such as cancer cells but also of stromal cells, such as immune cells, fibroblasts, and vascular cells. In this review, we studied current methods of spatial transcriptome sequencing based on their technical backgrounds, tissue preparation, and analytic procedures. With the pathology examples, useful recommendations for pathologists who are just getting started to use spatial sequencing analysis in research are provided here. In addition, leveraging spatial sequencing by integration with scRNA-seq is reviewed. With the advantages of simultaneous histologic and single-cell information, spatial sequencing may give a molecular basis for pathological diagnosis, improve our understanding of diseases, and have potential clinical applications in prognostics and diagnostic pathology.

Key Words: Single-cell sequencing; Spatial sequencing; Pathology; Histology; Transcriptome; Diseases

Received: November 14, 2022 **Revised:** December 7, 2022 **Accepted:** December 12, 2022

Corresponding Author: Sug Hyung Lee, MD, PhD, Department of Pathology, College of Medicine, The Catholic University of Korea, 222 Banpo-daero, Seocho-gu, Seoul 06591, Korea
 Tel: +82-2-2258-7311, Fax: +82-2-537-6586, E-mail: suhulee@catholic.ac.kr

Corresponding Author: Jinyong Choi, PhD, Department of Microbiology, College of Medicine, The Catholic University of Korea, 222 Banpo-daero, Seocho-gu, Seoul 06591, Korea
 Tel: +82-2-3147-8368, Fax: +82-2-537-0572, E-mail: jchoi@catholic.ac.kr

Because tissue cells represent the fundamental unit of biology, deciphering the phenotypic heterogeneity between cells, the intercellular interactions, and the spatial organization of cells in tissues are crucial for understanding the pathophysiology of disease [1]. Recently developed high-throughput technologies, such as single-cell RNA sequencing (scRNA-seq) and spatial transcriptomics (ST), have brought revolutionary insights into diverse research areas, including developmental biology, cancer, immunology, and neuroscience [2,3]. However, the necessary tissue dissociation step of scRNA-seq destroys information on their spatial context, which is crucial to understand the intercellular interactions underlying normal and disease tissues [4]. Moreover, integrating scRNA-seq and ST data can address this limitation and thus provide novel insights for homeostasis, development, and disease microenvironment, which cannot be informed by scRNA-seq alone [4]. In this review, from a pathologist's view, we aim to suggest the overview of the integrative analysis of scRNA-seq and ST and describe representative research studies.

THE INTRODUCTION OF SINGLE-CELL RNA SEQUENCING

Conventional transcriptome technologies, including microarrays and bulk RNA sequencing (RNA-seq), have shown a way to assay only the average expression RNA expression signal of all cell types within the tissue. However, gene expression is heterogeneous between many tissue cells and even between the same cell types, and thus these technologies are likely to miss important cell-to-cell variability [2]. After the introduction in 2009 [5], the droplet-based scRNA-seq has been the most popular scRNA-seq technology that can capture the transcriptomes in tens of thousands of single cells per sample to dissect transcriptomic heterogeneity masked in bulk RNA-seq [6]. Since there have been numerous reviews that comprehensively introduce the technological aspects and various analysis methodologies of scRNA-seq [2,7-12] and ST [3,13-16], we briefly introduce the overview of principles and analytical methods of scRNA-seq and ST in this

review. We summarize the strengths and limitations of clinical and experimental gene expression methods: recent scRNA-seq and ST, compared to conventional histopathology and bulk RNA-seq (Fig. 1).

The ordinary procedures for the generating scRNA-seq data include single-cell isolation and capture, cell lysis, reverse transcription, cDNA amplification, and library preparation [17]. Single-cell isolation and capture is the first process of acquiring

high-quality single cells from a tissue in which all transcripts from single-cell will be uniquely barcoded. Polyadenylated mRNA molecules are captured by poly[T]-primers, reverse transcribed, polymerase chain reaction amplified, and resulting cDNA from every cell is pooled and sequenced by next-generation sequencing (NGS) [18]. Many methodologies are different in terms of the number of cell per sample (the breadth of cellular profiling) and the number of genes per cell (the depth of cellular profil-

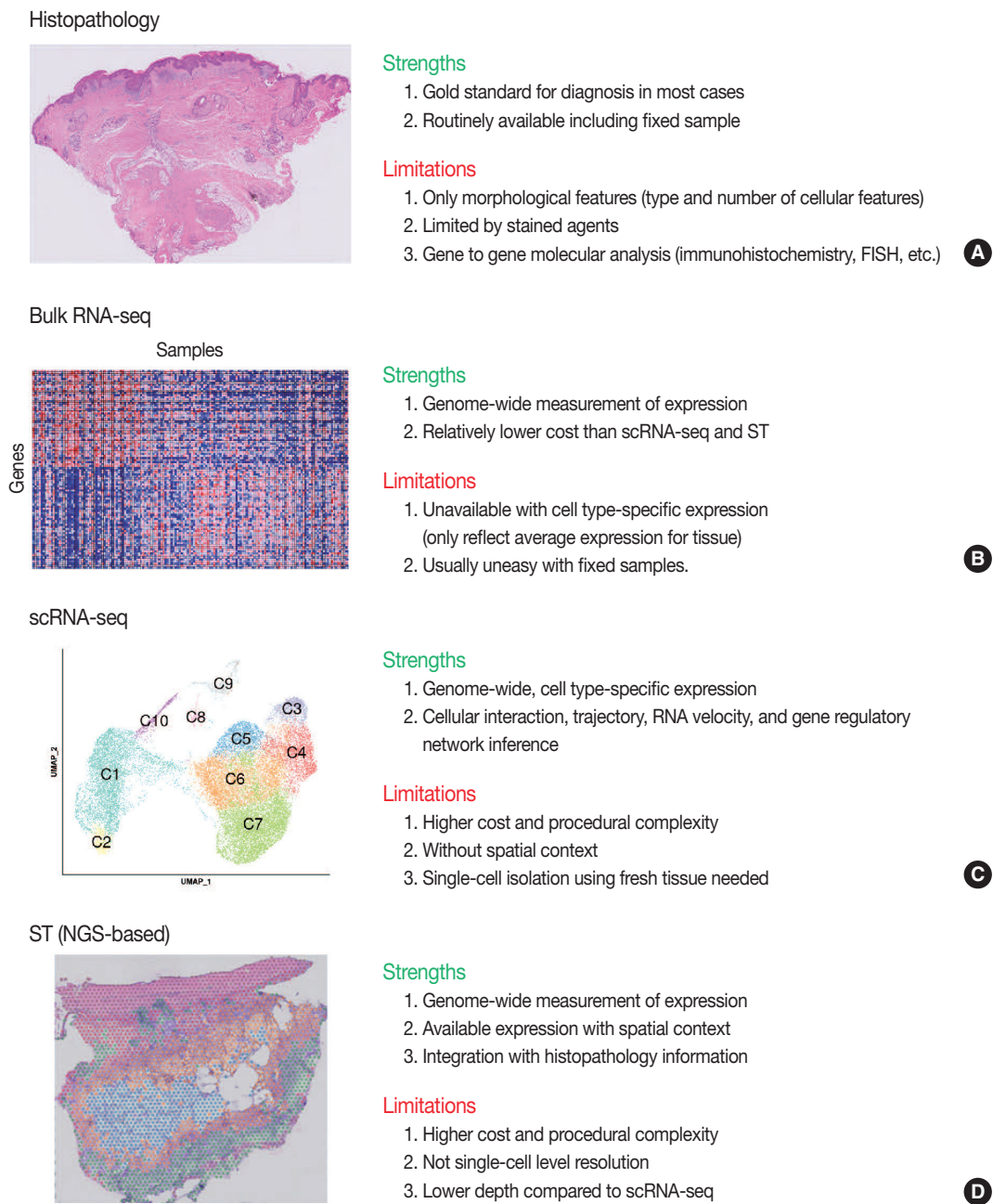


Fig. 1. Overview of strengths and limitations of clinical and experimental methods for gene expression. Conventional methods of histopathology (A) and bulk RNA sequencing (RNA-seq) (B). FISH, fluorescence in situ hybridization. Recent methods of single-cell RNA sequencing (scRNA-seq) (C) and next-generation sequencing (NGS)-based spatial transcriptomics (ST) (D).

ing) [11]. Some provide full-length transcript coverage, while others only partial sequences from either 3' or 5' end of the transcript [7]. The preparation of high-quality single-cell suspension is key to successful scRNA-seq studies, and researchers should acknowledge the possible protocol-specific biases that can be developed during single-cell isolation [19,20]. While scRNA-seq needs prior tissue dissociation of fresh tissue for the preparation of single-cell suspension, single-nucleus RNA-seq capturing only transcripts present in the nucleus can be prepared from frozen or fresh tissue without the need for tissue dissociation [1,21].

Workflows for scRNA-seq analysis include pre-processing (quality control, normalization, data correction, feature selection, and dimensionality reduction) and cell/gene-level downstream analysis (clustering, cluster annotation, trajectory inference, and differential expression analysis). The best-practice recommendations and details for each step of the analysis pipeline are comprehensively described elsewhere [8]. There have been various tools for analyzing scRNA-seq data, among which R-package Seurat is the most commonly used tool for analysis and visualization of scRNA-seq data [22]. Researchers easily find the sample analysis pipeline using Seurat R-package with the representative dataset at https://satijalab.org/seurat/articles/pbmc3k_tutorial.html. Major applications of scRNA-seq include the clustering and identification of known or novel cell types, inferring cellular trajectory, and inferring gene regulatory networks [2]. Unsupervised clustering is preferred in most cases for clustering and identification of cell types, although supervised clustering using prior assumptions and canonical marker genes is also available [18]. Dimensional reduction and visualization are performed using algorithms such as principal component analysis, t-distributed stochastic neighbor embedding, and uniform manifold approximation and projection, followed by cell clustering into subpopulations with biological significance using algorithms such as a graph-based clustering [18,20]. In addition to the unsupervised clustering, cell types can be determined by reference-based annotation using reference expression profiles from bulk RNA-seq [23]. Trajectory inference reconstructs dynamic cellular trajectories during the cellular transition between cell identities underlying biological process of interest [2]. Tools for trajectory inference have been developed for ordering single cells in pseudotime, an abstract unit of progress through the single-cell trajectory, by taking advantage of individual cells' asynchronous progression of transcriptional dynamics along the biological process [24]. For trajectory inference, RNA velocity that is the time derivative of the gene expression state, can be analyzed to predict the future

state of individual cells by distinguishing between unspliced and spliced mRNAs [25]. From scRNA-seq data, gene regulatory networks underlying gene expression by transcription factors, co-factors, and signaling molecules can be inferred, which may help to pinpoint key factors that determine phenotype in healthy systems as well as in diseases [26,27].

THE INTRODUCTION OF SPATIAL TRANSCRIPTOMICS

Overview of ST was summarized in Fig. 2. One of the major limitations of scRNA-seq is the loss of spatial context since cells should be liberated from whole tissue before scRNA-seq. The spatial location of a cell can reveal helpful information for defining cellular phenotypes, cell states, intercellular interactions, and cell functions [15]. Although histopathology is the gold standard for diagnosis in most cases, it is limited by the type and number of cellular features delineated by stained agents [3]. Traditional methodologies for applying technologies for analyzing expression within tissues (in situ) include in situ hybridization (ISH) and immunohistochemistry; however, these methods limit analysis to, at most, a handful of genes or proteins at a time [13]. The recent development of ST technologies enables profile the whole transcriptome in spatially resolved way [13]. ST technologies can describe an unbiased picture of spatial composition that may provide valuable biological insights into development, physiology, and diseases microenvironment.

As technologies and computational approaches for generating and analyzing ST data are rapidly evolving, there are various options for ST technologies that differ in terms of the number of genes and the size of tissues that can be assayed [13]. ST technologies are primarily categorized as (1) NGS-based, encoding positional information onto transcripts; and (2) imaging-based approaches, comprising in situ sequencing-based or ISH-based methods [28,29]. Recently introduced and widely used NGS-based ST have shown increased resolution (55 μm spot diameter with 100 μm center-to-center distance) and sensitivity (more than 10,000 transcripts per spot) compared to the previous ones [13]. Currently, commercial kits utilize fresh-frozen tissues for ST; however cutting-edge technologies have shown successful ST application to formalin-fixed, paraffin-embedded (FFPE) tissues that will expand the usages of ST for numerous FFPE samples in biobanks [30]. ISH-based high-plex RNA imaging (HPRI) is a targeted ST method that localizes and quantifies RNA transcripts of hundreds of genes in an intact tissue through multiplexed fluorescent microscopy [4]. Depth is a limiting factor for

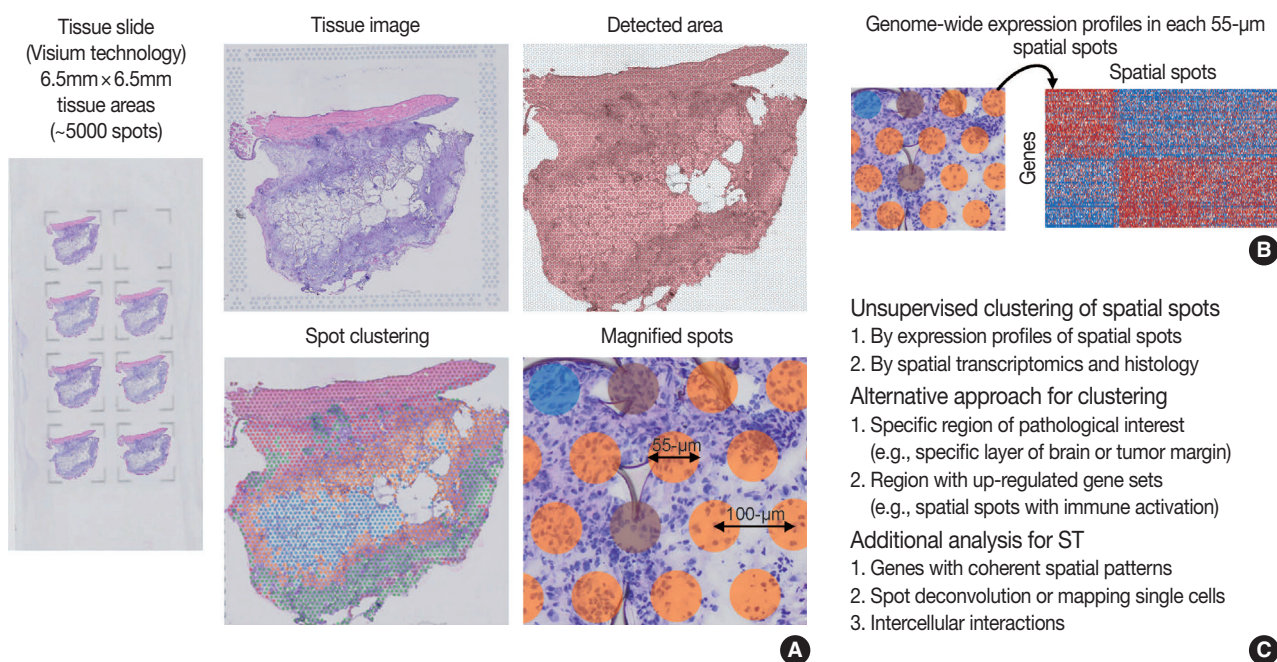


Fig. 2. Overview of spatial transcriptomics (ST) analysis. (A) Example of tissue slide (Visium technology) for ST. Original tissue image, detected area, spot clustering of ST data by unsupervised clustering (spatial spots colored by spot clusters), and magnified view of spatial spots are shown. Distance between spatial spots were 100-µm, and each spot has a diameter of 55-µm. (B) ST can measure genome-wide expression profiles in each 55-µm spatial spots. (C) Analysis strategies for ST data.

NGS-based techniques, while lack of transcriptome-wide coverage is for HPRI. Therefore, current ST technologies themselves still cannot reveal the deep transcriptomic information in tissue at single-cell level with accuracy, although they can shed light on the architecture of the cell-type distribution or the niches enriched for a specific gene set [4]. Until HPRI improves the transcriptome coverage and applicability of untargeted methods, the ST may stay advantageous, especially for obtaining an unbiased characterization of the spatial transcriptomics [4].

Compared to scRNA-seq, the workflows for ST analysis and its integration with scRNA-seq have emerged recently and rapidly evolved. As previously described, the workflows for ST analysis are akin to those in scRNA-seq. Several additional points are needed for analyzing ST: (1) to identify genes with coherent spatial patterns, (2) spot deconvolution or mapping single cells, and (3) analysis and visualization in the intercellular interactions [3,15]. Researchers can utilize various ST methodologies for clustering analysis of spatially coherent domains and identification of spatially domain-enriched genes [3]. Unsupervised clustering and subsequent characterization aim to identify clusters of spots and sets of genes with biological significances [13]. A cluster of spots may be characterized by pathological findings or by molecular marker genes [13], indicating pathologists' roles in the biological interpretation of ST data. Alternative to the un-

supervised clustering, researchers may focus on a specific region of interest, for example a specific layer in the brain or the interface between cancer and microenvironment, or on context-specific genes, for example known gene sets or highly variable genes [13]. Widely used techniques for ST utilize 50–100-µm spot diameters with mixture of 10–20 cells, indicating that the spatial spots in the ST dataset may correspond to mixture expressions of several cells [31]. The proportion of cell type (deconvolution) or the designation of cell type (mapping) can be analyzed using both scRNA-seq and ST data, which will be explained in detail in the later chapter of the manuscript [4]. Surely, while scRNA-seq analysis cannot distinguish short-distance (juxtacrine and paracrine) and long-distance (endocrine) intercellular signaling due to lack of spatial information, ST dataset can seek the spatial coordinate of cell signaling [3].

While currently often underused, the tissue image from ST analysis can be improved to show high-resolution information when combined with the knowledges in the field of histopathology [13]. For example, a previous study revealed that integrating ST data with high-resolution histology image data could improve the resolution of ST data [32]. Pathologists may play the main role in the integrative analysis and biological interpretation of ST for histopathology.

INTEGRATIVE ANALYSIS OF SINGLE-CELL AND SPATIAL RNA SEQUENCING

Integrated analysis of scRNA-seq and ST is summarized in Fig. 3. The major limitations for scRNA-seq and ST are loss of spatial information and low resolution, respectively. Furthermore, the lack of reliable ST methods to implement deep sequencing necessitates the need to integrate scRNA-seq and ST data. Thus, simultaneous measurements followed by the integrated analysis of scRNA-seq and ST from the same tissue may improve the data quality. Herein, we summarize strategies for integrating scRNA-seq and ST data: deconvolution, mapping, and spatially informed ligand-receptor analysis.

Because of the high read-depth and single-cell resolution of scRNA-seq compared with ST, cell subpopulations need to be defined firstly by scRNA-seq in a given tissue. There are two primary approaches for integration of scRNA-seq and ST data: first, deconvolution for ST without single-cell resolution such as spatial barcoding and second, mapping for ST with single-cell resolution such as HPRI [4]. Deconvolution refers to the process of quantifying the relative proportion of each cell type in spatial spots

[15]. There are two main ways of the deconvolution: (1) inferring the proportion of cellular subtypes for a given spot, and (2) scoring a given spatial transcriptomic spot for how strongly it corresponds to a single cellular subtype. SPOTlight tool is good at validating the deconvolution analysis in terms of the accuracy, sensitivity, and specificity of cell-type detection [31]. The mapping has two facets: mapping assigned scRNA-seq-based cell subtypes to each cell and mapping each scRNA-seq cell to a specific niche or region of a tissue [13]. For mapping, *pciSeq* is one of the popular tools that have shown effectiveness in classifying cell type [33]. Researchers can adopt following statistical models for deconvolution and mapping: regression-based deconvolution and probabilistic modeling for deconvolution, and cell-type scoring and cluster-based mapping for mapping [4]. The possible mismatch between cell subtypes present in scRNA-seq data and those in spatial sequencing data that may complicate deconvolution and mapping should be acknowledged [4].

Spatial data from ST, for example, the spot clusters from unsupervised clustering and the areas of pathological interests, can be analyzed for deconvolution or mapping of cell types identi-

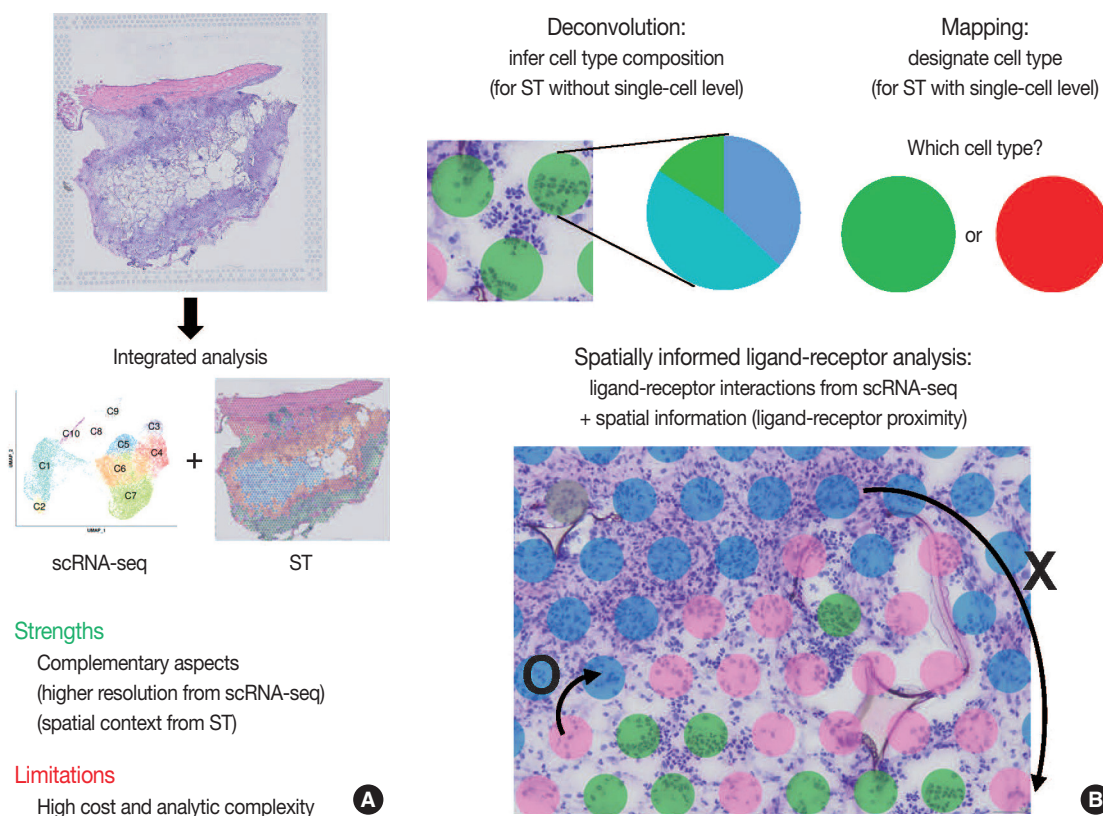


Fig. 3. Schematic view of integrated analysis of single-cell RNA sequencing (scRNA-seq) and spatial transcriptomics (ST). (A) Strengths and limitations of integrated analysis of scRNA-seq and ST. (B) Analysis strategies for integrated scRNA-seq and ST data.

fied by scRNA-seq. Unsupervised clustering of ST data can be performed using either gene expression of spatial spots alone or in combination with gene expression and histopathology [15], where pathologists may play an important role in the interpretation of pathological findings between identified cell subpopulations. Instead, the areas of pathological interests can be determined from the matched histological images by the pathologists, which are further investigated for distinct molecules of the areas: proportion of cell subtype, distinct expression, and intercellular interactions. For example, in cancer tissues, interesting areas of the tumor core and leading edges can be annotated by the pathologists for further investigations [34].

Since intercellular interactions, especially juxtacrine and paracrine communications, are spatially restricted, ST data is well suited to validate the ligand-receptor interactions computed from scRNA-seq [4,35]. Standard algorithms for predicting ligand-receptor interaction pairs adopt both scRNA-seq data and a known database for ligand-receptor interactions, such as Cell-

phoneDB [36]. In this, researchers can use ligand-receptor and ligand-receptor-target co-expression restriction to establish intercellular communications from scRNA-seq data. From ST data, a further restriction can be applied by ligand-receptor proximity where the spatial context can enhance the intercellular interaction analysis. Integrated analysis of scRNA-seq and ST can be used to nominate the receptors and ligands that mediate communication between the proximal cell subpopulations. The Giotto workflow is one of widely used tools for anticipating the likelihood that a given ligand-receptor interaction is used more or less based on the proximity of all of the co-expressing cells [37].

EXAMPLES FOR THE INTEGRATION OF SINGLE-CELL RNA SEQUENCING AND SPATIAL TRANSCRIPTOMICS TECHNOLOGIES

Our group previously published the integrative analysis of scRNA-seq and ST of a foreign body reaction, which character-

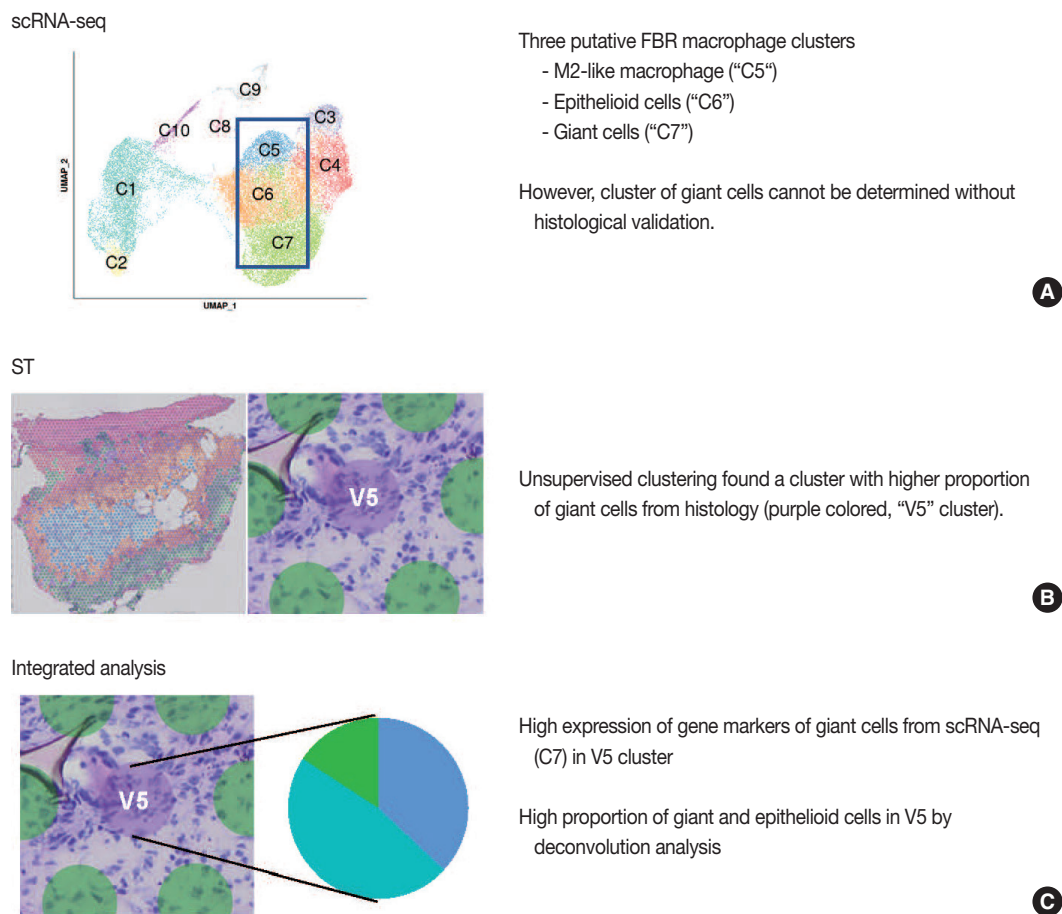


Fig. 4. Example study of integrated analysis [38]. Findings from single-cell RNA sequencing (scRNA-seq) (A), spatial transcriptomics (ST) (B), and integrated analysis of scRNA-seq and ST (C) are summarized. FBR, foreign body reaction.

ized the molecular signatures and cellular interactions of epithelioid cells and multinucleated giant cells in the foreign body reaction (Fig. 4) [38]. From the scRNA-seq data, we designated three putative clusters of macrophages, such as M2-like macrophage, epithelioid cells, and giant cells; however the designation of cell types cannot be completely from scRNA-seq data alone [38]. Unsupervised clustering of the ST data using the same foreign body reaction tissue found a cluster with the smallest number of spatial spots with scattered distribution, in which pathological examination found a relatively higher proportion of giant cells compared with other spot clusters [38]. Consistently, deconvolution analysis also supported a relatively high proportion of giant and epithelioid cells in this cluster [38]. scRNA-seq discovered the marker genes for giant cells, which were further validated by both ST and immunohistochemistry [38].

We also present another two integration studies for human cancer transcriptomics. Profiling of human cutaneous squamous cell carcinoma (cSCCs) and matched normal tissues was performed via scRNA-seq, ST, and multiplexed ion beam imaging in ten cSCC patients [39]. In the scRNA-seq, tumor cells in cSCC showed four subpopulations, three recapitulating normal skin epidermis and a tumor-specific keratinocyte population unique to the cancer [39]. Integration analysis of the scRNA-seq and ST found that tumor-specific keratinocytes expressing epithelial-to-mesenchymal signature were mainly located to the tumor leading edges with enrichment of adjacent stroma of fibrovascular niche, thus being a hub for intercellular communication [39]. Multiplexed ion beam imaging, ST technology at a single-cell level, was further performed for validation [39]. Next, an integrative study of scRNA-seq and ST were performed in two tumors from patients with pancreas ductal adenocarcinomas [40], where high concordance was found between pathological annotation by histological features and unsupervised clustering of ST data [40]. A statistical approach to overlap cell type-specific and tissue region-specific gene sets, called the multimodal intersection analysis, was used for identification and mapping of cell-type subpopulations across tissue regions [40]. A multimodal intersection analysis found that the subpopulations of ductal cells, macrophages, dendritic cells and cancer cells were spatially restricted [40]. Co-enrichment analysis of the multiple cell types found that inflammatory fibroblasts and cancer cells shared a stress-response gene module, which was further supported by a cancer genome database and immunofluorescence experiments [40].

These example studies in area of tissue pathology highlight the importance of integrated analysis of scRNA-seq and ST along with histopathological features, in which the integrated

approach helps to overcome the limitations of any individual method [38-40]. These studies confirmed that, the cellular subtypes in spatial spots by deconvolution or mapping from integrated scRNA-seq and ST were concordant with the histological findings, supporting the robustness of the integrative analysis [38-40]. Also, spatially informed ligand-receptor analysis suggested candidates of pivotal intercellular interactions in the pathological area of interest, which would lead to further mechanistic studies [38-40].

CONCLUSION

Integrated analysis of scRNA-seq and ST spatially maps cell subtypes identified from scRNA-seq to decipher how cell populations are spatiotemporally participated in shaping tissue phenotypes. Such integration can also see the high-resolution maps of cellular subpopulations and intercellular interactions within the tissues, bridging the gap between the molecular characterization of a disease by the transcriptomics and the classical histological approaches. Among various available options, the study methodology of scRNA-seq and ST should be carefully designed and selected according to the biological questions. Especially for pathologists, coupling scRNA-seq and ST information with traditional morphological details will suggest novel insights for the molecular characterization as well as the cellular and spatial context of a disease, which can help diagnose and manage the diseases. The analytic tools in ST are rapidly evolving, especially in the area of scRNA-seq and ST integration. Given the rapid development, we expect new methodologies of a genome-wide ST at high sensitivity with a real single-cell resolution. In addition, the future direction of this area would be multiple integrative analyses of scRNA-seq and ST with other single-cell multi-omics technologies such as the genome, chromatin accessibility, and DNA methylation sequencing [41-43].

Ethics Statement

Not applicable.

Availability of Data and Material

Not applicable.

Code Availability

Not applicable.

ORCID

Yoon-Seob Kim <https://orcid.org/0000-0003-1660-010X>
 Jinyong Choi <https://orcid.org/0000-0003-2474-2837>
 Sug Hyung Lee <http://orcid.org/0000-0001-6677-0487>

Author Contributions

Conceptualization: SHL. Data curation: YSK. Formal analysis: YSK. Funding acquisition: SHL. Investigation: YSK, SHL. Methodology: YSK, SHL. Project administration: SHL. Resources: SHL. Software: YSK. Supervision: SHL. Visualization: YSK. Writing—original draft: YSK, JC, SHL. Writing—review & editing: JC, SHL.

Conflicts of Interest

The authors declare that they have no potential conflicts of interest.

Funding Statement

This study was supported by grants from National Research Foundation of Korea (2019R1A5A2027588 and 2020R1A2C2005031).

References

- Stewart BJ, Clatworthy MR. Applying single-cell technologies to clinical pathology: progress in nephropathology. *J Pathol* 2020; 250: 693-704.
- Hwang B, Lee JH, Bang D. Single-cell RNA sequencing technologies and bioinformatics pipelines. *Exp Mol Med* 2018; 50: 1-14.
- Liu B, Li Y, Zhang L. Analysis and visualization of spatial transcriptomic data. *Front Genet* 2021; 12: 785290.
- Longo SK, Guo MG, Ji AL, Khavari PA. Integrating single-cell and spatial transcriptomics to elucidate intercellular tissue dynamics. *Nat Rev Genet* 2021; 22: 627-44.
- Tang F, Barbacioru C, Wang Y, et al. mRNA-Seq whole-transcriptome analysis of a single cell. *Nat Methods* 2009; 6: 377-82.
- Zheng GX, Terry JM, Belgrader P, et al. Massively parallel digital transcriptional profiling of single cells. *Nat Commun* 2017; 8: 14049.
- Chen G, Ning B, Shi T. Single-cell RNA-seq technologies and related computational data analysis. *Front Genet* 2019; 10: 317.
- Luecken MD, Theis FJ. Current best practices in single-cell RNA-seq analysis: a tutorial. *Mol Syst Biol* 2019; 15: e8746.
- Andrews TS, Kiselev VY, McCarthy D, Hemberg M. Tutorial: guidelines for the computational analysis of single-cell RNA sequencing data. *Nat Protoc* 2021; 16: 1-9.
- Kashima Y, Sakamoto Y, Kaneko K, Seki M, Suzuki Y, Suzuki A. Single-cell sequencing techniques from individual to multiomics analyses. *Exp Mol Med* 2020; 52: 1419-27.
- Papalexi E, Satija R. Single-cell RNA sequencing to explore immune cell heterogeneity. *Nat Rev Immunol* 2018; 18: 35-45.
- Ziegenhain C, Vieth B, Parekh S, et al. Comparative analysis of single-cell RNA sequencing methods. *Mol Cell* 2017; 65: 631-43.
- Rao A, Barkley D, Franca GS, Yanai I. Exploring tissue architecture using spatial transcriptomics. *Nature* 2021; 596: 211-20.
- Lewis SM, Asselin-Labat ML, Nguyen Q, et al. Spatial omics and multiplexed imaging to explore cancer biology. *Nat Methods* 2021; 18: 997-1012.
- Williams CG, Lee HJ, Asatsuma T, Vento-Tormo R, Haque A. An introduction to spatial transcriptomics for biomedical research. *Genome Med* 2022; 14: 68.
- Moor AE, Itzkovitz S. Spatial transcriptomics: paving the way for tissue-level systems biology. *Curr Opin Biotechnol* 2017; 46: 126-33.
- Jovic D, Liang X, Zeng H, Lin L, Xu F, Luo Y. Single-cell RNA sequencing technologies and applications: a brief overview. *Clin Transl Med* 2022; 12: e694.
- Haque A, Engel J, Teichmann SA, Lonnberg T. A practical guide to single-cell RNA-sequencing for biomedical research and clinical applications. *Genome Med* 2017; 9: 75.
- Denisenko E, Guo BB, Jones M, et al. Systematic assessment of tissue dissociation and storage biases in single-cell and single-nucleus RNA-seq workflows. *Genome Biol* 2020; 21: 130.
- Lafzi A, Moutinho C, Picelli S, Heyn H. Tutorial: guidelines for the experimental design of single-cell RNA sequencing studies. *Nat Protoc* 2018; 13: 2742-57.
- Slyper M, Porter CBM, Ashenberg O, et al. A single-cell and single-nucleus RNA-Seq toolbox for fresh and frozen human tumors. *Nat Med* 2020; 26: 792-802.
- Hao Y, Hao S, Andersen-Nissen E, et al. Integrated analysis of multimodal single-cell data. *Cell* 2021; 184: 3573-87.
- Aran D, Looney AP, Liu L, et al. Reference-based analysis of lung single-cell sequencing reveals a transitional profibrotic macrophage. *Nat Immunol* 2019; 20: 163-72.
- Trapnell C, Cacchiarelli D, Grimsby J, et al. The dynamics and regulators of cell fate decisions are revealed by pseudotemporal ordering of single cells. *Nat Biotechnol* 2014; 32: 381-6.
- La Manno G, Soldatov R, Zeisel A, et al. RNA velocity of single cells. *Nature* 2018; 560: 494-8.
- Pratapa A, Jalihal AP, Law JN, Bharadwaj A, Murali TM. Benchmarking algorithms for gene regulatory network inference from single-cell transcriptomic data. *Nat Methods* 2020; 17: 147-54.
- Skok Gibbs C, Jackson CA, Saldi GA, et al. High-performance single-cell gene regulatory network inference at scale: the Inferelator 3.0. *Bioinformatics* 2022; 38: 2519-28.
- Zhuang X. Spatially resolved single-cell genomics and transcriptomics by imaging. *Nat Methods* 2021; 18: 18-22.
- Larsson L, Frisen J, Lundeberg J. Spatially resolved transcriptomics adds a new dimension to genomics. *Nat Methods* 2021; 18: 15-8.
- Villacampa EG, Larsson L, Mirzazadeh R, et al. Genome-wide spatial expression profiling in formalin-fixed tissues. *Cell Genomics* 2021; 1: 100065.
- Elosua-Bayes M, Nieto P, Mereu E, Gut I, Heyn H. SPOTlight: seeded NMF regression to deconvolute spatial transcriptomics spots with single-cell transcriptomes. *Nucleic Acids Res* 2021; 49: e50.
- Bergenstrahle L, He B, Bergenstrahle J, et al. Super-resolved spatial transcriptomics by deep data fusion. *Nat Biotechnol* 2022; 40: 476-9.
- Qian X, Harris KD, Hauling T, et al. Probabilistic cell typing enables fine mapping of closely related cell types in situ. *Nat Methods* 2020; 17: 101-6.
- Arora R, Cao C, Kumar M, et al. Spatial transcriptomics reveals distinct and conserved tumor core and edge architectures that predict survival and targeted therapy response. Preprint at: <https://doi.org/10.1101/2022.09.04.505581> (2022).
- Armingol E, Officer A, Harismendy O, Lewis NE. Deciphering cell-cell interactions and communication from gene expression. *Nat Rev Genet* 2021; 22: 71-88.
- Efremova M, Vento-Tormo M, Teichmann SA, Vento-Tormo R. CellPhoneDB: inferring cell-cell communication from combined expression of multi-subunit ligand-receptor complexes. *Nat Protoc* 2020; 15: 1484-506.
- Dries R, Zhu Q, Dong R, et al. Giotto: a toolbox for integrative analysis and visualization of spatial expression data. *Genome Biol* 2021; 22: 78.
- Kim YS, Shin S, Choi EJ, et al. Different molecular features of epithelioid and giant cells in foreign body reaction identified by single-

- cell RNA sequencing. *J Invest Dermatol* 2022; 142: 3232-42.
39. Ji AL, Rubin AJ, Thrane K, et al. Multimodal analysis of composition and spatial architecture in human squamous cell carcinoma. *Cell* 2020; 182: 497-514.
40. Moncada R, Barkley D, Wagner F, et al. Integrating microarray-based spatial transcriptomics and single-cell RNA-seq reveals tissue architecture in pancreatic ductal adenocarcinomas. *Nat Biotechnol* 2020; 38: 333-42.
41. Argelaguet R, Clark SJ, Mohammed H, et al. Multi-omics profiling of mouse gastrulation at single-cell resolution. *Nature* 2019; 576: 487-91.
42. Abascal F, Harvey LM, Mitchell E, et al. Somatic mutation landscapes at single-molecule resolution. *Nature* 2021; 593: 405-10.
43. Lee J, Hyeon DY, Hwang D. Single-cell multiomics: technologies and data analysis methods. *Exp Mol Med* 2020; 52: 1428-42.

Perspectives on single-nucleus RNA sequencing in different cell types and tissues

Nayoung Kim^{1,2*}, Huiram Kang^{1,2*}, Areum Jo^{1,2}, Seung-Ah Yoo^{2,3}, Hae-Ock Lee^{1,2,4}

¹Department of Microbiology, College of Medicine, The Catholic University of Korea, Seoul;

²Department of Biomedicine and Health Sciences, Graduate School, The Catholic University of Korea, Seoul;

³Department of Medical Life Sciences, College of Medicine, The Catholic University of Korea, Seoul;

⁴Precision Medicine Research Center, College of Medicine, The Catholic University of Korea, Seoul, Korea

Single-cell RNA sequencing has become a powerful and essential tool for delineating cellular diversity in normal tissues and alterations in disease states. For certain cell types and conditions, there are difficulties in isolating intact cells for transcriptome profiling due to their fragility, large size, tight interconnections, and other factors. Single-nucleus RNA sequencing (snRNA-seq) is an alternative or complementary approach for cells that are difficult to isolate. In this review, we will provide an overview of the experimental and analysis steps of snRNA-seq to understand the methods and characteristics of general and tissue-specific snRNA-seq data. Knowing the advantages and limitations of snRNA-seq will increase its use and improve the biological interpretation of the data generated using this technique.

Key Words: Single-cell analysis; RNA sequencing; Transcriptome

Received: November 15, 2022 **Revised:** December 19, 2022 **Accepted:** December 19, 2022

Corresponding Author: Seung-Ah Yoo, PhD, Department of Biomedicine and Health Sciences, Graduate School, The Catholic University of Korea, 222 Banpo-daero, Seocho-gu, Seoul 06591, Korea

Tel: +82-2-3147-8410, Fax: +82-2-532-6537, E-mail: youcap78@catholic.ac.kr

Corresponding Author: Hae-Ock Lee, PhD, Department of Biomedicine and Health Sciences, Graduate School, The Catholic University of Korea, 222 Banpo-daero, Seocho-gu, Seoul 06591, Korea

Tel: +82-2-3147-8365, Fax: +82-2-532-6537, E-mail: haeocklee@catholic.ac.kr

*Nayoung Kim and Huiram Kang contributed equally to this work.

The introduction of single-cell RNA sequencing (scRNA-seq) opened a new era in cell biology, where cellular identity and heterogeneity can be defined by transcriptome data [1]. One cell type with tremendous phenotypic and functional heterogeneity is neurons in the brain. Indeed, scRNA-seq has revealed diverse neuronal cell types in the mouse brain [2]. However, cell isolation by enzymatic tissue dissociation may damage neurons, and most human brain samples are not available as fresh tissues. Among the alternative approaches attempted, the isolation of single nuclei and subsequent RNA sequencing have enabled high-throughput transcriptome profiling at a single-cell resolution [3,4]. In addition to neurons, single-nucleus RNA sequencing (snRNA-seq) has been applied to diverse hard-to-dissociate tissues and cell types, including the kidney, heart, liver, adipocytes, and myofibers [5-9]. For most tissues, snRNA-seq is more powerful at recovering attached cell types, whereas scRNA-seq is bi-

ased towards immune cell types [5,10-12]. Moreover, the enzymatic dissociation required for scRNA-seq induces a stress response that alters the cellular transcriptome [9,10,13]. Using snRNA-seq can reduce cellular and stress response biases. The different gene expression fractions in the nucleus and cytoplasm make it necessary to generate snRNA-based data references, and these have recently been provided [14]. Combining scRNA-seq and snRNA-seq data will enable more comprehensive transcriptome profiling and cell-type annotation in tissues.

EXPERIMENTAL PROCEDURES FOR SINGLE-NUCLEUS RNA SEQUENCING

snRNA-seq was developed as a method to obtain transcriptome data from cells that cannot be successfully dissociated due to their size and/or fragility, such as neurons, adipocytes, and epi-

thelial cell types from the kidney (Fig. 1A). Multi-nucleated cells, such as trophoblasts, osteoclasts, and skeletal myocytes, can be inimitably interrogated using snRNA-seq. Archived frozen tissues with broken cell membranes are also the primary targets of this method. The isolation of single nuclei, instead of whole cells, is achieved by cell membrane lysis, and nuclear transcriptome data are generated using scRNA-seq workflows (Fig. 1B). Both chemical and mechanical forces are used for cell membrane lysis. Competent buffers with nonionic detergents that disrupt cell membranes, but preserve nuclear membranes, have been tested for nuclear isolation [12]. Mechanical force is exerted using a Dounce

homogenizer or other types of tissue lysers. To obtain high-quality nuclei containing transcripts, the buffers and wash conditions are important and need to be optimized for different tissue types. The inclusion of bovine serum albumin and a high concentration of RNase inhibitors, during and after the isolation process, is critical. After isolation, nuclear morphology indicative of intact nuclei are confirmed by microscopy at 40–60× magnification (Fig. 1C). Overlysis results in clumping and poor transcript recovery, whereas under-lysis causes contamination by cytoplasmic RNAs.

In addition to the isolation of intact nuclei, brain tissues require an additional clean-up process to remove excessive myelin debris.

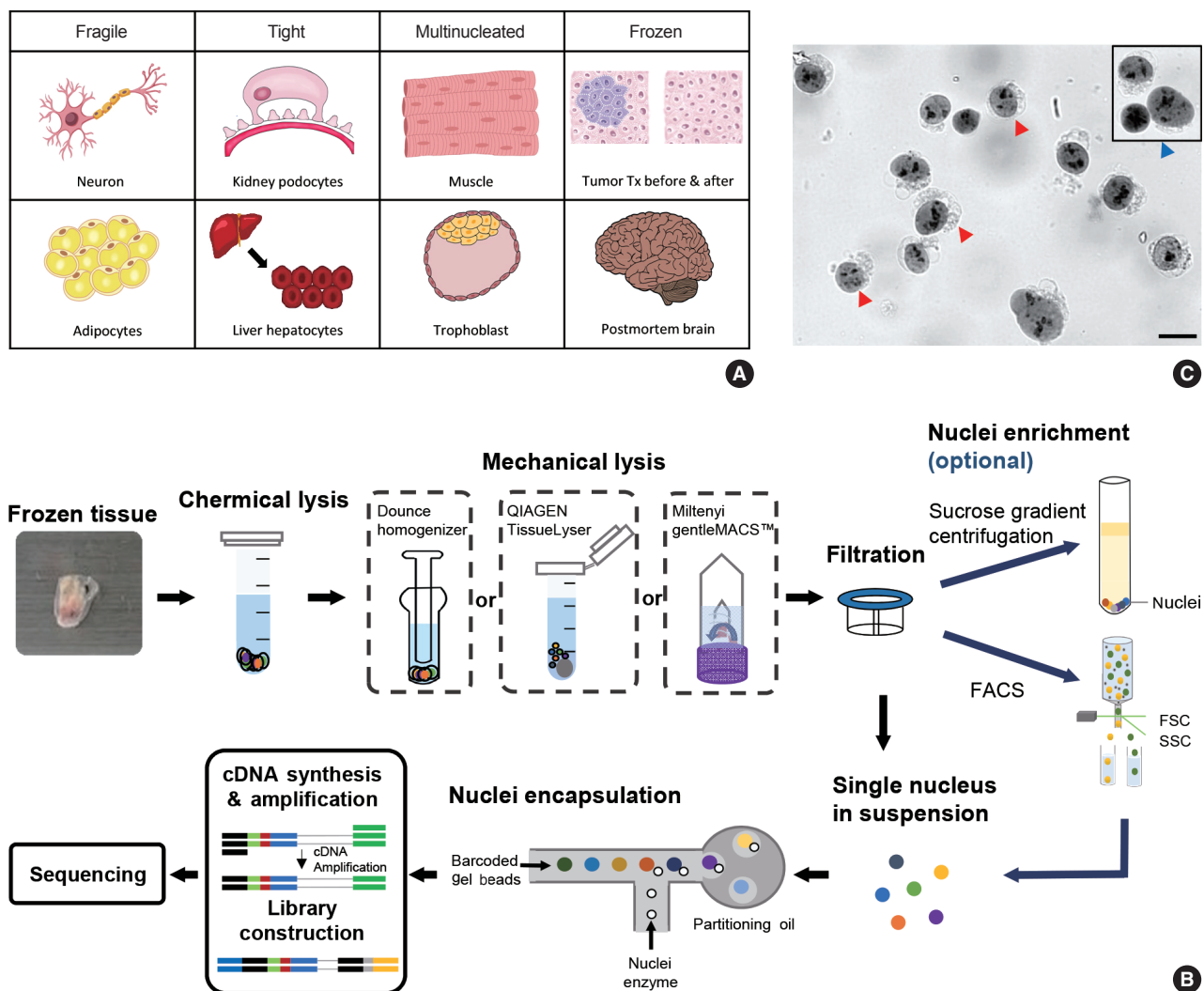


Fig. 1. Summary of the single-nucleus RNA sequencing (snRNA-seq) experimental process. (A) Representative cell types and tissues fit for snRNA-seq-based transcriptome profiling. (B) Experimental workflow to isolate intact nuclei for snRNA-seq. Frozen tissue is dissected, chemically and mechanically lysed, and then filtered to obtain a single-nucleus suspension. Sucrose gradient centrifugation or flow cytometry analysis is used for nuclei enrichment (Optional). After reverse transcription and amplification, a cDNA library is constructed for sequencing. (C) Representative image of extracted nuclei stained with Trypan blue. High-quality (blue arrowhead) and poor-quality (red arrowhead) nuclei are marked. Scale bar = 20 μm. FACS, fluorescence-activated cell sorting; FSC, forward scatter; SSC, side scatter.

Iodixanol (OptoPrep, San Diego, CA, USA) or a sucrose gradient [15], a myelin removal column (Miltenyi, Bergisch Gladbach, Germany), and sorting by flow cytometry have been used for this extra clean-up process (Fig. 1B). The most frequently used buffer recipe for neurons in the brain is a combination of 250–320 mM sucrose and a low-concentration of non-ionic detergent, whereas the commercial EZ Prep Kit (Sigma, St. Louis, MO, USA) is the method of choice for kidney preparations. Sorting by flow cytometry is not recommended for kidney tissue. The use of commercial buffers other than EZ Prep, such as those from 10× Genomics (Pleasanton, CA, USA) is also increasing, because of the minimal optimization requirement. Studies providing nuclear isolation protocols for snRNA-seq are listed in Table 1. The details of the buffer recipes and complete protocols can be found in these publications.

SINGLE-NUCLEUS RNA SEQUENCING DATA PROCESSING AND ANALYSIS

The data analysis pipeline for snRNA-seq is similar to the pipeline used for scRNA-seq (Fig. 2A). The most frequently used se-

quencing procedure for snRNA-seq is Chromium 3' scRNA-seq (10× Genomics), and the sequencing read mapping process (Cell Ranger 7.0, 10× Genomics) currently used is identical for scRNA-seq and snRNA-seq. During this process, both exonic and intronic reads that map the sense orientation to a single gene are used for gene counting using the default option. In previous Cell Ranger versions, intronic mapped reads were not used for the default read count option in the scRNA-seq pipeline, and the option parameter, "--include-introns = true" needed to be added for snRNA-seq read counting. The inclusion of intronic reads in snRNA-seq is critical, as more than 50% of nuclear RNAs are typically intronic compared to 15%–25% of total RNAs [13,16]. Immune cell populations such as neutrophils and other granulocytes are more likely to be identified when intronic reads are included. Detection of neutrophils is difficult because of their low RNA content and low gene count [17]. Since neutrophils have a higher amount of introns compared to other cell types [18,19], the inclusion of intronic reads may enhance the recovery of neutrophils. According to the guideline by 10× genomics, experimental steps are also important to enhance the neutrophil recovery such as immediate processing, sample preparation at room

Table 1. Representative studies reporting nuclei isolation protocols for the single-nucleus RNA sequencing

Tissue type	PMID	Nuclei extraction buffer components and additional nuclei clean up steps ^a
Frozen human brain	26890679	250 mM Sucrose/0.1% Tritonx-100/optional iodixanol gradient/FACS
Frozen human brain	27339989	1% NP40 or nuclear extraction buffer (320 mM sucrose, 0.1% Triton X-100)/iodixanol gradient
Frozen human/mouse brain	28846088	EZ lysis buffer
Mouse brain	29220646	250 mM Sucrose/0.1% Tritonx-100/sucrose gradient
Frozen human/mouse brain	31932797	0.025% NP-40/sucrose gradient
Mouse	32507042	10× Genomics reagent and protocol
Human brain	32997994	320 mM Sucrose/0.1% Igepal (0.1%)/iodixanol gradient
Frozen human/mouse brain	33495627	1% Formaldehyde fixation/100 mM sucrose/0.5% Triton-X-100/sucrose gradient
Frozen human brain	33972803	0.05% NP-40/iodixanol gradient
Human kidney	31249312	320 mM Sucrose/0.1% Triton X-100
Human kidney	31506348	EZ lysis buffer
Mouse kidney	30510133	EZ lysis buffer
Mouse kidney	32571916	EZ lysis buffer
Mouse kidney	32673289	EZ lysis buffer
Mouse kidney	33239393	EZ lysis buffer
Mouse kidney	33444290	EZ lysis buffer
Mouse kidney	34155061	EZ lysis buffer
Mouse heart	30939177	320 mM Sucrose/0.2% Triton-X-100
Brown adipose tissue	33116305	0.1% CHAPS (human) or EZ lysis buffer (mouse)
Human pancreas	33212097	250 mM Sucrose
Mouse skeletal muscle	33311464	250 mM Sucrose/0.4% Triton-X100/FACS
Mouse skeletal muscle	34382019	0.1% NP-40/FACS
Human liver	34792289	CST/NST/TST
Human liver	35581624	0.1% IGEPAL
Human tumor	32405060	EZ lysis buffer or ST (salts and tris) with 0.49% CHAPS (CST), with 0.03% Tween20 (TST) or with 0.2% NP-40 (NST)

FACS, fluorescence-activated cell sorting.

^aCell membrane disruption was achieved using isotonic sucrose and/or a nonionic detergent. The other buffer components were omitted from the analysis.

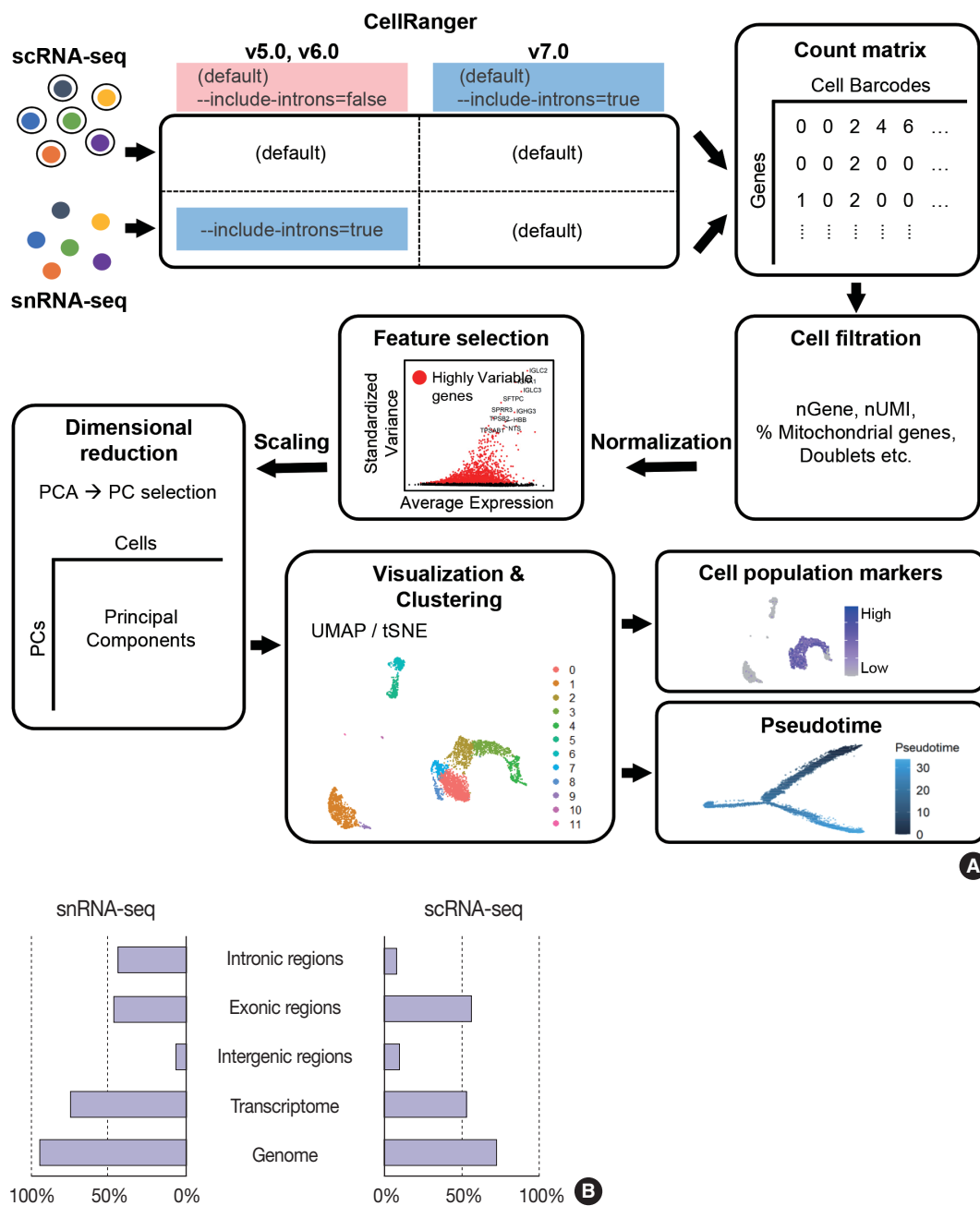


Fig. 2. Summary of single-nucleus RNA sequencing (snRNA-seq) and single-cell RNA sequencing (scRNA-seq) analyses. (A) Schematic workflow of snRNA-seq and scRNA-seq analysis processes. (B) Distribution of confidently mapped snRNA-seq and scRNA-seq reads. Transcriptome, the fraction of reads mapped to the exons of an annotated transcript. Genome, fraction of reads mapped to exonic and non-exonic loci. PC, principal cells; PCA, principal component analysis; UMAP, uniform manifold approximation and projection.

temperature, increasing polymerase chain reaction cycles during cDNA amplification, adding RNase inhibitors in the wash and suspension buffers, and enrichment by fluorescence-activated cell sorting into 0.04% bovine serum albumin solution in scRNA-seq [20].

From the filtered cell by gene matrices of snRNA-seq data, fur-

ther quality control (QC) filtering, normalization, feature selection, scaling, dimensional reduction, and clustering can be performed for cell-type annotation, as in scRNA-seq data analyses. Mitochondrial or ribosomal gene contents, which are often used as QC parameters for scRNA-seq, are not robustly used in snRNA-seq, as mitochondria and ribosomes are excluded during the ex-

perimental procedure. The differences in sequencing reads between scRNA-seq and snRNA-seq are shown in Fig. 2B.

Differential expression analysis using bulk RNA sequencing data has demonstrated a high correlation between nuclei and whole-cell samples [21,22]. However, at the single-cell or single-nucleus levels, cell-to-cell or nucleus-to-nucleus correlations decrease and replicate variations become larger than the bulk samples [22]. Direct comparisons of matched scRNA-seq and snRNA-seq data from S1 cortex neurons have demonstrated differences in genomic read mapping to coding sequences, introns, or untranslated regions [23]. Significant gene length bias exists, such that nuclear-biased genes show a length of 17 kb compared with 188 kb for genes detected in both whole cells and nuclei. The total gene expression correlation between single-cell and single-nucleus data ranges from 0.21 to 0.74. In a study of adipocytes, the average gene expression correlation between whole-cell and nuclei data for white cells was found to be 0.5 or 0.6 (after normalization)

[24]. Despite the relatively low correlations, diverse batch correction algorithms allow the co-clustering of identical cell types at a global scale in scRNA-seq and snRNA-seq data [24].

While data integration allows the combined clustering analysis of scRNA-seq and snRNA-seq data, direct comparisons of the two are difficult because of the differences in cellular and nuclear gene expression patterns. In addition, over-representation of immune cells by scRNA-seq and the superior representation of epithelial cell types by snRNA-seq suggest that complementary analysis is more appropriate than integrated analysis (Fig. 3).

SPECIFIC TISSUE OR CELL TYPE APPLICATIONS

Neurons in the brain

A high-throughput snRNA-seq protocol has been described for transcriptomic analysis of individual neurons from archived

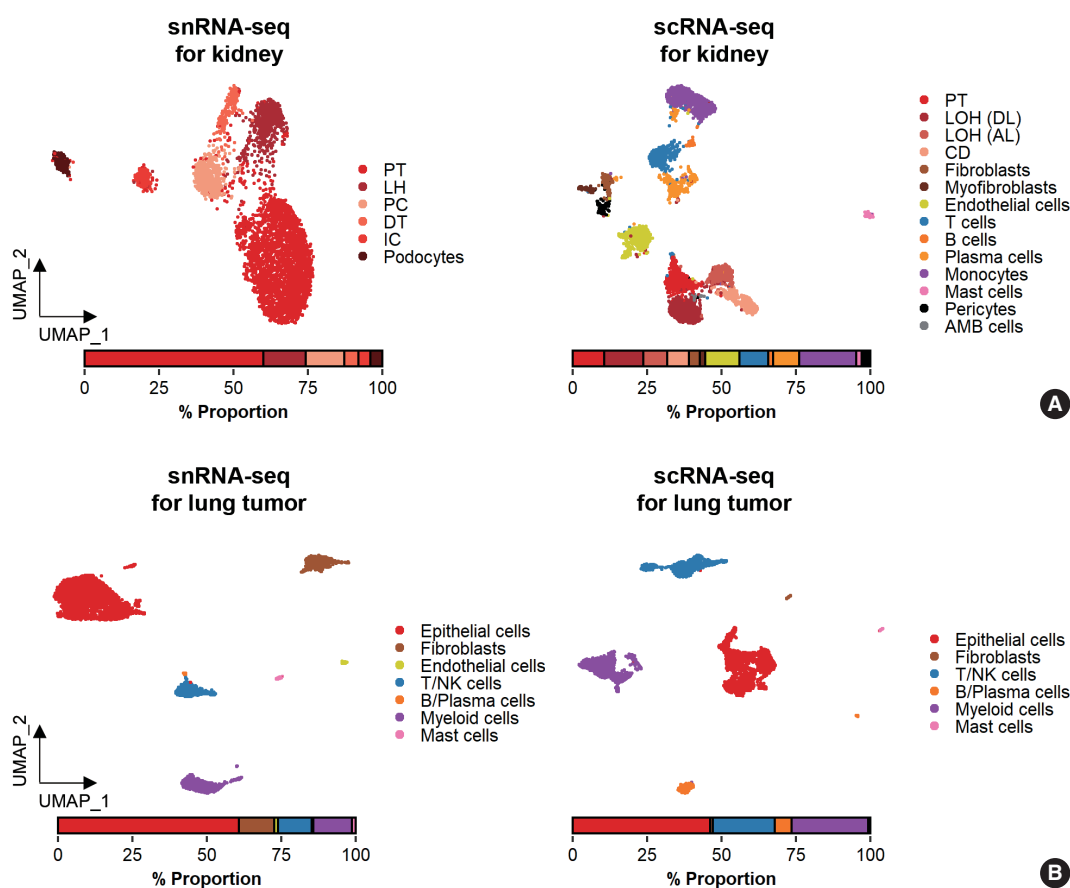


Fig. 3. Comparison of cell types detected by single-nucleus RNA sequencing (snRNA-seq) and single-cell RNA sequencing (scRNA-seq). (A) Uniform manifold approximation and projection (UMAP) plots of snRNA-seq and scRNA-seq data for the human kidney. A bar plot representing the percentages of annotated nuclei and cell identities. AMB, ambiguous; CD, collecting duct; DT, distal tubule; IC, intercalated cells; LH, loop of Henle; LOH (AL), loop of Henle, ascending limb; LOH (DL), loop of Henle, distal limb; NK, natural killer; PC, principal cells; PT, proximal tubule. (B) UMAP plots of snRNA-seq and scRNA-seq data for lung tumors from a lung cancer patient.

postmortem human brain tissues [25]. Before the introduction of high-throughput applications, low-throughput methods, such as intracellular tagging by transcription in vivo analysis [26] and extraction of the cytoplasmic contents using a glass microcapillary [27,28] or laser-capture microdissection [29] were explored, along with low-throughput snRNA-seq [22]. Lake and colleagues [4] applied snRNA-seq and identified 16 neuronal subtypes of the cerebral cortex from a postmortem brain.

Currently, snRNA-seq is extensively used to determine brain cell type complexity. The U.S. government's Brain Research Through Advancing Innovative Neurotechnologies (BRAIN) Initiative [30] launched a project known as the BRAIN Initiative Cell Census Consortium to pursue a comprehensive human brain cell atlas [31]. These resources will serve as a reference for delineating brain functions and alterations in neurodegenerative and neurological diseases. To construct the brain cell atlas, electrophysiological, morphological, and transcriptional features were used for neuronal cell type specifications, signifying the importance of transcriptome-based cell type annotation in functional and anatomical contexts. Transcriptome-based neuronal identification was accomplished using both scRNA-seq and snRNA-seq [31] after regional dissection. Due to the under-representation of neuronal cell types in scRNA-seq data and the availability of frozen postmortem brains, more recent cell applications have concentrated on snRNA-seq.

Nonetheless, differences in the nuclear and cytoplasmic gene expression patterns, and limitations of snRNA-seq in the capture and characterization of non-neuronal cell types [32] necessitate the complementary use of scRNA-seq and snRNA-seq for cell type identification in the brain.

Epithelial cells in the kidney

Whereas the studies agree that average nephron number is approximately 900,000 to 1 million per kidney, numbers for individual kidneys range from approximately 200,000 to >2.5 million [33]. Each nephron contains a glomerulus, which is a bundle of vessels through which waste materials are filtered from the blood. The glomerulus is enclosed in Bowman's capsule, and filtered water, ions, and small molecules are collected in Bowman's space. Podocytes in the epithelial lining of the Bowman's capsule wrap around the capillaries of the glomerulus and leave filtration slits between them. Filtered materials leave Bowman's space through a proximal tubule where reabsorption occurs. Epithelial cells lining the proximal tubule are covered with dense microvilli to facilitate transport. The modular characteristics of the kidney make biopsy an accessible and efficient sampling method for the

characterization of the glomerulus.

Glomerular cell types in the kidney have been characterized using both scRNA-seq and snRNA-seq protocols. For the mouse kidney, an snRNA-seq experimental protocol yielded 20-fold more podocytes than an scRNA-seq protocol [9,34]. The Kidney Precision Medicine Project developed a reference tissue atlas for the human kidney with single-cell resolution and spatial context [35]. Rare epithelial cell types and states can be captured by snRNA-seq; however, immune components in the kidney are not well captured by snRNA-seq (Fig. 3A) [36]. Thus, the kidney atlas data incorporate snRNA-seq and scRNA-seq data for tissue atlas generation [37].

Tumors from frozen tissues

A diverse range of solid tumor tissues have been subjected to scRNA-seq, and the biological features of tumor cells and their surrounding microenvironments have been extensively studied. However, scRNA-seq data shows a heavy bias towards immune cell types when compared with bulk tissue data after cell type deconvolution (Fig. 3B). The use of snRNA-seq data may resolve this problem [12]. Side-by-side comparisons of scRNA-seq and snRNA-seq analyses of hepatocellular carcinoma [38] demonstrated the predominant capture of hepatocytes and carcinoma cells in snRNA-seq data compared with the immune cell-dominant landscape in scRNA-seq data. In a pancreatic cancer study, a combination of snRNA-seq and digital spatial profiling revealed that gene expression programs in malignant tumor cells and fibroblasts were enriched after chemotherapy and radiotherapy [39]. In addition to tumor-centric data analysis, snRNA-seq can be performed on longitudinal samples stored as frozen tissues. Similar to brain and kidney examples, immune cells in the tumor microenvironment can be efficiently captured by scRNA-seq.

CONCLUSION

Transcriptome-based cell type profiling by scRNA-seq has remarkably enhanced our understanding of cellular diversity. While scRNA-seq shows good performance at capturing immune cell diversity, the cellular landscape depicted is biased against for attached cell types and is missing fragile cells. In most tissues, snRNA-seq can be used to obtain more information about these cell types, including epithelial cells, fibroblasts, neurons, and adipocytes. In addition, snRNA-seq can be used for frozen tissues, such as postmortem brain and archived tumor samples. After the successful isolation of nuclei, experimental and analysis pipelines used for scRNA-seq can be adopted for snRNA-seq. In the anal-

ysis, data from the two methods should be combined with caution, considering the differences in cellular and nuclear RNA gene expression patterns.

Ethics Statement

Not applicable.

Availability of Data and Material

The datasets analyzed during the current study are available in the Gene Expression Omnibus repository at GSE137444 [<https://www.ncbi.nlm.nih.gov/geo/query/acc.cgi?acc=GSE137444>], GSE114156 [<https://www.ncbi.nlm.nih.gov/geo/query/acc.cgi?acc=GSE114156>], and GSE109564 [<https://www.ncbi.nlm.nih.gov/geo/query/acc.cgi?acc=GSE109564>].

Code Availability

Not applicable.

ORCID

Nayoung Kim <https://orcid.org/0000-0003-3202-750X>
 Huiram Kang <https://orcid.org/0000-0002-7136-9724>
 Areum Jo <https://orcid.org/0000-0001-7815-8439>
 Seung-Ah Yoo <https://orcid.org/0000-0003-4878-8733>
 Hae-Ock Lee <https://orcid.org/0000-0001-5123-0322>

Author Contributions

Conceptualization: SAY, HOL. Data curation: NK. Funding acquisition: HOL. Investigation: NK, HK, AJ. Supervision: SAY, HOL. Visualization: NK, HK, AJ. Writing—original draft: NK, HK, SAY, HOL, AJ. Writing—review & editing: NK, HK, SAY, HOL, AJ. Approval of final manuscript: all authors.

Conflicts of Interest

The authors declare that they have no potential conflicts of interest.

Funding Statement

This study was supported by the Bio & Medical Technology Development Program of the National Research Foundation, funded by the Ministry of Science and ICT (NRF-2019M3A9B6064691).

References

- Kolodziejczyk AA, Kim JK, Svensson V, Marioni JC, Teichmann SA. The technology and biology of single-cell RNA sequencing. *Mol Cell* 2015; 58: 610-20.
- Zeisel A, Munoz-Manchado AB, Codeluppi S, et al. Brain structure. Cell types in the mouse cortex and hippocampus revealed by single-cell RNA-seq. *Science* 2015; 347: 1138-42.
- Habib N, Avraham-Davidi I, Basu A, et al. Massively parallel single-nucleus RNA-seq with DroNc-seq. *Nat Methods* 2017; 14: 955-8.
- Lake BB, Ai R, Kaeser GE, et al. Neuronal subtypes and diversity revealed by single-nucleus RNA sequencing of the human brain. *Science* 2016; 352: 1586-90.
- Andrews TS, Atif J, Liu JC, et al. Single-cell, single-nucleus, and spatial RNA sequencing of the human liver identifies cholangiocyte and mesenchymal heterogeneity. *Hepatol Commun* 2022; 6: 821-40.
- Petrany MJ, Swoboda CO, Sun C, et al. Single-nucleus RNA-seq identifies transcriptional heterogeneity in multinucleated skeletal myofibers. *Nat Commun* 2020; 11: 6374.
- Sun W, Dong H, Balaz M, et al. snRNA-seq reveals a subpopulation of adipocytes that regulates thermogenesis. *Nature* 2020; 587: 98-102.
- Tucker NR, Chaffin M, Fleming SJ, et al. Transcriptional and cellular diversity of the human heart. *Circulation* 2020; 142: 466-82.
- Wu H, Kirita Y, Donnelly EL, Humphreys BD. Advantages of single-nucleus over single-cell RNA sequencing of adult kidney: rare cell types and novel cell states revealed in fibrosis. *J Am Soc Nephrol* 2019; 30: 23-32.
- Denisenko E, Guo BB, Jones M, et al. Systematic assessment of tissue dissociation and storage biases in single-cell and single-nucleus RNA-seq workflows. *Genome Biol* 2020; 21: 130.
- Yamawaki TM, Lu DR, Ellwanger DC, et al. Systematic comparison of high-throughput single-cell RNA-seq methods for immune cell profiling. *BMC Genomics* 2021; 22: 66.
- Slyper M, Porter CB, Ashenberg O, et al. A single-cell and single-nucleus RNA-Seq toolbox for fresh and frozen human tumors. *Nat Med* 2020; 26: 792-802.
- Bakken TE, Hodge RD, Miller JA, et al. Single-nucleus and single-cell transcriptomes compared in matched cortical cell types. *PLoS One* 2018; 13: e0209648.
- Eraslan G, Drokhyansky E, Anand S, et al. Single-nucleus cross-tissue molecular reference maps toward understanding disease gene function. *Science* 2022; 376: eabl4290.
- Zhou Y, Song WM, Andhey PS, et al. Human and mouse single-nucleus transcriptomics reveal TREM2-dependent and TREM2-independent cellular responses in Alzheimer's disease. *Nat Med* 2020; 26: 131-42.
- La Manno G, Soldatov R, Zeisel A, et al. RNA velocity of single cells. *Nature* 2018; 560: 494-8.
- Hay SB, Ferchen K, Chetal K, Grimes HL, Salomonis N. The Human Cell Atlas bone marrow single-cell interactive web portal. *Exp Hematol* 2018; 68: 51-61.
- Ullrich S, Guigo R. Dynamic changes in intron retention are tightly associated with regulation of splicing factors and proliferative activity during B-cell development. *Nucleic Acids Res* 2020; 48: 1327-40.
- Wong JJ, Ritchie W, Ebner OA, et al. Orchestrated intron retention regulates normal granulocyte differentiation. *Cell* 2013; 154: 583-95.
- Xie X, Shi Q, Wu P, et al. Single-cell transcriptome profiling reveals neutrophil heterogeneity in homeostasis and infection. *Nat Immunol* 2020; 21: 1119-33.
- Barthelson RA, Lambert GM, Vanier C, Lynch RM, Galbraith DW. Comparison of the contributions of the nuclear and cytoplasmic compartments to global gene expression in human cells. *BMC Genomics* 2007; 8: 340.
- Grindberg RV, Yee-Greenbaum JL, McConnell MJ, et al. RNA-sequencing from single nuclei. *Proc Natl Acad Sci U S A* 2013; 110: 19802-7.
- Lake BB, Codeluppi S, Yung YC, et al. A comparative strategy for single-nucleus and single-cell transcriptomes confirms accuracy in predicted cell-type expression from nuclear RNA. *Sci Rep* 2017; 7: 6031.
- Gupta A, Shamsi F, Altemose N, et al. Characterization of transcript enrichment and detection bias in single-nucleus RNA-seq for mapping of distinct human adipocyte lineages. *Genome Res* 2022; 32: 242-57.
- Krishnaswami SR, Grindberg RV, Novotny M, et al. Using single nuclei for RNA-seq to capture the transcriptome of postmortem neurons. *Nat Protoc* 2016; 11: 499-524.
- Lovatt D, Ruble BK, Lee J, et al. Transcriptome in vivo analysis

- (TTVA) of spatially defined single cells in live tissue. *Nat Methods* 2014; 11: 190-6.
27. Citri A, Pang ZP, Sudhof TC, Wernig M, Malenka RC. Comprehensive qPCR profiling of gene expression in single neuronal cells. *Nat Protoc* 2011; 7: 118-27.
 28. Qiu S, Luo S, Evgrafov O, et al. Single-neuron RNA-Seq: technical feasibility and reproducibility. *Front Genet* 2012; 3: 124.
 29. Lovatt D, Bell T, Eberwine J. Single-neuron isolation for RNA analysis using pipette capture and laser capture microdissection. *Cold Spring Harb Protoc* 2015; 2015: pdb prot072439.
 30. Ngai J. BRAIN 2.0: Transforming neuroscience. *Cell* 2022; 185: 4-8.
 31. Ecker JR, Geschwind DH, Kriegstein AR, et al. The BRAIN Initiative Cell Census Consortium: lessons learned toward generating a comprehensive brain cell atlas. *Neuron* 2017; 96: 542-57.
 32. Thrupp N, Sala Frigerio C, Wolfs L, et al. Single-nucleus RNA-seq is not suitable for detection of microglial activation genes in humans. *Cell Rep* 2020; 32: 108189.
 33. Bertram JF, Douglas-Denton RN, Diouf B, Hughson MD, Hoy WE. Human nephron number: implications for health and disease. *Pediatr Nephrol* 2011; 26: 1529-33.
 34. Park J, Shrestha R, Qiu C, et al. Single-cell transcriptomics of the mouse kidney reveals potential cellular targets of kidney disease. *Science* 2018; 360: 758-63.
 35. Hansen J, Sealton R, Menon R, et al. A reference tissue atlas for the human kidney. *Sci Adv* 2022; 8: eabn4965.
 36. Wu H, Malone AF, Donnelly EL, et al. Single-cell transcriptomics of a human kidney allograft biopsy specimen defines a diverse inflammatory response. *J Am Soc Nephrol* 2018; 29: 2069-80.
 37. O'Sullivan ED, Mylonas KJ, Hughes J, Ferenbach DA. Complementary roles for single-nucleus and single-cell RNA sequencing in kidney disease research. *J Am Soc Nephrol* 2019; 30: 712-3.
 38. Wen F, Tang X, Xu L, Qu H. Comparison of single-nucleus and single-cell transcriptomes in hepatocellular carcinoma tissue. *Mol Med Rep* 2022; 26: 339.
 39. Hwang WL, Jagadeesh KA, Guo JA, et al. Single-nucleus and spatial transcriptome profiling of pancreatic cancer identifies multicellular dynamics associated with neoadjuvant treatment. *Nat Genet* 2022; 54: 1178-91.

Inflammatory bowel disease—associated intestinal fibrosis

Ji Min Park¹, Jeongseok Kim², Yoo Jin Lee², Sung Uk Bae³, Hye Won Lee¹

¹Department of Pathology, ²Division of Gastroenterology and Hepatology, Department of Internal Medicine, ³Division of Colorectal Surgery, Department of Surgery, Keimyung University School of Medicine, Daegu, Korea

Fibrosis is characterized by a proliferation of fibroblasts and excessive extracellular matrix following chronic inflammation, and this replacement of organ tissue with fibrotic tissue causes a loss of function. Inflammatory bowel disease (IBD) is a chronic inflammation of the gastrointestinal tract, and intestinal fibrosis is common in IBD patients, resulting in several complications that require surgery, such as a stricture or penetration. This review describes the pathogenesis and various factors involved in intestinal fibrosis in IBD, including cytokines, growth factors, epithelial-mesenchymal and endothelial-mesenchymal transitions, and gut microbiota. Furthermore, histopathologic findings and scoring systems used for stenosis in IBD are discussed, and differences in the fibrosis patterns of ulcerative colitis and Crohn's disease are compared. Biomarkers and therapeutic agents targeting intestinal fibrosis are briefly mentioned at the end.

Key Words: Fibrosis; Inflammatory bowel disease; Crohn disease; Colitis, ulcerative

Received: October 21, 2022 **Revised:** November 1, 2022 **Accepted:** November 2, 2022

Corresponding Author: Hye Won Lee, MD, PhD, Department of Pathology, Keimyung University School of Medicine, 1095 Dalgubeol-daero, Dalseo-gu, Daegu 42601, Korea
 Tel: +82-53-258-4260, Fax: +82-53-258-7382, E-mail: hwlee@dsmc.or.kr

Fibrosis is characterized by fibroblastic proliferation and the deposition of excessive extracellular matrix (ECM) and hard collagen layers through chronic inflammatory and reparative responses [1-4]. Fibrosis can also occur during the wound healing process, and it is an end-stage phenomenon that causes chronic damage to solid organs, such as the liver, lungs, and kidneys [5]. Hepatitis and cholestatic diseases with various etiologies eventually lead to liver cirrhosis, and various types of glomerulonephritis lead to glomerulosclerosis. In such cases, the organ is replaced with fibrous tissue instead of the original functional tissue, resulting in a loss of function. However, in contrast to those solid organs, the phenomenon of fibrosis in the gastrointestinal tract, a hollow viscous organ, is poorly understood.

Inflammatory bowel disease (IBD) is characterized by persistent and refractory immuno-mediated inflammation in the gastrointestinal tract [6]. To date, studies on disease activity in IBD have focused on the presence or absence of ulcers and the degree of infiltration of inflammatory cells. However, intestinal fibrosis is a common pathogenic feature of IBD and has several related complications, including stricture, fistula, and bowel penetration [7,8]. Intestinal fibrosis can occur through several etiologies, including a desmoplastic reaction, radiation enteropathy,

solitary rectal ulcer, graft-versus-host disease, post-surgical adhesions, desmoid tumors, collagenous colitis, and eosinophilic enteropathy. IBD is the leading cause of intestinal fibrosis, and it is thus necessary to understand its unique form of intestinal fibrosis [9-11].

Intestinal fibrosis is a pathological complication of great interest not only to radiologists and pathologists but also to clinicians due to its association with the risk of major complications that require surgical treatment, prognosis after surgery, and the risk of recurrence [12].

PATHOGENESIS

Fibrosis is an irreversible process that occurs as a consequence of chronic inflammation. It results in persistent luminal narrowing and strictures. Anti-inflammatory agents do not prevent or treat fibrosis in IBD, even if they improve the inflammation [13]. Because the fibrotic process is not affected by various IBD treatments, researchers have focused on inflammation-independent mechanisms, such as genetic factors, environmental risks, and the gut microbiota, which are known to affect the prognosis of fibrosis [14]. Moreover, intestinal fibrosis can be observed alongside ex-

cessive deposition of ECM and activated mesenchymal cells in the intestinal wall [15]. The main known drivers of this fibrosis mechanism are soluble molecules (cytokines and growth factors), the epithelial-mesenchymal transition (EMT), the endothelial-mesenchymal transition (EnMT), and the gut microbiota.

Genetic factors

Genetic research on IBD has proposed several genetic pathways for its pathogenesis [16,17]. However, relations between those gene mutations and intestinal fibrosis have not yet been well studied. In one bioinformatics study, researchers hypothesized that similar molecular pathways would be involved in fibrosis in various organs and thus measured gene expressions found in kidney fibrosis and liver cirrhosis in Crohn's disease (CD) and ulcerative colitis (UC). They found that fibrosis in different organs had different gene signatures. C-X-C motif chemokine ligand 9 (*CXCL9*) and *CD52* were upregulated in both CD and UC, whereas thrombospondin 2 (*THBS2*), matrix gla protein (*MGP*), protein tyrosine phosphatase receptor type C (*PTPRC*), and decorin (*DCN*) were upregulated only in CD. In UC, *CXCL9*, *CD52*, and granzyme A (*GZMA*) were upregulated, and *DCN*, which was elevated in CD, was downregulated [18].

Nucleotide binding oligomerization domain containing 2 (*NOD2*) has been most studied in association with IBD. Various polymorphisms related to the *NOD2* gene have been reported and are known to be related to fibrogenesis in UC and CD [19-23]. The *NOD2* gene was also suggested as a predictive marker for the progression of CD fibrosis [24]. Within the innate immune system, Toll-like receptors 4 (*TLR*) and signal transducers

and activators of the transcription 3 (*STAT3*) might be a mechanism for intestinal fibrosis [19,25,26], and interleukin-23 receptor (*IL23R*), interleukin-12 subunit beta (*IL12B*), and Janus kinases 2 (*JAK2*), which are related to the Th17 pathway, could also be involved [25,27-29]. *CX3CR1*-mediating chemokines [30] and autophagy genes (autophagy related 16 like 1 [*ATG16L1*] and immunity-related GTPase family M protein [*IRGM*]) were reported to have an association with stricture disease [25,31]. However, the exact mechanism remains obscure because fucosyltransferase 2 (*FUT2*) appears to change the composition of the gut microbiota, which is presumed to be able to induce fibrosis [32]. Transforming growth factor β (*TGF- β*) plays a broad role in initiating inflammation and fibrosis [33,34]. Matrix metalloproteinase 3 (*MMP3*) encodes a proteinase that degrades most components of the ECM. Membrane-associated guanylate kinase inverted 1 (*MAGI1*), which is associated with a mechanism that disrupts the tight junction of intestinal epithelial cells, is a gene factor potentially associated with fibrosis (Table 1) [35,36]. Because the number of studies is too small for generalization, more genome-wide association studies and next generation sequencing studies are needed to reveal genetic factors involved with fibrosis in IBD [16].

Cytokines and growth factors

Local fibroblasts in fibrotic foci proliferate in response to various growth factors and cytokines. platelet derived growth factor (PDGF), basic-fibroblast growth factor, insulin like growth factor 1, epidermal growth factor, CTGF, tumor necrosis factor α (*TNF- α*), IL-1 β , and IL-6 can act as major proliferating factors

Table 1. Potential genetic factors of IBD-associated fibrosis

Related genes	Disease entity	Mechanism	Reference
<i>NOD2</i>	CD and UC	Apoptosis and activates NF- κ B, induce interleukin 1-beta	[19-23]
<i>TLR4</i>	CD	Initiating innate immune responses	[19]
<i>IL23R</i>	CD and UC	Activation of Th17 lymphocytes	[27,28]
<i>IL12B</i>	CD	Activation of Th17 lymphocytes	[25]
<i>JAK2</i>	CD	Activation of Th17 lymphocytes	[29]
<i>CX3CR1</i>	CD	Leukocyte chemotaxis and adhesion	[30]
<i>STAT3</i>	CD and UC	Innate immune mechanisms	[25,26]
<i>ATG16L1</i>	CD	Autophagocytosis	[31]
<i>IRGM</i>	CD	Autophagocytosis	[25]
<i>FUT2</i>	CD	Affects the composition of the gut microbiota	[32]
<i>TGF-β</i>	CD	Initiation of inflammation	[33,34]
<i>MMP3</i>	CD and UC	Mediate degradation of components of the extracellular matrix	[35]
<i>MAGI1</i>	CD	Disruption of epithelial barrier via abnormality of tight junction of intestinal epithelial cells	[36]

IBD, inflammatory bowel disease; *NOD2*, nucleotide-binding oligomerization domain-containing protein 2; CD, Crohn disease; UC, ulcerative colitis; NF- κ B, nuclear factor κ B; *TLR4*, Toll-like receptors 4; *IL23R*, interleukin-23 receptor; *IL12B*, interleukin-12 subunit beta; *JAK2*, Janus kinases 2; *CX3CR1*, C-X3-C motif chemokine receptor 1; *STAT3*, signal transducers and activators of the transcription 3; *ATG16L1*, autophagy-related 16-like 1; *IRGM*, immunity-related GTPase family M protein; *FUT2*, fucosyltransferase 2; *TGF- β* , transforming growth factor beta; *MMP-3*, matrix metalloproteinase-3; *MAGI1*, membrane-associated guanylate kinase inverted 1.

[12,14,37]. The proliferating fibroblasts recruit various inflammatory cells, T cells, eosinophils, and mast cells. Inflammatory mediators, such as PDGF-A, PDGF-B, IGF-1, and fibronectin, are also involved in local fibroblastic proliferation and the migration of fibroblasts to the ECM of an inflamed area. In addition, intestinal stellate cells are differentiated into fibroblasts at inflammatory sites using TGF- β [38]. Furthermore, though the molecular pathway is not well established, the capacity of adult bone marrow to derive fibroblast precursors recently became clear, and several cytokines, such as IL-10 or other growth factors, are considered to be part of that pathway [14,39,40].

Critical role of adipose tissue

The role of adipose tissue is essential in inducing hyperplasia of the muscularis propria and subsequent stricture formation in CD [41]. In IBD research, interest is increasing in the role of various bioactive substances secreted by mesenteric fat [42]. Creeping fat is a unique and pathognomonic phenomenon in CD that was first reported by Crohn in 1932 [43]. Creeping fat is defined as > 50% coverage of the exterior intestinal surface with proliferation and ectopic extension of mesenteric adipose tissue (Fig. 1). In the proliferated adipose tissue surrounding the intestine, numerous mediators play crucial roles in inflammation and immunity that lead to the development and progression of IBD [41,44]. Mediators secreted by fat tissue include adipokines (adiponectin, leptin, resistin, C1q/TNF-related protein 3 [CTRP-3], and fatty acids), cytokines (TNF- α , peroxisome proliferator-activated receptor- γ [PPAR- γ], macrophage colony-stimulating factor, monocyte chemoattracted protein-1, IL-1, IL-6, IL-8, IL-10, and chemokine (C-C motif) ligand 5), and growth factors (ghrelin and vascular endothelial growth factor). Those secretions attract and activate various immune cells [45,46]. Therefore, cases of cobblestone mucosa and proper muscle hyperplasia are common in specimens surgically resected to treat CD complications and result in a thick intestinal wall and stricture formation (Fig. 1) [47].

EMT and EnMT

The EMT is a well-known phenomenon in malignant neoplasms and literally describes a phenomenon in which tumor cells with epithelial features acquire a mesenchymal tendency to break the resistance of the surrounding ECM, facilitate local migration and invasion, and exhibit aggressive behavior [48]. It is also a mechanism of distant metastasis, in which epithelial cells are attacked by immune cells, or an apoptotic program is initiated when epithelial cells float away from their location, especially when they enter the blood flow, which is the starting point of



Fig. 1. Gross finding of resected large intestine specimen of 30-year-old patient with Crohn's disease. Creeping fat covers more than 50% of the intestinal circumference surface with mesenteric proliferation. Cobblestone mucosa and proper muscle hyperplasia that result in intestinal stricture are also noted.

distant metastases [49].

In IBD, damaged intestinal epithelial cells are activated, and the EMT pathway is initiated. This change can be shown by a loss of epithelial marker expression (such as cytokeratins and E-cadherin) in the enterocytes of inflamed foci and increased expression of mesenchymal markers (especially fibroblast markers, MMP-2, MMP-9, ferroptosis suppressor protein 1, α -smooth muscle actin [α -SMA], and vimentin) [50].

In addition, IBD can damage vascular endothelial cells [14]. In the presence of an excessive inflammatory response, such as hypoxia and secondary mechanical stress, endothelial cells are activated and converted into cells with fibroblast properties. This is called the EnMT, in which endothelial markers (VE-cadherin, Von Willebrand factor, and CD31) expressed in cells are lost, and the expression of fibroblast markers increases. In the EnMT, TGF- β , insulin-like growth factor 2, and IL-1b or TNF- α , which are pro-inflammatory components, are inducers [48,51,52]. Occasionally, this process is reversible. Bone morphogenetic protein-7 or hepatocyte growth factor can convert fibroblasts back into endothelial cells. However, the conditions under which this reversal pathway works remain unknown [53,54]. Cellular transitions, i.e., the EMT and EnMT, are sources of new fibroblasts and result in excessive ECM deposition. Fibroblasts also exhibit enhanced migratory ability. Therefore, the submucosal layer, which is composed of loose connective tissue, is replaced with various ECM components. As a result, the condition of the intestinal wall impedes its flexible movement [13].

Gut microbiota

The gut microbiota is one key factor in the development of fibrosis in IBD [16]. It consists of bacteria, viruses, archaea, pro-

tists, and yeast. The composition of the intestinal microbiota affects the host metabolism and immune systems in various ways, and chronic inflammatory status caused by the gut microbiota can ultimately produce the complications of intestinal fibrosis or strictures [55]. The stability of the intestinal microbiota supports the barrier function of intestinal epithelial cells [56]. If the balance between beneficial and harmful bacteria is destroyed, the intestinal microbial barrier and anti-inflammatory regulatory pathway can be damaged, which can eventually cause severe colitis [57,58]. In one study, the intestinal bacterial diversity of mice was reduced using intestinal radiation and an antibiotic cocktail treatment, and that produced decreased levels of TGF β , phosphorylated SMAD3, and SMA proteins, which in turn reduced the chronic inflammation that plays a crucial role in intestinal fibrosis [59]. Preliminary studies of fibrosis and the microbiome have been done [24]. Several studies have suggested that fibronectin and collagen deposition in the intestinal wall is a response to bacterial stimulation of the intestine [60,61]. In addition, several studies have reported that strictures are more frequent in patients with CD who have higher levels of antibacterial antibodies [56,58].

HISTOPATHOLOGY

In IBD-associated fibrosis, the change in the muscular layer, which contributes to the presence of a thickened bowel wall, is notable (Fig. 2A). This results in both hypertrophy and hyper-

plasia [47]. Although chronic inflammation, represented by basal plasmacytosis, is predominant, IBD can also show a mixed inflammation pattern that is accompanied by active inflammation (Fig. 2B, C). As the disease progresses, increased activation of intestinal myofibroblasts results in the gradual synthesis of ECM and contractile proteins (α -SMA and MYLK) [60]. Young fibroblasts begin to be deposited and gradually progress to fibrosis with increased deposition of ECM (collagen, fibronectin, etc.) [55]. In addition, slowed blood flow is caused by damage to highly branched vessels (Fig. 2D). This condition often becomes refractory to medication. Neuronal cell changes are usually observed in surgical specimens from patients with chronic constipation without a certain organic cause, and similarly in IBD patients, neuronal hypertrophy can be a secondary reactive change [62]; however, it can also act as a mechanism for intestinal stiffening (Fig. 2E). In trichrome stain results, dissection between hyperplastic smooth muscle bundles is observed to be interspersed with fibrosis (Fig. 2F).

Histopathology scoring systems for stenosis

In IBD, many scoring systems have been developed to express disease activity, including the Geboes score and Nancy Index of UC and the Crohn's Disease Activity Index [63,64]. These evaluation methods consider not only the presence of ulcers but also the degree of infiltration of inflammation, submucosal fibrosis, and thickened muscularis propria. Following a recent discussion at the Stenosis Therapy and Antifibrotic Research Consortium, a

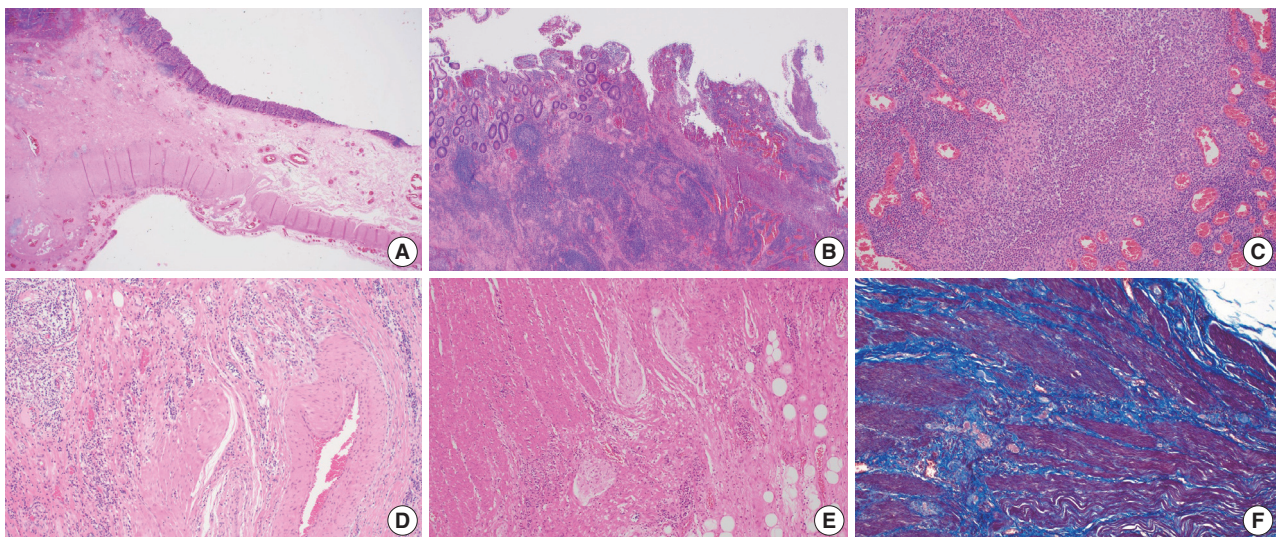


Fig. 2. Histologic findings of Crohn's disease. (A) Hypertrophy and hyperplasia of the submucosa and muscularis propria are present. (B) Chronic inflammation with lymphoid aggregates and lymphoid follicles is dominant. (C) Although chronic inflammation is predominant, active inflammation that consists of extensive neutrophilic infiltrates is also noted. (D) Fibromuscular hyperplasia of damaged submucosal vessels causes slow blood flow. (E) Neural hypertrophy is also noted. (F) Trichrome stain reveals that dissection between the hyperplastic smooth muscle bundles is interspersed with fibrosis.

four-tiered system (none, mild, moderate, and severe) was constructed to include an evaluation of the inflammatory and fibrotic components of each mural layer [55]. In this artificial intelligence era, researchers have endeavored to develop a deep learning model to evaluate intestinal fibrosis in surgical specimens for postoperative recurrence prediction [65,66].

Differences of intestinal fibrosis in UC and CD

UC and CD, which belong to the same IBD category but differ in their mechanisms of development and clinical features, also show differences in IBD-related fibrosis [67]. In UC, fibrotic changes are limited to the mucosal and submucosal layers [55]. This can shorten or stiffen the intestine, leading to motility disorders. Because strictures in UC are rare and can be either benign or malignant, a persistent stricture should raise suspicions of cancer [68]. Complications that are mainly due to bowel wall thickening, such as stricture and stenosis, are problematic in CD. Furthermore, diffuse transmural collagen layers down to the muscularis propria and proliferative fibroblastic infiltration are observed. In UC, on the other hand, the progression of intestinal fibrosis does not correlate with disease duration or location; however, inflammatory activity does correlate with medical treatment. In contrast, in CD, the duration and location of the disease and type of treatment are related to the risk of intestinal fibrosis [55,69,70].

Biomarkers and potential antifibrotic agents

Gene variants, epigenetic modifiers, antimicrobial antibodies, ECM components, and clinical, endoscopic, or environmental factors can be used to evaluate and predict fibrosis in IBD patients [71]. Fibrosis in CD, which causes several serious sequelae, is reversible, and thus it is important to develop therapeutic agents targeting it [72]. However, no effective therapeutic agents are available to prevent or repair the progression of fibrosis except by suppressing inflammation, though diverse potential antifibrotic therapies have been proposed. Although their mechanism is still unknown, statins (simvastatin) have been reported to effectively inhibit the progression of CD fibrosis [73,74]. In CD, pirfenidone, Rho kinase inhibitors, TGF- β signaling inhibitors, IL-13 inhibitors, and G31P (an antagonist of CXCL8) are also known to be effective [75,76]. GED-0507-34, an agent with a strong affinity for PPAR- γ , has been suggested as an anti-fibrotic agent in UC patients [77].

CONCLUSION

IBD-related intestinal fibrosis is the starting point for serious complications in patients with refractory and poorly controlled chronic IBD. If the uniquely activated profibrotic pathway observed in IBD can be identified, it could be used as a biomarker for targeted therapy. In addition, the gene expression signature of fibrogenesis at diagnosis could predict the risk of surgery. Intestinal fibrosis is an unfavorable result of the harmonic action of intestinal epithelial cells, the microbiota, and various mesenchymal components, such as the adipose tissue, fibroblasts, smooth muscle, neural tissue, and vascular endothelial cells, at the lesion site. It is thus necessary to pay attention to these mechanisms, from analyzing the ECM to developing therapeutic agents that target the main factors affecting pathogenesis, as well as elucidating the mechanisms involved by using various advanced research methods.

Ethics Statement

Not applicable.

Availability of Data and Material

All data generated or analyzed during the study are included in this published article (and its supplementary information files).

Code Availability

Data sharing not applicable to this article as no datasets were generated or analyzed during the study.

ORCID

Ji Min Park	https://orcid.org/0000-0002-6062-0418
Jeongseok Kim	https://orcid.org/0000-0003-1007-564X
Yoo Jin Lee	https://orcid.org/0000-0003-1799-0146
Sung Uk Bae	https://orcid.org/0000-0002-7876-4196
Hye Won Lee	https://orcid.org/0000-0001-8540-524X

Author Contributions

Conceptualization: SUB. Figures and data: JMP. Writing—original draft: JMP, JK, YJL. Writing—review & editing: HWL. Approval of final manuscript: all authors.

Conflicts of Interest

The authors declare that they have no potential conflicts of interest.

Funding Statement

No funding to declare.

References

1. Leask A, Abraham DJ. TGF-beta signaling and the fibrotic response. *FASEB J* 2004; 18: 816-27.
2. Kumar V, Abbas AK, Aster JC. Robbins and Cotran pathologic basis of disease. Amsterdam: Elsevier, 2020.
3. Jun JI, Lau LF. Resolution of organ fibrosis. *J Clin Invest* 2018; 128:

- 97-107.
4. Di Gregorio J, Robuffo I, Spalletta S, et al. The epithelial-to-mesenchymal transition as a possible therapeutic target in fibrotic disorders. *Front Cell Dev Biol* 2020; 8: 607483.
 5. Rockey DC, Bell PD, Hill JA. Fibrosis: a common pathway to organ injury and failure. *N Engl J Med* 2015; 372: 1138-49.
 6. Zhang YZ, Li YY. Inflammatory bowel disease: pathogenesis. *World J Gastroenterol* 2014; 20: 91-9.
 7. Zidar N. Histopathology of fibrosis in Crohn's disease: the importance of understanding its pathogenesis. *Gastroenterology* 2020; 158: 2313-4.
 8. Hanna MH, Kaiser AM. Update on the management of sigmoid diverticulitis. *World J Gastroenterol* 2021; 27: 760-81.
 9. Specia S, Giusti I, Rieder F, Latella G. Cellular and molecular mechanisms of intestinal fibrosis. *World J Gastroenterol* 2012; 18: 3635-61.
 10. Wynn TA. Cellular and molecular mechanisms of fibrosis. *J Pathol* 2008; 214: 199-210.
 11. Burke JP, Mulsow JJ, O'Keane C, Docherty NG, Watson RW, O'Connell PR. Fibrogenesis in Crohn's disease. *Am J Gastroenterol* 2007; 102: 439-48.
 12. Franze E, Monteleone I, Laudisi F, et al. Cadherin-11 is a regulator of intestinal fibrosis. *J Crohns Colitis* 2020; 14: 406-17.
 13. Rieder F, Fiocchi C, Rogler G. Mechanisms, management, and treatment of fibrosis in patients with inflammatory bowel diseases. *Gastroenterology* 2017; 152: 340-50.
 14. Rieder F, Fiocchi C. Intestinal fibrosis in inflammatory bowel disease: current knowledge and future perspectives. *J Crohns Colitis* 2008; 2: 279-90.
 15. Derkacz A, Olczyk P, Olczyk K, Komosinska-Vassev K. The role of extracellular matrix components in inflammatory bowel diseases. *J Clin Med* 2021; 10: 1122.
 16. Graham DB, Xavier RJ. Pathway paradigms revealed from the genetics of inflammatory bowel disease. *Nature* 2020; 578: 527-39.
 17. Zhang H, Massey D, Tremelling M, Parkes M. Genetics of inflammatory bowel disease: clues to pathogenesis. *Br Med Bull* 2008; 87: 17-30.
 18. Jerala M, Hauptman N, Kojc N, Zidar N. Expression of fibrosis-related genes in liver and kidney fibrosis in comparison to inflammatory bowel diseases. *Cells* 2022; 11: 314.
 19. Gazouli M, Pachoula I, Panayotou I, et al. *NOD2/CARD15*, *ATG16L1* and *IL23R* gene polymorphisms and childhood-onset of Crohn's disease. *World J Gastroenterol* 2010; 16: 1753-8.
 20. Andriulli A, Annese V, Latiano A, et al. The frame-shift mutation of the *NOD2/CARD15* gene is significantly increased in ulcerative colitis: an *IG-IBD study. *Gastroenterology* 2004; 126: 625-7.
 21. Wehkamp J, Harder J, Weichenthal M, et al. *NOD2 (CARD15)* mutations in Crohn's disease are associated with diminished mucosal alpha-defensin expression. *Gut* 2004; 53: 1658-64.
 22. Nimmo ER, Prendergast JG, Aldhous MC, et al. Genome-wide methylation profiling in Crohn's disease identifies altered epigenetic regulation of key host defense mechanisms including the Th17 pathway. *Inflamm Bowel Dis* 2012; 18: 889-99.
 23. Chuang AY, Chuang JC, Zhai Z, Wu F, Kwon JH. *NOD2* expression is regulated by microRNAs in colonic epithelial HCT116 cells. *Inflamm Bowel Dis* 2014; 20: 126-35.
 24. Rieder F, Lawrance IC, Leite A, Sans M. Predictors of fibrostenotic Crohn's disease. *Inflamm Bowel Dis* 2011; 17: 2000-7.
 25. Henckaerts L, Van Steen K, Verstreken I, et al. Genetic risk profiling and prediction of disease course in Crohn's disease patients. *Clin Gastroenterol Hepatol* 2009; 7: 972-80.
 26. Nijhuis A, Biancheri P, Lewis A, et al. In Crohn's disease fibrosis-reduced expression of the miR-29 family enhances collagen expression in intestinal fibroblasts. *Clin Sci (Lond)* 2014; 127: 341-50.
 27. Duerr RH, Taylor KD, Brant SR, et al. A genome-wide association study identifies *IL23R* as an inflammatory bowel disease gene. *Science* 2006; 314: 1461-3.
 28. Glas J, Seiderer J, Wetzke M, et al. rs1004819 is the main disease-associated *IL23R* variant in German Crohn's disease patients: combined analysis of *IL23R*, *CARD15*, and *OCTN1/2* variants. *PLoS One* 2007; 2: e819.
 29. Cleynen I, Gonzalez JR, Figueroa C, et al. Genetic factors conferring an increased susceptibility to develop Crohn's disease also influence disease phenotype: results from the IBDchip European Project. *Gut* 2013; 62: 1556-65.
 30. Brand S, Hofbauer K, Dambacher J, et al. Increased expression of the chemokine fractalkine in Crohn's disease and association of the fractalkine receptor T280M polymorphism with a fibrostenosing disease Phenotype. *Am J Gastroenterol* 2006; 101: 99-106.
 31. Fowler EV, Doecke J, Simms LA, et al. *ATG16L1* T300A shows strong associations with disease subgroups in a large Australian IBD population: further support for significant disease heterogeneity. *Am J Gastroenterol* 2008; 103: 2519-26.
 32. Forni D, Cleynen I, Ferrante M, et al. ABO histo-blood group might modulate predisposition to Crohn's disease and affect disease behavior. *J Crohns Colitis* 2014; 8: 489-94.
 33. Hume GE, Fowler EV, Lincoln D, et al. Angiotensinogen and transforming growth factor beta1: novel genes in the pathogenesis of Crohn's disease. *J Med Genet* 2006; 43: e51.
 34. Adams AT, Kennedy NA, Hansen R, et al. Two-stage genome-wide methylation profiling in childhood-onset Crohn's disease implicates epigenetic alterations at the *VMP1/MIR21* and HLA loci. *Inflamm Bowel Dis* 2014; 20: 1784-93.
 35. Meijer MJ, Mieremet-Ooms MA, van Hogezaand RA, Lamers CB, Hommes DW, Verspaget HW. Role of matrix metalloproteinase, tissue inhibitor of metalloproteinase and tumor necrosis factor-alpha single nucleotide gene polymorphisms in inflammatory bowel disease. *World J Gastroenterol* 2007; 13: 2960-6.
 36. Alonso A, Domenech E, Julia A, et al. Identification of risk loci for Crohn's disease phenotypes using a genome-wide association study. *Gastroenterology* 2015; 148: 794-805.
 37. Rieder F, Brenmoehl J, Leeb S, Scholmerich J, Rogler G. Wound healing and fibrosis in intestinal disease. *Gut* 2007; 56: 130-9.
 38. Rockey DC. Hepatic fibrosis, stellate cells, and portal hypertension. *Clin Liver Dis* 2006; 10: 459-79.
 39. Bamba S, Lee CY, Brittan M, et al. Bone marrow transplantation ameliorates pathology in interleukin-10 knockout colitic mice. *J Pathol* 2006; 209: 265-73.
 40. Brittan M, Wright NA. Gastrointestinal stem cells. *J Pathol* 2002; 197: 492-509.
 41. Mao R, Kurada S, Gordon IO, et al. The mesenteric fat and intestinal muscle interface: creeping fat influencing stricture formation in Crohn's disease. *Inflamm Bowel Dis* 2019; 25: 421-6.
 42. Peyrin-Biroulet L, Gonzalez F, Dubuquoy L, et al. Mesenteric fat as a source of C reactive protein and as a target for bacterial translocation in Crohn's disease. *Gut* 2012; 61: 78-85.
 43. Crohn BB, Ginzburg L, Oppenheimer GD. Regional ileitis: a pathologic and clinical entity. *JAMA* 1932; 99: 1323-9.
 44. Goncalves P, Magro F, Martel F. Metabolic inflammation in inflam-

- matory bowel disease: crosstalk between adipose tissue and bowel. *Inflamm Bowel Dis* 2015; 21: 453-67.
45. Desreumaux P, Ernst O, Geboes K, et al. Inflammatory alterations in mesenteric adipose tissue in Crohn's disease. *Gastroenterology* 1999; 117: 73-81.
 46. Levine JA, Jensen MD, Eberhardt NL, O'Brien T. Adipocyte macrophage colony-stimulating factor is a mediator of adipose tissue growth. *J Clin Invest* 1998; 101: 1557-64.
 47. Chen W, Lu C, Hirota C, Iacucci M, Ghosh S, Gui X. Smooth muscle hyperplasia/hypertrophy is the most prominent histological change in Crohn's fibrostenosing bowel strictures: a semiquantitative analysis by using a novel histological grading scheme. *J Crohns Colitis* 2017; 11: 92-104.
 48. Kalluri R, Neilson EG. Epithelial-mesenchymal transition and its implications for fibrosis. *J Clin Invest* 2003; 112: 1776-84.
 49. Zhang D, Wang S, Chen J, et al. Fibulin-4 promotes osteosarcoma invasion and metastasis by inducing epithelial to mesenchymal transition via the PI3K/Akt/mTOR pathway. *Int J Oncol* 2017; 50: 1513-30.
 50. Frid MG, Kale VA, Stenmark KR. Mature vascular endothelium can give rise to smooth muscle cells via endothelial-mesenchymal transdifferentiation: in vitro analysis. *Circ Res* 2002; 90: 1189-96.
 51. Bates RC, Mercurio AM. Tumor necrosis factor-alpha stimulates the epithelial-to-mesenchymal transition of human colonic organoids. *Mol Biol Cell* 2003; 14: 1790-800.
 52. Strutz F, Zeisberg M, Ziyadeh FN, et al. Role of basic fibroblast growth factor-2 in epithelial-mesenchymal transformation. *Kidney Int* 2002; 61: 1714-28.
 53. Yang J, Dai C, Liu Y. A novel mechanism by which hepatocyte growth factor blocks tubular epithelial to mesenchymal transition. *J Am Soc Nephrol* 2005; 16: 68-78.
 54. Kagawa T, Takemura G, Kosai K, et al. Hepatocyte growth factor gene therapy slows down the progression of diabetic nephropathy in db/db mice. *Nephron Physiol* 2006; 102: p92-102.
 55. D'Alessio S, Ungaro F, Noviello D, Lovisa S, Peyrin-Biroulet L, Danese S. Revisiting fibrosis in inflammatory bowel disease: the gut thickens. *Nat Rev Gastroenterol Hepatol* 2022; 19: 169-84.
 56. Chu H, Khosravi A, Kusumawardhani IP, et al. Gene-microbiota interactions contribute to the pathogenesis of inflammatory bowel disease. *Science* 2016; 352: 1116-20.
 57. Qiu P, Ishimoto T, Fu L, Zhang J, Zhang Z, Liu Y. The gut microbiota in inflammatory bowel disease. *Front Cell Infect Microbiol* 2022; 12: 733992.
 58. Alfredsson J, Wick MJ. Mechanism of fibrosis and stricture formation in Crohn's disease. *Scand J Immunol* 2020; 92: e12990.
 59. Zhao Z, Cheng W, Qu W, Shao G, Liu S. Antibiotic alleviates radiation-induced intestinal injury by remodeling microbiota, reducing inflammation, and inhibiting fibrosis. *ACS Omega* 2020; 5: 2967-77.
 60. Zhao S, Dejanovic D, Yao P, et al. Selective deletion of MyD88 signaling in alpha-SMA positive cells ameliorates experimental intestinal fibrosis via post-transcriptional regulation. *Mucosal Immunol* 2020; 13: 665-78.
 61. Porrás AM, Zhou H, Shi Q, et al. Inflammatory bowel disease-associated gut commensals degrade components of the extracellular matrix. Preprint at: <https://doi.org/10.1101/2022.08.09.503432> (2022).
 62. Knowles CH, Farrugia G. Gastrointestinal neuromuscular pathology in chronic constipation. *Best Pract Res Clin Gastroenterol* 2011; 25: 43-57.
 63. Mosli MH, Parker CE, Nelson SA, et al. Histologic scoring indices for evaluation of disease activity in ulcerative colitis. *Cochrane Database Syst Rev* 2017; 5: CD011256.
 64. Hutchings H, Alrubaiy L. Crohn's disease activity index. In: Michalos AC, ed. *Encyclopedia of quality of life and well-being research*. Dordrecht: Springer Netherlands, 2014; 1354-7.
 65. Sofo L, Caprino P, Schena CA, Sacchetti F, Potenza AE, Ciociola A. New perspectives in the prediction of postoperative complications for high-risk ulcerative colitis patients: machine learning preliminary approach. *Eur Rev Med Pharmacol Sci* 2020; 24: 12781-7.
 66. Udristoiu AL, Stefanescu D, Gruionu G, et al. Deep learning algorithm for the confirmation of mucosal healing in Crohn's disease, based on confocal laser endomicroscopy images. *J Gastrointest Liver Dis* 2021; 30: 59-65.
 67. Flynn S, Eisenstein S. Inflammatory bowel disease presentation and diagnosis. *Surg Clin North Am* 2019; 99: 1051-62.
 68. Gumaste V, Sachar DB, Greenstein AJ. Benign and malignant colorectal strictures in ulcerative colitis. *Gut* 1992; 33: 938-41.
 69. Mitomi H, Okayasu I, Bronner MP, et al. Comparative histologic assessment of proctocolectomy specimens from Japanese and American patients with ulcerative colitis with or without dysplasia. *Int J Surg Pathol* 2005; 13: 259-65.
 70. Yamagata M, Mikami T, Tsuruta T, et al. Submucosal fibrosis and basic-fibroblast growth factor-positive neutrophils correlate with colonic stenosis in cases of ulcerative colitis. *Digestion* 2011; 84: 12-21.
 71. Bettenworth D, Bokemeyer A, Baker M, et al. Assessment of Crohn's disease-associated small bowel strictures and fibrosis on cross-sectional imaging: a systematic review. *Gut* 2019; 68: 1115-26.
 72. Agrawal M, Spencer EA, Colombel JF, Ungaro RC. Approach to the management of recently diagnosed inflammatory bowel disease patients: a user's guide for adult and pediatric gastroenterologists. *Gastroenterology* 2021; 161: 47-65.
 73. Li C, Yang CW, Park JH, et al. Pravastatin treatment attenuates interstitial inflammation and fibrosis in a rat model of chronic cyclosporine-induced nephropathy. *Am J Physiol Renal Physiol* 2004; 286: F46-57.
 74. Abe Y, Murano M, Murano N, et al. Simvastatin attenuates intestinal fibrosis independent of the anti-inflammatory effect by promoting fibroblast/myofibroblast apoptosis in the regeneration/healing process from TNBS-induced colitis. *Dig Dis Sci* 2012; 57: 335-44.
 75. Gordon JR, Zhang X, Li F, Nayyar A, Town J, Zhao X. Amelioration of pathology by ELR-CXC chemokine antagonism in a swine model of airway endotoxin exposure. *J Agromedicine* 2009; 14: 235-41.
 76. Stillie R, Farooq SM, Gordon JR, Stadnyk AW. The functional significance behind expressing two IL-8 receptor types on PMN. *J Leukoc Biol* 2009; 86: 529-43.
 77. Specá S, Rousseaux C, Dubuquoy C, et al. Novel PPARgamma modulator GED-0507-34 levo ameliorates inflammation-driven intestinal fibrosis. *Inflamm Bowel Dis* 2016; 22: 279-92.

The proteomic landscape shows oncologic relevance in cystitis glandularis

Jun Yong Kim¹, Dohyun Han^{2,3}, Hyeyoon Kim^{3,4}, Minsun Jung¹, Han Suk Ryu⁴

¹Department of Pathology, Yonsei University College of Medicine, Seoul;

²Transdisciplinary Department of Medicine and Advanced Technology, Seoul National University Hospital, Seoul;

³Proteomics Core Facility, Biomedical Research Institute, Seoul National University Hospital, Seoul;

⁴Department of Pathology, Seoul National University College of Medicine, Seoul, Korea

Background: The relationship between cystitis glandularis (CG) and bladder malignancy remains unclear. **Methods:** We identified the oncologic significance of CG at the molecular level using liquid chromatography-tandem mass spectrometry-based proteomic analysis of 10 CG, 12 urothelial carcinoma (UC), and nine normal urothelium (NU) specimens. Differentially expressed proteins (DEPs) were identified based on an analysis of variance false discovery rate <0.05, and their functional enrichment was analyzed using a network model, Gene Set Enrichment Analysis, and Gene Ontology annotation. **Results:** We identified 9,890 proteins across all samples and 1,139 DEPs among the three entities. A substantial number of DEPs overlapped in CG/NU, distinct from UC. Interestingly, we found that a subset of DEP clusters (n=53, 5%) was differentially expressed in NU but similarly between CG and UC. This “UC-like signature” was enriched for reactive oxygen species (ROS) and energy metabolism, growth and DNA repair, transport, motility, epithelial-mesenchymal transition, and cell survival. Using the top 10 shortlisted DEPs, including SOD2, PRKCD, CYCS, and HCLS1, we identified functional elements related to ROS metabolism, development, and transport using network analysis. The abundance of these four molecules in UC/CG than in NU was consistent with the oncologic functions in CG. **Conclusions:** Using a proteomic approach, we identified a predominantly non-neoplastic landscape of CG, which was closer to NU than to UC. We also confirmed a small subset of common DEPs in UC and CG, suggesting that altered ROS metabolism might imply potential cancerous risks in CG.

Key Words: Cystitis; Urinary bladder neoplasms; Carcinoma, transitional cell; Proteomics; Tandem mass spectrometry

Received: September 22, 2022 **Revised:** October 22, 2022 **Accepted:** October 24, 2022

Corresponding Author: Minsun Jung, MD, PhD, Department of Pathology, Yonsei University College of Medicine, 50-1 Yonsei-ro, Seodaemun-gu, Seoul 03722, Korea
Tel: +82-2-2228-1771, Fax: +82-2-362-0860, E-mail: jjunglammy@yuhs.ac

Corresponding Author: Han Suk Ryu, MD, PhD, Department of Pathology, Seoul National University College of Medicine, 103 Daehak-ro, Jongno-gu, Seoul 03080, Korea
Tel: +82-2-740-8277, Fax: +82-2-743-5530, E-mail: nash77@snu.ac.kr

Cystitis glandularis (CG), a common glandular lesion of the urinary bladder, is a cystic structure with a glandular lumen surrounded by outer urothelial cells that usually evolve from von Brunn's nests after long-standing inflammation or irritation [1]. CG with intestinal metaplasia (IM) or the presence of mucin-containing goblet cells can produce abundant extracellular mucin that requires differentiation from primary adenocarcinoma, urachal adenocarcinoma, or metastatic adenocarcinoma from other organs [1,2]. CG can also develop a mass-like florid lesion that mimics bladder cancer on radiologic and cystoscopic examinations [3].

In addition to the clinical and histopathological disguise characteristics of CG, its relationship with malignancy has been discussed in studies with contrasting results [2]. For example, the

co-occurrence of CG and adenocarcinoma has been frequently reported in the urinary bladder, which may indicate a connection between these two entities [1]. Furthermore, prior studies, using single gene or chromosome assays, underlaid the molecular basis supporting the premalignant nature of CG with or without IM by elucidating telomere shortening and chromosomal instability [4], p53 loss of heterozygosity and overexpression [5], and nuclear β -catenin expression [6]. In contrast, other studies failed to find a clear indication that CG, with or without IM, increased the future risk of developing bladder cancer during years of retrospective observation [7,8]. Comprehensive characterization would greatly help identify the pathobiology and clinical implications of CG.

In this study, we compared the proteomic landscape of CG with that of urothelial carcinoma (UC) and normal urothelium (NU). Differentially expressed proteins (DEPs) with functional enrichment were analyzed in CG, UC, and NU to identify the oncologic significance of CG at the molecular level.

MATERIALS AND METHODS

Patient selection

From the Seoul National University Hospital, 10 CG, 12 UC, and 9 NU specimens were collected after excluding patients who previously had any bladder tumor or intravesical treatment. Experienced pathologists (M.J. and H.S.R.) reviewed the diagnoses using hematoxylin-eosin slides based on the 2022 World Health Organization (WHO) classification [9]. All samples were obtained by transurethral resection of the urinary bladder, except for one NU, which was obtained from the ureter.

Liquid chromatography-tandem mass spectrometry

Formalin-fixed paraffin-embedded slides were scrapped and lysed in a sodium dodecyl sulfate-extraction buffer. After protein isolation, samples were sonicated and precipitated using acetone. Proteins were digested according to the filter-aided sample preparation procedure [10]. Tandem mass tag 6-plex labeling was employed for the peptide samples according to the manufacturer's instructions, with modifications. After pooling the labeled peptides, the sample was separated into 12 fractions using Agilent 1290 bioinert high-pH reverse-phase liquid chromatography (Agilent, Santa Clara, CA, USA). For each peptide fraction, liquid chromatography-tandem mass spectrometry (LC-MS/MS) analysis was conducted using a Q-ExactivePlus mass spectrometer (Thermo Fisher, Waltham, MA) with an Ultimate 3000 RSLC system (Dionex, Sunnyvale, CA, USA), as previously described, with modifications [11]. Peptides were identified using a false discovery rate (FDR) of 1% as cutoff. Raw data are available in the ProteomeXchange Consortium (PXD027602) [12,13].

Proteomic data analysis

The MS raw data were processed using MaxQuant ver. 1.5.3.1 (Max Planck Institute of Biochemistry, Munich, Germany) [14] with the Andromeda engine [15]. For label-free quantification, the iBAQ algorithm was used on MaxQuant platform [16]. Using normalized abundance, we identified DEPs among CG, UC, and NU based on an analysis of variance (ANOVA) [14] test as a cutoff for permutation-based FDR < 0.05. Subsequently, the DEPs were hierarchically clustered based on Euclidean distance.

Following a review of their abundance, we enlisted "UC-like" DEP clusters as "UC-like signature", for which CG and UC overlapped but NU did not. All analyses were conducted using Perseus ver. 1.6.14.0 (Max Planck Institute of Biochemistry).

Functional enrichment analysis

To determine the biological processes represented by the lists of DEPs, we investigated protein-protein interactions (PPIs) using String database [17], Gene Ontology-biologic process (GOBP) annotation using ToppGene Suite [18], and the Molecular Signatures Database (MSigDB) Hallmark gene sets using pre-ranked Gene Set Enrichment Analysis (GSEA) [19]. To examine the associations among GOBPs, we reconstructed a network model using REVIGO [20]. Network models of PPI and GOBP were visualized using Cytoscape ver. 3.7.2 [21]. The z-scores of the selected proteins were compared between the group with and without IM using a two-tailed t-test.

RESULTS

We investigated 31 urothelial specimens, including 10 CGs, 12 UCs, and nine NUs, using a proteomic approach. A schematic outline of this study is shown in Fig. 1. The median ages were 40, 70, and 63.5 years, respectively, and the male-to-female ratios were 1.0, 0.4, and 0.9, respectively. Half of the specimens that contained CG were accompanied by IM. All UCs were confined to the mucosa (stage Ta), and eight (67%) were of WHO high grade.

From LC-MS/MS analysis, we identified 9,890 proteins across all samples and 1,139 DEPs among the three entities (ANOVA FDR < 0.05). With unsupervised hierarchical clustering, a substantial number of DEPs were discovered to overlap with CG/NU in a way distinct from UC (Fig. 2). CG was not differentiated by the presence of IM (Fig. 2, asterisks). Interestingly, we found a subset of DEP clusters (n = 53, 5%) that were differentially expressed in NU but similarly expressed between CG and UC (Fig. 2, arrows); thus, these proteins were named as "UC-like signature" (Fig. 3A). Since the signature were similar within each group, the patterns of these signatures were thought to represent the general profile of CG.

We hypothesized that this signature might represent the UC-like characteristics of the CG. Using PPI analysis, we explored cellular processes represented by the "UC-like signature". This resulted in sets of DEP networks within the "UC-like signature", which were enriched for reactive oxygen species (ROS) and energy metabolism [22-24], growth and DNA repair [25,26], transport [27,28], motility and epithelial-mesenchymal transition (EMT)

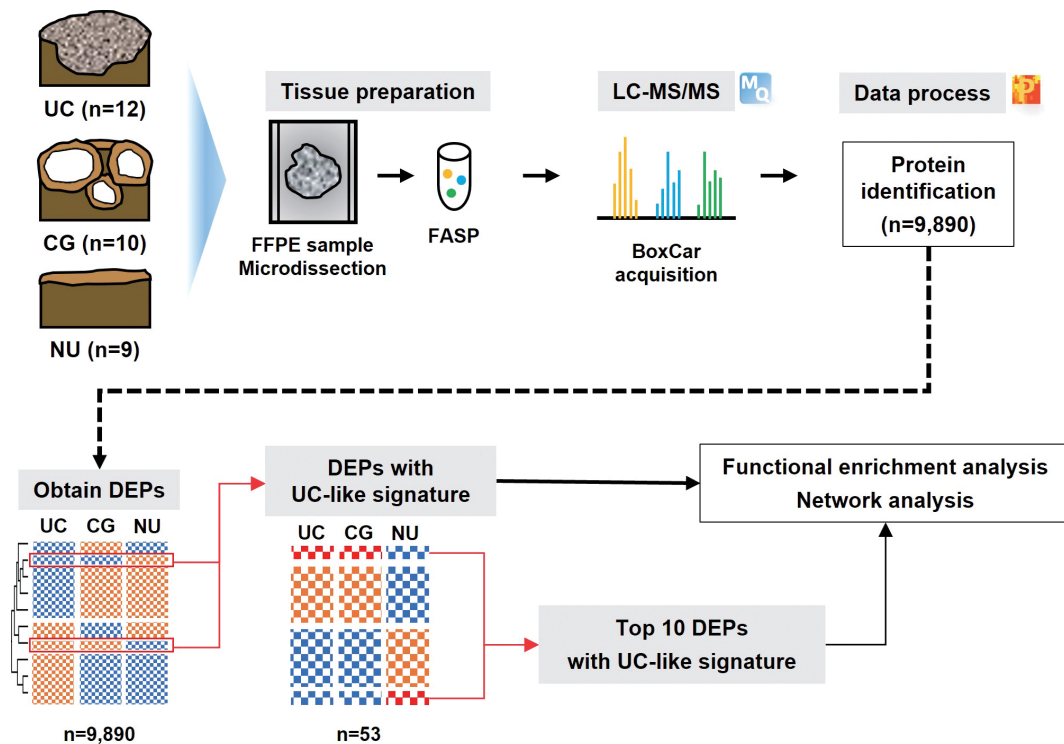


Fig. 1. Schematic outline of the study. (Top) Liquid chromatography-tandem mass spectrometry (LC-MS/MS)-based proteomic analysis of 12 urothelial carcinoma (UC), 10 cystitis glandularis (CGs), and nine normal urothelial (NU) specimens identified 9,890 proteins. Formalin-fixed paraffin-embedded (FFPE) slides were scrapped and proteins were isolated. After sonication and precipitation of samples, proteins were digested according to the filter-aided sample preparation (FASP) procedure. (Bottom) Differentially expressed proteins (DEPs) were discovered based on analysis of variance (false discovery rate <math>< 0.05</math>), and DEPs with UC-like signatures were revealed in CG. Functional enrichment analysis was performed for the DEPs and top 10 DEPs, respectively.

[29,30], and cell survival [31,32] (Fig. 3B). The unit associated with ROS and energy metabolism, which was connected to the one with growth and DNA repair functions, included the top-ranked DEPs (e.g., SOD2, PRKCD, CYCS, and MRPL23) (Fig. 3B). Using the official pre-ranked GSEA of the “UC-like signature”, we also identified significant enrichment of ultraviolet (UV) response (normalized enrichment score = 1.772, FDR = 0.03) for SOD2, PRKCD, and MRPL23 (Fig. 3C). UV radiation stimulates carcinogenic sequences by promoting ROS generation and DNA damage [33]. These data suggest that CG is predominantly a benign lesion, but oxidative stress might be a gateway theme representing oncogenic potential in CG.

To further characterize the “UC-like signature”, we shortlisted the top 10 most significant DEPs (Fig. 3A, asterisk), followed by GOBP analysis (Fig. 4A). Subsequently, we constructed a network of connections between the GOBP terms. Consistent with the aforementioned single-protein networks, functional elements related to ROS metabolism, development, and transport were highlighted by GOBPs (Fig. 4B), which suggests that these functions could collectively substantiate the cancerous risks in CG.

Of note, GOBPs were represented almost exclusively by four molecules, i.e., SOD2, PRKCD, CYCS, and HCLS1 (Fig. 4A), and their abundance in UC/CG compared to NU accordantly pointed toward oncologic functions. For example, previous studies have shown an association of decreased level of SOD2 and increased level of PRKCD, as observed in CG/UC versus NU, with ROS production [22,24]. Overt oxidative stress by activating oncogenic signaling pathways, DNA mutations, EMT, and stromal remodeling promotes bladder cancer development and progression [22]. In line with this, altered expression of CYCS and HCLS1 might deregulate oxidative respiration and the RAS signaling pathway, thereby enhancing the malignant behavior of bladder cancer [23,34]. We further examined whether these four statistically and functionally significant molecules were differentially expressed with IM and found no significant differences related to IM (Fig. 4C).

DISCUSSION

The malignant risk of CG and its association with bladder can-

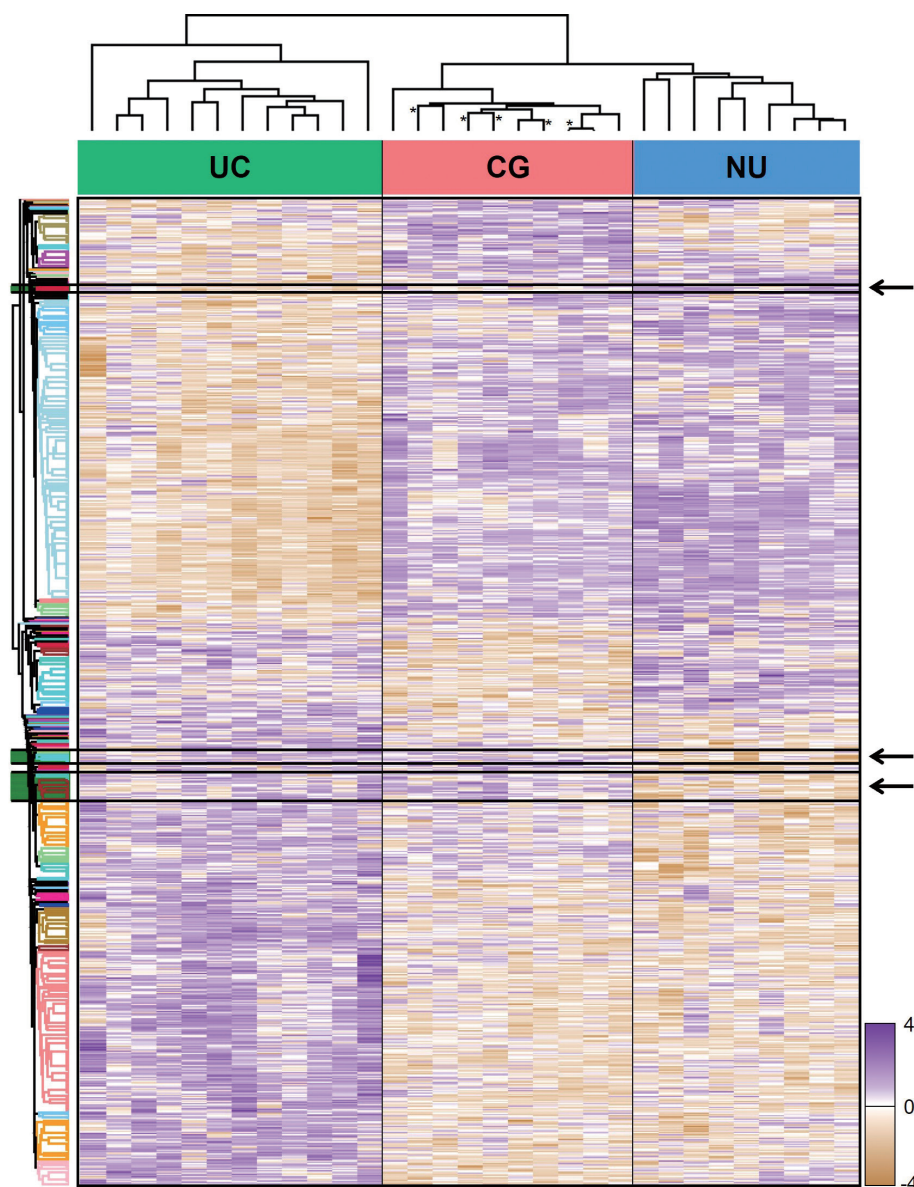


Fig. 2. Unsupervised hierarchical clustering of 1,139 differentially expressed proteins identified by an analysis of variance test of urothelial carcinoma (UC), cystitis glandularis (CG), and normal urothelium (NU). Arrows indicate a “UC-like signature” that showed disparity between UC/CG and NU. Asterisks indicate CG samples showing intestinal metaplasia.

cer have been disputed [1,2]. Considering the high prevalence of CG, there is a dire need to clarify its oncologic implications. Using LC-MS/MS, we revealed the proteomic landscape of CG in relation to malignant (UC) and normal (NU) urothelial tissues. CG generally presented an NU-like profile, in contrast to UC, indicating the overall benign nature of CG. By retrospectively observing a handful of patients with CG, consistent with this result, previous studies failed to confirm clear association between UC and CG [7,8]. Conversely, we confirmed that some of the clustered DEPs showed an opposite pattern across the diagnosis; these proteins

were shared by CG and UC but not by NU. Using functional and network analyses, we found that these DEPs coded for ROS and energy metabolism, growth and DNA repair, transport, motility and EMT, and cell survival, further supporting the relation of this “UC-like signature” with the malignant risk in CG. To our knowledge, this is the first study to determine the oncogenic characteristics of CG using a comprehensive proteomic analysis. Further large-scale studies are required to determine the risks of UC development in patients with CG.

Using an interconnected functional network analysis of the

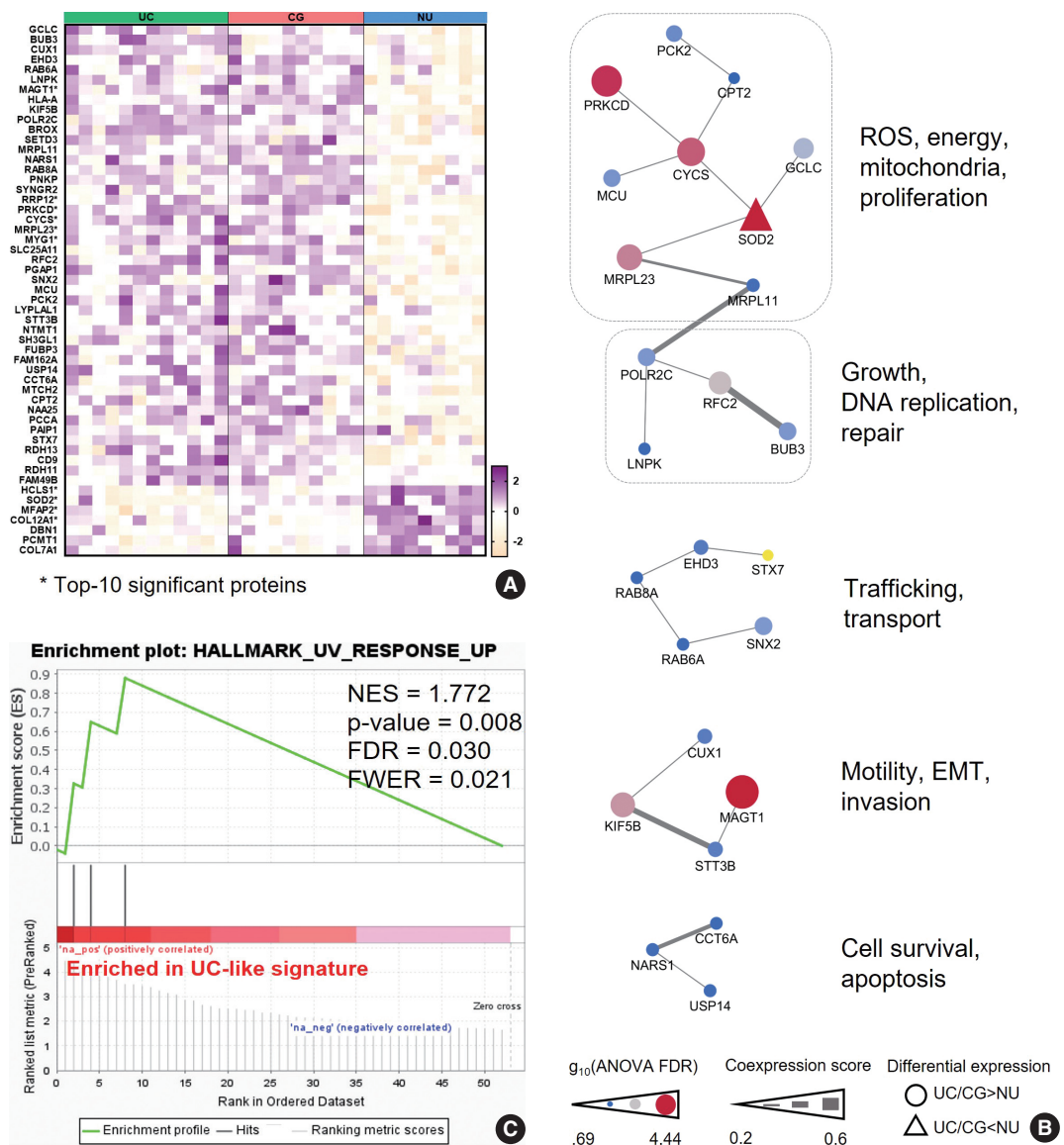


Fig. 3. Pathobiologic characteristics of the “urothelial carcinoma (UC)-like signature”. (A) The UC-like signature proteins. Asterisks denote the 10 top-listed proteins by false discovery rate (FDR). (B) Protein-protein interaction networks of the “UC-like signature” proteins with their common functions. (C) Gene Set Enrichment Analysis of the “UC-like signature” shows enrichment of response to ultraviolet in molecular hallmark function. CG, cystitis glandularis; EMT, epithelial-mesenchymal transition; FWER, family wise error rate; NES, normalized enrichment score; NU, normal urothelium; ROS, reactive oxygen species.

shortlisted proteins, including SOD2, PRKCD, CYCS, and HCLS1, ROS metabolism, structural development, and transport functions were concordantly found to be significantly enriched in the “UC-like signature.” ROS are tightly regulated in normal cellular environments, and increased ROS act as versatile transducers for the generation and progression of bladder cancer [22]. For example, both UC and CG showed downregulation of SOD2, a scavenging molecule, and upregulation of PRKCD, an oxidative enzyme associated with ROS accumulation. ROS im-

balance induces oxidative DNA damage, mutations, propagation of oncogenic signals including RAS, mitogen-activated protein kinases, phosphoinositide 3-kinase, and nuclear factor κB pathways, EMT, and stromal modification in bladder cancer [22,24]. Consistent with this, a previous study suggested that alterations in ROS metabolism participate in inflammation-associated cancer sequences [35,36]. In addition, upregulation of PRKCD can further support a malignant phenotype in bladder cancer by promoting migration and invasion [37]. CYCS is instrumental

in regulating oxidative phosphorylation and energy metabolism, and high maintenance of CYCS, as identified in UC/CG, could induce metabolic modification in bladder cancer, or War-

burg effect [23]. In addition, UC and CG showed lower HCLS1 levels than NU. HCLS1, an actin-binding molecule supporting cellular transport and trafficking, has been shown to result in

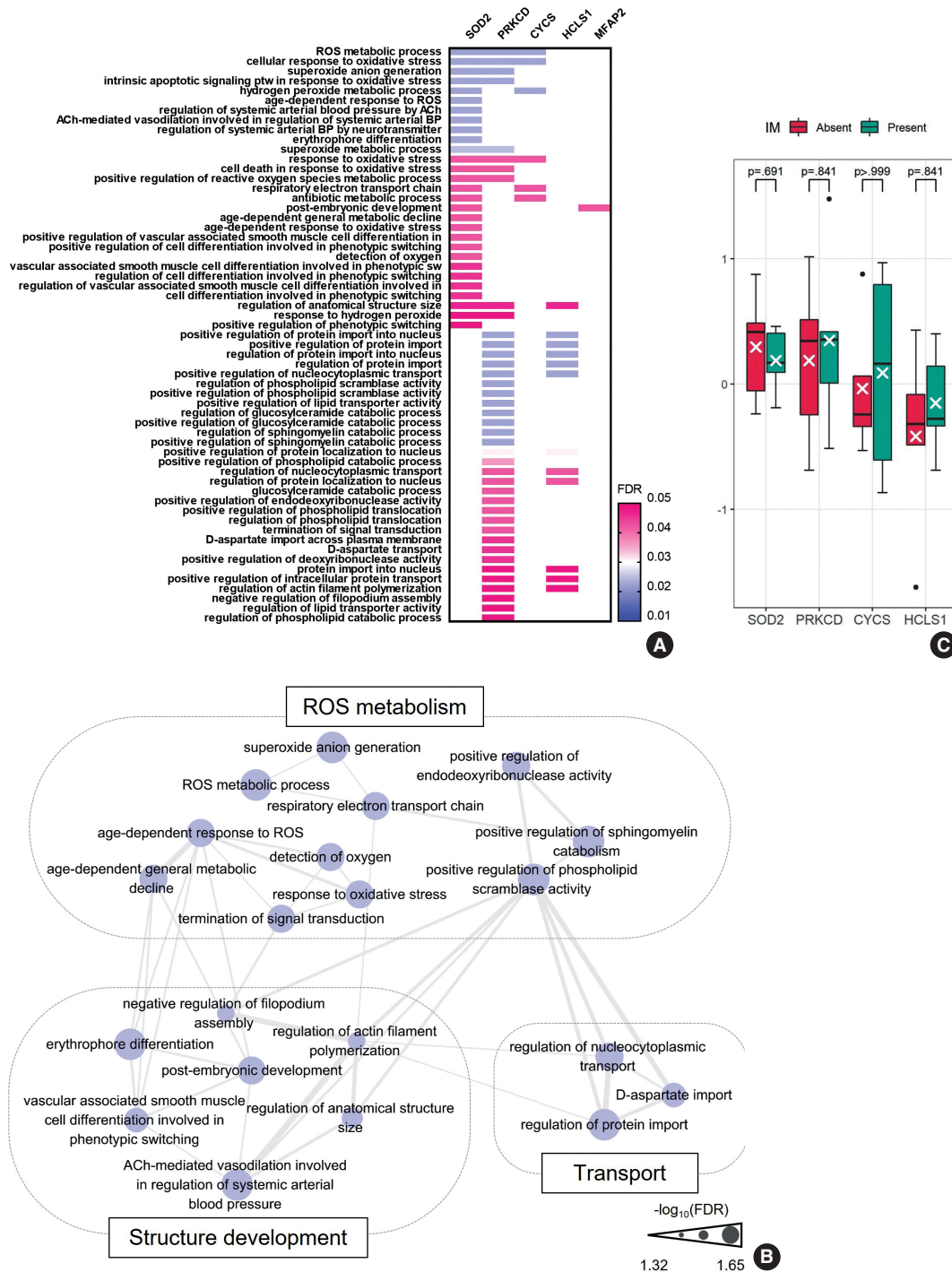


Fig. 4. Imperative functions enriched in the “urothelial carcinoma-like signature”. (A) Gene Ontology-biologic processes (GOBPs) represented by the top 10 shortlisted proteins of “urothelial carcinoma-like signature”. (B) Network analysis of the GOBPs identifies reactive oxygen species (ROS) metabolism, structure development, and transport as common functional themes. (C) SOD2, PRKCD, CYCS, and HCLS1 were comparable between cystitis glandularis with and without intestinal metaplasia (IM). The value is expressed with z-scores of the proteome abundance. FDR, false discovery rate.

adverse outcomes in bladder cancer [34,38]. We believe that the “UC-like signature” might reflect the oncogenic pathway related to altered ROS and energy metabolism and structural modification in CG, and the expression of these signature proteins deserves further study to determine the risk of aggression in CG.

This study lacked specimens with adenocarcinoma in the analysis. The malignant association of CG with IM has been conjectured, typically in terms of bladder adenocarcinoma, but definite evidence has not been confirmed [1]. Instead, altered ROS and energy metabolism have been implicated in the transformation of dysplasia to adenocarcinoma in the esophagus, consistent with the functions enriched in the “UC-like signature” [35]. In addition, the overall proteomic profile and biomarkers relevant to such functions showed no difference regardless of the presence of IM in CG. However, previous studies have suggested that CG with IM may be more advanced than CG without IM regarding tumorigenic potential, as exemplified by more robust telomere shortening or β -catenin activation [4,6]. Therefore, we reasonably speculate that the “UC-like signature” might reflect the malignancy risk encoded in CG irrespective of IM at a global level.

In conclusion, using comprehensive proteomic profiling, we identified a predominantly non-neoplastic landscape of CG that is closer to NU than to UC. Furthermore, we confirmed a small subset of common DEPs in UC and CG, suggesting altered functions of ROS metabolism that might imply potential cancerous risks in CG.

Ethics Statement

All procedures performed in the current study were approved by the Institutional Review Board (IRB) (H-2009-163-1160; 05 October 2020) per the 1964 Helsinki Declaration and its later amendments. Formal written informed consent was not required, with a waiver by the appropriate IRB.

Availability of Data and Material

The datasets generated or analyzed during the current study are available in the ProteomeXchange Consortium (<http://www.proteomexchange.org/>) via the PRIDE database (accession: PXD027602).

Code Availability

Not applicable.

ORCID

Jun Yong Kim <https://orcid.org/0000-0002-4313-9032>
 Dohyun Han <https://orcid.org/0000-0002-0841-1598>
 Hyeyoon Kim <https://orcid.org/0000-0002-8197-6114>
 Minsun Jung <https://orcid.org/0000-0002-8701-4282>
 Han Suk Ryu <https://orcid.org/0000-0003-2508-9796>

Author Contributions

Conceptualization: HSR. Data curation: HSR. Formal analysis: JYK, MJ, HSR. Funding acquisition: MJ. Investigation: JYK, MJ, HSR. Methodology:

HSR. Project administration: HSR. Resources: HSR. Software: DH, HK, HSR. Supervision: HSR. Validation: DH, HK, MJ, HSR. Visualization: JYK, MJ, HSR. Writing—original draft: JYK, MJ. Writing—review and editing: MJ, HSR.

Conflicts of Interest

The authors declare that they have no potential conflicts of interest.

Funding Statement

This research was supported by the Korean Society of Pathologists Grant (No. KSPG2020-04).

References

- Williamson SR, Lopez-Beltran A, Montironi R, Cheng L. Glandular lesions of the urinary bladder: clinical significance and differential diagnosis. *Histopathology* 2011; 58: 811-34.
- Samaratunga H, Martignoni G, Egevad L, Delahunt B. Premalignant lesions of the urinary bladder. *Pathology* 2013; 45: 243-50.
- Song YS, Jang KS, Jang SH, et al. The intestinal type of florid cystitis glandularis mimics bladder tumor: a case report. *Korean J Pathol* 2007; 41: 116-8.
- Morton MJ, Zhang S, Lopez-Beltran A, et al. Telomere shortening and chromosomal abnormalities in intestinal metaplasia of the urinary bladder. *Clin Cancer Res* 2007; 13: 6232-6.
- Srivastava S, Yan B, Chin SY, Muliana T, Salto-Tellez M, Teh M. Nuclear p53 expression is associated with allelic imbalance (TP53) in glandular dysplasia and typical cystitis glandularis: a LCM-based molecular analysis. *Clin Genitourin Cancer* 2012; 10: 57-9.
- Bryan RT, Nicholls JH, Harrison RE, Jankowski JA, Wallace DM. The role of beta-catenin signaling in the malignant potential of cystitis glandularis. *J Urol* 2003; 170: 1892-6.
- Corica FA, Husmann DA, Churchill BM, et al. Intestinal metaplasia is not a strong risk factor for bladder cancer: study of 53 cases with long-term follow-up. *Urology* 1997; 50: 427-31.
- Smith AK, Hansel DE, Jones JS. Role of cystitis cystica et glandularis and intestinal metaplasia in development of bladder carcinoma. *Urology* 2008; 71: 915-8.
- WHO Classification of Tumours Editorial Board. Urinary and male genital tumours. Lyon: International Agency for Research on Cancer, 2022; 131-92.
- Wisniewski JR, Zougman A, Nagaraj N, Mann M. Universal sample preparation method for proteome analysis. *Nat Methods* 2009; 6: 359-62.
- Han D, Moon S, Kim Y, Kim J, Jin J, Kim Y. In-depth proteomic analysis of mouse microglia using a combination of FASP and StageTip-based, high pH, reversed-phase fractionation. *Proteomics* 2013; 13: 2984-8.
- Jung M, Lee C, Han D, et al. Proteomic-based machine learning analysis reveals PYGB as a novel immunohistochemical biomarker to distinguish inverted urothelial papilloma from low-grade papillary urothelial carcinoma with inverted growth. *Front Oncol* 2022; 12: 841398.
- Kim B, Jung M, Moon KC, et al. Quantitative proteomics identifies TUBB6 as a biomarker of muscle-invasion and poor prognosis in bladder cancer. *Int J Cancer* 2022 Sep 10 [Epub]. <https://doi.org/10.1002/ijc.34265>.
- Tyanova S, Temu T, Cox J. The MaxQuant computational platform for mass spectrometry-based shotgun proteomics. *Nat Protoc* 2016;

- 11: 2301-19.
15. Cox J, Neuhauser N, Michalski A, Scheltema RA, Olsen JV, Mann M. Andromeda: a peptide search engine integrated into the MaxQuant environment. *J Proteome Res* 2011; 10: 1794-805.
 16. Schwanhaussner B, Busse D, Li N, et al. Global quantification of mammalian gene expression control. *Nature* 2011; 473: 337-42.
 17. Szklarczyk D, Gable AL, Lyon D, et al. STRING v11: protein-protein association networks with increased coverage, supporting functional discovery in genome-wide experimental datasets. *Nucleic Acids Res* 2019; 47: D607-13.
 18. Chen J, Bardes EE, Aronow BJ, Jegga AG. ToppGene Suite for gene list enrichment analysis and candidate gene prioritization. *Nucleic Acids Res* 2009; 37: W305-311.
 19. Liberzon A, Birger C, Thorvaldsdottir H, Ghandi M, Mesirov JP, Tamayo P. The Molecular Signatures Database (MSigDB) hallmark gene set collection. *Cell Syst* 2015; 1: 417-25.
 20. Supek F, Bosnjak M, Skunca N, Smuc T. REVIGO summarizes and visualizes long lists of gene ontology terms. *PLoS One* 2011; 6: e21800.
 21. Shannon P, Markiel A, Ozier O, et al. Cytoscape: a software environment for integrated models of biomolecular interaction networks. *Genome Res* 2003; 13: 2498-504.
 22. Mendes F, Pereira E, Martins D, et al. Oxidative stress in bladder cancer: an ally or an enemy? *Mol Biol Rep* 2021; 48: 2791-802.
 23. Herrmann PC, Herrmann EC. Oxygen metabolism and a potential role for cytochrome c oxidase in the Warburg effect. *J Bioenerg Biomembr* 2007; 39: 247-50.
 24. Talior I, Tennenbaum T, Kuroki T, Eldar-Finkelman H. PKC-delta-dependent activation of oxidative stress in adipocytes of obese and insulin-resistant mice: role for NADPH oxidase. *Am J Physiol Endocrinol Metab* 2005; 288: E405-11.
 25. Bywater MJ, Pearson RB, McArthur GA, Hannan RD. Dysregulation of the basal RNA polymerase transcription apparatus in cancer. *Nat Rev Cancer* 2013; 13: 299-314.
 26. Yuniati L, Lauriola A, Gerritsen M, et al. Ubiquitylation of the ER-shaping protein lunapark via the CRL3 (KLHL12) ubiquitin ligase complex. *Cell Rep* 2020; 31: 107664.
 27. Chukkapalli S, Amessou M, Dekhil H, et al. Ehd3, a regulator of vesicular trafficking, is silenced in gliomas and functions as a tumor suppressor by controlling cell cycle arrest and apoptosis. *Carcinogenesis* 2014; 35: 877-85.
 28. Nakamura N, Yamamoto A, Wada Y, Futai M. Syntaxin 7 mediates endocytic trafficking to late endosomes. *J Biol Chem* 2000; 275: 6523-9.
 29. Wang G, Li Y, Li J, et al. microRNA-199a-5p suppresses glioma progression by inhibiting MAGT1. *J Cell Biochem* 2019; 120: 15248-54.
 30. Moamer A, Hachim IY, Binothman N, Wang N, Lebrun JJ, Ali S. A role for kinesin-1 subunits KIF5B/KLC1 in regulating epithelial mesenchymal plasticity in breast tumorigenesis. *EBioMedicine* 2019; 45: 92-107.
 31. Sharma A, Almasan A. USP14 regulates DNA damage response and is a target for radiosensitization in non-small cell lung cancer. *Int J Mol Sci* 2020; 21: 6383.
 32. Wang L, Li Z, Sievert D, et al. Loss of NARS1 impairs progenitor proliferation in cortical brain organoids and leads to microcephaly. *Nat Commun* 2020; 11: 4038.
 33. Bosch R, Philips N, Suarez-Perez JA, et al. Mechanisms of photoaging and cutaneous photocarcinogenesis, and photoprotective strategies with phytochemicals. *Antioxidants (Basel)* 2015; 4: 248-68.
 34. Tikoo A, Shakri R, Connolly L, et al. Treatment of ras-induced cancers by the F-actin-bundling drug MKT-077. *Cancer J* 2000; 6: 162-8.
 35. O'Farrell NJ, Phelan JJ, Feighery R, et al. Differential expression profiles of oxidative stress levels, 8-oxo-dG and 4-HNE, in Barrett's esophagus compared to esophageal adenocarcinoma. *Int J Mol Sci* 2019; 20: 4449.
 36. Wigner P, Grebowski R, Bijak M, Saluk-Bijak J, Szemraj J. The interplay between oxidative stress, inflammation and angiogenesis in bladder cancer development. *Int J Mol Sci* 2021; 22: 4483.
 37. Garg R, Benedetti LG, Abera MB, Wang H, Abba M, Kazanietz MG. Protein kinase C and cancer: what we know and what we do not. *Oncogene* 2014; 33: 5225-37.
 38. Sanchez-Carbayo M, Socci ND, Lozano J, Saint F, Cordon-Cardo C. Defining molecular profiles of poor outcome in patients with invasive bladder cancer using oligonucleotide microarrays. *J Clin Oncol* 2006; 24: 778-89.

Metallic implant-associated lymphoma: ALK-negative anaplastic large cell lymphoma associated with total knee replacement arthroplasty

Jai-Hyang Go

Department of Pathology, Dankook University College of Medicine, Cheonan, Korea

Metallic implant-associated lymphomas are extremely rare. Only seven cases have been reported in association with knee joint arthroplasty, and all tumors were large B-cell lymphomas. This report is the first case of anaplastic large cell lymphoma occurring after total knee replacement arthroplasty. An 80-year-old female patient was admitted because of right knee pain for 2 years. She had undergone total knee replacement arthroplasty 10 years prior. Computed tomography showed an irregular osteolytic lesion in the right lateral femoral condyle, adjacent to the metallic prosthesis. Histologic findings reveal sheets of anaplastic tumor cells that were positive for CD2, CD4, CD5, CD43, and CD30 but negative for CD3, CD20, CD15, and anaplastic lymphoma kinase. Epstein-Barr encoding region in situ hybridization was negative. Analysis of T-cell receptor γ gene rearrangement studies using BIOMED-2-based multiplex polymerase chain reaction confirmed monoclonal T cell proliferation. The woman was finally diagnosed with ALK-negative anaplastic large cell lymphoma.

Key Words: Anaplastic large cell lymphoma; Knee; Prosthesis

Received: August 16, 2022 **Revised:** September 26, 2022 **Accepted:** October 30, 2022

Corresponding Author: Jai-Hyang Go, MD, Department of Pathology, Dankook University College of Medicine, 119 Dandae-ro, Dongnam-gu, Cheonan 31116, Korea
Tel: +82-41-550-6974, Fax: +82-41-550-6034, E-mail: cyjy555@daum.net

Primary lymphoma of the bone and joint is rare. Malignant lymphomas related to metallic implants from an orthopedic procedure, called metallic implant-associated lymphomas, are extremely rare [1]. Only seven cases of malignant lymphomas complicating total knee replacement arthroplasty have been reported and occur several years after operation; all cases were large B-cell lymphoma [1-7].

Herein, we describe the first reported case of anaplastic large cell lymphoma (ALCL) presenting as periprosthetic joint infection occurring 10 years after total knee replacement arthroplasty, suggesting that patients with an inflammatory response to orthopedic prostheses should be monitored carefully for an extended time.

CASE REPORT

An 80-year-old female patient was admitted because of right knee pain for 2 years. The pain had recently increased, although there was no history of trauma. She had undergone total knee replacement arthroplasty 10 years prior. Computed tomography

demonstrated an irregular osteolytic mass-like lesion in the right lateral femoral condyle, adjacent to the metallic prosthesis, and a large amount of joint effusion with periarticular soft tissue swelling (Fig. 1), which suggested metallosis, or aseptic lymphocyte-dominant vasculitis-associated lesion, and infectious arthritis. Arthrotomy, hardware removal, and anti-cement insertion were performed under the clinical impression of septic knee. Intraoperatively, synovial hypertrophy, inflammatory change, necrotic tissue, and a mass-like lesion were observed in the right knee joint. Histologically, several fragments of bone and soft tissues were composed of sheets of anaplastic tumor cells, which had irregularly folded nuclei, prominent nucleoli, and a moderate amount of amphophilic cytoplasm (Fig. 2A). Most of the tumor cells were positive for CD30 (Fig. 2B). The tumor cells were also positive for CD2, CD4 (Fig. 2C), CD5, CD43 (Fig. 2D), epithelial membrane antigen, TIA-1, perforin, and granzyme B but negative for CD3, CD7, CD8, CD20, Pax5, CD15, CD68, lysozyme, CD1a, and S100. These cells did not express anaplastic lymphoma kinase (ALK). Epstein-Barr encoding region in situ hybridization was negative. Analysis of T-cell receptor γ gene rear-

rangement studies using BIOMED-2–based multiplex polymerase chain reaction confirmed monoclonal T-cell proliferation (Fig. 3). The woman was finally diagnosed with ALK-negative



Fig. 1. Computed tomography shows an irregular osteolytic mass-like lesion (arrow) in the right lateral femoral condyle, adjacent to the metallic prosthesis.

ALCL. Whole body bone scan showed high ^{18}F -fluorodeoxyglucose uptake in bone and synovium at the right knee arthroplasty removal site, with overlying soft tissue inflammation and joint effusion. There was no evidence of other site involvement in systemic workup, consistent with stage 1 disease. Postoperative definite radiotherapy was administered, and the patient was in good health at the latest follow-up (1 year). Follow-up position emission tomography–computed tomography (PET-CT) revealed no residual mass.

DISCUSSION

Medical devices such as breast, hip, knee, and vascular prostheses can be associated with malignant lymphomas. A prototype is an entity related to breast implants, called breast implant-associated anaplastic large cell lymphoma (BIA-ALCL), and more than 300 cases have been described in the literature [8]. Genomic characterization of BIA-ALCL shows abnormalities similar to those of systemic ALCL [8]. The characteristic clinical features are late-onset implant-associated seroma occurring greater than 1-year post-operative and an indolent course. Most patients are cured by implant removal [9]. In addition to ALCL, other types

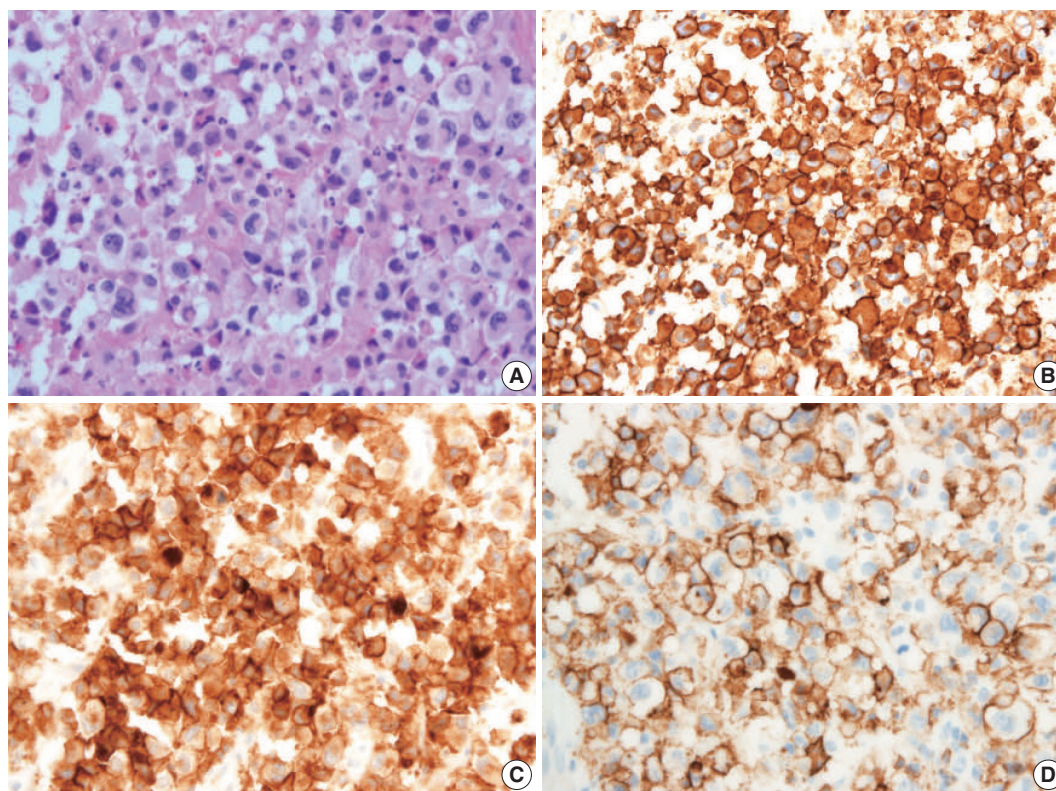


Fig. 2. Anaplastic tumor cells have irregularly folded nuclei, prominent nucleoli, and a moderate amount of amphophilic cytoplasm (A). Tumor cells are positive for CD30 (B), CD4 (C), and CD43 (D).

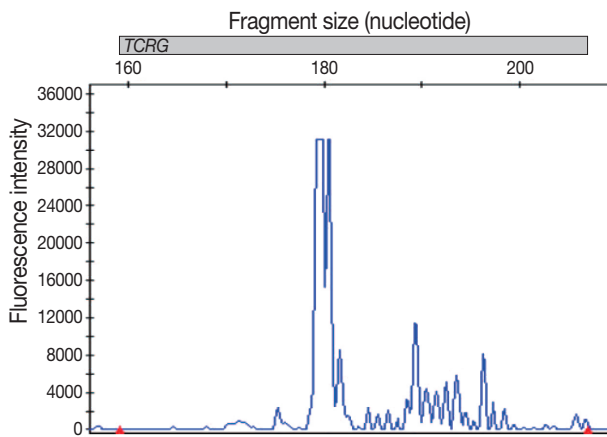


Fig. 3. Analysis of T-cell receptor γ gene (*TCRG*) rearrangement using BIOMED-2-based polymerase chain reaction shows a monoclonal peak.

of lymphomas have been reported to be associated with breast implants [9]. To date, 28 cases of implant-associated B-cell lymphoma have been reported, 18 of which were diffuse large B-cell lymphoma (DLBCL) [10]. Although the available data regarding causation and treatment are limited in BIA-DLBCL, the treatments of BIA-ALCL and DLBCL might be similar. The majority of these two different lymphoma types is well-localized and show similar favorable clinical courses [10].

A prosthesis may act as an immune adjuvant [9], and an immune reaction to the prosthetic material may cause T cell infiltration with later clonal expansion of T lymphocytes. A reaction to biofilms can generate a response by stimulating toll-like receptors on immune cells. Bacterial cell-wall components are potent stimulators of these responses. Contamination of the implant with bacterial fragments can maintain a chronic inflammatory response [8,9]. In contrast, the implants elicit chronic immune system stimulation against the prosthetic material, particularly in genetically susceptible hosts. Therefore, polyclonal activation leads to autoantibody formation, polyclonal hypergammaglobulinemia progressing to monoclonality, and B-cell lymphoma in at-risk hosts [9].

Metallic implant-associated lymphomas are exceedingly rare [1], with only a few cases reported. This raises suspicion of possible oncogenic properties of such materials [9]. The wear debris of implanted synthetic materials is not biologically inert [11], and microparticle detachment from implants might be involved in lymphoproliferative responses and is an important factor in the development of lymphomas [8]. Metallic implant-associated lymphoma is thought to resemble lymphomas associated with other chronic inflammatory conditions such as chronic osteomy-

elitis and pyothorax, and the two share several clinicopathologic features including development in the setting of prolonged chronic inflammation, localization to a confined body space, a long latency period, and the presence of large cell phenotype [11]. Most metallic implant-associated lymphomas were of B-cell origin, in contrast to breast implants. To the best of my knowledge, only one case of ALCL for a tibial metal implant has been published in the English literature [11], and another case of metallic dental implant-associated mucosal CD30-positive T-cell lymphoproliferative disorder was reported in Korea [12].

Only seven cases of malignant lymphomas complicating total knee replacement arthroplasty have been reported in the medical literature [1-7]. The mean time between implantation of the prostheses and lymphoma diagnosis was 7 years (range, 6 months to 16 years). All tumors were classified as large B-cell lymphomas. All cases arose in the bone and five of them were found in wear debris adjacent to the prosthesis or periprosthetic membrane. Three cases were presented as osteolytic bone lesions with soft tissue extension as is the case described above. Four patients were treated with radiotherapy and chemotherapy, one was treated with radiotherapy, one was treated with chemotherapy, and one patient was not treated. Follow-up was reported in six patients, all of them being free of disease for 8 months to 3 years. In particular, one patient was alive for 2 years without evidence of disease, even though no additional treatment was received other than revision arthroplasty [6].

In conclusion, this is the first reported case of ALCL complicating total knee replacement arthroplasty, which can cause prosthesis failure long after the placement operation. Periprosthetic primary lymphoma of the bone should be included in the differential diagnosis of a patient presenting with knee pain, knee mass, or lytic destruction after knee arthroplasty [5].

Ethics Statement

The Institutional Review Board of Dankook University Hospital (2022-03-028) approved this case report and informed consent was waived.

Availability of Data and Material

All data generated or analyzed during this study are included in this published article and available from the corresponding author.

Code Availability

Not applicable.

ORCID

Jai-Hyang Go <https://orcid.org/0000-0002-2105-7837>

Conflicts of Interest

The author declares that I have no potential conflicts of interest.

Funding Statement

No funding to declare.

References

1. Cheuk W, Chan AC, Chan JK, Lau GT, Chan VN, Yiu HH. Metallic implant-associated lymphoma: a distinct subgroup of large B-cell lymphoma related to pyothorax-associated lymphoma? *Am J Surg Pathol* 2005; 29: 832-6.
2. Chaudhry MS, Mather H, Marks A, Naresh K. Diffuse large B cell lymphoma complicating total knee arthroplasty: case report and literature review of the association of diffuse large B cell lymphoma with joint replacement. *Acta Haematol* 2011; 126: 141-6.
3. Sanchez-Gonzalez B, Garcia M, Montserrat F, et al. Diffuse large B-cell lymphoma associated with chronic inflammation in metallic implant. *J Clin Oncol* 2013; 31: e148-51.
4. Sunitsch S, Gilg M, Kashofer K, Leithner A, Liegl-Atzwanger B, Beham-Schmid C. Case report: Epstein-Barr-virus negative diffuse large B-cell lymphoma detected in a peri-prosthetic membrane. *Diagn Pathol* 2016; 11: 80.
5. Ibrahim I, Haughom BD, Fillingham YA, Brown N, Gitelis S. Primary lymphoma of bone complicating total knee arthroplasty: an unexpected mode of prosthesis failure: a case report. *JBJS Case Connect* 2015; 5: e34.
6. Hall J, Kampfer C, Williams N, et al. Fibrin-associated diffuse large B cell lymphoma found on revision arthroplasty of the knee. *South Med J* 2021; 114: 708-13.
7. Agrawal K, Agrawal N, Levin M. Primary synovial diffuse large B-cell lymphoma presenting as loosening of prosthetic joint: a case report and review of literature. *World J Oncol* 2019; 10: 181-5.
8. Ramos-Gallardo G, Carballo-Zarate AA, Cuenca-Pardo J, et al. What is the evidence of lymphoma in patients with prostheses other than breast implants? *Aesthetic Plast Surg* 2020; 44: 286-94.
9. Bizjak M, Selmi C, Praprotnik S, et al. Silicone implants and lymphoma: the role of inflammation. *J Autoimmun* 2015; 65: 64-73.
10. Morgan S, Tremblay-LeMay R, Lipa JE, et al. Breast implant-associated EBV-positive diffuse large B-cell lymphoma: two case reports and literature review. *Pathol Res Pract* 2021; 226: 153589.
11. Palraj B, Paturi A, Stone RG, et al. Soft tissue anaplastic large T-cell lymphoma associated with a metallic orthopedic implant: case report and review of the current literature. *J Foot Ankle Surg* 2010; 49: 561-4.
12. Yoon HJ, Choe JY, Jeon YK. Mucosal CD30-positive T-cell lymphoproliferative disorder arising in the oral cavity following dental implants: report of the first case. *Int J Surg Pathol* 2015; 23: 656-61.



What's new in neuromuscular pathology 2022: myopathy updates and gene therapies

Chunyu Cai

Department of Pathology, University of Texas Southwestern Medical Center, Dallas, TX, USA

Received: September 22, 2022

Accepted: October 14, 2022

Corresponding Author: Chunyu Cai, MD, PhD
 Department of Pathology, University of Texas Southwestern Medical Center, Dallas, Texas, USA
 E-mail: Chunyu.Cai@utsouthwestern.edu

ORCID

Chunyu Cai
<https://orcid.org/0000-0001-8808-4779>

This article has been published jointly, with consent, in both Journal of Pathology and Translational Medicine and PathologyOutlines.com.

Abstract

This compilation of new changes in the diagnosis and treatment of muscle and nerve disease is extracted from the latest publications from the European Neuromuscular Centre International workshops, FDA.gov and clinicaltrials.gov.

MYOPATHY UPDATES

Classification of idiopathic inflammatory myopathies (IIM)

- European Neuromuscular Centre (ENMC) clinico-sero-pathological classification divides IIM into 4 subclasses, which are associated with myositis specific antibodies (MSAs), as outlined in Table 1.
- MSA testing is preferentially performed prior to immune suppression treatment but should also be performed in patients with suspected IIM or interstitial lung disease of unknown etiology without prior MSA testing.
- Polymyositis no longer exists as an IIM subclass.

Dermatomyositis (DM)

- A classification of DM cannot be made in the absence of DM rash (Gottron's sign, Gottron's papules, heliotrope rash).

Table 1. IIM subtypes and their associated autoantibodies

Dermatomyositis (DM)	Mi2, NXP2, TIF1γ, MDA5, SAE
Inclusion body myositis (IBM)	cN1A*
Immune mediated necrotizing myopathy (IMNM)	SRP, HMGCR
Anti-synthetase syndrome (ASyS)	Jo-1, PL7, PL12, EJ, OJ, KS, Zo, Ha

*MSAs are usually mutually exclusive and specific for IIM subclasses, with the exception of cN1A

- In the presence of DM-like rash, DM can be diagnosed if a DM-specific autoantibody is present, or if definitive DM muscle biopsy features are present and are combined with clinical signs of proximal muscle weakness or elevated muscle enzymes.
- Definitive DM muscle biopsy findings: perifascicular atrophy and/or perifascicular MxA overexpression (Fig. 1) with rare or absent perifascicular necrosis.
- Suggestive DM muscle biopsy findings: lymphocytic infiltrates (often perivascular), evidence of perifascicular disease (perifascicular predominant fibers that are pale on COX staining and/or positive on NCAM staining).
- DM specific autoantibodies: Mi2, NXP2, TIF1γ, MDA5, SAE. Patients are subclassified according to that autoantibody (e.g., anti-TIF1γ DM, anti-NXP2 DM). Patients who have DM without a DM-specific autoantibody are subclassified as having "autoantibody negative DM."

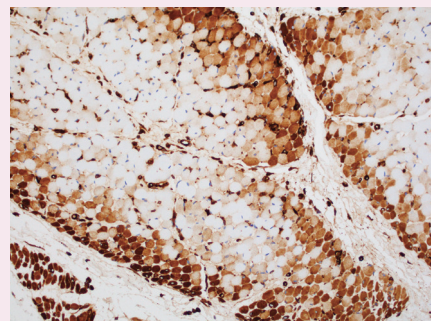


Fig. 1. Sarcoplasmic MxA expression is considered a sensitive and specific marker for dermatomyositis.

Antisynthetase syndrome (ASyS)

- Defined by the presence of an antibody to aminoacyl tRNA synthetase (ARS), together with a single or combination of the following clinical manifestations:
 - Myositis
 - Polyarthritis
 - Interstitial lung disease
 - Mechanic hands
 - Raynaud phenomenon
- ASyS patients with a DM-like rash are not classified as DM, but as "ASyS with a DM-like rash."
- Pathology is characterized by:
 - Perifascicular pathology with necrotic myofibers and nonnecrotic fibers with sarcolemmal C5b-9 (MAC) expression
 - Perimysial connective tissue with substantial edema, fragmentation, and mixed mononuclear inflammation
 - MHC1 sarcoplasmic expression and nuclear actin inclusions in myofibers

Immune mediated necrotizing myopathies (IMNM)

- Anti-HMGCR and anti-SRP autoantibodies are considered specific for IMNM.
- Patients with anti-HMGCR antibody and a DM-like rash will be classified as having "anti-HMGCR myopathy with a DM-like rash," while patients with anti-SRP antibody and a DM-like rash will be classified as having "anti-SRP myopathy with a DM-like rash."
- Pathology requires diffusely scattered necrotic fibers at different stages of resolution and macrophage dominant, pauci-lymphocytic inflammation.

Sporadic inclusion body myositis (sIBM)

- The pathologic criteria for sIBM include:
 - Endomysial T cell inflammation with invasion of non-necrotic fibers
 - Rimmed vacuoles
 - P62 or TDP-43 positive protein aggregates or 15-18 nm filaments (tubulofilamentous inclusions) on electron microscopy
- Anti-cN1A autoantibody is present in 30%–70% of sIBM patients but has also been found in DM and other systemic autoimmune diseases such as Sjögren's and lupus.
- Clinically, elderly patients with asymmetric muscle weakness and atrophy of proximal and distal muscle groups, with predilection for wrist and finger flexors and knee extensors.
- Usually refractory to immunosuppressive therapies.

Limb girdle muscular dystrophies (LGMD)

- The definition and nomenclature of LGMD have been re-defined in the 2017 ENMC international workshop as a genetically inherited condition that primarily affects skeletal muscle leading to progressive, predominantly proximal muscle weakness at presentation caused by a loss of muscle fibers.
- All LGMD subclasses must fulfill all of the following:
 - Described in at least two unrelated families
 - Patients have achieved independent walking (to differentiate from congenital muscular dystrophies)
 - Elevated serum creatine kinase
 - Degenerative changes on muscle imaging over the course of disease
 - Dystrophic changes on muscle histology, ultimately leading to end-stage pathology
- New nomenclature: change from the alphanumeric system to include the name of the affected protein and mode of inheritance (D for dominant, R for recessive, X for X-linked); examples listed in Table 2.
- Some previous LGMD subclasses no longer fulfill the new LGMD definition (Table 3).

Table 2. Old vs new LGMD nomenclature

Previous name	Gene	New name
LGMD 1D	<i>DNAJB6</i>	LGMD D1 DNAJB6-related
LGMD 1I	<i>CAPN</i>	LGMD D4 Calpain3-related
LGMD 2A	<i>CAPN</i>	LGMD R1 Calpain3-related
LGMD 2B	<i>DYSF</i>	LGMD R2 Dysferlin-related

Table 3. Previous LGMD subtypes that are no longer considered LGMD

Previous name	Gene	New name
LGMD 1A	<i>MYOT</i>	Myofibrillar myopathy
LGMD 1B	<i>LMNA</i>	Emery–Dreifuss muscular dystrophy
LGMD 1C	<i>CAV3</i>	Rippling muscle disease
LGMD 1E and 2R	<i>DES</i>	Myofibrillar myopathy
LGMD 1H	unknown	n/a
LGMD 2V	<i>GAA</i>	Pompe disease/acid maltase deficiency

n/a, not available

Myofibrillar myopathies (MFM)

- MFM is a group of disorders associated with myofibrillar degradation that begins in the Z disk.
- Histologically characterized by sarcoplasmic pleomorphic amorphous, granular or hyaline protein aggregates on Gomori trichrome (Fig. 2), and positive for desmin immunostain.
- Most contain mutations in Z disk associated protein coding genes: *DES*, *CRYAB*, *MYOT*, *ZASP*, *FLNC*, *BAG3*.
- Patients with mutations in *FHL1*, *DNAJB6*, *HSBP8*, *TTN*, *ACTA1*, *PLEC*, and *LMNA* have also been associated with MFM phenotype.

Myotonic dystrophy (DM1/DM2)

- Autosomal dominant multi-system diseases with the common features of myotonia and progressive muscle weakness. There are two main forms: DM1 and DM2.
- DM1 is caused by CTG trinucleotide repeats in the 3' untranslated region of *DMPK*. DM1 shows striking anticipation, with age at onset decreasing by 20-30 years per generation.
- DM1 muscle pathology is characterized by markedly increased internalized nuclei, often in chains and ring fibers, in a background of chronic myopathy.
- DM2 is caused by CCTG repeat expansion in intron 1 of *CNBP* (*ZNF9*). Additionally, *CLCN1* and *SCN4A* are disease modifying genes whose mutations may exaggerate DM2 phenotype; they therefore should be included

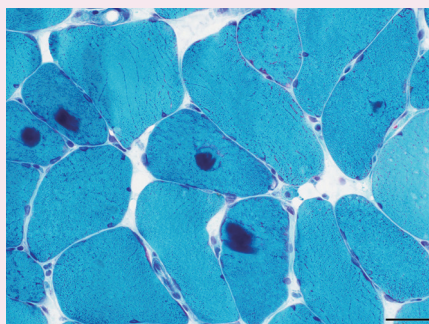


Fig. 2. Myofibrillar myopathy on Gomori trichrome stain.

in DM2 genetic screening.

- DM2 muscle pathology is characterized by type 2 atrophy and frequent internalized nuclei predominantly in type 2 fibers.

GENE THERAPIES

Gene replacement therapies for hereditary neuromuscular diseases

- Adeno-associated virus (AAV) based gene delivery vectors can produce replacement proteins in patients with loss of function mutations, such as spinal muscular atrophy (SMA) or Duchenne's muscular dystrophy. The vector does not integrate into the patient's genome and has a low immunogenicity.
- CRISPR-Cas9-mediated gene editing does incorporate into the patient's genome and can permanently replace a deleterious mutation in patient with conditions such as hereditary transthyretin-mediated (*hATTR*) amyloidosis.
- Both methods entail only a single intravenous injection and thus have a clear advantage over siRNA based and antisense oligonucleotide (ASO) based therapies, which require serial infusions.

FDA approved gene therapy for neuromuscular diseases

- Zolgensma (Novartis) is the first ever FDA approved (2019), intravenously delivered, AAV9 vector mediated *SMN* gene therapy for spinal muscular atrophy.

New gene therapies currently in clinical trials

- NTLA-2001 is a CRISPR-Cas9-mediated gene editing construct that targets *hATTR* amyloidosis in a phase II-III trial for adults with polyneuropathy or cardiomyopathy (NCT04601051).
- SRP-9001 (Sarepta), SGT-001 (Solid Biosciences) and PF-06939926 (Pfizer) are AAV based micro-dystrophin constructs in phase III trials for DMD (NCT03375164, NCT03769116, NCT04281485).
- SPK-3006 (Spark Therapeutics) is an AAV based human *GAA* gene construct in a phase I/II trial for adult onset Pompe disease (NCT04093349).

Meet the Author

Dr. Chunyu Cai has been part of the PathologyOutlines.com editorial board and the Deputy Editor in Chief for Neuropathology since 2020. He is a pathologist and an Associate Professor at University of Texas Southwestern Medical Center. His research focuses on neuromuscular diseases and brain tumors.

